In-depth analysis of the purine biosynthetic pathway of *Corynebacterium glutamicum*

-

From local pathway analysis to global phenotype profiling

Dissertation

zur Erlangung des Grades

des Doktors der Naturwissenschaften

der Naturwissenschaftlich-Technischen Fakultät III

Chemie, Pharmazie, Bio- und Werkstoffwissenschaften

der Universität des Saarlandes

von

Susanne Peifer

Saarbrücken

2012

Tag des Kolloquiums:	21.12.2012
Dekan:	Prof. Dr. Volkhard Helms
Berichterstatter:	Prof. Dr. Elmar Heinzle
	Prof. Dr. Dietrich A. Volmer
Vorsitz:	Prof. Dr. Uli Müller
Akad. Mitarbeiter:	Prof. Dr. Gert-Wieland Kohring

An experiment is a question which [the scientist] poses to Nature,

and a measurement is the recording of Nature's answer.

Max Planck

(1858-1947)

Meiner Familie

Danksagung

Table of contents

Quantitation of intracellular purine intermediates in different *Corynebacteria* using electrospray LC-MS/MS

Metabolic engineering of the purine biosynthetic pathway in *Corynebacterium glutamicum* results in increased intracellular pool sizes of IMP and hypoxanthine

Restriction of the metabolic flexibility due to *pgi* gene deletion triggers a unique adaptation process in *C. glutamicum* involving increased oxygen uptake

List of abbreviations

The following abbreviations are used throughout this thesis. In addition, amino acids are referred to by their common 3 letter codes.

Metabolites

3PG	3-phosphoglycerate
AcCoA	acetyl-coenzyme A
AKG	α-ketoglutarate
ATP/ADP/AMP	adenosine tri/di/monophosphate
DHAP	dihydroxyacetone phosphate
E4P	erythrose 4-phosphate
F16BP	fructose 1,6-bisphosphate
F6P	fructose 6-phosphate
$FAD^+/FADH_2$	flavin adenine dinucleotide; (ox/red)
Fum	fumarate
G6P	glucose 6-phosphate
GAP	glyceraldehyde 3-phosphate
g_{CDW}	cell dry weight [g]
glc	glucose
GTP/GDP/GMP	guanosine tri/di/monophosphate
IMP	inosine 5-monophosphate
Iso	isocitrate
K_m	michaelis constant
Mal	malate
$NAD^+/NADH$	nicotinamide adenine dinucleotide; (ox/red)
$NADP^+/NADPH$	nicotinamide adenine dinucleotide phosphate; (ox/red)
OAA	oxaloacetate
P5P	pentose 5-phosphate
PEP	phosphoenolpyruvate

P_i	inorganic phosphate
PP_i	pyrophosphate
PRPP	5-phosphoribosyl 1-pyrophosphate
Pyr	pyruvate
S7P	sedoheptulose 7-phosphate
Suc	succinate
THF	tetrahydrofolate
Tre	trehalose
V_{max}	maximal enzymatic activity
XMP	xanthosine 5-monophosphate

Enzymes, reactions and pathways

6PGDH	6-phosphogluconate dehydrogenase
G6PDH	glucose 6-phosphate dehydrogenase
GuaB2/*guaB2*	IMP dehydrogenase (enzyme/gene)
ICD	isocitrate dehydrogenase
MalE/*malE*	malic enzyme (enzyme/gene)
Pck	PEP carboxykinase
pgi	glucose 6-phosphate isomerase (gene)
PPP	pentose phosphate pathway
PTS	phosphotransferase system
PurA/*purA*	adenylosuccinate synthase (enzyme/gene)
PurF/*purF*	amidophosphoribosyltranferase (enzyme/gene)
PurF^{K348Q}/*purF*^{K348Q}	amidophosphoribosyltranferase with point mutation K348Q (enzyme/gene)
Pyk	pyruvate kinase
rpm	rounds per minute
SacB/*sacB*	levansucrase (enzyme/gene)
TCA cycle	tricarboxylic acid cycle

Others

μ	specific growth rate [h^{-1}]
AMM	atom mapping matrix
ATCC	American Type Culture Collection
BM	biomass
BSTFA	N,O-bis-(trimethylsilyl)trifluoroacetamide
CE	collision energy
CE-MS	capillary electrophoresis-mass spectrometry
CID	collision-induced dissociation
CPR	CO$_2$ production rate [mmol L^{-1} h^{-1}]
DNA	desoxynucleic acid
DP	declustering potential
DSMZ	Deutsche Sammlung von Mikroorganismen und Zellkulturen
DTT	dithiothreitol
et al.	and others (*et alii*)
GC	gas chromatography
HPLC	high performance liquid chromatography
IDV	isotopomer distribution vector
IEC	ion-exchange chromatography
IMM	isotopomer mapping matrix
IPC	ion-pairing chromatography
IS	internal standard
Kan	kanamycin
LC	liquid chromatography
LLOQ	lower limit of quantification
m/z	mass to charge ratio [-]
MBDSTFA	N-methyl-N-*t*-butyldimethylsilyl-trifluoroacetamide
MCS	multiple cloning site
MDV	mass distribution vector
MFA	metabolic flux analysis
MRM	multiple reaction monitoring

MS	mass spectrometry
NMR	nuclear magnetic resonance
OD	optical density
ori	origin of replication
OUR	oxygen uptake rate [mmol L^{-1} h^{-1}]
PCA	perchloric acid
PCR	polymerase chain reaction
pH	negative decimal logarithm of the proton activity
QC	quality control
q_{CO2}	specific CO_2 production rate [mmol g^{-1} h^{-1}]
q_{O2}	specific O_2 consumption rate [mmol g^{-1} h^{-1}]
q_P	specific product formation rate [mmol g^{-1} h^{-1}]
q_s	specific substrate consumption rate [mmol g^{-1} h^{-1}]
SAX	strong anion-exchange chromatography
t	time [h]
TOF	time of flight
U	units
v	metabolic flux
$Y_{P/S}$	product yield [mol mol^{-1}]
$Y_{X/S}$	biomass yield [g $mmol^{-1}$]
ε	molar extinction coefficient [mM^{-1}]

Abstract

This thesis focused on the purine biosynthetic pathway of *C. glutamicum* in order to increase the general understanding of this essential pathway.

In a first step, a suitable approach for the reliable quantitation of intracellular purine pools was established and validated, thus allowing *targeted metabolite profiling* of genetically engineered *C. glutamicum* strains. Based on a metabolic engineering strategy, site-directed mutants were generated and comprised modifications of the purine precursor supply (*pgi*), deletions of degrading reactions (*purA* and *guaB2*) and a point mutation (*purF*^{K348Q}) targeting at a deregulation of the feedback inhibitory control.

The individual modifications were combined in *C. glutamicum ΔpurA ΔguaB2 purF*^{K348Q} *Δpgi*. Conducting a systems-level approach, a *metabolic shift* of the purine intermediate distribution was revealed, promoting a tremendous increase of the intracellular concentration of the degradation product hypoxanthine at the expense of IMP. Furthermore, a global phenotypic adaptation, expressed in transient growth stagnation, was observed. These adverse effects were attributed to a decline in the ATP generating capacity and imbalances of the NADPH metabolism caused by the deletion of the first glycolytic enzyme, glucose 6-phosphate isomerase (*pgi*). Cultivations applied on complex substrates showed a release of these adverse effects, temporarily delaying the growth stagnation phenomenon.

Zusammenfassung

Im Mittelpunkt der Arbeit stand die Untersuchung des Purinbiosynthesewegs in *C. glutamicum*, welche auf eine Erweiterung des vorliegenden Kenntnisstandes über diesen essentiellen Stoffwechselweg abzielte.

Zunächst wurde ein geeignetes Verfahren zur Quantifizierung intrazellulärer Purinpools etabliert und validiert. Dies bildete die Grundlage zur Erstellung gezielter metabolischer Profile genetisch veränderter *C. glutamicum* Stämme. Die eingebrachten genetischen Veränderungen umfassten die Modifizierung der Purin-Vorläuferbereitstellung (*pgi*), die Deletion beteiligter Abbauwege (*purA* und *guaB2*), sowie die Einführung einer Punktmutation (*purF^{K348Q}*). Letztere hatte die Deregulation der *Feedback*-Inhibierung zum Ziel.

Eine system-orientierte Analyse der Mutante *C. glutamicum ΔpurA ΔguaB2 purF^{K348Q} Δpgi* wies eine ausgeprägte Verschiebung der intrazellulären Purinpools auf, die zu einem drastischen Konzentrationsanstieg des Abbauproduktes Hypoxanthin führte. Desweiteren resultierten die genetischen Veränderungen in einer phänotypisch-globalen Adaption, die sich durch einen vorübergehenden Wachstumsstillstand auszeichnete. Die nachteiligen Effekte – die sich sowohl lokal im Hinblick auf den Purinweg, aber auch global mit Auswirkungen auf den gesamten Phänotyp – zeigten, wurden auf ein verringertes Potential zur Energiegewinnung, sowie auf ein Ungleichgewicht im NADPH-Metabolismus zurückgeführt. Diese Effekte wurden durch den Einsatz komplexer Medienbestandteile teilweise eliminiert.

Chapter I

General introduction

Microorganisms

–

Tailor-made cell factories in the scope of systems biotechnology

The exploitation of microorganisms, representing the most diverse group on earth and the basis of life itself (Schaechter et al., 2004), has been performed for thousands of years. Possessing a tremendous repertoire of biochemical capabilities, those *"conversion agents"* emerged as irreplaceable instruments in the era of biotechnological manufacturing, *e.g.* for product synthesis or degradation of undesired and harmful compounds.

Whereas *trial and error*-driven advancements characterized traditional bioprocess improvements over the last century, thereby primarily relying on classical breeding (Becker and Wittmann, 2012; Nakayama et al., 1978; Vallino and Stephanopoulos, 1993), the focus nowadays is more and more shifting towards targeted approaches, *e.g. genetic* and *metabolic engineering*. The creation of microorganisms with modified cellular properties, so called *designer microbes* (Cameron and Tong, 1993) requires knowledge on *how* these cellular systems operate, ultimately targeting a global and comprehensive picture of the dynamic properties and especially the interconnectivity of the diverse cellular components. Therefore various platforms, allowing quantitative analyses *i.e. genomics, proteomics, transcriptomics, metabolomics* and *fluxomics* are being combined.

Recent developments in the fields of molecular biology, biochemistry, biophysics, microbiology, analytical chemistry and computational modeling and the increasing ability to understand and utilize the vast amount of data, drastically promoted this field. One of the microbial milestones within the scope of industrial manufacturing was the discovery and following exploitation of the Gram-positive microbe *Corynebacterium glutamicum*. This organism, exhibiting an outstanding significance in the biotechnological industry, represents a model system within the field of systems biotechnology. This integrative field, composed by the joined terms of *systemsbiology* and *biotechnology*, aims at uncovering emerging system properties and the refinement of cellular properties to the point of the

redefinition of whole cellular systems, always based on a profound basis of research knowledge, ideally in the form of predictive mathematical models.

The purine biosynthetic pathway and corresponding intermediates are in this context of special interest, as these metabolites exhibit various functions within the cellular system, ranging from carrying the genetic information to signal mediation and energy supply (Cordell et al., 2008; Guimaraes and Londesborough, 2008; Pang et al., 2011; Traut, 1994). In addition imbalances in their pool sizes are reported to be directly linked to increased mutation rates (Bebenek et al., 1992; Pang et al., 2011). Enzymatic defects, perturbing the purine metabolism further cause a large number of human diseases by metabolic dysfunctions (van Gennip et al., 2006). Furthermore some of those compounds exhibit additional functions as flavor-enhancing agents (inosine monophosphate (IMP) and guanosine monophosphate (GMP) (Halpern, 2002; Shimaoka et al., 2005)), putting them into focus of biotechnological manufacturing. Particularly the biotechnological production using *Corynebacteria* (*e.g. Corynebacterium ammoniagenes)* has been successfully performed over the past decades (Abbouni et al., 2004; Furuya et al., 1968; Furuya et al., 1969; Furuya et al., 1970). Flavor-enhancing agents are defined as compounds not possessing a taste on their own but amplifying that of other substances. Thereby, the purine 5-ribonucleotides IMP and GMP synergistically increase the savory taste associated with meat, cheese or seafood (*umami* taste), generated by small amounts of L-glutamate added to food (Abbouni et al., 2004; Halpern, 2002).

In sharp contrast to the development of amino acid producing strains – for example for lysine or glutamate biosynthesis – which have been derived mostly by (targeted) metabolic engineering (Wendisch et al., 2006a), the microbial production of IMP and GMP has been (and still *is*) relying on classical strain optimization applying random mutagenesis and screening (Mori et al., 1997; Shimaoka et al., 2007; Teshiba and Furuya, 1989). Thus, genetic perturbations allowing increased secretion of those compounds and hence regulation and linkage of this essential pathway branch with the central metabolism are not known in detail, promoting this subject into focus of systems biotechnological research.

Aim and outline of the thesis

The objective of this research project aimed towards an in-depth analysis of the purine biosynthetic pathway of the Gram-positive soil bacterium *Corynebacterium glutamicum*. This microorganism, exhibiting an extraordinary significance within the field of biotechnology, provides on one side a powerful and complex platform for industrial processes (Becker and Wittmann, 2012); on the other side, due to its close scientific study and increasing elucidation of global regulatory structures and interactions within the cell, it serves as a model organism in systems biotechnology targeting the ultimate understanding of its metabolic and regulatory potential (Burkovski, 2008; Eggeling and Bott, 2005).

While one section of this thesis focused on global understanding of the essential pathway of the purine metabolites, another section studied the requirements and consequences of increased intracellular concentrations of the industrially relevant purine intermediate inosine 5-monophosphate (IMP), investigating regulatory parameters and the interconnection of this pathway with the central metabolism. Thereby, far-reaching connection of terminal and central pathways via mutual precursor molecules like ATP, NADH or NADPH – *system multiplayers* – but also the unique complexity of this pathway within the whole metabolic network should be outlined, employing *metabolomic* and *fluxomic* analyses.

Each chapter thereby tackles a particular problem or challenge. In addition, result parts of this thesis are summarized in two separate parts (**Part I** and **II**), particularly depicting utilization of alternate carbon sources: whereas cultivations performed on glucose as sole carbon source were studied in **Part I**, metabolization of complex medium supplements, *i.e.* peptone was investigated in **Part II**.

A general introduction is outlined in **Chapter I**.

In **Chapter II** the organism *Corynebacterim glutamicum*, its physiological principles – especially focusing on the purine biosynthetic pathway and its interconnection to the central carbon metabolism – and analytical approaches for the investigation of the

metabolome and fluxome are described. Furthermore, fundamentals for targeted genetic engineering of this bacterium are outlined.

In the initial chapter of **Part I** (**Chapter III**), the challenge of an adequate, reproducible, sensitive and selective analytical platform for quantitative determination of purine intermediates, *i.e. targeted metabolite profiling*, was addressed. In particular, the question for a suitable extraction procedure, ensuring maintenance of unchanged, intracellular *in vivo* concentrations was raised. Usage of a high-sensitive and selective detection system, ESI-MS/MS, set the basis for further in-depth analyses of different *C. glutamicum* mutant strains performed in **Chapter IV**. In this chapter, a metabolic engineering strategy was realized, focusing on the rigidity analysis of the pathway branch of the purine intermediates. Furthermore, influences arising from readjustment processes of the central metabolism, *i.e.* increased activity of the pentose phosphate pathway due to genetic perturbations were addressed and studied based on physiological analyses, *targeted metabolite profiling* and *fluxomics*. This allowed the identification of basic regulatory patterns, *e.g.* impacts emanating from a perturb ATP generation capacity.

Chapter V addressed the problem of deleting the key enzyme glucose 6-phosphate isomerase, targeting an increased precursor availability of ribose 5-phosphate, simultaneously detracting the flexibility and adaptation capabilities of the metabolic network. Effects on the intracellular purine distributions determined and analyzed in **Chapter IV**, were addressed in **Chapter V** with respect to the overall growth performance, especially focusing on the specific growth rates, and redox state of different deletion mutants of *C. glutamicum*. The focus thereby was the elucidation of the impact on the central metabolism emerging from targeted improvements of the purine precursor supply of ribose 5-phosphate, pursued by the deletion of the *pgi* gene.

In Part II, glucose-decoupled growth and intracellular purine accumulation of a site-directed *C. glutamicum* mutant strain (*C. glutamicum ΔpurA ΔguaB2 purF^{K348Q} Δpgi*) were investigated (**Chapter VII**), a response to the observations obtained in previous chapters, especially **Chapters III** and **IV**. The objective was to investigate the intracellular alteration of metabolite concentrations and their distributions as well as that of carbon fluxes of the purine accumulating strain *C. glutamicum ΔpurA ΔguaB2 purF^{K348Q} Δpgi*. The corresponding wild type strain served as reference and was used to implement a

suitable method to study dynamic metabolic flux redistributions on complex media (**Chapter VI**).

Finally reflections, summarizing the results obtained in this thesis, and prospects for future analyses are presented and discussed in **Chapter VIII**, illustrating that new insights had been gained but also new questions have been raised.

Chapter II

Theoretical principles

C. glutamicum and its significance within the field of systems biotechnology

The Gram-positive microorganism *Corynebacterium glutamicum* belongs to the family of the *Corynebacteriaceae*, a heterogeneous group within the actinomycetes subphylum (Liebl, 2005; Stackebrandt et al., 1997). Besides the human pathogenic species *Mycobacterium tuberculosis*, *Mycobacterium leprea* and *Corynebacterium diphteriae* (Tauch et al., 2002), the family of *Corynebacteriaceae* comprises commercially relevant species *e.g. C. glutamicum* and *C. ammoniagenes* (Hirasawa et al., 2000).
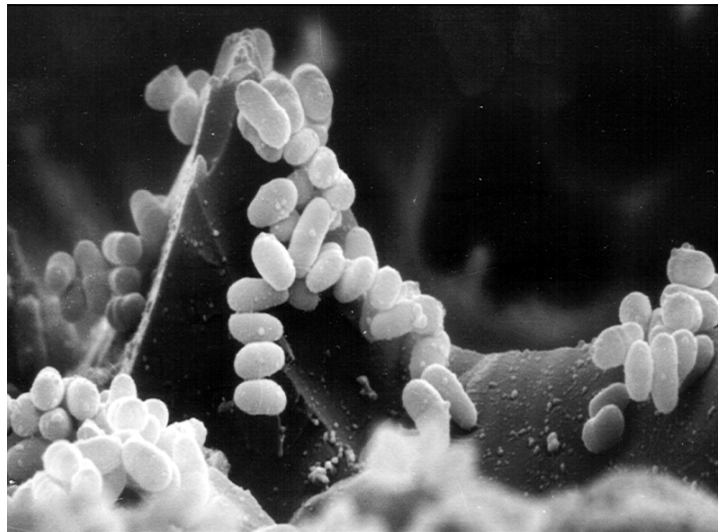
Figure II-1. Electron microscopical image of the soil bacterium *Corynebacterium glutamicum* (source: DBU (Deutsche Bundesstiftung Umwelt; http://www.dbu.de/533bild14952__1959.html).

The rod-shaped, non-sporulating, aerobic, non-motile soil bacterium *C. glutamicum* (Figure II-1) characterized by a high GC content (Pfefferle et al., 2003) and the *"GRAS"* status (*generally regarded as safe*) has first been discovered in Japan in 1957 as natural

producer of the amino acid L-glutamate (Kinoshita et al., 1957; Udaka, 1960). It requires biotin for growth (Schneider et al., 2012) and can be isolated from various ecological niches (Liebl, 2005). Since then this microorganism started its advancement within systems biotechnology, writing a remarkable success story (Becker and Wittmann, 2012) as one of today's most important bacterial species for biotechnological production (Burkovski, 2008). Its product portfolio comprises various compounds *e.g.* amino acids, flavors, diamines, polymers but also biofuels, further driven by systems metabolic engineering concepts (Becker and Wittmann, 2012). In addition to its conversion capabilities, this organism is characterized by low nutritional requirements.

Since its discovery numerous production strains have been created empirically by random mutagenesis and selection (Sahm et al., 2000; Vallino and Stephanopoulos, 1994). Although being successful in the past, these approaches have the huge disadvantages of high labor and resource intensities due to the associated *trial and error* principle, and the fact that the phenotype-modifying alterations of the genome remain unknown. Furthermore, the pronounced accumulation of undesired mutations leads to weak and slowly growing strains (Ohnishi et al., 2002).

The determination of the genome sequence in 2003 (Ikeda and Nakagawa; Kalinowski et al.), marked an essential advancement and allowed the transition from so-far untargeted approaches towards rational strain optimization by *metabolic engineering*, driven by global analytical techniques – the *omic* platforms – promoting a fundamental understanding of the underlying cellular concepts.

Fundamentals of metabolic physiology

The metabolism of cellular systems is a complex, highly intertwined network of interactions, linking central and terminal metabolic branches while maintaining comprehensive and selective regulation mechanisms. Thus, in order to understand the concept behind proper and improper functioning, extensive in-depth analyses are required.

The metabolic branch of the purine biosynthesis involves several pathway branches, supplying the essential precursor molecules *i.e.* ribose 5-phosphate, glutamine, glycine, C_1 groups derived from tetrahydrofolate derivates, aspartate, as well as energy and reduction power. In addition, the synthesis of these compounds can be accomplished by two distinct biosynthetic routes: the *de novo pathway* – assembly of the corresponding purine bases directly onto the carbon skeleton of the precursor ribose 5-phosphate – and the *salvage pathway* – recycling of intact purine bases, either obtained by degradation of nucleotides or by extracellular supplementation, and attachment to 5-phosphoribosyl 1-pyrophosphate (PRPP).

Purine biosynthetic pathway

De novo nucleotide synthesis starts with the activation of the PPP intermediate and direct precursor ribose 5-phosphate (R5P) to 5-phosphoribosyl 1-pyrophosphate (PRPP) (Messenger and Zalkin, 1979), which is further converted to IMP in a twelve-step biosynthetic pathway (Figure II-2).

This step, catalyzed by the ribose-phosphate pyrophosphokinase (PrsA, EC 2.7.6.1) is further accompanied with the conversion of 1 molecule ATP to AMP. The next step catalyzed by the amidophosphoribosyltranferase (PurF, EC 2.4.2.14) represents a transamination reaction with glutamine acting as amino group donor. This rate-determining

step of the purine biosynthesis is controlled by a synergistic feedback-inhibition of the two end products AMP and GMP, acting as competitive inhibitors with respect to PRPP (Messenger and Zalkin, 1979). Thereby, GMP exhibits the highest inhibition efficiency. The corresponding product 5-phosphoribosylamine (PRA) is converted to glycineamide ribonucleotide (GAR) by glycineamide ribonucleotide synthetase (PurD, EC 6.3.4.13) concomitantly consuming 1 molecule glycine and 1 molecule ATP. The transfer of a formyl group derived from N^{10} formyltetrahydrofolate by GAR transformylase (PurN, EC 2.1.2.2) completes the successive reaction to formylglycineamide ribonucleotide (FGAR). FGAR is then converted to phosphoribosyl formylglycineamidine (FGAM) by FGAM synthetase (PurL, EC 3.6.5.3) utilizing 1 molecule ATP and 1 molecule glutamine. The hydrolysis of 2 molecules ATP and the incorporation of 1 molecule hydrogencarbonate represent the two successive reaction steps catalyzed by AIR synthetase (PurM, EC 6.3.3.1) and N_5-CAIR synthetase (PurK, EC 6.3.4.18), respectively. N_5-CAIR mutase (PurE, EC 5.4.99.18) catalyzes the isomerisation of N_5-CAIR (N_5-carboxyaminoimidazole ribonucleotide) into carboxyaminoimidazole ribonucleotide (CAIR). The conversion of CAIR into SAICAR (phosphoribosylaminoimidazole succinocarboxamide) is catalyzed by SAICAR synthetase (HemH, EC 6.3.2.6) consuming 1 molecule aspartate and 1 molecule ATP. Adenylosuccinate lyase (PurB, EC 4.3.2.2) catalyzes the reaction to AICAR (phosphoribosylaminoimidazole carboxamide) releasing fumarate. The final carbon atom is added from formyltetrahydrofolate by AICAR formyltransferase/ IMP cyclohydrolase (PurH, EC 2.1.2.3) generating formamido phosphoribosylimidazole carboxamide (FAICAR) that is finally converted to inosine 5-monophosphate (IMP).
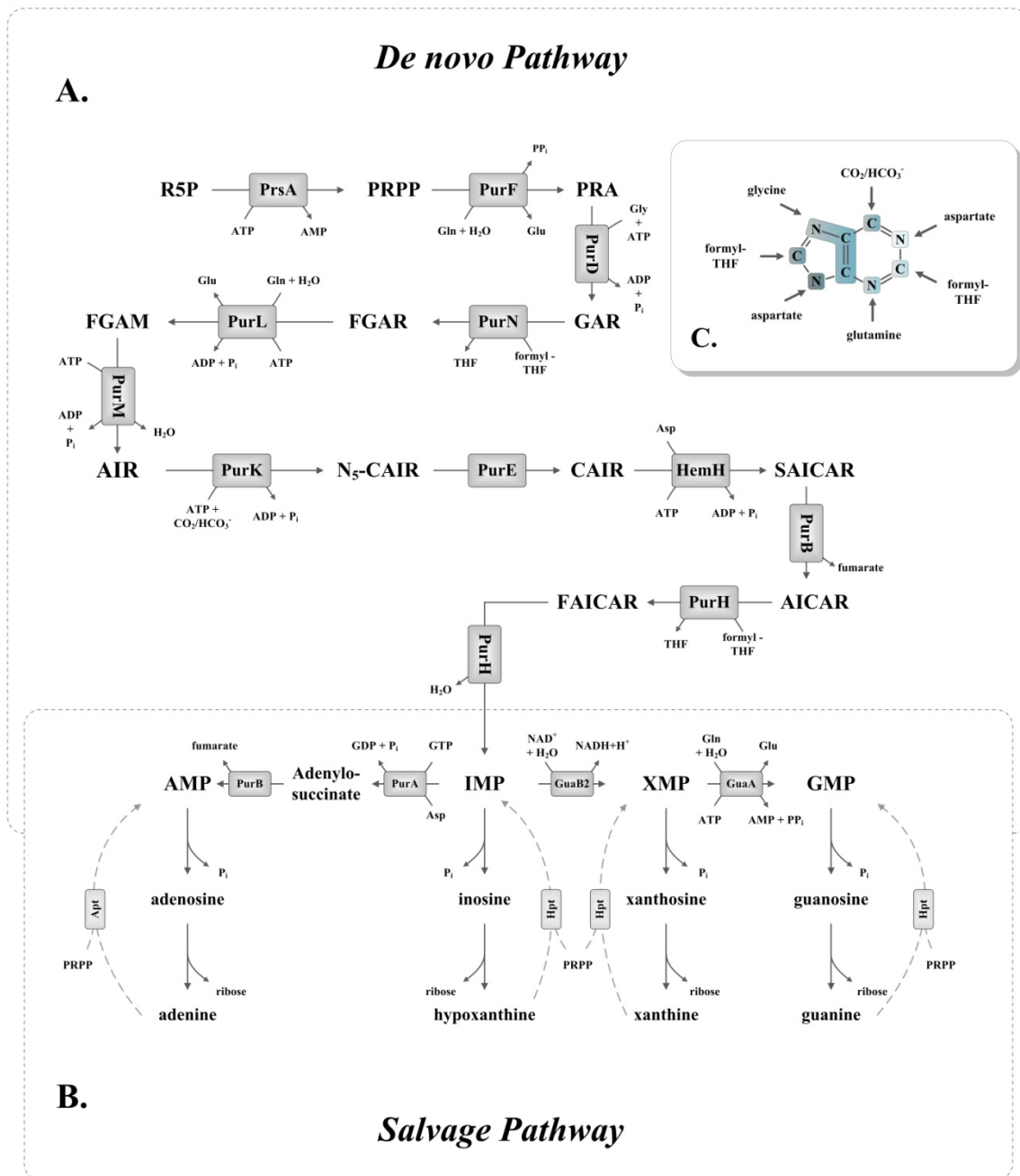
Figure II-2. Purine biosynthetic pathway in *C. glutamicum* comprising reactions end corresponding enzymes from *de novo* (**A.**) and *salvage pathway* (**B.**). Origin of base ring atoms is illustrated in (**C.**).

AMP and GMP are derived from IMP via two-step biosyntheses (Pang et al., 2011; Saxild and Nygaard, 1991): synthesis of AMP starts via the conversion to adenylosuccinate by adenylosuccinate synthase (PurA, EC 6.3.4.4) in the presence of aspartate and GTP.

Adenylosuccinate is further converted to AMP by adenylosuccinate lyase (PurB, EC 4.3.2.2) releasing in addition 1 molecule of fumarate. GMP is generated via the reactions of IMP dehydrogenase (GuaB2, EC 1.1.1.205) and GMP synthase (GuaA, EC 6.3.5.2), leading to XMP (in the presence of 1 molecule NAD^+) and GMP and glutamate (in the presence of ATP and glutamine), respectively.

Due to the complexity of the underlying biosynthetic process, the atoms contained in the purine ring are derived from various precursor molecules (Figure II-2) highly interconnecting this pathway with the central carbon metabolism and – due to the high demand of ATP (10 mol ATP for 1 molecule IMP starting from glucose) – with the energy metabolism.

Central carbon metabolism

The central carbon metabolism fulfills the task to constantly meet the demand for carbon precursors and cofactors draining the intracellular metabolite pools and supplying the anabolic pathways. Varying demands, *e.g.* caused by altered product syntheses or a changing availability of carbon sources, lead to flux redistributions and fine-tunings of the metabolic activities to assure the sufficient supply for precursor and cofactor molecules (NADH, NADPH and ATP). The metabolic flexibility and adaption potential to varying environmental conditions allows *C. glutamicum* to utilize several carbon sources. Carbohydrates as glucose, fructose and sucrose are taken up by phosphotransferase systems (PTS) (Dominguez et al., 1998; Moon et al., 2005; Moon et al., 2007; Mori and Shiio, 1987). In addition, lactate and mannose as well as organic acids *e.g.* acetate can be used as carbon sources (Gourdon et al., 2000; Neuner and Heinzle, 2011; Veit et al., 2009).

The central metabolism of *C. glutamicum* comprises the metabolic pathways of glycolysis, pentose phosphate pathway (PPP), tricarboxylic acid (TCA) cycle and anaplerosis (Figure II-3).
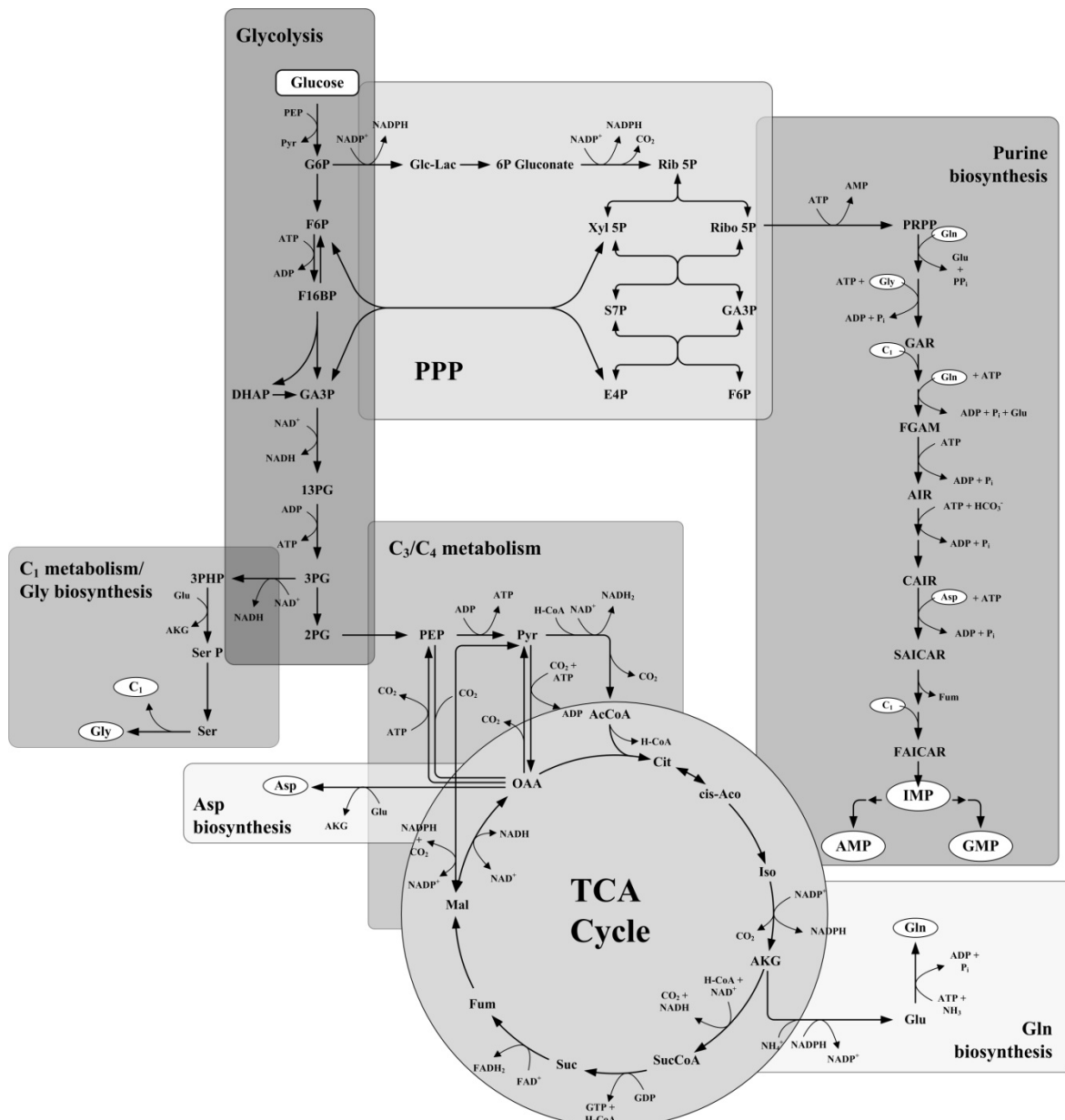
Figure II-3. Central carbon metabolism of *Corynebacterium glutamicum* including glycolysis, pentose phosphate pathway (PPP), TCA cycle, C_3/C_4 metabolism (anaplerosis), C_1 metabolism (simplified), purine biosynthesis and biosynthetic pathways of amino acids required for purine biosynthesis (glycine, glutamine and aspartate).

The latter includes the two C_3-carboxylating enzymes phosphoenolpyruvate carboxylase (Ppc, EC 4.1.1.31) and pyruvate carboxylase (Pyc, EC 6.4.1.1), replenishing the TCA cycle at the level of OAA (Eikmanns et al., 1989; Sauer and Eikmanns, 2005). The glyconeogenic C_4-decarboxylating enzymes phosphoenolpyruvate carboxykinase (Pck, EC

4.1.1.32), OAA-decarboxylase (Oad, EC 4.1.1.3) and malic enzyme (MalE, EC 1.1.1.40) contribute to refill the PEP/pyruvate pools (Gourdon et al., 2000; Jetten and Sinskey, 1993; Jetten and Sinskey, 1995; Netzer et al., 2004a; Sauer and Eikmanns, 2005). Glucose uptake in *C. glutamicum* is generated via a PEP-dependent phosphotransferase system (PTS^{Glc}). Thereby, glucose is phosphorylated and enters the glycolysis as glucose 6-phosphate (Mori and Shiio, 1987; Parche et al., 2001; Yokota and Lindley, 2005). The required phosphate group is derived from PEP. The glucose uptake is thus linked to the availability of PEP and glucose uptake might be constricted under PEP limitations.

With ribose 5-phosphate representing the starting point for the purine biosynthesis – the purine ring system is assembled onto this molecule – the activity of the PPP for supply of this initial precursor is crucial. In addition, serine as precursor for glycine synthesis and also serving as linking point to the C_1 (tetrahydrofolate-) metabolism, is generated during glycolysis. Aspartate and glutamate are synthesized in the TCA cycle. Besides the supply of precursors, glycolysis generates 2 mol ATP and 2 mol NADH per mol glucose; TCA cycle delivers 3 mol NADH, 1 mol FADH$_2$ and 1 mol GTP. One key enzyme of the TCA cycle is the strictly NADP$^+$-dependent isocitrate dehydrogenase (Icd, EC 1.1.1.42) controlling the flux activity of this pathway branch while supplying NADPH and α-ketoglutarate (Eikmanns et al., 1995). In *C. glutamicum* NADPH supply is provided by 4 strictly NADP$^+$-dependent enzymes, located in the PPP – glucose 6-phosphate dehydrogenase (Zwf, EC 1.1.1.49) and 6-phosphogluconate dehydrogenase (Gnd, EC 1.1.1.44) – the TCA cycle – isocitrate dehydrogenase – and anaplerosis – malic enzyme (Gourdon et al., 2000; Marx et al., 1996; Sugimoto and Shiio, 1987a; Sugimoto and Shiio, 1987b). With respect to the purine biosynthesis, especially ATP generation is one of the key points as 1 molecule IMP – the initial purine nucleotide – consumes 10 mol ATP starting from glucose. Furthermore, the intracellular distribution of the purine intermediates is reported to be influenced by the ATP supply. Diminished ATP supply thereby provokes a metabolic shift towards degradation products (Noguchi et al., 2003). In *C. glutamicum* NADH generated in different pathway branches, is oxidized by oxidative phosphorylation and used for ATP formation. In contrast to the utilization of NADH, usage of NADPH in an energy-generating function has, so far, not been described for

C. glutamicum. A NADPH oxidizing capacity of the respiratory chain, *i.e.* the NADH-ubiquinone-1 oxidoreductase, however has been suggested by Matsushita et al. (2001).

Metabolic engineering toolbox

Recent developments of novel molecular biology tools *(genetic engineering)* provide the capability to control but also to understand and link cellular properties with corresponding genetic perturbations. In addition, while entering the post genome era, high throughput sequencing techniques and improvements of bioinformatic tools in data mining allow the elucidation of genetic repertoires of diverse biological systems (Wendisch et al., 2006b) leading from local pathway identification towards global phenotype analysis (Ikeda and Nakagawa, 2003). Techniques of *proteomics* and *transcriptomics* are undergoing rapid developments and facilitate the determination of regulatory function mechanisms. In combination with quantitative *metabolomics* and *fluxomics*, these techniques depict a global approach to perform in-depth system profiling (Dunn, 2008; Ikeda and Nakagawa, 2003; Nielsen et al., 2003; Niklas and Heinzle, 2011; Niklas et al., 2010) (Figure II-4).
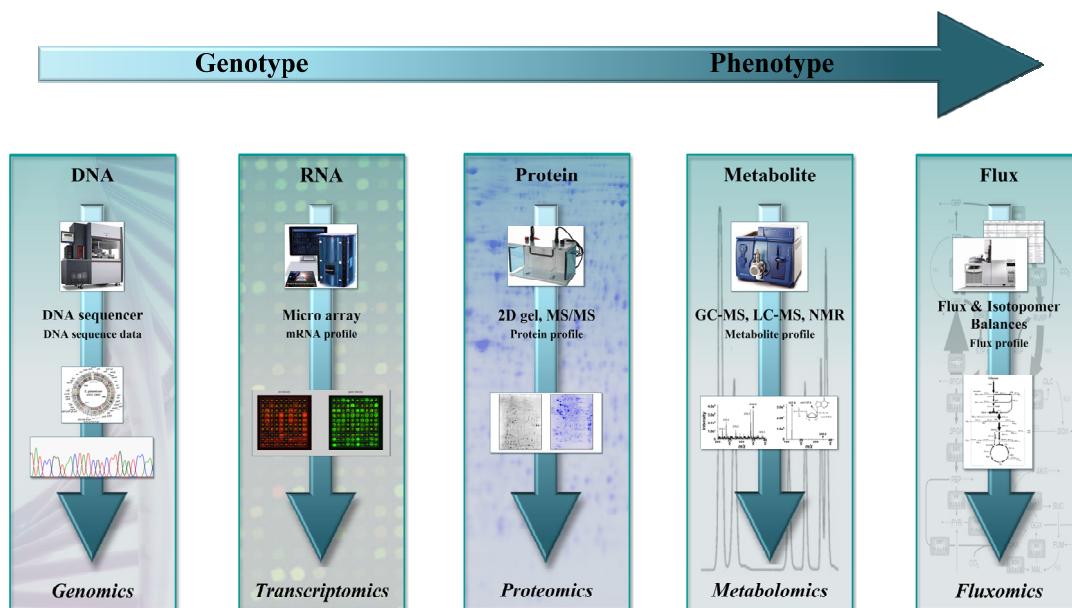
Figure II-4. Schematic illustration of the *metabolic engineering toolbox* comprising the different omic platforms: Targeting the understanding of complex metabolic networks and their regulatory pattern, systems bio(techno)logy represents a global and integrative approach.

Quantitative metabolomics

Linking genotypes and phenotypes

While focusing on the study of different hierarchical levels, which comprise comprehensive regulatory actions (Nielsen and Oliver, 2005), especially the metabolome exhibits distinct advantages for investigating phenotypes (Dunn, 2008; Klein and Heinzle, 2012). As final downstream product of the genome, the *metabolome* – next to the *fluxome* – is seen to be closest to describing the actual phenotype. The study of metabolites and their concentration changes due to altered physiological states, *e.g.* caused by genetic perturbations or varied environmental conditions, provides valuable insights into regulatory principles as well as the interconnectivity of biological systems.

With the development of MS-based analytical platforms *e.g.* LC-MS, LC-MS/MS, CE-MS, GC-MS or GC-TOF, which provide the capabilities for high-sensitive multi-analyte determination, *metabolomics* progressed into a mainstream science (Dunn, 2008; Shulaev, 2006; Sumner et al., 2003). The high accuracy and selectivity of the applied analytical platforms allow the quantitative determination of molecules even in complex biological matrices such as cell extracts.

Due to the complexity and size of the metabolome, analytical procedures might be restricted to a defined metabolic *"section"*. The investigation of an isolated pathway is thereby described as *targeted metabolite profiling*. *Metabolite target analysis* (Fiehn, 2002) solely describes the analysis of a small number of predefined metabolites *e.g.* exclusive analysis of the corresponding substrates and products of a targeted reaction (Figure II-5). Such punctual investigations drastically reduce the analytical requirements in contrast to a whole metabolome analysis (*metabolomics*) (Dunn, 2008) but still elucidate limiting and inhibiting effects or simply provide metabolite concentrations, that can be optimized in an iterative strain improvement process (Buchholz et al., 2002). The field of metabolomic analyses finds important applications in bioscience, *e.g.* profiling whole metabolomes, performing profile comparisons or analyzing dynamic cell behavior.
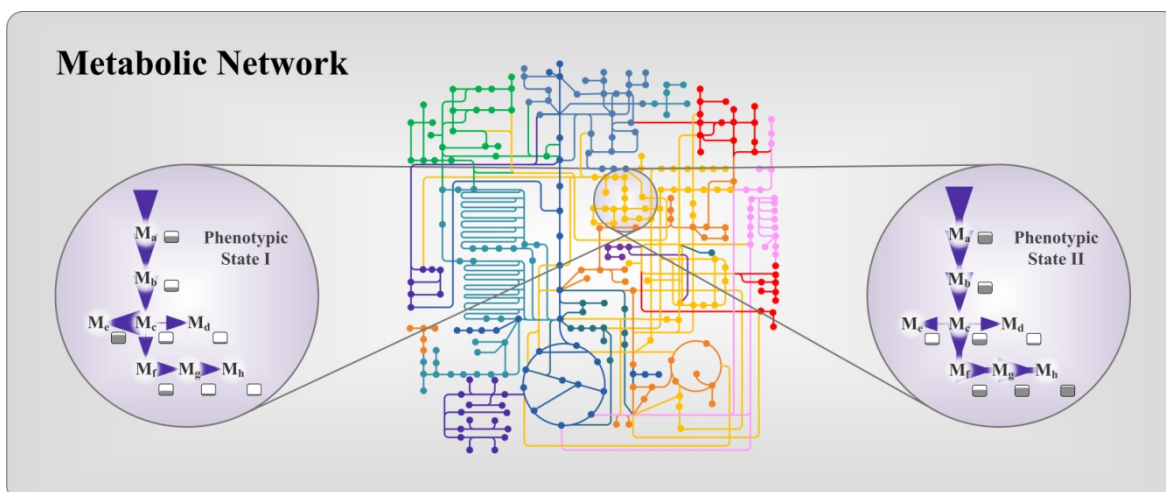
Figure II-5. *Targeted metabolite profiling* of a biological system representing two distinct physiological states with differential metabolite concentrations and metabolic fluxes (based on Sauer and Zamboni (2008)).

In order to actually represent physiological states of biological systems, the extraction of metabolites has to maintain the *in vivo* conditions. Thus extraction-based degradation, insufficient extraction efficiency and enzymatic conversions due to an inadequate arrest of metabolic activity have to be prevented (for further references see Chapter III).

Based on the interconnectivity of the various reactions within metabolic systems, small – sometimes not even detectable – perturbations of the fluxome can cause significant changes of the metabolome (de Koning and van Dam, 1992; Nielsen and Oliver, 2005). Thus metabolome data represent the ultimate, integrative response to genetic or environmental alterations (Villas-Boas et al., 2005), but concomitantly are themselves functions of metabolic fluxes and participating enzymes representing a crucial feedback regulation imposed on the system (Nielsen, 2003) (Figure II-5).

Fluxomics

Principles of metabolic flux analysis

Metabolic flux analysis (MFA) is a generally applicable characterization method in the field of metabolic engineering, targeting the quantitative analysis of intracellular carbon fluxes of a predefined metabolic network (Wittmann and de Graaf, 2005). While metabolome analyses provide data about various reactants (*metabolites*) and their pool sizes present in biological systems, fluxome analyses (*fluxomics*) describe the reactions interconnecting these molecules with each other. Thus, *in vivo* quantitation of intracellular fluxes further improves the in-depth analysis of physiological systems and in combination with metabolite data, represents a powerful tool to determine kinetic regulatory principles. Over the past years, MFA greatly contributed to identifying novel pathways or metabolic bottlenecks, improving strain optimizing processes and to the analysis of regulation and structural *design* of metabolic systems (Beste et al., 2011; Bonarius et al., 1996; Fong et al., 2006; Tang et al., 2008). Due to the presence of common metabolites as ATP, NADH or NADPH, the various metabolic pathways exhibit a high degree of interconnectivity. As a result, flux alterations affecting one distinct pathway branch disseminate to other parts, provoking a global network response (Nielsen, 2003).

Quantitation of intracellular flux rates, which represent time-dependent conversing reactions and are thus not directly measureable (Noh and Wiechert, 2011), can be performed using two approaches: metabolite balancing or ^{13}C MFA (Stephanopoulos, 1998; Stephanopoulos et al., 1998; Wittmann and de Graaf, 2005).

A detailed description of approach-specific advantages and disadvantages is given in Chapter VI, also covering basic principles. The following section only addresses the fundamental and analytical principles for the usage of isotope-labeled substrates. A detailed description of computational modeling and mathematical optimization algorithms is given by Yang et al., 2008 and 2009.

As explained in Chapter VI, metabolization of isotope-labeled substrates, *e.g.* ^{13}C labeled glucose, leads to the distribution of the labeled carbon atoms throughout the entire metabolic network, resulting in stable (fluxome-) specific isotopic enrichment of cellular components – macromolecules as well as free intermediates (Wittmann, 2002). In the field of isotope-base MFA, usage of ^{13}C labeling is the most prominent, as carbon transfer reactions within a biological network are exactly defined by the enzyme specificities and are in addition very well studied (Wittmann, 2002; Yang et al., 2009). The specific labeling patterns can be analyzed by NMR (*nuclear magnetic resonance*) or MS (*mass spectrometry*) (Wittmann, 2002). The combination of measured extracellular fluxes, *i.e.* biomass and by-product formation, and determined labeling pattern of metabolites, allows the computational estimation of intracellular carbon fluxes overcoming the limitations representative for sole metabolite balancing (Wittmann and de Graaf, 2005). Based on the isotopomer distributions of the individual metabolites and the corresponding metabolic network, the relative reaction activities generating those distributions can be calculated (Wittmann and Heinzle, 1999). This includes important physiological parameters *e.g.* the flux partitioning at the glucose 6-phosphate node (de Graaf et al., 2001). In order to determine proper flux distributions, the existence of other stable isotopes other than ^{13}C has to be corrected for (Fernandez et al., 1996; van Winden et al., 2002; Wittmann and Heinzle, 1999).

The term *isotopomer* – composed of the two terms *isotope* and *isomer* (Schmidt et al., 1997) – thereby describes the labeling state of a metabolite (Malloy et al., 1988; Wiechert, 2001). Isotope enrichment analysis carried out by mass spectrometry can resolve single mass isotopomers, while NMR allows for the differentiation between positional isotopomers (Wittmann and de Graaf, 2005). Positional isotopomers are thereby described by uniquely determined labeling patterns of the molecule (Christensen and Nielsen, 1999) *i.e.* the specific number of the labeled carbon atoms (^{13}C atoms) at specific positions within the molecule is defined (Wittmann and de Graaf, 2005). Mass isotopomers however, solely describe the number of ^{13}C atoms within the molecule but not their exact positions. In conclusion, a positional isotopomer distribution precisely determines the corresponding mass isotopomer distribution while the mass isotopomer distribution only impose certain constraints but does not deliver a unique solution for the corresponding positional isotopomer distribution (Christensen and Nielsen, 1999). This principle has to be

considered during the parameter estimation process *i.e.* it has to be specified if either *mass* (MDVs) or *isotopomer distribution vectors* (IDVs) are used (Figure II-6) or an IDV has to be converted into a MDV (Wittmann, 2002).

2^n positional isotopomers   n+1 mass isotopomers

$$IDV = \begin{bmatrix} X_{(000)} \\ X_{(001)} \\ X_{(010)} \\ X_{(011)} \\ X_{(100)} \\ X_{(101)} \\ X_{(110)} \\ X_{(111)} \end{bmatrix} \leftarrow \qquad \rightarrow \begin{bmatrix} X_{(m+0)} \\ X_{(m+1)} \\ X_{(m+2)} \\ X_{(m+3)} \end{bmatrix} = MDV$$
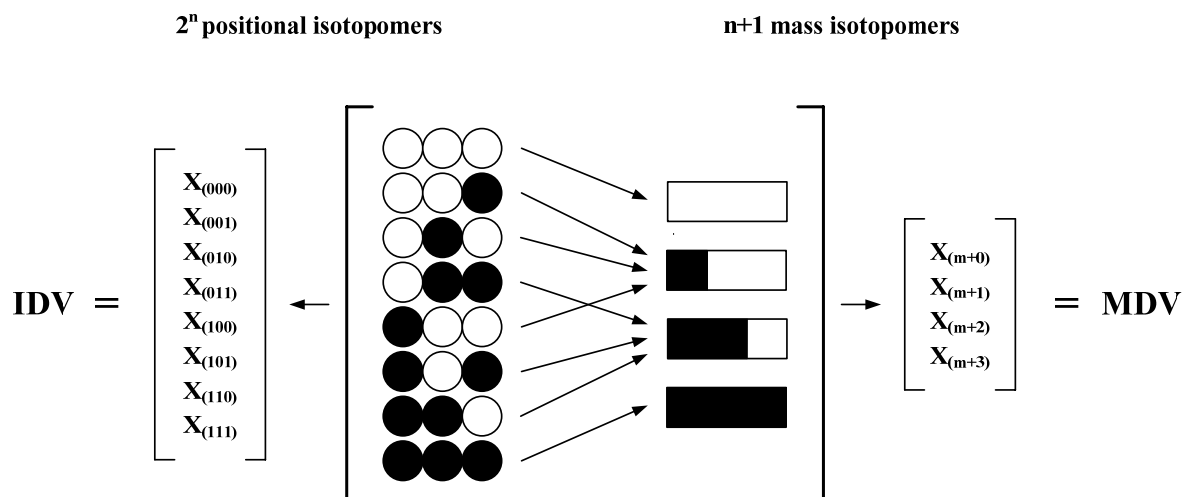
Figure II-6. Positional and mass isotopomers with corresponding IDV and MDV exemplarily for a molecule comprising 3 carbon atoms (white circles illustrate ^{12}C, black circles illustrate ^{13}C; based on Wittmann (2002)). Arrows represent conversion (grouping) of different positional isotopomers into mass isotopomers. Fractions of individual mass and positional isotopomers add up to 1.

The carbon transition network, in form of an *atom mapping matrix* (AMM), precisely defines the transfer of the individual carbon atoms from reactants to products (Zupke and Stephanopoulos, 1994). AMMs thereby depict $m \, x \, n$ matrices with m representing the carbon atoms of the product and n those of the substrate. The reaction catalyzed by pyruvate carboxylase, converting pyruvate and CO_2 to OAA is highlighted as illustrative example (equation 1, [**1**]). A carbon transfer from the educt to the corresponding position of the product is indicated by the element 1. In 1997, *isotopomer mapping matrices* (IMM) were introduced by Schmidt et al. (1997). IMMs define the precise transfer of the positional isotopomers of a substrate to the corresponding product and can be deduced from the corresponding AMM (Wittmann, 2002). The $m \, x \, n$ AMM is thereby converted

into a $2^m \times 2^n$ IMM with m corresponding to the number of carbon atoms of the product and n to those of the substrates.

$$\text{AMM}_{\text{Pyr} \rightarrow \text{OAA}} = \begin{bmatrix} 1 & 0 & 0 \\ 0 & 1 & 0 \\ 0 & 0 & 1 \\ 0 & 0 & 0 \end{bmatrix} \qquad \text{AMM}_{\text{CO}_2 \rightarrow \text{OAA}} = \begin{bmatrix} 0 \\ 0 \\ 0 \\ 1 \end{bmatrix} \qquad \text{[1]}$$

The combination of the *isotopomer distribution vectors* (IDV) – comprising information about the experimentally determined labeling pattern – and the *isotopomer mapping matrices* (IMMs) – comprising information about the carbon transfer based on the underlying enzymatic reactions – are further used to solve the complex equation system (Schmidt et al., 1997). For a description of the parameter estimation and the mathematical modeling see Yang et al., 2008 and 2009.

The experimental principle of ^{13}C MFA is depicted in Figure II-7. Incorporation of the stable ^{13}C carbon isotope into cellular components *e.g.* into cellular protein, is accomplished by cultivations performed on ^{13}C labeled glucose. The corresponding MDVs are determined by *e.g.* GC-MS after isotopic steady state of the corresponding metabolites was reached (*stationary* MFA (Noack et al., 2011)). In combination with additionally determined physiological parameters, *i.e.* biomass and by-product formations, flux calculations are performed. The unknown flux activities are estimated, fitting simulated isotopomer distributions to those experimentally determined via an optimizing algorithm (Wittmann, 2007; Yang et al., 2008).
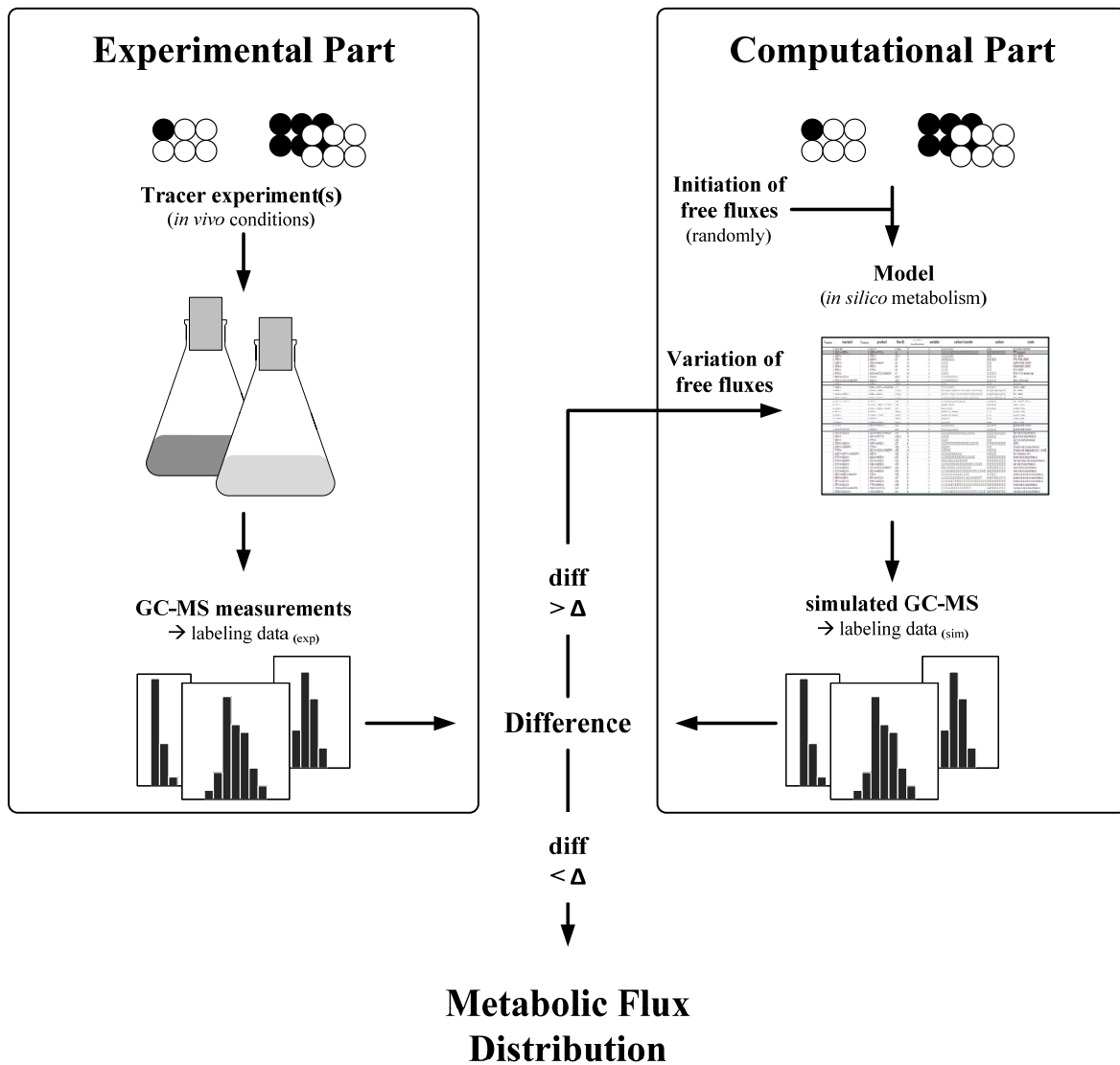
Figure II-7. Schematic representation of the strategy for ^{13}C metabolic flux analysis: the experimental part comprises tracer experiment(s) and the determination of the corresponding labeling pattern by GC-MS; the computational part comprises the simulation of the labeling pattern (based on Wittmann (2007)).

Genetic engineering

Principles of strain construction

Traditional strain optimizing processes of the last century were primarily based upon *classical mutagenesis* and *selection* (Rowlands, 1984). One of the most crucial disadvantages of these processes is the fact that genetic alterations triggering the *"superior qualities"* remained unknown (Sahm et al., 2000). This depicted a huge challenge for further optimizations as neither identified beneficial properties could be combined, nor "unwanted" – often harmful – modifications could be eliminated. Decryption of the *C. glutamicum* genome sequence in 2003 (Kalinowski et al.) and development of methods for recombinant DNA technology marked the advent of *targeted mutagenesis* approaches (Eggeling et al., 1997; Ikeda, 2003; Sahm et al., 1995). Targeted genetic perturbations further provide the basis for the elucidation of genotype-phenotype relationships (Dunn, 2008) and are therefore an indispensable tool within the field of metabolic engineering.

The portfolio of genetic engineering tools *i.e.* amplification and over expression (Neuner and Heinzle, 2011), deletion (Mascarenhas et al., 1991), introduction of point mutations (Becker et al., 2007; Kim et al., 2006) or foreign DNA (heterologous gene expression) as well as codon optimization (Kind et al., 2010), offered new opportunities for targeted strain optimization (Sahm et al., 1995). The introduction of stable genetic modifications of the chromosome, which are maintained and passed on without the need for selective pressure, can be accomplished by homologous recombination employing integrative plasmids (Tauch et al., 2002). Theses plasmids are characterized by an origin of replication (*ori*) for *E. coli* but not for the organism to be modified *e.g. C. glutamicum*. Two selection markers – additionally encoded within the plasmid DNA sequence – allow the identification of two (separate) recombination events: the Kan[R] selection marker, conferring resistance to kanamycin, is employed for the selection of the first recombination event which leads to the integration of the whole plasmid DNA into the genome. The second selection marker, the *sacB* positive selection system introduced by Jager et al. (1992) facilitates the identification of the second recombination event. Thereby, the *sacB* gene sequence encoding for the exoenzyme levansucrase from *Bacillus subtilis* catalyzes the conversion of sucrose into levan that is lethal to *C. glutamicum*. The presence of sucrose in the corresponding media will lead to the cell death of transformants still containing the

plasmid DNA and expressing the *sacB* gene. Thus, solely cells that performed the double crossover event *i.e.* the second recombination randomly initiated without selective pressure, and eliminated the plasmid DNA from the genome, are selected (Nesvera and Patek, 2011).

The first step comprises the design of the targeted genetic modification: performing a SOE-PCR (*splicing by overlapping extension*, (Ho et al., 1989)) hybrid-DNA molecules are constructed (Figure II-8).
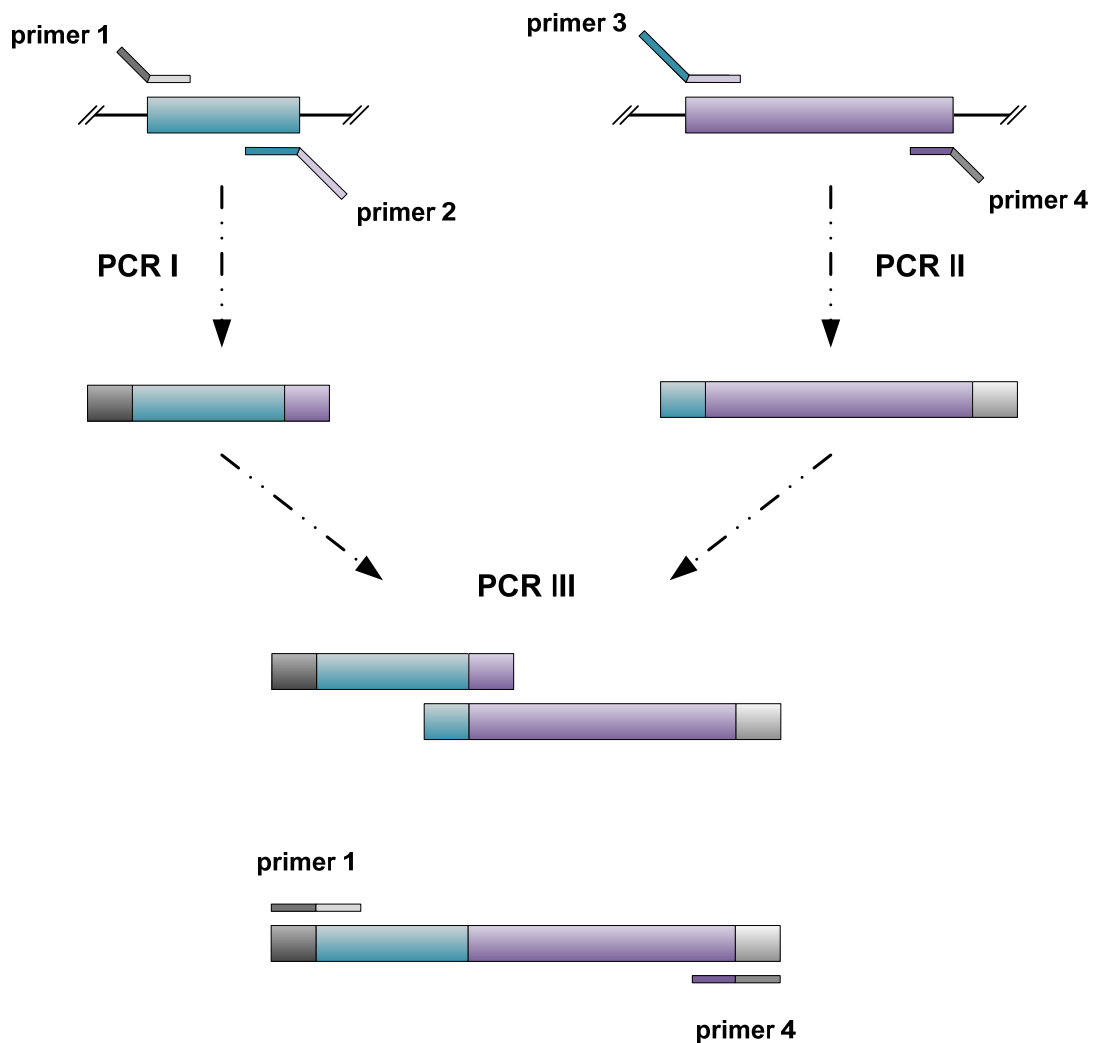
Figure II-8. Fusion (SOE) PCR: connection of two separate DNA molecules. Primer 2 and primer 3 exhibit complementary DNA sequences to each other, while primer 1 und 4 are complementary to the corresponding 3' and 5' ends of the gene(s) additionally comprising specific restriction sites.

Therefore specific primers (1 and 4) – complementary to the 3' and 5' ends of the gene(s) – and in addition fusion primers (2 and 3) – exhibiting complementary DNA sequences to each other – are used. In the first two PCR reactions (primer pairs 1-2 and 3-4) overlapping complementary extensions are created. These overlaps are used in the third PCR reaction to fuse the two single PCR segments. Existence of differential restriction sites, contained and attached by primers 1 and 4, allows a targeted ligation into the integrative vector. This vector is then amplified in *E. coli* employing the selection marker Kan^R. After isolation from *E. coli*, the plasmid is transferred into the recipient *C. glutamicum* by electroporation (Kirchner and Tauch, 2003; Tauch et al., 2002) where the two recombination events take place (Figure II-9).
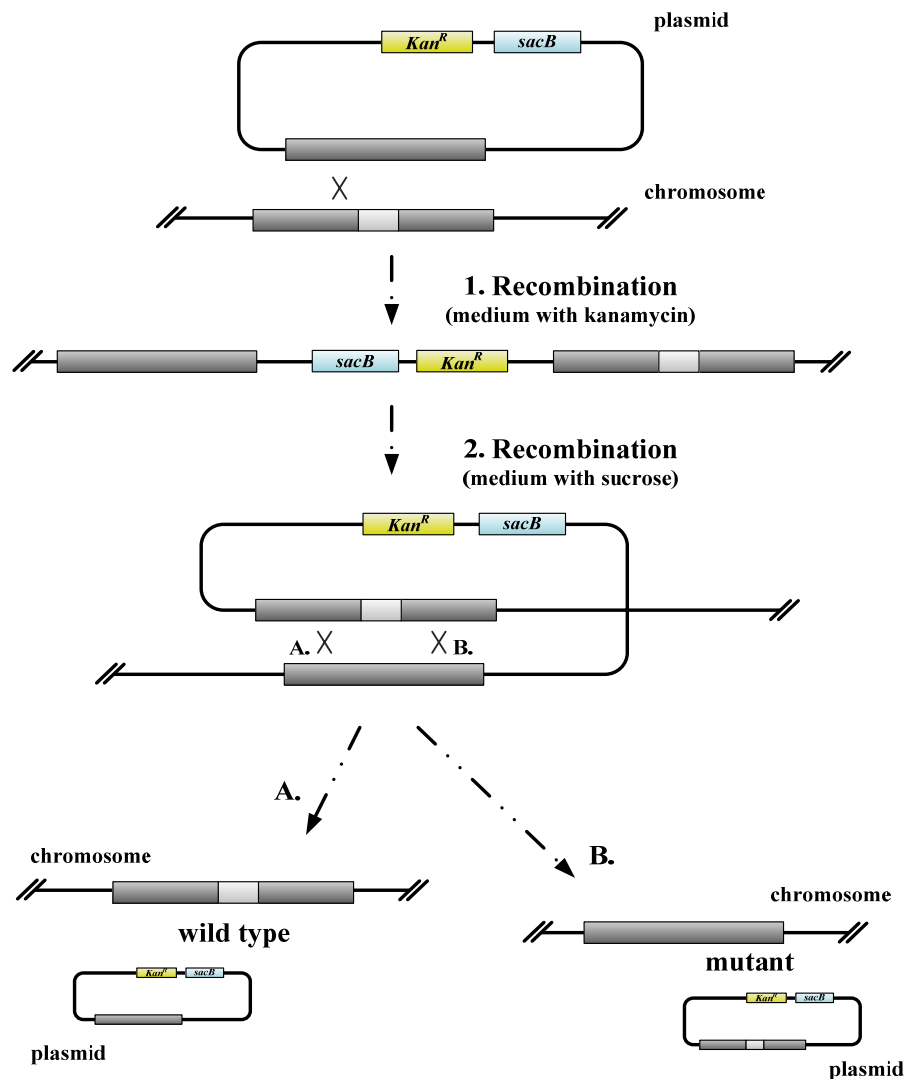
Figure II-9. Implementation of stable genetic modifications by homologous recombination in *C. glutamicum.*

In order to avoid degradation of the introduced (foreign) DNA and to increase the transformation efficiency (Bonamy et al., 2003; Bonnassie et al., 1990; Tzvetkov et al., 2003) the plasmid is methylated in *E. coli* using an additional plasmid (pTC) carrying the corynespecific methyltransferase gene. After the second recombination event − the complete removal of the plasmid DNA from the genome of *C. glutamicum* − either the native (wild type) or the manipulated gene sequence are eliminated, yielding either wild type cells or site-directed mutants.

PART I

Phenotype characterization on minimal medium

The following chapters of Part I present results obtained from cultivations on a defined, fully synthetic medium with glucose as the sole carbon source. Metabolic behavior of different genetically engineered *Corynebacterium glutamicum* strains was investigated, starting with the implementation of a suitable analytical procedure for quantitative metabolite profiling of the purine biosynthetic pathway. Modifying the genetic background of this organism resulted in a complete metabolic shift and uncovered essential regulatory processes, that monitor and control the distribution patterns of the purine intermediates. Furthermore, adverse effects on the overall growth performance were determined, which were related to the deletion of the glucose 6-phosphate isomerase (*pgi*), interrelating the terminal pathway branch of the purine metabolites with the central metabolism. These topics are described in the following chapters:

- Quantitation of intracellular purine intermediates in different C*orynebacteria* using electrospray LC-MS/MS (**Chapter III**).
- Metabolic engineering of the purine biosynthetic pathway in *Corynebacterium glutamicum* results in increased intracellular pool sizes of IMP and hypoxanthine (**Chapter IV**).
- Restriction of the metabolic flexibility due to *pgi* gene deletion triggers a unique adaptation process in *C. glutamicum* involving increased oxygen uptake (**Chapter V**).

Chapter III

It is all about numbers

Quantitation of intracellular purine intermediates in different

Corynebacteria using electrospray LC-MS/MS

Abstract*

Intermediates of the purine biosynthesis pathway play key roles in cellular metabolism including nucleic acid synthesis and signal mediation. In addition, they are of major interest to the biotechnological industry as several intermediates either possess flavor-enhancing characteristics or are applied in medical therapy. In this study, we have developed an analytical method for quantitation of 12 intermediates from the purine biosynthesis pathway including important nucleotides and their corresponding nucleosides and nucleobases. The approach comprised a single-step acidic extraction/quenching procedure, followed by quantitative electrospray LC-MS/MS analysis. The assay was validated in terms of accuracy, precision, reproducibility and applicability for complex biological matrices. The method was subsequently applied for determination of free intracellular pool sizes of purine biosynthetic pathway intermediates in the two Gram-positive bacteria *Corynebacterium glutamicum* and *Corynebacterium ammoniagenes*. Importantly, no ion pair reagents were applied in this approach as usually required for liquid chromatography analysis of large classes of diverse metabolites.

Introduction

Nucleotides and their corresponding nucleosides and nucleobases are essential biomolecules and fulfill various functions in the living cell. In addition to being central building blocks for DNA and RNA (Traut, 1994), they also act as co-substrates in enzymatic reactions, play crucial roles in activating metabolites and serve as signal mediators (Cordell et al., 2008). Furthermore, several intermediates of the purine biosynthesis pathway exhibit additional characteristics – ranging from flavor-enhancing qualities (inosine monophosphate (IMP) and guanosine monophosphate (GMP) (Halpern, 2002; Shimaoka et al., 2005)) to drug-assisted therapy (*e.g.* inosine and purine analogues (Cohen et al., 2010; Hofmann et al., 2012)). These properties make them attractive targets for the pharmaceutical and biotechnological industries. Particularly the fermentative production using *Corynebacteria* (*e.g. Corynebacterium ammoniagenes)* has been successfully performed over the past decades (Abbouni et al., 2004; Furuya et al., 1968; Furuya et al., 1969; Furuya et al., 1970). *Corynebacterium glutamicum*, a most relevant industrial producer of amino acids and other metabolites, may serve as a starting organism to develop a new, powerful producer strain for purine pathway intermediates. As a result, quantifying these substances from biological matrices such as bacteria is crucial to assess the potential of the underlying cellular systems.

The quantitative determination of these compounds, however, is very challenging due to their diverse chemical properties (Cordell et al., 2008), the possibility for chemical and biological degradation during extraction and sample treatment, and the wide concentration range observed in biological systems (Carlucci et al., 1992; Traut, 1994). Over the past several decades, quantitation of nucleotide concentrations has been performed by liquid chromatography and UV detection. The poor retention of phosphorylated polar substances on conventional reversed-phase HPLC columns using mixtures of water and organic solvents as mobile phases led to the frequent application of ion-exchange chromatography (IEC). IEC using high salt concentrations was first described in the 1950s (Cohn). Long run times (Carlucci et al., 1992; Faletto et al., 1997) and incompatibility with mass spectrometry however, have limited its application for nucleotide quantification mostly to

in vitro studies (Qian et al., 2004). Alternatives are ion suppression HPLC (Witters et al., 1996) and ion-pairing chromatography (IPC). The latter has been used for many years with a broad application range in nucleotide analysis (Buziol et al., 2002; Cai et al., 2002; Carlucci et al., 1992; Cohen et al., 2010; Cordell et al., 2008; Gayden et al., 1991; Naydenova et al., 2008). The addition of cationic reagents such as alkylamines leads to formation of adducts between negatively-charged nucleotides and positively-charged ion pair reagent, increasing the retention factors for these compounds and thus improving retention. In addition to this *classical ion-pairing* model, which describes ion formation solely as a mobile phase phenomenon, an alternate *dynamic ion-exchange* model has been proposed (Kissinger, 1977) utilizing stationary phase modification processes. Here, modification of the stationary phase is attributed to active adsorption of the ion-pairing reagent to the stationary phase, in turn modifying its surface charge and providing ion-exchange sites for analyte ions (Hoffman and Liao, 1977). The extent to which these two alternate mechanisms are contributing to analyte retention has been shown to depend on experimental conditions (Bidlingmeyer et al., 1979).

Although HPLC/UV systems have been successfully applied (de Abreu et al., 1982; Gill and Indyk, 2007; Werner et al., 1989), the increasing need for higher sensitivity and improved selectivity has prompted the use of LC-MS approaches in this field.

High salt conditions required for strong anion-exchange chromatography (SAX) and the non-volatile nature of ion-pairing reagents such as tetraalkylamines and ammonium phosphates, are not readily compatible with LC-MS detection systems (Luo et al., 2007; Seifar et al., 2009). Thus, new alternative separation methods have been developed including HPLC coupled to electrochemical detection (Deng et al., 2003) or CE-MS (Auriola et al., 1997).

Nevertheless, LC-MS remains the method of choice for quantification of nucleotides in complex biological matrices. Since even low concentrations of non-volatile ion-pairing reagents such as trialkylamines and dialkylamines lead to a contamination of the ion source (Witters et al., 1997), careful choice of the ion-pairing reagent is crucial for hyphenation ion pair separations to MS (Cordell et al., 2008). Considerable efforts have been made to improve the compatibility of ion-pairing reagents for LC-MS over the recent years, usually based on volatile ion-pair reagents. This led to simplified routines with significantly reduced operator intervention. Even though reduced ion-pair concentrations have been

reported by several groups (Cordell et al., 2008; Crauste et al., 2009; Klawitter et al., 2007; Yamaoka et al., 2010), developing a method for quantitative determination of nucleotides, nucleosides and nucleobases from complex biological samples without any ion-pairing reagent has, to our knowledge, not been reported yet.

The aim of the present study therefore was the development of a LC-MS method for *targeted metabolite profiling* of the purine biosynthesis pathway in bacteria, without the need for any ion-pairing reagents in the mobile phase. The assay allowed the quantitative determination of 12 intermediates of this pathway in complex biological samples in less than 15 min run time.

Materials and methods

Chemicals and reagents

99% ^{13}C enriched [U-^{13}C$_6$] glucose was purchased from Cambridge Isotope Laboratories (Andover, Mass., USA). Ultrapure water was obtained from a Milli-Q purifier (Millipore, Eschborn, Germany) and HPLC-grade acetonitrile was purchased from Sigma-Aldrich (Taufkirchen, Germany). All other chemicals and reagents of analytical grade were obtained from Sigma-Aldrich (Taufkirchen, Germany).

Standard mixtures, quality control (QC) and biological samples

Standard mixtures and QC samples

Standards were prepared for guanosine 5'-monophosphate (GMP), adenosine 5'-monophosphate (AMP), inosine 5'-monophosphate (IMP), xanthosine 5'-monophosphate (XMP), adenosine, guanosine, inosine, xanthosine, adenine, guanine, hypoxanthine and xanthine in ultrapure water (1 mM each). Subsequently all compounds were mixed and diluted with perchloric acid (PCA, final concentration 500 mM) to give a final concentration of 100 μM of each compound. A series of working standard solutions for external calibration and a set of quality control (QC) samples were prepared by adding increasing amounts of the standard mixture to the ^{13}C-labeled cell extract reaching concentration ranges from 0.001 μM to 5 μM.

Biological samples

Wild type strain *Corynebacterium glutamicum* (ATCC 13032) and *Corynebacterium ammoniagenes* (DSM 20306) were purchased from the American Type Culture Collection (Manassas, VA, USA) and the Deutsche Sammlung von Mikroorganismen und Zellkulturen (Braunschweig, Germany).

Precultures and main cultures were performed using an orbital shaker (Multitron 2, Infors AG, Bottmingen, Switzerland) at 230 rpm and 30°C on minimal medium (pH 7.2) containing (per liter): 15 g glucose, 4 g KH_2PO_4, 16 g Na_2HPO_4, 500 mg $MgCl_2 \cdot 6 H_2O$, 300 mg 3,4-dihydroxybenzoic acid, 100 mg $CaCl_2 \cdot 2 H_2O$, 100 μg cyanocobalamin, 750 μg thiamine, 4 μg pyridoxal phosphate, 100 μg biotin, 400 μg calcium pantothenate, 2 μg folic acid, 400 μg nicotinic acid, 200 μg 4-aminobenzoic acid, 400 μg pyridoxine · HCl, 2 mg inositol, 10 mg $FeCl_2 \cdot 4 H_2O$, 1 mg $ZnCl_2$, 100 μg $CuCl_2$, 20 μg $NiCl_2 \cdot 6 H_2O$, 20 μg $Na_2MoO_4 \cdot 2 H_2O$, 500 μg boric acid, 100 μg KI, 100 μg $CoCl_2 \cdot 6 H_2O$, 10 mg $MnCl_2 \cdot 4 H_2O$. Cultures of *C. ammoniagenes* DSM 20306 were supplied additionally with 300 mg L^{-1} methionine. *C. glutamicum* and *C. ammoniagenes* main cultures were inoculated from overnight precultures with initial optical densities of 0.5 and 0.8, respectively (660 nm, Novospec II, Parmacia Biotech, Uppsala, Sweden). Cultivations were carried out in 500 mL baffled shake flasks using 10% liquid volume.

Cells were grown until an optical density of 6.5 and 11.8 for *C. glutamicum*, and 4.0 and 8.0 for *C. ammoniagenes*. During this period cells grew exponentially under balanced growth conditions (Provost and Bastin, 2004) and concentrations of internal metabolites were expected to be constant assuming a quasi-steady-state.

^{13}C-labeled biomass extract

Wild type *C. glutamicum* ATCC 13032 precultures were performed under the same conditions as mentioned above, except using [U-$^{13}C_6$] glucose. Cells were grown on [U-$^{13}C_6$] glucose to an optical density of 4.0 and used as inoculum for the main culture. Main cultivations were carried out in a 500 mL stirred tank bioreactor (Meredos, Bovenden, Germany) containing 75 mL minimal medium and [U-$^{13}C_6$] glucose at 30°C and 1,000 rpm maintaining dissolved oxygen concentrations above 60% air duration throughout the cultivation. The gas flow was controlled at 1 vvm (vessel volume per minute) (WMR Compact4, Brooks Instruments, Veenedaal, Netherlands) using a nitrogen/oxygen gas mixture to avoid CO_2 derived ^{12}C incorporation into biomass. Temperature, pH and agitation were collected using the Lucullus process control system (Lucullus PIMS 2.1, Biospectra, Schlieren, Switzerland). Cells were cultivated until mid-exponential growth phase (OD_{660nm} 6.7).

Sample preparation and extraction procedure

Extraction was performed by mixing preheated PCA (55°C, final concentration 500 mM) with the sample followed by incubation at 55°C. Exact sample volumes were determined gravimetrically. Sampling setups and incubation times varied according to validation parameters and nature of samples.

Stability of standard compounds under extraction conditions

1 mL standard mixture containing all 12 compounds (initial concentration 3 µM each) was mixed with 1 mL preheated extraction solution (1 M PCA). Incubation at 55°C was carried out for 3, 5, 10 and 30 min, followed by incubation on ice (10 min). Supernatants were obtained by centrifugation (10 min, 4°C, 6,000 g), and stored at -20°C until further analysis.

Extraction of biological samples

Biological samples for metabolite profiling were taken at balanced growth during the mid-exponential growth phase. To ensure instantaneous mixing 2 mL sample were drawn into a syringe filled with 2 mL preheated extraction solution. Generated turbulence guaranteed instantaneous mixing of sample and extraction solution as verified by colored test solutions (phenolphthalein). Incubation at 55°C (3 min) was followed by 10 min incubation on ice. Cell debris and insoluble macromolecules were precipitated by centrifugation (10 min, 4°C, 6,000 g). Prior to the LC-ESI-MS/MS analysis, the naturally labeled cell extracts of *C. glutamicum* and *C. ammoniagenes* were mixed with uniformly ^{13}C-labeled cell extract of *C. glutamicum* treated under the same conditions (see *"^{13}C-labeled biomass extract – Materials and Methods"*). As a result, the ^{13}C-labeled cell extract served a dual function: firstly, by acting as internal standard (IS) providing isotope standard analytes (Wu et al., 2005) at relevant concentration levels, *i.e.* at levels of the analytes to be determined. The IS corrects for influences of precipitation and degradation on metabolite levels during extraction as well as for variabilities during LC-MS injection. Secondly, addition of labeled cell extract provided a suitable biological matrix with identical properties to the

samples to be analyzed, while still allowing discrimination between the added analytes and those naturally present due to isotopic *m/z* differences. As a result, ^{13}C-labeled cell extract was chosen as internal standard and was mixed with standard and sample solutions in all experiments, except when the biological matrix was interrogated for matrix effects (see below).

To prevent matrix effects during extraction stability studies, no cell extract was added to the samples.

LC-MS/MS conditions

Liquid chromatography

Chromatographic separation was carried out using a Phenomenex (Torrance, CA, USA) Kinetex reversed-phase PFP core-shell column (2.6 µm pore size, 100 Å particle size, 100 x 2.1 mm). All separations were performed at 25°C with a constant flow rate of 200 µL min^{-1} using a Shimadzu (Duisburg, Germany) UFLC Prominence system. The autosampler (SIL20AC) temperature was set to 4°C. Separation of single purine intermediates was performed isocratically as proposed by Nichthauser and Stepnowski (2009) using 0.1% formic acid in water (eluent A). Solely elution of xanthosine required an organic mobile phase (0.1% formic acid in acetonitrile) of the following elution profile: after an initial isocratic step at 0% B for 5.5 min, B was increased to 30% within 10 min, followed by a flushing step at 100% B for a further 5 min. The column was reconditioned at 0% B (initial concentration) for 5 min. The standard injection volume was 1 µL, but was increased to 10 µL in some experiments when needed.

Mass spectrometry

LC-MS/MS analysis was carried out on a API5500 QTRAP quadrupole linear ion trap (AB Sciex, Concord, Ontario, Canada) equipped with a Turbo-V electrospray ionization source. Nitrogen was used as curtain (20 psi), nebulizer (GS1; 60 psi) and auxiliary gas (GS2; 60 psi). The ESI voltage was set to 5500 V and a source temperature of 200°C was used.

Multiple reaction monitoring (MRM) was performed in positive mode with the following parameters: collision gas (nitrogen), medium; dwell time, 250 ms. The declustering potentials (DP) and collision energies (CE) were optimized for each MRM transition by direct injection of 5 µM standard solution in ACN/water (50/50, v/v) using a syringe pump at a constant flow rate of 10 µL min^{-1} for each metabolite.

Data analysis/ quantitative analysis

Calibration curves were created by plotting the peak area ratios of analytes and IS, *i.e.* the biological ^{13}C-labeled cell extract, (area$_{compound}$/area$_{internal\ standard}$) against the nominal concentration of each analyte (µM) in the cell extract and assessed by linear least square regression analysis. Analyte concentrations in unknown samples were interpolated using the calculated calibration curves.

Validation procedure

The impact of extraction was validated for metabolite stability and recovery using standard solutions. In this procedure, the values of standard concentrations were compared with experimentally determined concentrations after the extraction. Time-dependent stability of metabolites was assessed at different incubation times at 55°C (3, 5, 10, 30 min). In addition, the impact of varying freeze-thaw cycles on compound stability was assessed. In these experiments, up to 10 freeze-thaw cycles of standard solutions mixed with ^{13}C-labeled cell extract to mimic the presence of biological matrix were performed and resulting degradation determined.

The validation procedure for MS quantification included linearity, accuracy, precision, lower limit of quantification (LLOQ) and influence of matrix effects.

For all MS validation procedures, standard solutions at a concentration range between 1 nM to 5 µM were spiked with biological matrix (^{13}C-labeled cell extract). Precision and lower limits of quantification were calculated by determining coefficients of variation

(CV %) of standard deviation and measured concentrations of spiked QC samples. Accuracy was assessed by comparing the determined concentrations of the spiked QC samples with calculated values obtained from standard calibration curves. In this study, LLOQ was defined as the lowest concentration for which precision values of 15% or better and an accuracy bias of 20% or better were observed. All calibrations were performed in the presence of a biological matrix. To investigate long term reproducibility, analysis of precision and accuracy was performed over a period of 4 weeks.

Matrix effects were determined by a post-extraction addition approach (Taylor, 2005). Peak areas from extracted standards *spiked* post-extraction with an extracted biological sample (^{13}C-labeled) were compared to extracted standards *spiked* with diluted extraction solution (1:1 dilution in water, v/v). Comparison was carried out for all compounds at two different concentration levels, similar to observed concentration levels in biological samples analyzed in this study.

Results and discussion

The present work describes the development of an assay aimed at the quantitation of 12 important metabolites from the purine biosynthesis pathway of bacteria, namely 5'-nucleoside monophosphates as well as their corresponding nucleosides and nucleobases.

Although several reports have investigated quantification of nucleotides and nucleosides in mammalian cells, tissues or fluids (Carlucci et al., 1992; Giannattasio et al., 2003; Gill and Indyk, 2007; Naydenova et al., 2008; Traut, 1994; Werner et al., 1989), this is, to the best of our knowledge, the first assay combining an extraction procedure for Gram-positive bacteria with simultaneous quantification of compounds from all three compound classes, including IMP, its nucleoside and nucleobase. Turnover rates for intracellular metabolites are reported to be within milliseconds (Moritz et al., 2000) and pool sizes are considerably small (Wittmann et al., 2004c). Therefore, the first essential step was the quenching of cellular metabolism maintaining actual *in vivo* concentrations and thereby yielding a representative metabolic snapshot of the current growth phase of the organism.

Validation of the extraction method

Metabolic freeze-frame by acidic extraction

Since *Corynebacterium glutamicum* belongs to bacteria affected by the unspecific cold shock phenomenon (Wittmann et al., 2004c), quenching using cold methanol or other low temperature-based quenching methods should not be applied for absolute quantification of intracellular metabolite pool sizes. We have therefore developed a one-step quenching/extraction method for quantitative metabolite extraction suited to the subsequent LC-ESI-MS/MS analysis.

In this procedure, it was important to assess the acidic extraction method for intermediates with respect to their stability and recovery after incubation at 55°C. Results clearly indicate that temperature or acid-dependent decomposition was not observed except for XMP,

xanthosine and xanthine (Table III-1). Recoveries for AMP, GMP, IMP, adenosine, guanosine, inosine, adenine, guanine and hypoxanthine were > 90%. Only intermediates of the xanthine family (XMP, xanthosine and xanthine) exhibited time-dependent decomposition of up to 50% (Table III-1) in 30 min.

Table III-1. Extraction recoveries and stabilities of standard solutions[a].

compound	extraction times			
	3 min	5 min	10 min	30 min
AMP	99.5 ± 1.7	100.3 ± 2.3	98.3 ± 0.9	99.0 ± 1.6
adenosine	100.5 ± 2.6	93.2 ± 2.1	93.3 ± 3.2	94.1 ± 1.2
adenine	101.4 ± 4.6	101.6 ± 2.2	101.3 ± 3.1	102.1 ± 0.9
GMP	115.5 ± 6.3	110.0 ± 3.2	112.3 ± 1.2	120.3 ± 4.3
guanosine	102.1 ± 2.7	105.4 ± 2.7	104.9 ± 0.4	101.8 ± 1.1
guanine	95.0 ± 2.2	94.7 ± 2.1	93.4 ± 3.8	95.5 ± 4.8
IMP	103.2 ± 2.3	100.8 ± 1.1	103.4 ± 0.7	103.3 ± 2.3
inosine	108.3 ± 0.9	102.1 ± 3.1	104.1 ± 2.1	111.3 ± 1.8
hypoxanthine	105.9 ± 3.9	98.1 ± 8.6	96.6 ± 1.2	90.3 ± 2.3
XMP	93.8 ± 2.1	90.2 ± 2.5	82.8 ± 1.5	60.8 ± 1.0
xanthosine	89.7 ± 1.1	82.8 ± 2.1	69.5 ± 0.8	46.3 ± 2.3
xanthine	92.6 ± 1.6	94.9 ± 2.9	92.2 ± 5.3	81.1 ± 2.8

[a] standard concentrations were 3 µM each. Results from n = 3 for each compound.

The degradation of the xanthine family intermediates was therefore studied in greater detail, to assess the impact on the determination of the other compounds. Fortunately, no negative effects were observed.

Unspecific metabolite leakage and secretion during the cultivation were also investigated for the purine intermediates studied in this work. Sole intracellular localization of the quantified metabolites is a prerequisite for application of a whole culture quenching procedure as performed in this work and neglecting this fact may otherwise result in significant errors. Therefore, medium supernatants were analyzed at different time points throughout the entire cultivation process. However, no detectable amounts were observed for the minimal medium used for cultivation. Thus, the described extraction procedure was well suited for the extraction and quantitation of *in vivo* free intracellular concentrations of the metabolites analyzed in this work. Importantly, unspecific leakages or secretions have to be considered when medium compositions are changed or different organisms are analyzed.

Application of PCA as quenching/extraction solution resulted in precipitation of cell debris and insoluble macromolecules. The obtained sample solution was of sufficient purity for direct LC-ESI-MS/MS analysis. However, extraction with PCA has to be validated for each substance due to varying chemical stabilities. Thus, PCA extraction is only suitable for analytes stable during acidic extraction.

To assess the extent of degradation of the individual purine intermediates caused by multiple freeze-thaw cycles, up to 10 freeze-thaw cycles using a standard solution were consistently performed on ice (concentrations: 1 µM each in PCA as described in *"Materials and Methods"*). The recovery rate (as percentage normalized to the relative initial concentrations) was then determined. As matrix effects from the complex biological samples might interfere with stability properties, the standard solution was mixed with IS (*i.e.* the ^{13}C-labeled cell extract, 1/1; v/v).

As is clearly seen in Table III-2, the freeze-thaw procedure was found to trigger a significant reduction in the concentration levels, particularly for AMP, GMP, IMP and XMP. The recovery rates for AMP were found to exhibit the greatest loss at 12% after 10 cycles, while even after 2 cycles a significant reduction was determined.

Table III-2. Recovery for standard solutions (1µM each) after freeze-thaw-cycles[a].

compound	freeze-thaw-cycles					
	0	1	2	3	5	10
AMP	102.1 ± 2.3	105.0 ± 3.0	94.0 ± 1.8	90.6 ± 1.0	89.2 ± 0.8	87.7 ± 0.5
adenosine	100.2 ± 0.6	100.6 ± 0.1	101.6 ± 0.1	102.1 ± 0.1	101.6 ± 0.2	103.0 ± 0.4
adenine	98.9 ± 1.3	100.0 ± 0.7	99.2 ± 0.8	99.5 ± 0.2	99.9 ± 0.2	98.5 ± 0.3
GMP	99.8 ± 0.7	98.2 ± 0.3	92.0 ± 0.3	92.0 ± 0.2	92.2 ± 0.5	93.8 ± 0.5
guanosine	98.6 ± 2.0	98.1 ± 3.6	104.7 ± 2.1	104.1 ± 1.1	99.6 ± 0.1	101.7 ± 0.6
guanine	103.1 ± 2.3	99.7 ± 1.5	101.4 ± 0.7	100.7 ± 0.1	101.0 ± 0.3	101.2 ± 0.2
IMP	99.7 ± 0.6	98.9 ± 0.1	96.7 ± 0.2	96.4 ± 0.7	95.2 ± 0.2	96.5 ± 0.2
inosine	99.6 ± 3.8	103.0 ± 2.8	101.9 ± 0.9	105.1 ± 2.5	94.2 ± 2.8	99.0 ± 0.3
hypoxanthine	98.9 ± 1.9	101.2 ± 2.0	97.8 ± 0.5	98.3 ± 0.1	98.7 ± 0.2	98.4 ± 0.9
XMP	100.3 ± 0.1	98.0 ± 0.6	98.6 ± 0.7	96.9 ± 1.3	95.8 ± 3.9	96.1 ± 0.6
xanthosine	101.9 ± 1.8	100.4 ± 1.5	101.3 ± 0.3	100.6 ± 0.2	98.3 ± 0.9	99.8 ± 1.9
xanthine	98.8 ± 2.2	101.7 ± 2.5	101.5 ± 0.1	100.5 ± 0.8	100.0 ± 0.4	99.5 ± 0.4

[a] results derived from n = 3 and determined in the presence of a biological matrix.

The susceptibility of the individual analytes to degradation was determined to be highly variable, as neither nucleosides nor nucleobases showed any freeze-thaw-related degradation (Table III-2). An extended extraction procedure at 55°C (Table III-1) for 30 min, however, yielded increased degradation mainly of xanthine, xanthosine and XMP. Therefore, to obtain reproducible and quantitative results, unnecessary freeze-thaw cycles should be avoided, and extreme care should be taken in terms of unnecessary extraction cycles.

Validation of the LC-ESI-MS/MS method

Separation and MS-MS optimization

Several studies have attempted the simultaneous quantification of nucleosides and nucleotides (Cordell et al., 2008; Czarnecka et al., 2005; Meyer and Wagner, 1985; Werner et al., 1989; Yamaoka et al., 2010). No method for all purine nucleoside monophosphates, nucleosides and nucleobases without the necessity for ion-pairing reagents, however, has yet been reported in the literature.

The MRM chromatograms for the 12 purine intermediates are shown in Figure III-1, which demonstrates the simultaneous analysis by LC-ESI-MS/MS.
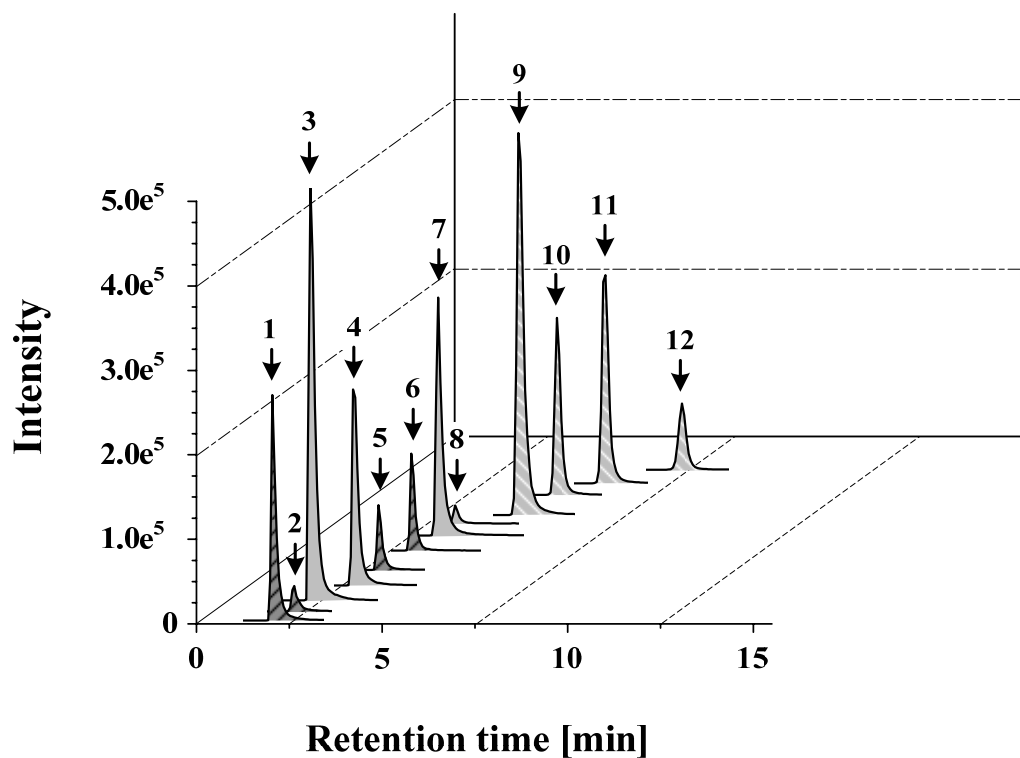
Figure III-1. MRM chromatograms for the 12 investigated purine intermediates. 1 = guanine, 2 = adenine, 3 = AMP, 4 = GMP, 5 = hypoxanthine, 6 = xanthine, 7 = IMP, 8 = XMP, 9 = adenosine, 10 = inosine, 11 = guanosine, 12 = xanthosine.

To describe active adsorption processes and retention effects for the different analytes, retention factors (*k*), were calculated ($k = (t_a-t_0)/t_0$). The net analyte retentions (t_a) were corrected using the void volume ($t_0 = 0.95$) of the column and *k* values were determined as shown in Table III-3.

Table III-3. Retention factors (k) of the purine analytes.

compound	k
AMP	1.6
adenosine	4.0
adenine	1.4
GMP	2.0
guanosine	5.1
guanine	1.3
IMP	2.6
inosine	4.2
hypoxanthine	2.3
XMP	2.7
xanthosine	6.6
xanthine	2.4

These values were found to be the lowest for guanine (1.3), adenine (1.4) and AMP (1.6), whereas all other analytes exhibited retention factors $k > 2.0$, indicating active adsorption by the stationary phase.

Fragmentation of protonated molecules of the investigated nucleotides and nucleosides by *collision-induced dissociation* (CID) resulted in the highly-specific protonated nucleobase as major product ions, allowing selection of specific product ions for quantitation by MRM (Table III-4). The CID spectra, fragmentation patterns as well as specific product ions for quantification of IMP, inosine and hypoxanthine are shown in Figure III-2 as illustrative examples.

Table III-4. MRM transitions and settings for LC-ESI-MS/MS[a].

ID	monoisotopic mass (amu)	Q1 (amu)	Q3 (amu)	DP	CE
adenine	135.0545	136	119	234	42
adenosine	267.0968	268	136	16	25
AMP	347.0631	348	136	72	25
GMP	363.0580	364	152	26	19
guanine	151.0494	152	135	18	27
guanosine	283.0917	284	152	42	17
hypoxanthine	136.0385	137	110	147	29
IMP	348.0471	349	137	64	19
inosine	268.0808	269	137	42	32
xanthine	152.0334	153	136	50	21
xanthosine	284.0757	285	153	32	19
XMP	364.0420	365	153	21	23

[a] for each compound the following parameters are indicated: compound name (ID), monoisotopic mass, selected ions on quadrupoles Q1 and Q3 (Q1 mass and Q3 mass, respectively), declustering potential [V] (DP), collision energy [V] (CE).
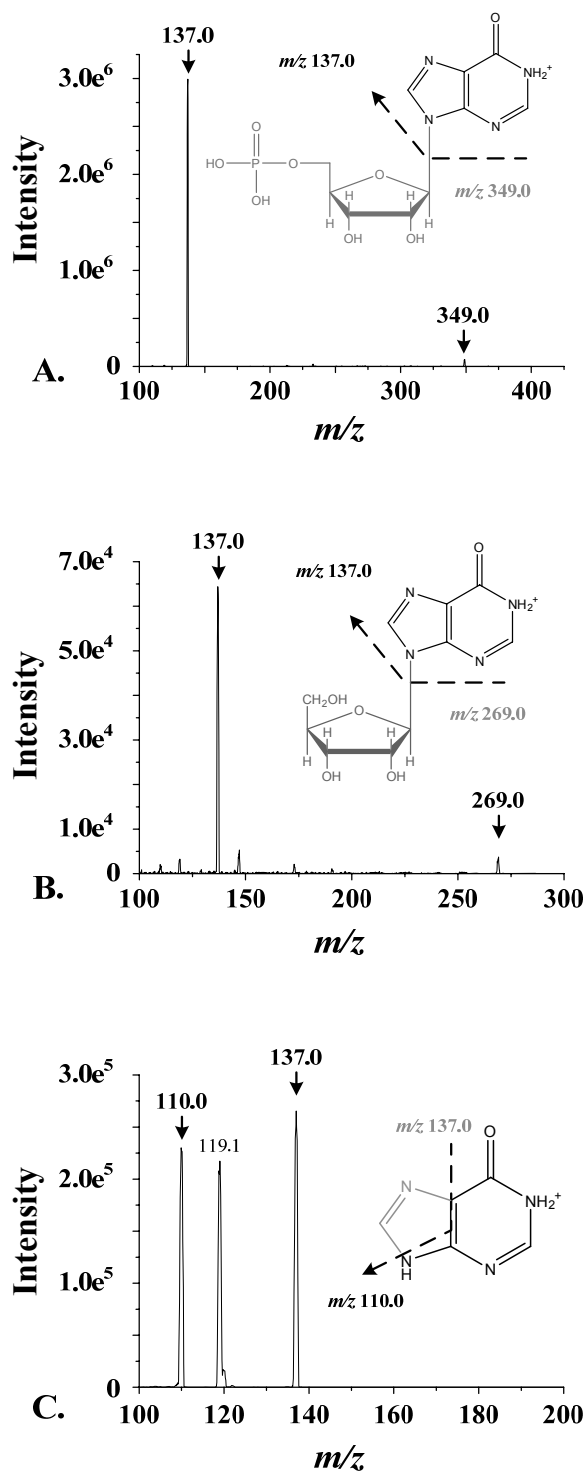
Figure III-2. CID spectra, fragmentation patterns and product ions of the [M+H]⁺ ions of IMP
(**A.**), inosine (**B.**) and hypoxanthine (**C.**). Chemical structures shown in gray represent the parent
ions, and chemical structures shown in black the corresponding product ions.

Linearity, sensitivity and long term reproducibility

Calibration curves were obtained from a series of working standard solutions over a wide concentration range, using ^{13}C-labeled cell extract as internal standards (IS). To ensure thorough incorporation of ^{13}C-labeled carbon (derived from the sole carbon source [U-$^{13}C_6$] glucose) into cellular components and intermediates, the mass isotopomer distributions of the nucleotide IMP were determined (Figure III-3).
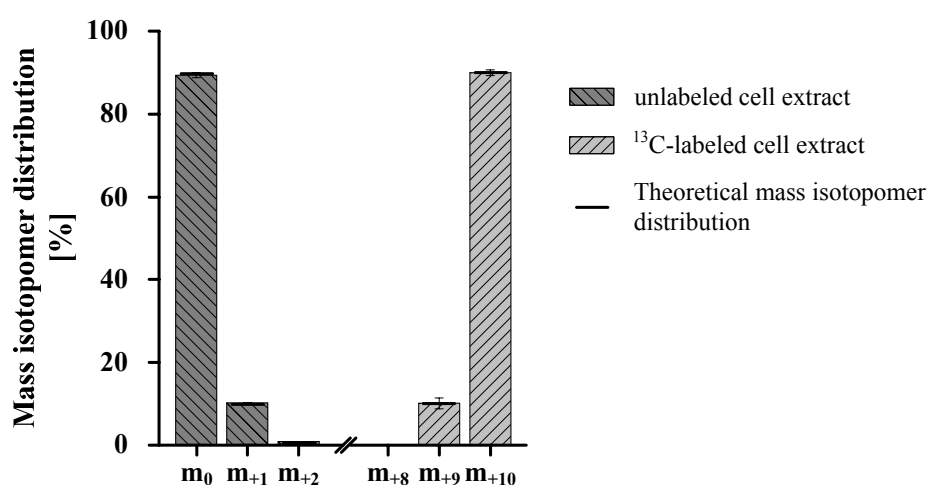
Figure III-3. Mass isotopomer distributions of the intracellular purine metabolite IMP, unlabeled (extracted from unlabeled cell extract) and uniformly labeled (extracted from ^{13}C-labeled cell extract). The theoretical distributions were corrected for the natural abundance of ^{13}C with 1.1% (unlabeled cell extract) and for the 99% enrichment of [U-$^{13}C_6$] glucose (labeled cell extract).

The ^{13}C-labeled cell extract was shown to exhibit the uniformly labeled isotopomer at 90%, whereas the remaining 10% comprised incorporation of 1 molecule of ^{12}C carbon (m_{+9}) due to the 99% enrichment of [U-$^{13}C_6$] glucose. The non-labeled cell extract was found to exhibit the natural distribution of the corresponding isotopes from the natural presence of ^{13}C (1.1% (Boehlke et al., 2005)) (Figure III-3). In addition to utilizing glucose as carbon source, the purine biosynthesis comprises incorporation of 1 molecule of CO_2 from hydrogencarbonate. Thus, to preclude any ^{12}C assimilation, carbon dioxide free synthetic air was used. This was validated by mass spectrometric analysis of the CO_2

released during the whole fermentation process. This released CO_2 was found to consist exclusively of $^{13}CO_2$. Therefore, the mass isotopomer distribution, as exemplarily determined for IMP, did not posses any detectable amounts of naturally-occurring mass isotopomers (*i.e.* m_0, m_{+1} and m_{+2}). This allowed non-interfered analyte quantitation using ^{13}C-labeled cell extract as internal standard. Peak area ratios of each analyte relative to the IS, *i.e.* the biological matrix, were plotted against the standard concentrations and linear regression was applied. The correlation coefficients (r^2) were consistently >0.99 for concentration levels >0.001 µM for GMP and IMP and 0.0075 µM for AMP, adenosine, inosine and guanosine. The highest LLOQ of 0.015 µM were observed for XMP, xanthosine, adenine, hypoxanthine, guanine and xanthine. Applying QC samples at the lower limit of quantification (LLOQ), precision was always better than 15% and accuracy deviated less than 20% (Table III-5) for all analytes.

Table III-5. Lower limits of quantification (LLOQ), accuracy and precision of QC samples[a].

compound	LLOQ mean [nM]	accuracy [%]	precision [CV %]
AMP	9.4	106.0	13.7
adenosine	8.2	108.5	13.6
adenine	16.1	97.2	10.0
GMP	0.8	103.8	13.2
guanosine	7.2	109.3	12.4
guanine	17.5	101.8	7.9
IMP	0.8	107.4	7.6
inosine	7.0	99.4	6.2
hypoxanthine	15.2	90.6	7.3
XMP	18.8	94.8	5.9
xanthosine	16.1	93.0	5.1
xanthine	19.0	98.3	10.9

[a] LLOQ corresponds to lower limits of quantification; acceptance criteria for LLOQs were 15 CV % or better for precision and a bias of 20% or better for accuracy. Results derived from n = 4 and determined in the presence of a biological matrix.

This was also true for all concentrations above LLOQ. To accurately quantify *in vivo* concentrations in biological samples, all validation steps, including linearity, precision and accuracy, were performed in the presence of a biological matrix. Standard working solutions containing ^{13}C-labeled cell extract were used for the calibration, which allowed for compensation of matrix effects. Matrix effects, which are specified as any interference of ionization efficiency caused by co-eluting substances (Taylor, 2005), usually result in a signal attenuation. To analyze the influence of possible matrix effects on the 12 analytes, a post-extraction-addition experiment was performed and the recovery for all analytes was determined. The resulting recoveries are summarized in Table III-4 and did not show any significant matrix effects for all analytes. This recovery study not only evaluated possible matrix effects, it also illustrated quantitative determination of purine intermediate pool concentrations in *Corynebacteria*, since the concentration range (Table III-6) covered the observed biological concentration levels (Table III-7) except for guanosine.

Table III-6. Recovery for standard solutions[a].

compound	conc [µM]	recovery [%]
AMP	3.1	102.0 ± 3.5
	0.2	102.1 ± 5.1
adenosine	2.7	102.8 ± 4.7
	0.1	106.7 ± 3.9
adenine	2.2	105.0 ± 1.1
	0.1	101.7 ± 6.6
GMP	2.7	98.1 ± 6.9
	0.1	95.1 ± 2.5
guanosine	2.4	104.0 ± 1.1
	0.1	105.7 ± 1.8
guanine	2.4	100.1 ± 4.1
	0.1	103.6 ± 3.3
IMP	2.9	99.8 ± 1.7
	0.1	97.9 ± 0.4
inosine	2.3	101.8 ± 1.7
	0.1	104.4 ± 0.2
hypoxanthine	2.1	99.0 ± 3.7
	0.1	92.3 ± 4.6
XMP	2.6	100.2 ± 1.5
	0.1	98.8 ± 0.1
xanthosine	2.2	96.7 ± 0.5
	0.1	99.6 ± 1.3
xanthine	2.6	101.0 ± 2.0
	0.1	98.8 ± 2.4

[a] determined recoveries for standard solutions in two different concentrations in order to estimate matrix effects.

To ensure accurate and precise quantitation of guanosine and other low level analytes or of those exhibiting lower detection sensitivities, the injection volume was adapted accordingly (see *"LC-MS/MS conditions - Materials and Methods"*).

All compounds exhibited a linear dynamic range of at least two orders of magnitude, which was considered sufficient for quantitation in this study.

Application to pathway analysis

Samples from two Gram-positive *Corynebacterium* species, *C. glutamicum* and *C. ammoniagenes*, were extracted and quantitation of intracellular purine pools was performed. *Multiple reaction monitoring* (MRM) chromatograms of purine biosynthetic pathway intermediates in biological samples are shown in Figure III-4. The corresponding concentration levels for detected nucleotides, nucleosides and nucleobases normalized to the cell volume (Gutmann et al., 1992) are summarized in Table III-7.
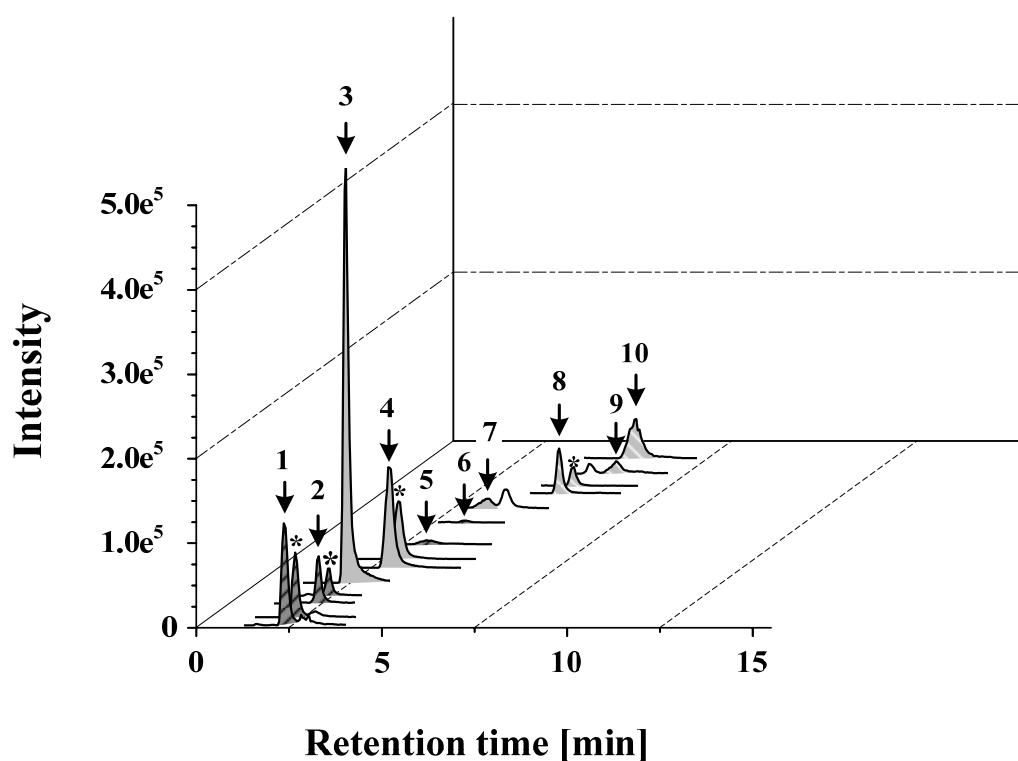
Figure III-4. MRM chromatogram of a *C. glutamicum* extract. 1 = guanine, 2 = adenine, 3 = AMP, 4 = GMP, 5 = hypoxanthine, 6 = xanthine, 7 = IMP, 8 = adenosine, 9 = inosine and 10 = guanosine. Isotope peaks (exemplary for 1, 2, 4 and 8) are marked with an asterisk.

Table III-7. Concentrations of purine intermediates (μmol mL$^{-1}_{cell\ volume}$) in *Corynebacterium glutamicum* and *Corynebacterium ammoniagenes*[a].

compound	*C. glutamicum*				*C. ammoniagenes*			
				[b.]				[b.]
AMP	4.09	±	0.20	(4.33)	1.19	±	0.12	(1.41)
GMP	1.35	±	0.08	(1.40)	0.15	±	0.01	(0.20)
IMP	0.23	±	0.02	(0.26)	0.06	±	0.00	(0.08)
XMP	[c.]				[c.]			
adenosine	0.05	±	0.00	(0.06)	0.17	±	0.01	(0.20)
guanosine	0.02	±	0.00	(0.02)	[c.]			
inosine	0.05	±	0.00	(0.07)	[c.]			
xanthosine	[c.]				[c.]			
adenine	1.47	±	0.08	(1.40)	0.78	±	0.05	(1.05)
guanine	1.67	±	0.11	(1.74)	1.16	±	0.05	(1.50)
hypoxanthine	0.13	±	0.01	(0.15)	0.07	±	0.01	(0.09)
xanthine	0.06	±	0.00	(0.06)	0.05	±	0.00	(0.06)

[a] concentrations and corresponding standard deviations were determined using 4 biological and 2 technical replicates for each compound and standardized to the cell volume (Gutmann et al., 1992).

[b] concentrations in μM from LC-MS quantitation, not related to biomass.

[c] below detection limit.

Concentrations in μM, obtained from LC-MS quantitations are additionally provided, to allow evaluation of an adequate and suitable concentration range. For *C. glutamicum,* all compounds except for XMP and xanthosine (which were below the detection limit) were quantified with precision values of less than 12%. AMP and GMP, central building blocks for DNA and RNA and co-substrates for activation of metabolites, exhibited the highest intracellular nucleotide concentrations of 4.1 μmol mL^{-1} and 1.3 μmol mL^{-1}, respectively. Other purine pathway intermediates showed a broad range of concentration levels varying between 0.02 μmol mL^{-1} and 1.7 μmol mL^{-1}. However, nucleosides exhibited the lowest levels of all analyzed metabolites at 0.02 μmol mL^{-1}. The observed concentrations for all quantified analytes were 1 to 3 orders of magnitude above the determined quantification limits, indicating that the investigated sample volumes could be further reduced if required.

Analysis of *C. ammoniagenes* revealed the same distribution pattern of intracellular concentrations of purine pathway intermediates, however, all quantified compounds (except for adenosine) exhibited significantly reduced intracellular concentration levels compared to *C. glutamicum*. Furthermore, no free intracellular nucleosides were detected, except for adenosine. The relatively decreased intracellular purine concentration levels detected in *C. ammoniagenes* could indicate differing regulatory mechanism of these species, eventually favoring reduced intracellular concentrations in *C. ammoniagenes*. This might be linked to the increased capability of *C. ammoniagenes* for nucleotide and nucleoside secretion (Furuya et al., 1968), resulting in decreased intracellular concentrations. This organism, which is characterized by its potential for extracellular purine accumulation, has been exploited for large-scale production of diverse compounds, *i.e.* IMP, GMP, XMP and inosine (Auriola et al., 1997), whereas *Corynebacterium glutamicum*, an outstanding model organism in the field of systems biotechnology and producer of various substances such as amino acids, polymers or biofuels (Becker and Wittmann, 2012) only possesses poor nucleotide secretion capabilities (Demain et al., 1965; Demain et al., 1966). A further deduction of the information based on the inter-species variations, however, has to be performed carefully, as the resulting pool sizes do not allow any interpretation of the participating enzymes; the alteration of intracellular metabolite pool sizes cannot directly be linked to varying enzyme activities and can only provide indications of differing underlying mechanisms.

Additional investigation of extended extraction at 55°C times up to 15 min did not result in increased metabolite concentrations (data not shown), indicating that a temperature of 55°C in combination with an incubation time of 3 min was sufficient for complete metabolite extraction. Incubating for more than 3 min caused degradation of analytes belonging to the xanthine family and should therefore be avoided.

Conclusions

In this study, a LC-ESI-MS/MS approach in conjunction with a single-step extraction procedure was developed and validated for quantitation of 12 major purine biosynthetic pathway intermediates from biological samples. Chromatographic separation of polar nucleotides and non-polar nucleosides and nucleobases was achieved in less than 15 min using reversed-phase HPLC-MS without using any ion-pairing reagents. The method exhibited excellent selectivity, precision and accuracy in the presence of a biological matrix. As no ion-pairing reagents were used, the method was much more rugged than existing methodologies and required significantly less instrument maintenance and operator intervention. Other advantages over previous methods include the simplified extraction procedure, the straightforward quantitation routine and the exclusive use of inexpensive reagents, making this approach particular suitable for high throughput, multi-user laboratories. Even though addition of ion-pairing reagents might sometimes have a positive effect on retention performance, in particular for phosphorylated compounds, the separations achieved in this work were found to fully meet the requirements in this study, without the need for troublesome ion-pairing reagents.

Acknowledgments

Chapter IV

Let's take a look inside

Metabolic engineering of the purine biosynthetic pathway in

Corynebacterium glutamicum results in increased

intracellular pool sizes of IMP and hypoxanthine

Abstract*

An in-depth analysis of the purine biosynthetic pathway was performed in *Corynebacterium glutamicum* in order to study the influence of directed rational strain design on intracellular IMP accumulation. The metabolic engineering strategy applied in this work focused on reducing metabolizing reactions towards AMP and GMP, feedback-deregulation of the purine biosynthetic pathway itself and an enhanced precursor supply of ribose 5-phosphate. Blocking of the degrading reactions towards AMP and GMP lead to a 45-fold increased intracellular IMP pool of 22 µmol g_{CDW}^{-1}. Deletion of the *pgi* gene encoding glucose 6-phosphate isomerase in combination with the deactivated AMP and GMP generating reactions, however, resulted in a significantly decreased IMP pool (13 µmol g_{CDW}^{-1}). Targeted metabolite profiling of the purine biosynthetic pathway further revealed a metabolite shift towards the formation of the corresponding nucleobase hypoxanthine (102 µmol g_{CDW}^{-1}) derived from IMP degradation.

Introduction

The diverse class of purine intermediates comprises phosphorylated nucleotides, nucleosides and nucleobases, exhibiting multiple functions in the cellular system (Pang et al., 2011): for example, they serve as transmitters of the genetic information (Traut, 1994), as phosphate group donors, are involved in signal mediation (Cordell et al., 2008) and ensure the energy supply of the living cell (Guimaraes and Londesborough, 2008). Thus, these intermediates are involved in almost every aspect of cellular metabolism. Furthermore, some of these compounds possess secondary functions as flavor-enhancing substances, *i.e.* IMP and GMP (Halpern, 2002; Matsui et al., 2001b; Shimaoka et al., 2005), and act as potential drugs in medical therapy, *e.g.* inosine and purine analogs (Cohen et al., 2010; Hofmann et al., 2012; Li et al., 2011).

Their *de novo* synthesis, however, is energetically expensive and imbalances in their pool sizes are reported to be directly linked to increased mutation rates (Bebenek et al., 1992), which eventually leads to constant pool sizes (Traut, 1994). These are maintained by a balanced system with two compensatory operating parts: the *de novo* biosynthesis pathway, generating the purine intermediates from central carbon metabolism, and the *salvage pathway*, which can replenish corresponding pools (Figure IV-1) (Li et al., 2011; Matsui et al., 2001b; Shimaoka et al., 2005; Tozzi et al., 2006).

R5P ⟶ PRPP

de novo   *Pathway*

AMP ← *purB* ← adenylo-succinate ← *purA* ← IMP → *guaB2* → XMP → *guaA* → GMP

Salvage Pathway — *apt*

adenosine   *Salvage Pathway* — *hpt*   inosine   xanthosine   *Salvage Pathway* — *hpt*   guanosine   *Salvage Pathway* — *hpt*

adenine   hypoxanthine   xanthine   guanine
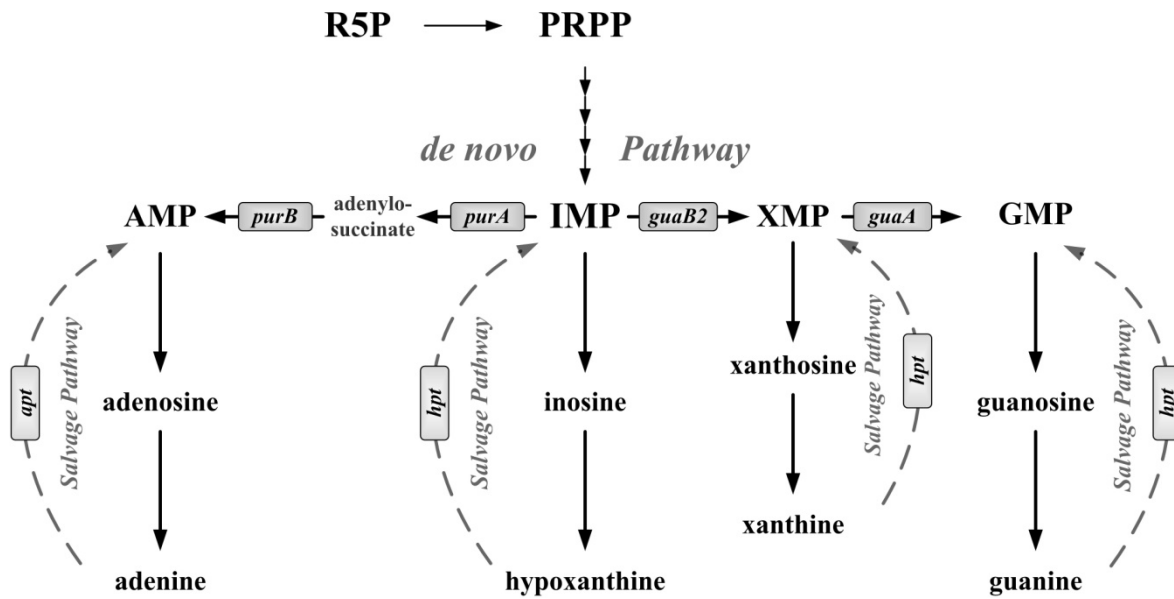
Figure IV-1. Metabolic map of the purine biosynthetic pathway. Dashed lines indicate multiple enzymatic steps; boxes denote contributing enzymes of *de novo* biosynthetic pathway (dark grey) and *salvage pathway* (light gray). **Abbreviations: R5P**, ribose 5-phosphate; **PRPP**, 5-phosphoribosyl 1-pyrophosphate; **IMP**, inosine 5-monophosphate; **AMP**, adenosine 5-monophosphate; **XMP** xanthosine 5-monophosphate; **GMP**, guanosine 5-monophosphate; *purA*, adenylosuccinate synthetase; *purB*, adenylosuccinate lyase; *guaB2*, IMP dehydrogenase; *guaA*, GMP synthase; *apt*, adenine phosphoribosyltransferase; *hpt*, hypoxanthine-guanine phosphoribosyltransferase.

De novo nucleotide synthesis begins with the activation of the PPP intermediate and direct precursor ribose 5-phosphate (Messenger and Zalkin, 1979), which is further converted to IMP in a twelve-step biosynthetic process with concomitant consumption of 10 mol ATP. AMP and GMP are derived from IMP as depicted in Figure IV-1 (Pang et al., 2011; Saxild and Nygaard, 1991). The *salvage pathway,* however, converts extracellular nucleobases or degraded purine compounds into the corresponding nucleosides and nucleotides (Abbouni et al., 2003; Abbouni et al., 2004), thereby preventing energetically-expensive *de novo* synthesis of these compounds.

Since primary metabolism is designed and optimized to deliver and sustain a more or less consistent distribution of metabolites (described as *network rigidity* (Stephanopoulos and Vallino, 1991)), which can be used as cellular building blocks, redox equivalents, energy and cofactors, any kind of overproduction or accumulation basically targets the deregulation of the underlying metabolism. In the present study, a strategy for increased IMP accumulation was developed by focusing on modifying the general key factors for overproduction: (i) increasing the precursor availability, (ii) de-bottlenecking regulation-restricted branch points, and (iii) deactivating the depleting reactions. The goal of this study was to identify essential nodes of this pathway and to uncover impacts from central and purine metabolism. Applying genetic engineering and in-depth metabolome analysis of the purine pathway intermediates, information of the extremely well-regulated purine pathway should be gathered (Mathews, 2006; Pang et al., 2011; Saxild and Nygaard, 1991; Wheeler et al., 2005). However, the underlying mechanisms and the contributions of different branches are not well described yet. In addition, identification of individual regulation factors (Fiehn, 2002; Nielsen, 2003) operating at different hierarchic levels (van Gulik and Heijnen, 1995) is challenging due to the comprehensive connectivity of the metabolic network. The interconnectivity of metabolome and fluxome therefore provides valuable insights into global dynamics (Fiehn, 2001; Nielsen and Oliver, 2005) resulting from single and multiple perturbations in the central and branch metabolism (Dunn, 2008).

Materials and methods

Microorganisms

Wild type *C. glutamicum* ATCC 13032 was obtained from the American Type Culture Collection (Manassas, VA, USA) and used as parent strain for further genetic modifications. *E. coli* DH5α was utilized as host strain for cloning and plasmid construction. *E. coli* NM522^{pTC} served as host for plasmid amplification and coryne-specific methylation. The pTC plasmid, harboring an origin of replication (*ori*), for *E. coli* a tetracycline resistance as selection marker and the DNA-methyltransferase gene from *C. glutamicum*, was co-expressed in *E. coli* NM522^{pTC} to transfer the methylation pattern of *C. glutamicum* to the integrative plasmids. The vector pClik, used for integrative genetic modifications, exhibited an *ori* for *E. coli* but not for *C. glutamicum*, a *multiple cloning site* (MCS) and kanamycin (Kan^R) and *sacB* selection markers. The constructed pClik-derivates were used for homologous replacement of the native gene sequences with the modified ones. Transformation of *C. glutamicum* and subsequent selection on Kan^R yielded transformants possessing genome-integrated plasmids via single crossover. The *sacB* positive selection system (Jager et al., 1992) on sucrose was applied to select clones from the second recombination event. Kan^R-sensitive and sucrose-insensitive clones were tested for the existence of the modified gene sequence via PCR and positive clones were additionally sequenced.

The modifications constructed in this study comprised single gene deletions (*ΔpurA, ΔguaB2* and *Δpgi*), an allelic replacement of the *purF* gene encoding amidophosphoribosyltranferase with a *purF*K348Q gene (*purF^{K348Q}*) and multiple gene deletions (*ΔpurA ΔguaB* and *ΔpurA ΔguaB2 purF^{K348Q} Δpgi*). The site-directed mutants and corresponding genetic modifications are summarized in Table IV-1. Allelic replacement of the modified *purF* gene was carried out by first deleting the native gene followed by a replacement step with the manipulated gene containing the point mutation. Primer sequences used for construction and verification are listed in Table IV-2.

Table IV-1. Genetically modified organisms constructed in the present study: Mutant strains of *C. glutamicum* based on the wild type strain (ATCC 13032) were constructed by site-directed mutagenesis. *E. coli* strains were employed for plasmid construction.

strain	genotype	reference
C. glutamicum ATCC 13032	wild type	American Type Culture Collection
C. glutamicum Δpgi	deletion of the *pgi* gene	This work
C. glutamicum ΔpurA	deletion of the *purA* gene	This work
C. glutamicum ΔguaB2	deletion of the *guaB2* gene	This work
C. glutamicum purF^{K348Q}	nucleotide exchange K348Q in the *purF* gene	This work
C. glutamicum ΔpurA ΔguaB2	double deletion of *purA* and *guaB2* genes	This work
C. glutamicum ΔpurA ΔguaB2 purF^{K348Q} Δpgi	deletion of *purA*, *guaB2* and *pgi* genes and allelic amino acid substitution K348Q in the *purF* gene	This work
E. coli DH5α	F⁻endA1, hsdR17(rk⁻mk⁺) supE44, thi-1λ⁻ recAI gyrA96 relA1 ^{Φ}80ΔlacAm15	(Hanahan, 1983)
E. coli NM522^{pTC}	*supE thi-1 Δ(lac-proAB) Δ(mcrB-hsdSM)5 (r*K⁻ *m*K⁺) [F′ *proAB lacIqZΔM15*]	Stratagene

Table IV-2. Mutant genotypes and corresponding site-specific primer sequences (F, forward; R, reverse) used for verification[a].

mutant genotype	primer	primer sequence
Δpgi	*Δpgi*-F	5′-GATCACGCGTATCCCTTCTCCGGCATC-3′
	Δpgi-R	5′-GATCTCTAGATCCAGCGACACGAATAATC-3′
ΔpurA	*ΔpurA*-F	5′-GATCTCTAGAATGGATCGGATGTGACG-3′
	ΔpurA-R	5′-GATCACGCGTCAATCGGTCAACCTGGT-3′
ΔguaB2	*ΔguaB2*-F	5′-GATCACGCGTGAGTTTCTACCGGAGGA-3′
	ΔguaB2-R	5′-GATCTCTAGATCAGACTGGAAGTAACG-3′
purF^{K348Q}	*purF^{K348Q}*-F	5′-GATCACGCGTGATTGCGGACTGGTTAC-3′
	purF^{K348Q}-R	5′-GATCTCTAGACTCCTGCTGCTGCGTATG-3′
	K348Q-1	5′-GGCCAAGGCATGGTCC<u>CAG</u>AACGCCTACGTTGGC-3′
	K348Q-2	5′-GCCAACGTAGGCGTT<u>CTG</u>GACCATGCCTTGGCC-3′

[a] for the single amino acid substitution in *purF^{K348Q}*, sequences for fusion primers (K348Q-1, K348Q-2) containing the point mutation (underlined) are additionally denoted.

DNA preparation and recombinant DNA modifications

Oligonucleotide synthesis was performed by Sigma-Aldrich (Steinheim, Germany) and DNA sequencing was carried out by GATC (Konstanz, Germany). Plasmid construction and DNA purification were performed using standard techniques. Preparation of genomic DNA from *C. glutamicum* was carried out with the MasterPure™ Gram Positive DNA Purification Kit (Biozym Scientific GmbH, Germany). PCR reactions were performed in a TGradient-Cycler (Whatman–Biometra^R) with Phusion polymerase (Biozym) for insert construction and JumpStart REDTaq Ready Mix (Sigma-Aldrich) for strain verification. PCR products were purified using NucleoSpin® Extract II Kit (Macherey-Nagel, Düren, Germany) and plasmids using HiYield® Plasmid Mini Kit (SLG, Gauting, Germany). Ligations were performed with Fast-Link™ DNA Ligation Kit (Epicentre Biotechnologies, Madison, WI, USA). FastDigest® restriction enzymes were obtained from Fermentas (St. Leon-Rot, Germany) as well as 10 mM dNTP Mix and 1-kb DNA O'GeneRuler™.

Transformation

Precultures used for transformation of *C. glutamicum*, were grown on BHI^{++} medium (10 mL in 100 mL baffled shake flasks) and incubated for 12 h at 30°C. The main culture in BHI^{++} medium (80 mL in 1000 mL baffled shake flasks) was inoculated from exponentially growing precultures to an optical density OD_{660nm} of 0.2. 400 mg isonicotinic acid hydrazide, 2.5 g glycine and 0.1 mL Tween 80 were dissolved in 20 mL H_2O, sterilized by filtration and added to the main culture at an OD_{660nm} of 0.6. Cells were further incubated until an OD_{660nm} of 0.8 was reached and harvested by centrifugation (7 min, 4,000 g, 4°C, Laborfuge 400R, Heraeus, Hanau, Germany). Cells were washed three times with pre-cooled wash buffer (10% glycerine, 8 mM tris hydrochloride, pH 7.4) and once with 10% glycerine. After the second resuspension in 6 mL 10% glycerine, 200 µL cells were subsequently used for transformation. Electroporation was performed using a BioRad Gene Pulser II (Hercules, California, USA) with the following parameters: 25 µF, 600 Ω and 2.5 kV. Cells were transferred into a 2 mL Eppendorf tube, mixed with 1 mL BHIS medium, followed by a heat shock for 5 min at 46°C. Regeneration was

performed for 90 min at 30°C to allow recovery of the cells, which were then spread on BHIS^{Kan} agar plates and incubated for 4 days.

Transformation of *E. coli* DH5α and NM522^{pTC} with the integrative pClik-derivates was performed by heat shock. Cells were incubated on ice for 30 min, heated at 45°C for 45 s and again cooled on ice for 2 min. Regeneration was performed for 1 h at 37°C after 900 μL SOC medium were added.

Targeted mutant generation

Site-directed mutations were introduced using the integrative vector pClik, which lacks an *ori* for *C. glutamicum*. Selection on Kan^R as resistance marker yielded transformed cells with genome-integrated plasmid DNA. The insertion of the plasmids thereby results from a single crossover recombination event. The second homologous recombination event, generated by the *sacB* positive selection system, causes the deletion of the *sacB* gene and therefore allows growth on corresponding selective agar plates. Due to the *sacB* associated additional deletion of the native or the modified gene sequence, transformants either contain the wild type gene sequence or exhibit the targeted mutation. Kan^R-sensitive and sucrose-insensitive clones were further verified by allelic-specific PCR for the presence of the targeted gene sequence. The corresponding gene sequence for a nucleotide exchange, *i.e. purF^{K348Q}*, was first deleted and then replaced.

Chemicals

Yeast extract, beef extract, polypeptone, casamino acids, and brain heart infusion (BHI) were purchased from Difco Laboratories (Detroit, USA). 99% enriched glucose, *i.e.* [1-^{13}C] and [1,2-^{13}C$_2$], were obtained from Cambridge Isotope Laboratories (Andover, MA., USA). All other chemicals and reagents of analytical grade were purchased from Sigma-Aldrich, Merck (Darmstadt, Germany), Fluka (Buchs, Switzerland) or Roth (Karlsruhe, Germany).

Growth Media

The first precultures were grown on complex media (pH 6.8) containing per liter: 10.0 g glucose, 2.5 g NaCl, 2.0 g urea, 5.0 g yeast extract, 5.0 g beef extract, 5.0 g polypeptone and 20.0 g casamino acids. For agar plates, the complex medium was supplemented with 20.0 g L^{-1} agar. Second precultures and main cultures were grown on minimal medium (pH 7.2) containing per liter: 15.0 g glucose, 4.0 g KH_2PO_4, 16.0 g Na_2HPO_4, 500 mg $MgCl_2 \cdot 6\,H_2O$, 300 mg 3,4-dihydroxybenzoic acid, 100 mg $CaCl_2 \cdot 2\,H_2O$, 100 µg cyanocobalamin, 750 µg thiamine, 4 µg pyridoxal phosphate, 100 µg biotin, 400 µg calcium pantothenate, 2 µg folic acid, 400 µg nicotinic acid, 200 µg 4-aminobenzoic acid, 400 µg pyridoxine $\cdot$ HCl, 2 mg inositol, 10 mg $FeCl_2 \cdot 4\,H_2O$, 1 mg $ZnCl_2$, 100 µg $CuCl_2$, 20 µg $NiCl_2 \cdot 6\,H_2O$, 20 µg $Na_2MoO_4 \cdot 2\,H_2O$, 500 µg boric acid, 100 µg KI, 100 µg $CoCl_2 \cdot 6\,H_2O$, 10 mg $MnCl_2 \cdot 4\,H_2O$. For tracer studies, naturally labeled glucose was replaced by 99% ^{13}C enriched $[1-^{13}C]$ or $[1,2-^{13}C]$ glucose. Mutants of *C. glutamicum* exhibiting deletions of adenylosuccinate synthetase (*purA*) or IMP dehydrogenase (*guaB2*) were grown on minimal media additionally supplemented with 200 mg L^{-1} adenine sulfate or 80 mg L^{-1} guanine hydrochloride, due to the introduced auxotrophies.

Media used for transformation experiments of *C. glutamicum* contained per liter: 37 g BHI, 26.4 g $(NH_4)_2SO_4$ and 40 g glucose for BHI^{++} and 37 g BHI and 46 g sorbitol for BHIS medium.

Cultivations

Cultivations were carried out in baffled shake flasks on an orbital shaker (Multitron 2, Infors AG, Bottmingen, Switzerland) at 230 rpm and 30°C. First precultures were grown on complex medium (25 mL medium in 250 mL baffled flasks) for 8 h and used for inoculation of the second precultures (25 mL medium in 250 mL baffled flasks). Second precultures and main cultures were performed in minimal medium. Main cultivations were performed in duplicates in minimal medium using 500 mL baffled shake flasks with 50 mL medium. For tracer experiments, which were conducted under the same conditions as main cultivations, naturally labeled glucose was replaced by $[1-^{13}C]$ glucose or $[1,2-^{13}C_2]$

glucose for analysis of glucose 6-phosphate isomerase (*pgi*) deletion mutants and the volume was adjusted to 5 mL in 50 mL baffled shake flasks.

Substrate and product analysis

Biomass concentration was determined by measuring the optical density of the culture at 660 nm (OD_{660nm}) using a photometer (Marsha Pharmacia Biotech, Freiburg, Germany) which was gravimetrically correlated with the cell dry weight. Extracellular substrates and secreted products were analyzed after 3 min centrifugation at 16,000 *g*. Quantification of glucose, α-ketoglutarate and trehalose was performed in diluted supernatants by HPLC (Kontron Instruments, Neufahrn, Germany). Separation was performed using an Aminex HPX-87H Bio-Rad column (300 x 7.8 mm; Hercules, USA), at 55°C with a constant flow rate of 0.8 mL min^{-1} (7 mM H_2SO_4 as mobile phase). Refraction index (RI) detection was used for quantification of sugars, and UV detection at 218 nm for organic acids. Determination of amino acids was performed as described previously (Kromer et al., 2005). Extracellular concentrations of adenine and guanine were determined by HPLC (Agilent 1290 Infinity; Agilent Technologies, Waldbronn, Germany) using a Phenomenex (Aschaffenburg, Germany) reversed-phase C_{18}-column (Gemini 5u 110Å, 150 x 4.6 mm). Separations were carried out at 10°C with a constant flow of 0.8 mL min^{-1}. Gradient elution was performed using 5 mM ammonium formate solution at pH 5.8 (eluent A) and acetonitrile:methanol:water mixture (45:45:10, eluent B) applying the following gradient: an initial isocratic step with 0% B (3.5 min) was followed by an increase to 30% within 10 min and to 100% within 1 min. The flushing step at 100% B was performed for 5 min. The column was reconditioned at 0% B for another 5 min.

Analysis of intracellular metabolites

Extraction and quantification of intracellular purine intermediates, *i.e.* nucleotides, nucleosides and nucleobases, by LC-ESI-MS/MS was performed as described previously (Peifer et al., 2012; Chapter III).

Mass spectrometric ^{13}C-labeling analysis

The mass isotopomer distributions of amino acids derived from cellular protein and of trehalose secreted during cultivation were determined by gas chromatography-mass spectrometry (GC-MS). Sample preparation and instrument settings were performed as described previously (Becker et al., 2005; Kiefer et al., 2004; Wittmann et al., 2004a).

Fluxome analysis

Calculation of the *in vivo* metabolic fluxes of the *C. glutamicum* strains was carried out by fitting simulated mass isotopomer distributions to experimentally determined labeling patterns of amino acids derived from cellular protein and trehalose secreted during cultivation. The calculations were based on the approach of Yang et al. (2008) implemented in Matlab (version 2008b, Mathworks Inc., Nattick, USA) using metabolite and isotopomer balancing. Anabolic demands for biomass synthesis and extracellular production rates were additionally considered and implemented in the metabolic network. A Monte Carlo approach with 100 independent runs was employed for the statistical analysis (Wittmann and Heinzle, 2002).

Data analysis

Mean concentration values for purine intermediates were calculated from four biological replicates for each strain for two biomass concentrations and corrected using ^{13}C-labeled cell extract as internal standard as described previously (Peifer et al., 2012; Chapter III). The metabolomics-based phenotype profiling was extended by principal component analysis (PCA) applying pareto scaling of the data. Data sets were compressed by reduction of dimension numbers and the metabolomic patterns were highlighted. PCA was performed using Matlab R2008b (The Math Works, Inc., Boston, USA) software.

Results

Metabolic snapshots of the purine pathway in wild type C. glutamicum

Intracellular metabolite concentrations in *C. glutamicum* were quantified after whole culture extraction using LC-ESI-MS/MS (Peifer et al., 2012; Chapter III). In order to verify balanced growth conditions (Provost and Bastin, 2004; Wittmann, 2007) and stable intracellular metabolite concentrations (Marx et al., 1996; Wiechert, 2001), respectively, quantification was performed for two different biomass concentrations, resulting in four biological replicates for each biomass concentration. The corresponding concentrations of nucleotides, nucleosides and nucleobases related to the cell dry weight are listed in Table IV-3.

All compounds except xanthosine and XMP, which were below the detection limit, were quantified with a precision better than 12%. AMP and GMP, as central building constituents for DNA and RNA and co-substrates for various enzyme reactions (Cordell et al., 2008; Traut, 1994), showed the highest concentration ranges of 8.13 and 2.63 μmol g_{CDW}^{-1}, respectively. Other intermediates varied within a broader concentration range from 0.04 to 3.27 μmol g_{CDW}^{-1}. The lowest concentrations were detected for nucleosides and reaching up to 0.04 μmol g_{CDW}^{-1} for guanosine.

Several genetic perturbations aiming at various metabolic key nodes were performed to evaluate the effects and impacts of changing activities of different metabolic branches of the metabolism on the intracellular purine pool sizes.

Table IV-3. Concentrations of purine intermediates [µmol g_{CDW}^{-1}] determined for *C. glutamicum* wild type (ATCC 13032) and site-directed mutants[a].

concentration [µmol g_{CDW}^{-1}]

compound	ATCC 13032	Δpgi	purF[K348Q]	ΔpurA[c]	ΔguaB2[c]	ΔpurA ΔguaB2	ΔpurA ΔguaB2 purF[K348Q] Δpgi
AMP	8.13 ± 0.50	9.07 ± 0.52	10.24 ± 0.78	10.66 (17.93) ± 0.22 (1.18)	10.11 (27.79) ± 0.05 (2.03)	3.69 ± 0.54	3.57 ± 0.20
adenosine	0.10 ± 0.01	0.09 ± 0.01	0.12 ± 0.02	0.13 ± 0.01	0.21 ± 0.01	0.05 ± 0.00	0.15 ± 0.03
adenine	2.63 ± 0.25	3.04 ± 0.11	3.36 ± 0.30	3.04 (5.58) ± 0.38 (0.26)	4.03 (8.32) ± 0.13 (0.53)	b.	b.
GMP	2.63 ± 0.16	3.65 ± 0.17	4.75 ± 0.27	9.47 (21.10) ± 0.12 (2.03)	3.92 (2.33) ± 0.19 (0.24)	0.65 ± 0.07	0.51 ± 0.03
guanosine	0.04 ± 0.00	b.	0.03 ± 0.00	0.03 ± 0.01	0.06 ± 0.01	0.10 ± 0.01	0.23 ± 0.02
guanine	3.27 ± 0.28	3.85 ± 0.17	5.08 ± 0.61	5.07 (10.27) ± 1.45 (0.62)	35.67 (9.38) ± 1.65 (0.64)	b.	b.
IMP	0.49 ± 0.06	0.42 ± 0.03	0.55 ± 0.05	30.72 (43.99) ± 0.48 (3.32)	6.39 (37.16) ± 0.21 (3.48)	21.91 ± 0.89	12.88 ± 0.74
inosine	0.13 ± 0.05	0.21 ± 0.04	0.38 ± 0.12	0.28 ± 0.06	0.85 ± 0.06	1.26 ± 0.08	2.53 ± 0.19

hypoxanthine	0.28 ± 0.03	0.29 ± 0.03	0.28 ± 0.03	11.87 (17.92)	1.00 (1.26)	3.55 (16.19)	0.04 (1.34)	80.65 ± 3.19	101.53 ± 1.09
XMP	b.	b.	b.	b.		n.d.		n.d.	n.d.
xanthosine	b.	b.	b.	b.		n.d.		n.d.	n.d.
xanthine	0.12 ± 0.01	0.22 ± 0.01	0.11 ± 0.00	0.17 ± 0.00		n.d.		n.d.	n.d.

a concentrations and corresponding standard deviations were determined using 4 biological replicates for each compound and biomass concentration and standardized to the cell dry weight.

b below detection limit.

c purine intermediate concentrations determined for *C. glutamicum ΔpurA* and *C. glutamicum ΔguaB2* represent values obtained for two biomass concentrations for each strain: numbers on top correspond to the first biomass concentration (1.3 g L^{-1} for *C. glutamicum ΔpurA* and 1.1 g L^{-1} for *C. glutamicum ΔguaB2*) and numbers in brackets for second biomass concentration (1.9 g L^{-1} for *C. glutamicum ΔpurA* and 1.8 g L^{-1} for *C. glutamicum ΔguaB2*).

n.d. not detected.

Manipulating the main carbon flux distribution

The first implemented modification affected the glucose 6-phosphate branch point and focused on amending the availability of the immediate precursor of IMP, ribose 5-phosphate. The carbon flux distribution was rerouted by deleting the first enzyme of the glycolysis, the glucose 6-phosphate isomerase encoded by the *pgi* gene, resulting in an entry block into glycolysis at that stage and thus restricting the metabolization of glucose 6-phosphate exclusively to the PPP. Growth parameters are depicted in Table IV-4. Specific growth rate of *C. glutamicum Δpgi* was slightly reduced compared to the wild type strain, as was biomass formation.

Table IV-4. Growth parameters for *C. glutamicum* ATCC 13032 and site-directed mutants.

parameter	strain			
	ATCC 13032	*Δpgi*	*purF*^{K348Q}	*ΔpurA*
μ	0.443 ± 0.00	0.376 ± 0.00	0.440 ± 0.01	0.455 ± 0.01
$Y_{x/s}$	0.095 ± 0.05	0.090 ± 0.00	0.091 ± 0.01	0.090 ± 0.00
q_S	4.67 ± 0.09	4.18 ± 0.02	4.82 ± 0.06	5.05 ± 0.02

	ΔguaB2	*ΔpurA ΔguaB2*	*ΔpurA ΔguaB2 purF*^{K348Q} *Δpgi*
μ	0.320 ± 0.00	0.317 ± 0.01	0.146 ± 0.00
$Y_{x/s}$	0.073 ± 0.00	0.075 ± 0.00	0.076 ± 0.00
q_S	4.38 ± 0.03	4.24 ± 0.01	1.92 ± 0.02

data represent mean values obtained from two parallel cultivations with corresponding standard deviations: specific growth rate (μ) [h^{-1}]; biomass yield ($Y_{X/S}$) [g mmol^{-1}] and the specific glucose consumption rate (q_S) [mmol g^{-1} h^{-1}].

Phenotypic analysis was further extended towards the determination of free intracellular purine pool sizes and a metabolic profile based on these analyses was generated (Table IV-3). Intracellular concentrations related to cell dry weight showed only minor changes compared to wild type *C. glutamicum*. GMP and AMP concentrations were slightly increased in *C. glutamicum Δpgi*, as were amounts of adenine, guanine and inosine. Adenosine and guanosine showed decreased concentrations. IMP and hypoxanthine were not affected significantly.

Targeted perturbations of the purine biosynthetic pathway

Further genetic manipulations were then aimed at the purine pathway itself, to estimate immediate effects emanating from this metabolic branch. The first target was the *purF* gene encoding the PRPP amidotransferase. This enzyme is generally regarded to act as key controller in the purine *de novo* synthesis, regulated by a feedback inhibition mainly caused by GMP and AMP (Matsui et al., 2001b; Shimaoka et al., 2007). An experimentally identified amino acid substitution (K326Q) in the *purF* gene is reported to offset this feedback inhibition by AMP and GMP in *E. coli* (Zhou et al., 1993) and should be incorporated into the corresponding position in the *purF* gene of *C. glutamicum*. In order to check for evolutionary conserved coding regions, a sequence alignment covering the complete amino acid sequence was performed (Zhou et al., 1993). Therefore, six organisms exhibiting a broad phylogenetic distinction, including *Escherichia coli, Corynebacterium glutamicum, Corynebacterium ammoniagenes, Bacillus subtilis, Salmonella typhimurium* and *Saccharomyces cerevisiae,* were analyzed. A conserved region comprising at least ten amino acids was identified for all organisms including the location of the amino acid substitution K326Q in *E. coli* identified by Zhou et al. (1993) The corresponding substitution K348Q in *C. glutamicum* was inserted into the genomic DNA. Verification of the base exchange was carried out by sequencing.

The amino acid substituent *C. glutamicum purF*K348Q (*purF^{K348Q}*) showed balanced growth with stable biomass formation and growth rate (Table IV-4). Intracellular purine intermediate pool sizes remained almost unchanged for adenosine, guanosine and

hypoxanthine (Table IV-3). The most striking changes were observed for intracellular inosine concentration which increased 2.9-fold. Compared to the wild type strain, the IMP concentration, however, showed only a minor change (10% increase). Intracellular concentrations of AMP and its corresponding nucleobase adenine increased by approximately 25% each. GMP and guanine pool sizes in *C. glutamicum purF*[K348Q] increased significantly by 80% and 55%, respectively compared to the wild type, indicating a global shift towards the main intermediates GMP, AMP and inosine. Direct determination of the *in vitro* activity of PurF following the method of Matsui et al. (2001a), employing HPLC quantitation of substrate (glutamine) and product (glutamate) concentrations over time in crude cell extracts, resulted in tremendous background activity, not permitting kinetic studies. In addition, heterologous expression using *Escherichia coli* as expression system resulted in enzyme inactivation, probably due to complex posttranslational events. Further studies will however focus on the determination of the *in vitro* activity.

In addition to the deregulation of PurF, further genetic manipulations were aimed at IMP degradation, affecting the synthesis of IMP-derived GMP and AMP. The biosynthesis of both intermediates was thus shifted from *de novo* biosynthesis to the purine *salvage pathway*, employing the two enzymes adenosine-phosphoribosyltransferase (APRT) and hypoxanthine-guanine-phosphoribosyltransferase (HGPRT) catalyzing the synthesis of AMP and GMP/IMP via a condensing reaction of adenine and guanine/hypoxanthine with PRPP maintaining a sustained supply of the necessary precursors. These genetic manipulations, however, lead to auxotrophies for adenine and/or guanine (Matsui et al., 2001a; Qian et al., 2006).

As initial strategy, the single gene deletions of the adenylosuccinate synthetase (*purA*) (catalyzing the conversion of IMP to AMP) and of the IMP-dehydrogenase (*guaB2*) (catalyzing the reaction of IMP to GMP) were analyzed. Due to the generated auxotrophies, the medium had to be supplied with adenine and guanine as discussed above and resulting phenotypes based on intracellular concentrations of the corresponding purine pathway intermediates were analyzed (Table IV-3).

The metabolic shift from *de novo* purine biosynthesis to the *salvage pathway* did not show any significant changes in the growth rate of the *purA* deletion strain. The *guaB2* deletion strain, however, showed a drastic response after redirecting GMP formation to the *salvage*

pathway: biomass yield was reduced by 25% (0.073 g mol$^{-1}_{glucose}$) of the wild type yield and the specific growth rate even dropped by 30% of the wild type rate, reaching a stable rate of 0.32 h^{-1}, thus indicating a restricted compensation efficiency of the *salvage pathway* concerning the GMP supply. Metabolic phenotyping revealed even more distinct alterations: most strikingly both deletion mutants were characterized by unbalanced intracellular pools sizes, exhibiting transient concentration changes which could not be related to biomass formation (Table IV-3). Degradation inefficiency of IMP towards the following nucleotides (GMP and AMP) led to maximal intracellular IMP concentrations of 44 µmol g$_{CDW}^{-1}$ (*ΔpurA*) and 37 µmol g$_{CDW}^{-1}$ (*ΔguaB2*) corresponding to a 90- and 80-fold increase compared to the wild type strain. Hypoxanthine concentrations were affected likewise.

The unbalanced metabolic state observed in *C. glutamicum ΔpurA* and *C. glutamicum ΔguaB2*, was further investigated in the double deletion mutant *C. glutamicum ΔpurA ΔguaB2*, exhibiting auxotrophies for adenine as well as for guanine. Specific growth parameters of the double deletion mutant, *i.e.* biomass yield (0.075 g$_{CDW}$ mmol$_{glucose}^{-1}$) and specific growth rate (0.317 h^{-1}), were consistent with those obtained for *C. glutamicum ΔguaB2*, indicating a mutual growth-related effect. However, the metabolic fingerprint for *C. glutamicum ΔpurA ΔguaB2* exhibited remarkable differences (Table IV-3): the unbalanced metabolic behavior observed in *C. glutamicum ΔpurA* and *C. glutamicum ΔguaB2* was completely reestablished resulting in constant intracellular purine intermediate concentrations for all substances quantified. The double deletion mutant showed a decreased intracellular IMP pool of 21.9 µmol g$_{CDW}^{-1}$ compared to the single gene deletion mutants which corresponds to a 44-fold increase compared to the wild type strain. The IMP reduction was accompanied by a significant increase of the inosine concentration (9.7-fold compared to the wild type strain) and especially hypoxanthine (290-fold compared to the wild type strain), indicating a metabolic shift from main purine intermediates; *i.e.*, the nucleotides, to the corresponding degradation products (nucleobases).

Extended metabolic manipulations – combination of central pathway and branch pathway modifications

Finally, the combined influence of the genetic modifications described in *"Manipulating the main carbon flux distributions"* and *"Targeted perturbations of the purine biosynthetic pathway"* (see section *"Results"*) were investigated. The rationally designed mutant *C. glutamicum ΔpurA ΔguaB2 purF^{K348Q} Δpgi* is characterized by the amino acid substitution (*purF*K348Q), supposed to affect the regulatory key enzyme for the *de novo* synthesis. In addition, the mutant exhibits gene deletions for the initiating reaction of glycolysis (*pgi*) and for the converting reactions leading from IMP to the successive purine nucleotides AMP (*purA*) and GMP (*guaB2*).

The biomass yield of 0.076 g$_{CDW}$ mmol$_{glucose}$$^{-1}$ for *C. glutamicum ΔpurA ΔguaB2 purF^{K348Q} Δpgi* was consistent with those obtained for *C. glutamicum ΔpurA ΔguaB2* and *C. glutamicum ΔguaB2*. Specific growth rate was however reduced to 0.146 h^{-1}. In contrast to the two single gene deletion mutants (*ΔpurA* and *ΔguaB2*), the previously observed IMP decline observed in the double deletion mutant *C. glutamicum ΔpurA ΔguaB2* was even more pronounced in the mutant containing the four genetic modifications (Table IV-3). In conjunction with these findings, an increased IMP degradation towards the corresponding nucleoside inosine and nucleobase hypoxanthine was observed.

Quantification of intracellular carbon flux distributions

Alterations of *in vivo* carbon flux distributions were investigated in order to assess the impact on the purine intermediate profile. The network contained reactions of glycolysis, TCA cycle, anaplerosis and PPP. Estimation of intracellular flux distributions was carried out based on measurable extracellular rates; *i.e.,* glucose consumption, biomass and by-product formation as well as the mass isotopomer data obtained from ^{13}C enriched cellular protein. Initial values were statistically varied and multiple parameter estimations were performed to guarantee finding of the global minimum solution.

The metabolic carbon flux distributions determined for the strains *C. glutamicum* ATCC 13032 (wild type), *C. glutamicum Δpgi, C. glutamicum ΔpurA ΔguaB2* and *C. glutamicum ΔpurA ΔguaB2 purF^{K348Q} Δpgi* are illustrated in Figure IV-2.

Deletion of the *pgi* gene strongly affected the carbon flux distribution and caused a complete carbon redirection towards the PPP. The reflux of ribose 5-phosphate via the non-oxidative part of the PPP entering glycolysis was almost tripled. Activity of the TCA cycle was only slightly affected, showing a small reduction from 47.3% in the wild type strain to 45.7% in the *pgi* deletion mutant.

In contrast, the double deletion mutant *C. glutamicum ΔpurA ΔguaB2,* possessing an intact *pgi* gene, exhibited the lowest flux through the oxidative part of the PPP (29%), which almost exclusively accounted for biomass formation. The relative reflux into glycolysis was less than 10%. TCA cycle activity was increased to 85%. The strain *C. glutamicum ΔpurA ΔguaB2 purF^{K348Q}Δpgi* showed a carbon flux redirection from glycolysis towards the PPP (97.8%) caused by the *pgi* gene deletion. The relative activity of the TCA cycle showed a significant decrease of approximately 35% compared to the double deletion mutant and dropped from 85% to 55.8%.

Glucose

$\frac{100}{\frac{100}{100}}$
100

0.4 ± 0.0 / $\overline{0.7 ± 0.0}$ / 0.5 ± 0.0 **G6P** **44.9 ± 1.3** 97.8 ± 0.1 / $\overline{29.0 ± 1.3}$ / 97.8 ± 0.1 **P5P**

Tre$_{ex}$ ● ◀ **1.0 ± 0.0**

52.2 ± 1.3 | $\frac{--}{\frac{68.8 ± 1.3}{--}}$

F6P

90.0 ± 0.1 / $\overline{22.3 ± 0.8}$ / 90.8 ± 0.1

36.1 ± 0.7

56.4 ± 0.1 / $\overline{80.6 ± 0.5}$ / 57.3 ± 0.1 **F16BP**
72.3 ± 0.4

DHAP ● **GAP**

140.1 ± 0.3 / $\overline{166.3 ± 0.6}$ / 142.3 ± 0.2
153.7 ± 0.4

Gly$_{ex}$ ● ◀ **0.9 ± 0.0** | $\frac{--}{\frac{--}{0.3 ± 0.0}}$ — **3PG**

128.7 ± 0.3 / $\overline{156.4 ± 0.6}$ / 131.5 ± 0.4
140.0 ± 0.4

PEP/Pyr

23.8 ± 3.7 / $\overline{39.7 ± 10.0}$ / 39.1 ± 6.3
11.1 ± 2.0

73.8 ± 0.7 / $\overline{109.3 ± 1.2}$ / 81.5 ± 0.7
78.8 ± 0.4

49.7 ± 3.8 / $\overline{62.0 ± 9.9}$ / 62.7 ± 6.3
40.1 ± 2.0

AcCoA

OAA/Mal

Iso

Suc

45.7 ± 0.9 / $\overline{85.0 ± 1.5}$ / 55.8 ± 0.9
47.3 ± 0.4

34.6 ± 0.9 / $\overline{75.5 ± 1.6}$ / 45.8 ± 1.0
35.0 ± 0.4 **AKG**

AKG$_{ex}$ ● ◀ **0.2 ± 0.0** | 0.2 ± 0.0 / $\overline{0.2 ± 0.0}$ / 0.1 ± 0.0

Figure IV-2. Intracellular carbon flux distributions with corresponding standard deviations of the central metabolism of the wild type *C. glutamicum* ATCC 13032 (in bold) and mutant strains *C. glutamicum Δpgi, C. glutamicum ΔpurA ΔguaB2* and *C. glutamicum ΔpurA ΔguaB2 purF*^{K348Q} *Δpgi* (displayed in that order from top to bottom). Net fluxes are given as molar percentage of the mean specific glucose uptake rates (4.67 mmol g^{-1} h^{-1} for *C. glutamicum* ATCC 13032; 4.18 mmol g^{-1} h^{-1} for *C. glutamicum Δpgi*; 4.24 mmol g^{-1} h^{-1} for *C. glutamicum ΔpurA ΔguaB2*;

1.92 mmol g^{-1} h^{-1} for *C. glutamicum ΔpurA ΔguaB2 purF^{K348Q} Δpgi*), which were set to 100%. Anabolic fluxes leading towards biomass formation were not displayed for the benefit of lucidity. Anabolic demands for auxotrophic mutant strains *C. glutamicum ΔpurA ΔguaB2* and *C. glutamicum ΔpurA ΔguaB2 purF^{K348Q} Δpgi* were corrected for the supplementation of adenine and guanine. **Abbreviations: G6P**, glucose 6-phosphate; **P5P**, pentose 5-phosphate; **F6P**, fructose 6-phosphate; **F16BP**, fructose 1,6-bisphosphate; **DHAP**, dihydroxyacetone phosphate; **GAP**, glyceraldehyde 3-phosphate; **3PG**, 3-phosphoglycerate; **PEP**, phosphoenolpyruvate; **Pyr**, pyruvate; **AcCoA**, acetyl-CoA; **Iso**, isocitrate; **AKG**, α-ketoglutarate; **Suc**, succinate; **OAA**, oxaloacetate; **Mal**, malate; **Gly$_{ex}$**, glycine (extracellular); **Tre$_{ex}$**, trehalose (extracellular).

Perturbation-caused alterations of the NADH metabolism

The inserted genetic changes also altered the redox metabolism, especially regarding the NADH/FADH$_2$ (XADH) supply. A surplus was detected in all strains investigated, which could be used for ATP generation by oxidative phosphorylation. However, the relative NADH production exhibited significant differences among the modified strains (Figure IV-3): *C. glutamicum* ATCC 13032 produced a XADH surplus of 369% which decreased to 346% in the *pgi* deletion mutant. An increased surplus of 502% was determined for *C. glutamicum ΔpurA ΔguaB2*. This difference can be ascribed to the low activity of the PPP (29%) and the contrariwise high TCA cycle activity (85%). In comparison to *C. glutamicum ΔpurA ΔguaB2, C. glutamicum ΔpurA ΔguaB2 purF^{K348Q} Δpgi* exhibited a decreased XADH surplus of 361%.
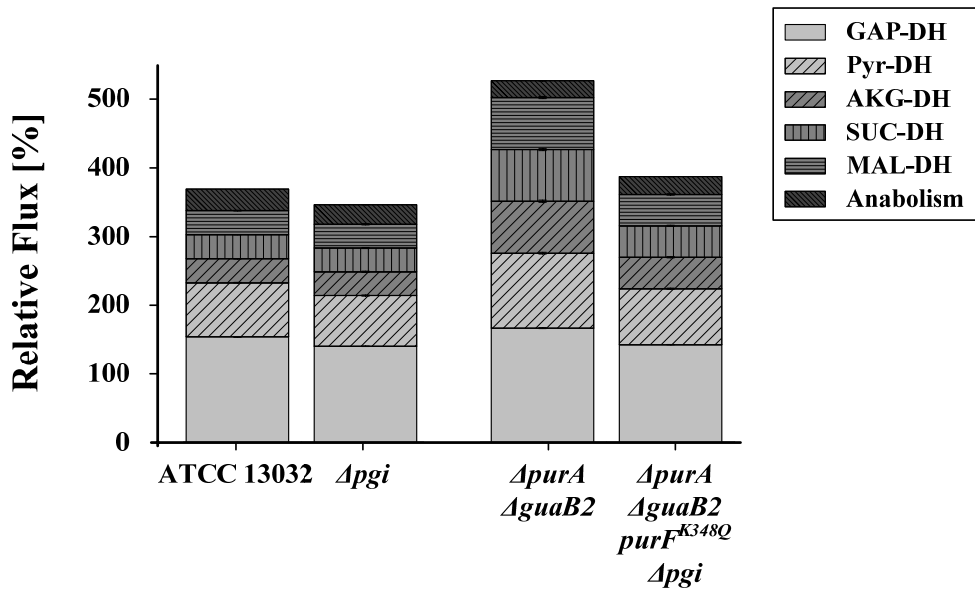
Figure IV-3. XADH formation for *C. glutamicum* ATCC 13032, *C. glutamicum Δpgi, C. glutamicum ΔpurA ΔguaB2* and *C. glutamicum ΔpurA ΔguaB2 purF^{K348Q} Δpgi*. Glyceraldehyde 3-phosphate dehydrogenase (GAP-DH), pyruvate dehydrogenase (Pyr-DH), α-ketoglutarate dehydrogenase (AKG-DH) and malate dehydrogenase (MAL-DH) were considered as NADH supplying reactions and succinate dehydrogenase (SUC-DH) as FADH$_2$ supplying reaction. Anabolically derived NADH was considered with 3.2 mmol g$_{CDW}^{-1}$ (Becker et al., 2007).

The consequences of the unequal NADH/FADH$_2$ supply are discussed in more detail below in *"Cluster analysis" (*see section *"Discussion").*

Discussion

Rerouting metabolic fluxes – contributions of individual pathway branches with respect to purine accumulation

(i) Targeted perturbations in the purine biosynthetic pathway

Imbalances in free intracellular purine pools are reported to be mutagenic and genotoxic (Mathews, 2006; Wheeler et al., 2005). Thus a prerequisite for balanced cellular growth is to maintain the intracellular pool sizes, which resulted in efficient regulatory mechanisms (Matsui et al., 2001a; Messenger and Zalkin, 1979; Pang et al., 2011; Saxild and Nygaard, 1991; Shimaoka et al., 2007; Zhou et al., 1994). This pool stability is on the one hand sustained by an interaction of *de novo* purine synthesis and the *salvage pathway*, ensuring a constant supply of purine nucleotides required for cellular growth (Messenger and Zalkin, 1979). On the other hand, increasing concentrations perturbing the system can easily be broken down via the present degrading and converting reactions.

In case of the *purA* gene deletion mutant (*C. glutamicum ΔpurA)*, extracellular supplementation with adenine completely restored cellular growth, resulting in comparable specific growth rates of the wild type (0.443 h^{-1}) and the *C. glutamicum ΔpurA* strain (0.455 h^{-1}), indicating a thorough compensatory effect by the *salvage pathway*.

On the contrary, extracellular guanine complementation was not sufficient to restore wild type growth behavior in the *guaB2* gene deletion mutant (*C. glutamicum ΔguaB2)*: specific growth rate as well as biomass yield were reduced by 25%, each compared to the wild type strain (Table IV-4). This can either be explained by insufficient uptake or converting systems for guanine. The latter is catalyzed by the *salvage pathway*. The observed phenotypic consequences reemerged in every genotype comprising this genetic perturbation (*C. glutamicum ΔguaB2* and *C. glutamicum ΔpurA ΔguaB2),* no matter if single or multiple genes were deleted. The attribution of this fundamental *salvage* branch restriction regarding uptake or conversion could not be answered definitely in this study. Decreasing intracellular guanine concentrations in *C. glutamicum ΔguaB2,* however

indicate an uptake insufficiency (and not a conversion insufficiency!). Decreasing metabolite concentrations are caused by increased consuming reactions (in this case by the *salvage pathway*).

In contrast, the *purA* gene deletion mutant *C. glutamicum ΔpurA* exhibited increasing adenine concentrations, supporting a sufficient adenine uptake, even exceeding converting reactions by the *salvage pathway*. This theory is additionally supported by the reduced guanine uptake (125 µmol g_{CDW}^{-1}) compared to the adenine uptake (243 µmol g_{CDW}^{-1}), indicating basic differences for both intermediates.

Regarding intracellular pool sizes, the single gene deletion mutants *C. glutamicum ΔpurA* and *C. glutamicum ΔguaB2* were found to exhibit the most promising rises in intracellular IMP concentration with maximal IMP pool sizes of 44.0 and 37.2 µmol g_{CDW}^{-1}, respectively. The associated transient concentration changes however showed no relation to biomass formation and resulted in unstable and thus unrepresentative results. This phenomenon may at least partially be associated with direct changes in the GMP and AMP pool sizes (Table IV-3). These two compounds are reported to act as the most stringent regulators for the purine biosynthetic pathway by a feedback-mediated inhibition of the PurF enzyme (Messenger and Zalkin, 1979). With both intermediates operating as regulators, it is not surprising that the individual gene deletions cause spreading influences on the whole branching pathway.

(ii) Targeted perturbation in the central carbon metabolism

Increasing the precursor supply via the oxidative branch of the PPP seemed to be a promising route to boost intracellular purine levels. This strategy has already been successfully applied for tryptophan production in *E. coli* (Mascarenhas et al., 1991) and lysine production in *C. glutamicum* (Becker et al., 2005; Becker et al., 2007), illustrating positive correlations between enhanced productivity and increased PPP activities (Wittmann and Becker, 2007).

Thus, the genetic modification (deletion of the *pgi* gene) was implemented into the genome. The resulting effects on the purine intermediate pool sizes (Table IV-3) however,

were rather limited compared to those observed for *purA* and *guaB2* gene deletion strains, indicating the strong regulation and rigidity of this pathway.

Effects of combined perturbations on intracellular purine pool sizes

Strains used for industrial manufacturing of purine intermediates are usually characterized by an adenine auxotrophy (Demain et al., 1966; Kamada et al., 2001; Matsui et al., 2001a; Mori et al., 1997; Qian et al., 2006). This perturbation seems to be fundamental, revealing the importance of an IMP conversion block for the accumulation of this intermediate metabolite (Villas-Boas et al., 2005). The extracellular supplementation with adenine, however, is linked to a repression of transcription initiation (Qian et al., 2006) of genes of the *pur* operone (Qian et al., 2006) via the depletion of PRPP. In order to counterbalance this phenomenon, the carbon flux was rerouted by introducing the *pgi* gene deletion, aiming at an increased PRPP supply (Figure IV-2).

The carbon flux was successfully rerouted. Intracellular purine levels though further shifted from nucleotides towards their degradation products, mainly inosine and hypoxanthine (Table IV-3).

Cluster analysis

In order to analyze correlations between the different manipulated pathway branches, *principal component analysis* (PCA) was performed. The result of the cluster analysis is illustrated in Figure IV-4. Pareto-scaled concentrations of purine pathway intermediates were used for the PCA, resulting in the global purine metabolite phenotype for each mutant.
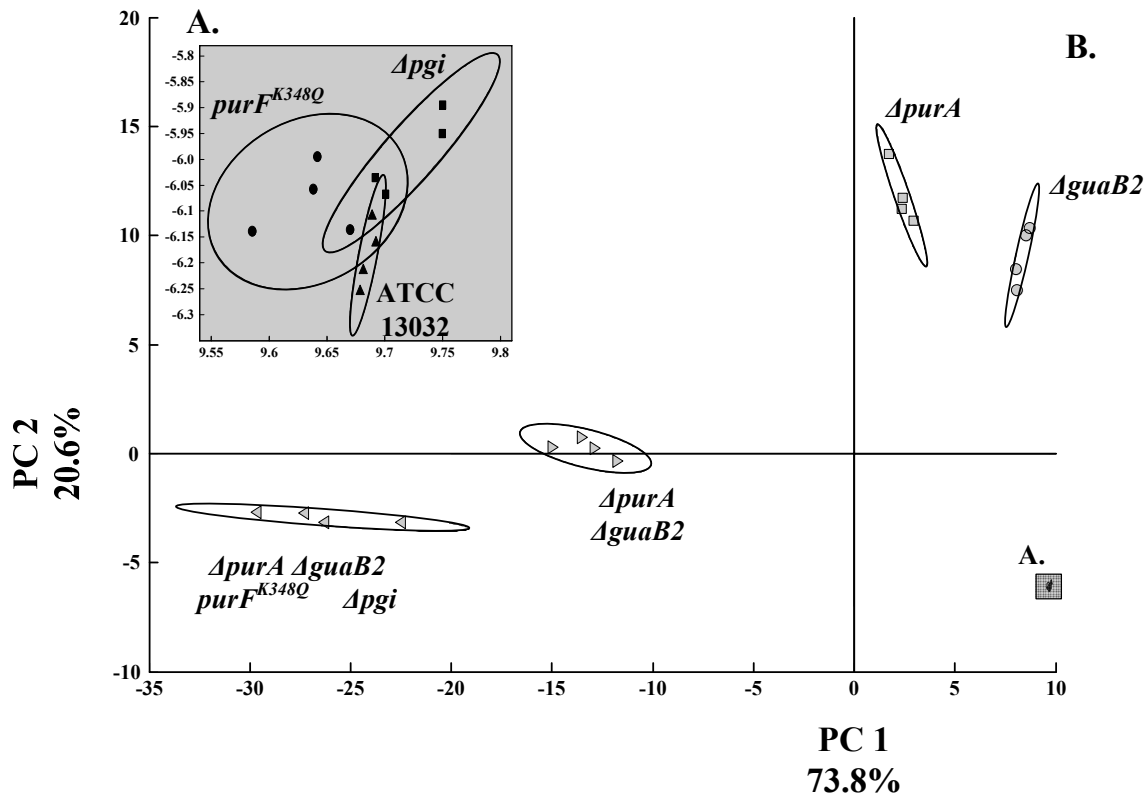
Figure IV-4. PCA score plots of principal components 1 and 2 for *C. glutamicum* ATCC 13032, *C. glutamicum Δpgi*, *C. glutamicum purF^K348Q*, *C. glutamicum ΔpurA*, *C. glutamicum ΔguaB2*, *C. glutamicum ΔpurA ΔguaB2* and *C. glutamicum ΔpurA ΔguaB2 purF^K348Q Δpgi*. The metabolite profiling was performed using cell extracts of exponentially growing cultures (n = 4 for each strain). The respective seven strains are shown with corresponding 95% confidence intervals. Data were pareto scaled. The gray insert depicts the analysis of *C. glutamicum* ATCC 13032, *C. glutamicum Δpgi* and *C. glutamicum purF^K348Q* (zoomed from the right lower corner). For *C. glutamicum ΔpurA* and *C. glutamicum ΔguaB2*, data obtained for phase 2 were considered (see Table IV-3).

The first two components contributed to more than 90% of the total variance. As shown in the score plot, a distinct separation pattern defining two groups could be derived (Figure IV-4). The first group (A.), comprising the wild type strain, the *pgi* deletion strain and the *purF* substituent, did not show any significant differences concerning intracellular purine intermediate pool sizes. As discussed earlier (see *"Manipulating the main carbon flux distribution"* and *"Targeted perturbations of the purine biosynthetic pathway"* –

"Results"), only minor changes with respect to intracellular concentration of purine pathway intermediates were caused by these genetic manipulations, which in direct comparison to the second group (B.) were quite consistent. The second group (B.), however, resulted in a broader clustering pattern comprising intrinsic dissimilarities. As shown by loading coefficients (Figure IV-5), the separation was mainly caused by the component IMP and its degradation product hypoxanthine, reflecting the observed shift from nucleotide accumulation towards increased degradation.
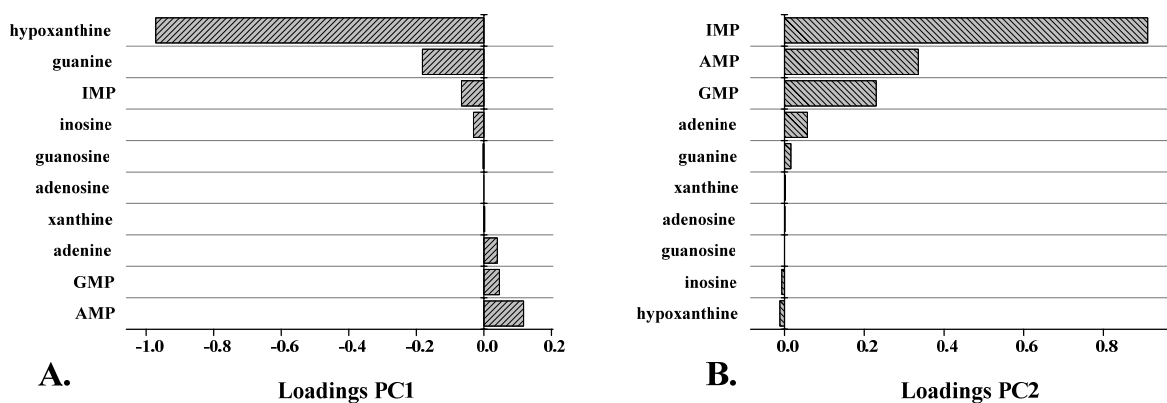
Figure IV-5. Loading coefficients for the first (**A.**) and second (**B.**) principal component obtained from multivariate analysis (Figure IV-4).

The disruption of critical nodes in the purine pathway itself, *i.e.* the conversion of IMP to AMP and GMP, provided the required fundamental basis for far-reaching effects when combined with additional modifications as the *pgi* gene deletion.

Solely based on the metabolome data, no clear link between the additional genetic manipulation of the *pgi* deletion and the increased degradation shift could be concluded. Therefore, the research was extended by an in-depth fluxome analysis to capture integrative effects of fluxome and metabolome.

Connectivity of targeted metabolome and fluxome analysis

In the context of purine accumulation, alterations in the PPP-TCA cycle ratio were of special interest, as their relative activities and especially the flux partitioning into these two main branches, mainly dictate the XADH ($NADH+FADH_2$) supply and thus ATP formation in the respiratory chain (Noguchi et al., 2003). The exclusive metabolization of glucose 6-phosphate via the PPP caused a major carbon flux redistribution in *C. glutamicum ΔpurA ΔguaB2 purF^{K348Q} Δpgi*, having an adverse effect on XADH formation compared to *C. glutamicum ΔpurA ΔguaB2* (Figure IV-3) and initiating a shift in the metabolic profile towards inosine and especially hypoxanthine formation. Since most XADH is generated in the TCA cycle, high PPP activities inevitably lead to an increased CO_2 production via a decarboxylation reaction in the oxidative part of the PPP and thus to a reduced carbon availability for other metabolic branches, as seen for *C. glutamicum ΔpurA ΔguaB2 purF^{K348Q} Δpgi* (Figure IV-2). Within the scope of the tightly regulated purine biosynthesis, Noguchi et al. (2003) presumed a connection between a declining ATP supply and an increasing degrading efficiency within this pathway. The results obtained in this study are consistent with those obtained previously (Noguchi et al., 2003). This suggests further metabolic engineering targets to increase intracellular IMP levels focusing on IMP degrading reactions.

Conclusions

In the present study, we performed an in-depth metabolic profiling of the purine biosynthetic pathway in *C. glutamicum*. Site-directed perturbations on the genetic level with subsequent studies of growth behavior and targeted metabolome analysis revealed a tight regulation of the underlying pathway with strong additional effects on the carbon flux distributions in the main metabolism as determined for *C. glutamicum ΔpurA ΔguaB2* and *C. glutamicum ΔpurA ΔguaB2 purF^{K348Q} Δpgi.*

Our results underline the importance of combined analyses employing different hierarchical levels such as fluxome and metabolome to reveal trends which indicate active regulation mechanisms. The regulatory processes maintaining balanced intracellular concentrations have not been fully discovered yet and necessitate further investigation. Complex future studies will thus focus on the redox and energy metabolisms, which were beyond the scope of the present analyses. In addition, it might be interesting to further analyze the metabolic instabilities – detected for *C. glutamicum ΔpurA* and *C. glutamicum ΔguaB2*. These instabilities were caused by the alteration of the complex regulatory structure of this pathway branch, opening up a way for in-depth surveys of this essential pathway in prokaryotes as well as in eukaryotes.

In order to achieve an understanding of the global cellular response, individual parts of the underlying network*, i.e.* precursor and cofactor supply, energy and redox metabolism, should not be assumed as independent, individual but interconnected units, linked by various key metabolites such as ATP or NAD(P)H.

Acknowledgments

Chapter V

Refining and redefining metabolic networks

Restriction of the metabolic flexibility due to *pgi* gene deletion triggers a unique adaptation process in *C. glutamicum* involving increased oxygen uptake

Abstract*

The flexibility and adaptability of the Gram-positive soil bacterium *Corynebacterium glutamicum* to various environmental as well as genetic perturbations provides the basis for the pronounced robustness of this organism. However, if essential key genes, as the glucose 6-phosphate isomerase (*pgi*), are deleted, the metabolic flexibility and concomitantly the overall growth performance is tremendously declining, ultimately resulting in complete growth stagnation, caused by NADPH imbalances.

This work describes physiological changes, triggered by *pgi* deletion in *C. glutamicum*. Thereby analysis of growth behavior, ^{13}C metabolic flux analyses and intracellular quantitation of the redox cofactors NADPH and NADP$^+$ were performed. Combining those approaches, a unique adaptation process of *C. glutamicum* upon *pgi* deletion was determined, resulting in increased specific oxygen uptake rates, surpassing the oxygen demand for NADH reoxidation in the respiratory chain. This phenomenon exclusively occurred in *pgi* deletion strains used in this work. Findings from ^{13}C metabolic flux analysis excluded malic enzyme as the sole reoxidation route for NADPH besides biomass formation, which was further confirmed by the deletion of this enzyme (*C. glutamicum ΔmalE Δpgi)*. Excessive oxygen not required for NADH reoxidation might partly participate in reoxidation of surplus NADPH.

Introduction

The carbon contained in metabolized substrates such as glucose gets distributed through the entire metabolic network depending on the flux activities of the contributing pathways to supply building blocks required for biomass formation. In addition to the supply of precursor molecules, redox equivalent requirements – NADH and NADPH – have to be covered and evenly balanced (Dominguez et al., 1998), as this would otherwise result in an impairment of cellular growth or even in its termination (Nissen et al., 2001).

The redox equivalents NADH and NADPH, chemically very similar, possess however fundamental distinctions within the cellular metabolism: NADH is linked to catabolic reactions (Verho et al., 2003) and used in the respiratory chain to meet the anabolic ATP demand, while NADPH, in contrast, functions as a reducing equivalent in anabolic reactions participating in biomass formation. These two systems – $NAD^+/NADH$ and $NADPH/NADP^+$ – are thus not in a thermodynamic equilibrium (Fuhrer and Sauer, 2009) while the $NAD^+/NADH$ ratio exhibits a rather oxidized state and the $NADPH/NADP^+$ ratio a rather reduced state.

During aerobic growth, NADH is generally produced in excess as the net anabolic biomass formation additionally generates NADH. This surplus is then used to drive ATP generation via the respiratory chain. NADPH, however, is used in anabolic reduction and – if present – product formation reactions. A question that has been addressed frequently, is the manner in which adequate amounts of NADPH are provided and excessive availability is equalized (Fuhrer and Sauer, 2009; Hua et al., 2003). Several mechanisms in different organisms have been reported so far, ensuring network-wide balancing of this redox equivalent (Fuhrer and Sauer, 2009).

One mechanism found to be essential in *E. coli*, is the employment of transhydrogenases, generating a biomass-decoupled system to convert NADPH and NADH (Canonaco et al., 2001; Sauer et al., 2004). This system was found to be active in terms of NADPH deficiencies, providing NADPH by the membrane-bound transhydrogenase PntAB, as well as oxidizing NADPH in case of overabundances, employing the soluble isoenzyme UdhA

(Sauer et al., 2004). Transhydrogenases are not limited to *E. coli* but mainly studied in this organism (Auriol et al., 2011) and were in addition found to be active *i.a.* in *Bacillus subtilis* and *Paracoccus versutus* as determined by Fuhrer and Sauer (2009).

In organisms lacking transhydrogenases, alternative systems evolved, such as for example usage of enzymes exhibiting dual cofactor specificities or the existence of different isoenzymes with distinct cofactor specificities (Fuhrer and Sauer, 2009) as observed in *Agrobacterium tumefaciens, Rhodobacter spaeroides, Sinorhizobium meliloti* and *Zymomonas mobilis.* One organism neither possessing an active transhydrogenase, isoenzymes nor enzymes exhibiting dual cofactor-specificities in terms of NADPH-dependencies (Kalinowski et al., 2003) is *C. glutamicum.*

In this work we addressed the question of alternative NADPH oxidizing systems that could balance catabolic NADPH formation and anabolic consumption under excessive NADPH generating conditions. We therefore restructured the central metabolism of *C. glutamicum* using rational metabolic engineering, forcing an increased PPP activity via a glucose 6-phosphate isomerase (*pgi*) deletion and thus elevated the NADPH generation. In a combined analysis, employing ^{13}C metabolic flux analysis, quantification of intracellular redox equivalents and off-gas analysis we investigated the metabolic response based on the implemented genetic modification.

Materials and methods

Strains and plasmids

The wild type strain *C. glutamicum* ATCC 13032 was purchased from the American Type Culture Collection (Manassas, VA, USA) and used as reference strain for further modifications. Cloning and plasmid construction was performed employing *E. coli* DH5α as host strain, whereas plasmid amplification and introduction of the coryne-specific methylation were carried out in *E. coli* NM522^{pTC}. In *E. coli* NM522^{pTC} the pTC plasmid, harboring an origin of replication (*ori*) for *E. coli*, a tetracycline resistance as selection marker and the DNA-methyltransferase gene from *C. glutamicum*, was co-expressed in order to transfer the methylation pattern of *C. glutamicum* to the integrative plasmids. The non-replicating vector used for integrative genetic modifications in *C. glutamicum*, pClik, contained a *multiple cloning site* (MCS), selection markers for kanamycin (Kan^R) and sacB and an *ori* for *E. coli*. The constructed pClik-derivates were used for homologous replacement of the native gene sequences with the modified ones. Transformation of *C. glutamicum* and subsequent selection on Kan^R yielded transformants with genome-integrated plasmids via single crossover. The second recombination event was depicted by the *sacB* positive selection system on sucrose (Jager et al., 1992). Kan^R-sensitive and sucrose-insensitive clones were tested for the existence of the modified gene sequence via PCR and positive clones were additionally sequenced.

In the present work, perturbations of the pentose phosphate pathway and the malic enzyme with regard to general growth behavior and metabolic flexibility were investigated. In order to manipulate these metabolic pathways, gene deletions affecting glucose 6-phosphate isomerase (*pgi*) and/or malic enzyme (*malE*) were performed.

The site-directed mutants and corresponding genetic modifications performed in this study are depicted in Table V-1. Primer sequences used for verification are listed in Table V-2.

Table V-1. *C. glutamicum* strains constructed in the present study: Mutant strains of *C. glutamicum* based on the wild type strain (ATCC 13032) were constructed by targeted mutagenesis. Plasmid construction and methylation were performed employing *E. coli* strains.

strain	genotype	reference
C. glutamicum ATCC 13032	wild type	American Type Culture Collection
C. glutamicum Δpgi	deletion of the *pgi* gene	This work
C. glutamicum ΔmalE	deletion of the *malE* gene	This work
C. glutamicum ΔmalE Δpgi	double deletion of *malE* and *pgi* genes	This work
E. coli DH5α	F⁻endA1, hsdR17(rk⁻mk⁺) supE44, thi-1λ⁻ recAI gyrA96 relA1 Φ80ΔlacAm15	(Hanahan, 1983)
E. coli NM522^{pTC}	*supE thi-1 Δ(lac-proAB) Δ(mcrB-hsdSM)5 (rK⁻ mK⁺) [F′ proAB lacIqZΔM15]*	Stratagene

Table V-2. Genotypes and corresponding site-specific primer sequences used for verification (F, forward; R, reverse).

mutant genotype	primer	primer sequence
Δpgi	*Δpgi*-F	5′-GATCACGCGTATCCCTTCTCCGGCATC-3′
	Δpgi-R	5′-GATCTCTAGATCCAGCGACACGAATAATC-3′
ΔmalE	*ΔmalE*-F	5′-GATCACGCGTTCAGCCCACTGAATCAAC-3′
	ΔmalE-R	5′-GATCTCTAGAGAATATCTACCACAAGACGC-3′

Recombinant DNA techniques and strain construction

Oligonucleotide synthesis was performed by Sigma-Aldrich (Steinheim, Germany) and DNA sequencing by GATC (Konstanz, Germany). Plasmid construction and DNA purification were performed applying standard techniques. Preparation of genomic DNA from *C. glutamicum* was carried out with the MasterPure[TM] Gram Positive DNA Purification Kit (Biozym Scientific GmbH, Germany). PCR reactions were performed in a TGradient-Cycler (Whatman – Biometra[R], Goettingen, Germany) with Phusion polymerase (Biozym, Hessisch Oldendorf, Germany) for insert construction and JumpStart REDTaq Ready Mix (Sigma-Aldrich) for strain verification. PCR products were purified using NucleoSpin® Extract II Kit (Macherey-Nagel, Düren, Germany) and plasmids using HiYield® Plasmid Mini Kit (SLG, Gauting, Germany). Ligation was done with Fast-Link[TM] DNA Ligation Kit (Epicentre Biotechnologies, Madison, WI, USA). FastDigest® restriction enzymes were obtained from Fermentas (St. Leon-Rot, Germany) as well as 10 mM dNTP Mix and 1-kb DNA O'GeneRuler[TM].

For transformation of *C. glutamicum,* cells were cultivated in BHI[++] medium (10 mL in 100 mL baffled shake flasks) for 12 hours. The main culture in BHI[++] medium (80 mL in 1000 mL baffled shake flasks) was inoculated from the exponentially growing preculture to an optical density OD_{660nm} of 0.2. 400 mg isonicotinic acid hydrazide, 2.5 g glycine and 0.1 mL Tween 80 were dissolved in 20 mL H_2O, sterilized by filtration and added to the main culture at an OD_{660nm} of 0.6. Cells were harvested by centrifugation (7 min, 4,000 *g*, 4°C, Laborfuge 400R, Heraeus, Hanau, Germany) when an OD_{660nm} of 0.8 was reached. Cells were washed three times with pre-cooled wash-buffer (10% glycerine, 8 mM tris hydrochloride, pH 7.4) and once with 10% glycerine. After the second resuspension in 6 mL 10% glycerine, 200 µL cells were subsequently used for transformation by electroporation as described previously (Tauch et al., 2002; van der Rest et al., 1999).

Transformation of *E. coli* DH5α and NM522[pTC] was performed by heat-shock (Inoue et al., 1990).

Chemicals

Yeast extract, polypeptone, casamino acids, beef extract and brain heart infusion (BHI) were purchased from Difco Laboratories (Detroit, USA). 99% enriched glucose, *i.e.* [1-^{13}C] and [1,2-^{13}C$_2$], were obtained from Cambridge Isotope Laboratories (Andover, MA, USA). All other chemicals and reagents were purchased from Sigma-Aldrich, Merck (Darmstadt, Germany), Fluka (Buchs, Switzerland), Roth (Karlsruhe, Germany) and Roche Diagnostics (Mannheim, Germany) and were of analytical grade unless stated otherwise.

Media

The first precultures were grown on complex media containing per liter (pH 6.8): 10.0 g glucose, 2.5 g NaCl, 2.0 g urea, 5.0 g yeast extract, 5.0 g beef extract, 5.0 g polypeptone and 20.0 g casamino acids. For agar plates, the complex medium was supplemented with 20.0 g L^{-1} agar. Second precultures and main cultures were cultivated in minimal medium (pH 7.2) containing per liter: 15.0 g glucose, 4.0 g KH$_2$PO$_4$, 16.0 g Na$_2$HPO$_4$, 500 mg MgCl$_2 \cdot$ 6 H$_2$O, 300 mg 3,4-dihydroxybenzoic acid, 100 mg CaCl$_2 \cdot$ 2 H$_2$O, 100 μg cyanocobalamin, 750 μg thiamine, 4 μg pyridoxal phosphate, 100 μg biotin, 400 μg calcium pantothenate, 2 μg folic acid, 400 μg nicotinic acid, 200 μg 4-aminobenzoic acid, 400 μg pyridoxine $\cdot$ HCl, 2 mg inositol, 10 mg FeCl$_2 \cdot$ 4 H$_2$O, 1 mg ZnCl$_2$, 100 μg CuCl$_2$, 20 μg NiCl$_2 \cdot$ 6 H$_2$O, 20 μg Na$_2$MoO$_4 \cdot$ 2 H$_2$O, 500 μg boric acid, 100 μg KI, 100 μg CoCl$_2 \cdot$ 6 H$_2$O, 10 mg MnCl$_2 \cdot$ 4 H$_2$O. For tracer studies, naturally labeled glucose was replaced by 99% ^{13}C enriched [1-^{13}C] or [1,2-^{13}C$_2$] glucose for analysis of glucose 6-phosphate isomerase (*pgi*) deletion mutants and the volume was adjusted to 5 mL in 50 mL baffled shake flasks.

Media applied for transformation experiments of *C. glutamicum* contained per liter: 37 g BHI, 26.4 g (NH$_4$)$_2$SO$_4$ and 40 g glucose for BHI^{++} and 37 g BHI and 46 g sorbitol for BHIS medium.

Cultivation conditions

Cultivations were carried out in baffled shake flasks on an orbital shaker (Multitron 2, Infors AG, Bottmingen, Switzerland) at 230 rpm and 30°C. First precultures were grown on complex medium (25 mL medium in 250 mL baffled flasks) for 8 h and used for inoculation of the second precultures (25 mL medium in 250 mL baffled flasks). Second precultures and main cultures were performed in minimal medium. Main cultivations were carried out in a 500 mL stirred tank bioreactor (Meredos, Bovenden, Germany) containing 75 mL minimal medium at 30°C and 1,000 rpm maintaining dissolved oxygen concentrations above 40% air saturation throughout the entire cultivation. The gas flow was controlled at 1 vvm (vessel volume per minute) by a mass flow controller (WMR Compact4, Brooks Instruments, Veenedaal, Netherlands). The composition of aeration and exhaust gas was determined by a quadrupole mass spectrometer (Omnistar, Pfeiffer). Process variables, *i.e.* temperature, pH, agitation, dissolved oxygen and gas composition were collected and stored using the Lucullus process control system (Lucullus PIMS 2.1, Biospectra, Schlieren, Switzerland).

Cell disruption and quantification of enzymatic activities

Determination of the *in vitro* enzyme activities was performed in crude cell extracts. Therefore cells were cultivated in 25 mL minimal medium in 250 mL baffled shake flasks (precultures) which were used for inoculation of the main culture performed in 50 mL minimal medium in 500 mL baffled shake flasks. Cells were harvested by centrifugation (5 min, 9,800 g, 4°C) during mid-exponential growth phase and washed twice in disruption buffer (100 mM Tris/HCl, 10 mM $MgCl_2$, pH 7.5, 4°C). After resuspension in disruption buffer and addition of DTT (dithiothreitol) to a final concentration of 0.75 mM, 1 mL cell suspension was mixed with 100 mg glass beads (Ø 0.25 mm). Cell disruption was performed using a bead mill (Retsch, MM301, Hahn, Germany) at 30 Hz for 5 min (two times). Between disruption periods, the cell suspension was cooled on ice for 10 min. Cell debris was removed by centrifugation (15 min, 16,000 g, 4°C). The remaining crude cell extract was used for determination of the total protein content and enzymatic activities. The protein content was determined by the method of Bradford (1976) and the reagent

solution from Sigma-Aldrich with bovine serum albumin as external standard. *In vitro* enzymatic activities were determined for the NADP$^+$-dependent malic enzyme (MalE) and the first enzyme of the glyoxylate pathway, isocitrate lyase (IsoLy). For reactions based on NADPH formation, the molar extinction coefficient of the reduced pyridine-dinucleotide (ε_{340nm} = 6.22 mM^{-1}) was used, for those based on phenylhydrazone formation the extinction coefficient ε_{324nm} (17.0 mM^{-1}).

Malic enzyme. The reaction mixture contained 100 mM Tris/HCl (pH 7.8), 200 mM KCl, 2 mM MgCl$_2$, 1 mM NADP$^+$, 40 mM malate and 50 µL of the crude cell extract. The final protein content was between 0.2-0.4 g L^{-1}. Determination of the *in vitro* malic enzyme activity was based on the change of absorption at 340 nm due to NADPH formation.

Isocitrate lyase. Determination of the *in vitro* activity of isocitrate lyase in crude cell extracts of *C. glutamicum* was based on the protocol of de Jong-Gubbels et al. (1995) with slight modifications. The reaction mixture contained 50 mM MOPS (pH 7.3), 2.5 mM MgCl$_2$, 2.5 mM cysteine, 4 mM phenylhydrazine, 2 mM isocitrate and 50 µL of the crude cell extract. The final protein concentration was between 0.2-0.4 g L^{-1}. Determination of the enzymatic activity was based on the change of absorption at 324 nm due to the formation of glyoxylate phenylhydrazone.

Measurements were started by addition of the substrates, performed at 30°C and monitored for 15-30 min. Negative controls were performed without substrate or crude cell extract, respectively. All measurements were performed in a total volume of 1 mL and carried out in triplicate.

Analytics for extracellular substrate and product analysis

Cell concentrations were determined by measuring the optical density at 660 nm (OD$_{660nm}$) using a photometer (Marsha Pharmacia Biotech, Freiburg, Germany) and gravimetrically correlated to the cell dry weight. Supernatants from the cultivations obtained after 3 min centrifugation at 16,000 g were used for quantification of extracellular substrates and secreted products. Glucose, α-ketoglutarate and trehalose were quantified in diluted supernatants by HPLC (Kontron Instruments, Neufahrn, Germany) using an Aminex HPX-

87H Bio-Rad column (300 x 7.8 mm; Hercules, USA) at 55°C with a constant flow rate of 0.8 mL min^{-1} (7 mM H_2SO_4 as mobile phase). Quantification of sugars was performed using refraction index (RI) detection and UV detection at 218 nm for organic acids. Determination of amino acids was performed as described previously (Kromer et al., 2005).

Analytics for intracellular metabolite quantification

Due to varying pH stabilities of oxidized and reduced species of pyridine nucleotides, different extraction procedures (alkaline and acidic) were applied, resulting in the complete degradation of either the oxidized or reduced form. Thus a separate determination allowing absolute quantification of both species was provided.

Extraction of intracellular pyridine nucleotides ($NADP^+$, NADPH) was based on the protocol of Franco et al. (1984) and modified as follows: for all extractions, 2 mL samples from exponentially growing *C. glutamicum* cells were drawn in a syringe filled with 2 mL of the corresponding extraction solution, preheated to 55°C. For acidic extraction 1 M $HClO_4$ was used, for alkaline extraction 1 M KOH (50% ethanol; v:v). Instantaneous mixing of sample and extraction solution was ensured by the generated turbulences and additionally verified by colored test solutions (bromphenol blue and phenolphthalein). Incubation at 55°C was performed for 3 min, followed by addition of 500 μL 0.5 M potassium phosphate buffer (pH 7.0) and of adequate volumes of 2 M KOH or 1 M HCl for neutralization. After incubation on ice for 10 min, cell debris and insoluble macromolecules were removed by centrifugation (10 min, 4°C, 6,000 *g*).

Quantification of the extracted pyridine nucleotides was performed employing an enzymatic cycling assay according to Bernofsky and Swan (1973) which was slightly modified. The reaction mixture contained 120 mM bicine (pH 5.8), 0.4 g L^{-1} 5-ethylphenazinium ethyl sulfate (PES), 0.125 g L^{-1} thiazolyl blue (MTT), 375 μM glucose 6-phosphate, 50 μM $MgSO_4 \cdot 7 H_2O$, 1.4 U mL^{-1} glucose 6-phosphate dehydrogenase and 150-325 μL mL^{-1} cell extract.

Measurements were started by addition of glucose 6-phosphate dehydrogenase at 30 °C and monitored for 60 min at 560 nm (Reader Biorad, model 680XR). Negative controls were performed without cell extract. All measurements were carried out in microtiter plates in a total volume of 200 μL.

Determination of intracellular pyridine nucleotide concentrations normalized to the cell dry weight was achieved by simultaneous determination of the optical density for each sampling process. To ensure metabolic steady state and thus stable metabolite concentrations over the whole cultivation period, cultivations were performed in duplicate and samples were taken for two biomass concentrations, each as duplicate, resulting in 8 biological samples. Concentrations were determined for two replicates for each sample. Calibrations were carried out using separate external standard series for each compound in the range from 0.0125 μM to 0.25 μM.

Respiration analysis

In order to perform an in-depth analysis of the redox metabolism of *C. glutamicum*, including NADH, FADH and NADPH as redox cofactors, a complete cofactor balance was set up and compared to the wild type strain as described by Yang et al. (2006).
Reoxidation of NADH and FADH$_2$ (XADH) was balanced assuming sole reoxidation of XADH by oxygen. Thus the amount of XADH to be reoxidized by cellular metabolism is restricted by the specific oxygen uptake rate of the microbial culture as follows:

$$qO_2 - \tfrac{1}{2}\, q_{XADH} - \tfrac{1}{2}\, q_{NADPH} = 0. \qquad\qquad \textbf{[2]}$$

qO_2 corresponds to the specific oxygen uptake rate determined using inert gas balancing (Heinzle et al., 1990). q_{XADH}, accounting for metabolic fluxes involved in the production of XADH (catabolic and anabolic), and q_{NADPH}, accounting for fluxes involved in the production and consumption of NADPH (catabolic and anabolic), which can be calculated from the metabolic flux distribution determined by ^{13}C MFA as described by Becker et al. (2007) and Yang et al. (2006).

The anabolic NADH production of 3.2 mmol NADH per gram biomass was adopted from literature for *C. glutamicum* (Yang et al., 2006), as was the anabolic demand of 15.9 mmol NADPH per gram biomass (Yang et al., 2006).

Metabolic network analysis

The metabolic network of *C. glutamicum* including all main metabolic pathways utilized during growth on glucose comprises *i.e.* glycolysis, pentose phosphate pathway (PPP), tricarboxylic acid (TCA) cycle and anaplerosis. Since usage of [1-^{13}C] labeled glucose is insufficient to distinguish between phosphoenolpyruvate and pyruvate as well as oxaloacetate and malate pools, these pools were lumped together and only the net anaplerotic fluxes were calculated. Glyoxylate pathway was shown to be inactive and was therefore neglected. Anabolic pathways towards biomass production and production pathways for α-ketoglutarate, trehalose and glycine were incorporated in the metabolic network topology. For determination of the metabolic fluxes of mutants comprising the *pgi* deletion [1,2-^{13}C$_2$] labeled glucose was used instead of [1-^{13}C] labeled glucose.

Calculation of the *in vivo* metabolic fluxes of the *C. glutamicum* strains was carried out by fitting simulated mass isotopomer distributions to experimentally determined labeling patterns of amino acids derived from cellular protein and trehalose secreted during cultivation. The calculations were based on the approach of Yang et al. (2008) implemented in Matlab (version 2008b, Mathworks Inc., Nattick, USA) using metabolite and isotopomer balancing. The hydrolyzed amino acids were analyzed by GC-MS and corresponding single mass isotopomer fractions were determined as described previously (Kiefer et al., 2004; Wittmann et al., 2004a). The labeling pattern of secreted trehalose was determined from supernatants as described by Wittmann et al. (2004b). All samples were analyzed in scan mode thereby exluding isobaric interferences between analytes and sample components.

Mass isotopomer fractions of amino acids and trehalose were determined using selective ion monitoring (SIM) mode in duplicates. In order to account for naturally occurring isotopes in the fragments and derivatization groups, measured GC-MS data were corrected (van Winden et al., 2002; Wittmann and Heinzle, 1999) and fitted to the simulated

isotopomer distributions. [13]C enrichment for amino acids was determined on the basis of the [M-57] fragments except for leucine ([M-157]). The mass isotopomer distribution of trehalose was analyzed for the *m/z* 361 fragment consisting of one glucose moiety. Anabolic demands for biomass synthesis and extracellular production rates ware additionally considered and implemented in the metabolic network. A Monte Carlo approach with 100 independent runs was employed for the statistical analysis of metabolic flux estimations (Wittmann and Heinzle, 2002).

Results and discussion

All strains analyzed in this study were characterized in terms of growth and carbon flux distribution, especially emphasizing redox metabolism. The metabolic flux analysis, focusing on the central metabolism of *C. glutamicum,* was performed in order to unravel the metabolic consequences of the genetic modifications and to highlight the cellular response due to manipulations of the cofactor metabolism of NADPH. All genetic modifications were validated on genomic level by PCR as well as on the physiological level by measuring enzymatic activities. In the case of the *pgi* deletion, validation was carried out using [1-^{13}C] labeled glucose and comparing the obtained isotopomer distribution for alanine. Due to the decarboxylating reaction in the oxidative branch of the PPP, the ^{13}C labeled carbon atom of glucose is completely decarboxylated resulting in the natural isotopomer distribution of alanine (data not shown). This proves the absence of any activity of the glycolysis pathway,

NADPH metabolism in C. glutamicum wild type ATCC 13032

Using a combination of ^{13}C flux analysis and a metabolomic approach focusing on the intracellular redox equivalent concentrations, NADPH metabolism of wild type strain *C. glutamicum* was investigated and compared with the mutant exhibiting the *pgi* deletion, *C. glutamicum Δpgi*. Since the PPP is considered to operate as the main pathway providing NADPH (Lee et al., 2010), modifications targeting this pathway were investigated in great detail with respect to NADPH demanding biotechnological product formation (Becker et al., 2007; Becker et al., 2011). However, even in case of high NADPH demands, the NADPH supply has to be balanced which is further complicated in strains lacking any additional NADPH sink. In this case a cellular response has to be triggered that eventually balances producing and consuming reactions. This metabolic modulation can generally be performed by a number of diverse mechanisms in different organisms, *e.g.* employing transhydrogenases (Sauer et al., 2004), applying unspecific cofactor dependencies of

different enzymes (Fuhrer and Sauer, 2009), or activating latent pathways (Fong et al., 2006; Hua et al., 2003).

Calculation of NADPH generating fluxes was based on the metabolic flux distributions determined for each strain and comprised reactions catalyzed by the glucose 6-phosphate dehydrogenase (G6PDH), the 6-phosphogluconate dehydrogenase (6PGDH) and the isocitrate dehydrogenase (ICD), where the carbon flux is equivalent to the NADPH generation. Calculations of the NADPH consuming fluxes considered the NADPH requirements for biomass formation which are linked to the stoichiometry of the biosynthetic reactions, the cell composition and the biomass yield. The activity of the malic enzyme (MalE), also involved in NADPH metabolism, was considered separately since previous studies reported no contribution to NADPH formation in the wild type strain (Kromer et al., 2008; Petersen et al., 2000) during growth on glucose.

Growth parameters are summarized in Table V-3 for the *C. glutamicum* strains subjected to the implemented genetic manipulations.

In addition, carbon balances were set up and determined to be statistically closed for all strains analyzed in this work, ensuring that all main products were considered.

Table V-3. Growth parameters (specific growth rates [µ], biomass yields [$Y_{X/S}$], specific uptake rates [q_S, q_{O2}] and production rates [q_{CO2}]) with corresponding standard deviations and carbon balances for the wild type strain (*C. glutamicum* ATCC 13032) and site-directed mutants (*C. glutamicum Δpgi, C. glutamicum ΔmalE* and *C. glutamicum ΔmalE Δpgi)* grown on glucose.

parameter		ATCC 13032			*Δpgi*			*ΔmalE*			*ΔmalE Δpgi*		
µ		0.443	±	0.004	0.376	±	0.001	0.439	±	0.002	0.345	±	0.002
$Y_{X/S}$		0.095	±	0.005	0.090	±	0.002	0.093	±	0.004	0.082	±	0.005
q_s		4.67	±	0.09	4.18	±	0.02	4.73	±	0.02	4.21	±	0.06
q_{O2}		8.55	±	0.21	8.71	±	0.26	10.84	±	0.32	9.98	±	0.29
q_{CO2}		8.85	±	0.19	9.56	±	0.12	11.26	±	0.23	10.41	±	0.21
Carbon balance	[%]	97.4	±	1.1	102.0	±	1.2	104.0	±	3.5	105.3	±	3.4

data represent mean values obtained from two parallel cultivations with corresponding standard deviations: specific growth rates (µ) [h^{-1}]; biomass yields ($Y_{X/S}$) [g $mmol^{-1}$], specific glucose consumption rates (q_S) [mmol g^{-1} h^{-1}], specific oxygen uptake rates (q_{O2}) [mmol g^{-1} h^{-1}] and specific CO_2 production rates (q_{CO2}) [mmol g^{-1} h^{-1}].

Metabolic flux distributions obtained for the different strains, as well as the corresponding NADPH balances are shown in Table V-4 and Figure V-1, respectively.

Table V-4. Intracellular carbon flux distributions [%] with corresponding standard deviations[a] determined for *C. glutamicum* ATCC 13032, *C. glutamicum Δpgi*, *C. glutamicum ΔmalE* and *C. glutamicum ΔmalE Δpgi*.

flux parameter	ATCC 13032			Δpgi			ΔmalE			ΔmalE Δpgi		
G6P isomerase	52.2	±	1.3		--		54.6	±	3.6		--	
G6P DH	44.9	±	1.3	97.8	±	0.1	43.0	±	3.6	97.7	±	0.1
transketolase 1	12.9	±	0.4	30.8	±	0.0	12.6	±	1.2	30.9	±	0.0
transketolase 2	10.3	±	0.4	28.4	±	0.0	10.4	±	1.2	28.7	±	0.0
aldolase	72.3	±	0.4	56.4	±	0.1	75.0	±	1.1	57.1	±	0.1
G3P DH	153.7	±	0.4	140.1	±	0.3	159.3	±	0.9	141.9	±	0.4
enolase	140.0	±	0.4	128.7	±	0.3	147.5	±	0.8	130.7	±	0.5
pyruvate DH	78.8	±	0.4	73.8	±	0.7	95.6	±	0.8	80.1	±	1.3
citrate synthase	47.3	±	0.4	45.7	±	0.9	68.9	±	1.0	54.1	±	1.6
α-ketoglutarate DH	35.0	±	0.4	34.6	±	0.9	58.4	±	1.1	44.0	±	1.8
pyruvate carboxylase[b]	29.0[c]	±	0.0	25.9[d]	±	0.2	24.6	±	0.2	23.9	±	0.4

data are given as relative fluxes [%] normalized to the specific glucose uptake rates q_S (see Table V-3), which were set to 100%.

[a] mean values and standard deviations were calculated from 100 independent Monte Carlo runs.

[b] given as net flux through anaplerotic reactions.

[c] carboxylating and decarboxylating reactions of the anaplerosis of *C. glutamicum* ATCC 13032 were 40.1 ± 2.0% and 11.1 ± 2.0%, respectively.

[d] carboxylating and decarboxylating reactions of the anaplerosis of *C. glutamicum Δpgi* were 49.7 ± 3.8% and 23.8 ± 3.7%, respectively.

The high biomass yield of 0.095 g_{CDW} $mmol_{glucose}^{-1}$ obtained for the wild type strain caused a high NADPH demand for anabolic reactions which was almost identical to combined generating reactions of the G6PDH, 6PGDH and ICD (Figure V-1).
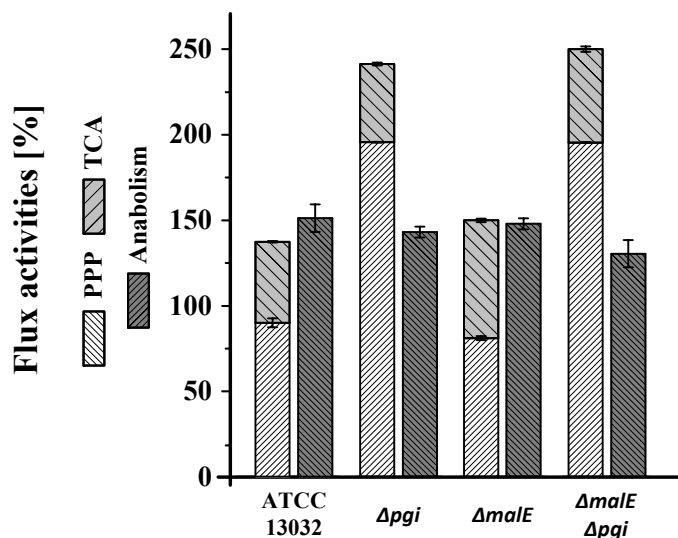
Figure V-1. NADPH balances for *C. glutamicum* ATCC 13032, *C. glutamicum Δpgi,* *C. glutamicum ΔmalE* and *C. glutamicum ΔmalE Δpgi* comprising NADPH generating reactions of the PPP (G6PDH and 6PGDH) and TCA cycle (ICD). Anabolism with a stoichiometric NADPH demand of 15.9 mmol g_{CDW}^{-1} (Yang et al., 2006) was considered as consuming reaction.

Deregulation of the pentose phosphate pathway activity

As depicted in Table V-4, *pgi* deletion caused a complete redirection of the carbon flux through the oxidative branch of the PPP (97.8%), resulting in a tremendous surplus of NADPH (98.1%) exceeding the anabolic capacities (Figure V-1), as was further supported by the increasing intracellular NADPH/NADP$^+$ ratio of 4.3 ± 2.8 (wild type 2.8 ± 1.4; Table V-5). As an evenly balanced redox metabolism is a prerequisite for balanced growth, additional so far unassigned NADPH consuming reactions must be present.

Table V-5. Intracellular concentrations [µmol g_{CDW}^{-1}] of NADPH and NADP$^+$ with corresponding ratios [-] for *C. glutamicum* ATCC 13032, *C. glutamicum Δpgi*, *C. glutamicum ΔmalE* and *C. glutamicum ΔmalE Δpgi*.

strain	NADPH concentration			NADP$^+$ concentration			NADPH/NADP$^+$ ratio [-]		
ATCC 13032	0.324	±	0.036	0.117	±	0.057	2.8	±	1.4
Δpgi	0.437	±	0.094	0.101	±	0.063	4.3	±	2.8
ΔmalE	0.356	±	0.030	0.100	±	0.008	3.6	±	0.4
ΔmalE Δpgi	0.699	±	0.043	0.041	±	0.005	17.1	±	2.4

A potential reported candidate for NADPH oxidation is malic enzyme (MalE) operating in carboxylating direction (Becker et al., 2007). Though even considering an exclusive carboxylating activity solely by MalE – determined by the anaplerotic flux activity derived from ^{13}C MFA – the NADPH surplus in *C. glutamicum Δpgi* (98.1%), could not be balanced (Table V-6). In sharp contrast to the transhydrogenase of *E. coli*, the electron-transferring capacity of MalE of *C. glutamicum* is restricted by the corresponding flux activity through the carboxylating reaction of the anaplerosis (49.7% maximal activity in *C. glutamicum Δpgi*; Table V-4).

As MalE however seems to be involved in this NADPH balancing process, it was deleted, resulting in a *malE* deficient strain (*C. glutamicum ΔmalE)* and a *pgi-malE* double deletion mutant (*C. glutamicum ΔmalE Δpgi)*. The consequences in terms of growth behavior, *i.e.* specific growth rate, were then investigated and the participation of this enzyme in relation to the different genetic perturbations was determined.

Perturbations of the malic enzyme activity

Tables V-3 and V-4 depict the growth characteristics and carbon flux distributions determined for *C. glutamicum ΔmalE*. Deletion of *malE* caused a slight reduction of the biomass yield while the growth rate was not affected significantly compared to the wild type strain (Table V-3). Figure V-1 illustrates the NADPH supply (154.9 ± 5.2%) and demand (148.2 ± 3.2%) with respect to the glucose uptake rate which were evenly balanced. The NADPH/NADP$^+$ ratio did not differ significantly in *C. glutamicum ΔmalE* (3.6 ± 0.4) compared to the wild type (2.8 ± 1.4). As malic enzyme was reported to be dispensable for growth of *C. glutamicum* on glucose, exhibiting no observable phenotype (Gourdon et al., 2000; Sauer and Eikmanns, 2005), its function was assumed to generate NADPH on substrates linked with low PPP activities *e.g.* lactate (Georgi et al., 2005). This hypothesis is consistent with the results obtained in this study.

Combined deletion of pgi and malE genes: probing the network rigidity

The previously investigated single deletions of *malic enzyme* and *glucose 6-phosphate isomerase* were combined and the carbon flux distributions as well as the NADPH requirements were analyzed. The double deletion mutant *C. glutamicum ΔmalE Δpgi* was constructed, forcing the carbon flux entirely through the oxidative branch of the PPP and simultaneously constraining the potential NADPH oxidizing possibilities by deleting the malic enzyme. Thus, the central metabolism was restructured towards a linear pathway lacking the possibility to adjust the NADPH producing pathways (PPP and TCA). As expected, excessive usage of the PPP caused a tremendous NADPH generation of 195.4%, clearly exceeding the anabolic demand of 130.4%. The additional NADPH generation by the TCA cycle led to a further increase in the NADPH overabundance, resulting in a total NADPH supply of 250.0% (Figure V-1). The NADPH/NADP$^+$ ratio increased immensely to 17.1 ± 2.4 compared to 2.8 ± 1.4 in the wild type.

As MalE did not exhibit any detectable activity under *in vitro* conditions (0.0 ± 0.1 mU mg$_{protein}^{-1}$) in *C. glutamicum ΔmalE Δpgi* , this potential NADPH oxidizing system could be excluded. Even though an *in vitro* activity of 133.3 ± 2.2 mU mg$_{protein}^{-1}$ was detected in *C. glutamicum Δpgi*, the NADPH surplus in *C. glutamicum Δpgi* was likewise found to

exceed the NADPH oxidizing capacities of MalE. Concluding, no metabolic reoxidation mechanism was found to match the NADPH requirements in either *C. glutamicum Δpgi* or *C. glutamicum ΔmalE Δpgi*. As a NADPH overabundance is deleterious, additional so far unconsidered reoxidizing mechanisms have to be present upon *pgi* deletion. One possibility *i.e.* the NADPH oxidizing capacity of the respiratory chain of *C. glutamicum* (Matsushita et al., 2001) was further investigated.

Investigations of the NADPH reoxidation capacity of C. glutamicum: alternative NADPH oxidizing mechanisms

Over the recent years, the NADPH metabolism of *C. glutamicum* and especially the corresponding balancing capacities were addressed in various works (Becker et al., 2007; Kromer et al., 2008; Kromer et al., 2004). An excellent study was published by Becker et al. (2007) investigating the problem of a NADPH surplus in genetically modified *C. glutamicum* strains considering the possibility of a NADPH oxidation via the respiratory chain. The NADH oxidizing enzyme NADH-ubiquinone-1 oxidoreductase of *C. glutamicum* exhibits an additional NADPH oxidizing function (Matsushita et al., 2001; Molenaar et al., 2000) which is linked with the deleterious generation of *reactive oxygen species* (ROS). The oxidation of NADPH via the respiratory chain by molecular oxygen would however lead to an increased oxygen consumption eventually surpassing the oxygen demand needed for NADH oxidation. The oxygen uptake rate determined for all strains in this work matched the required oxygen for complete NADH reoxidation in case of the wild type strain and *C. glutamicum ΔmalE* (Table V-6).

Table V-6. CO_2 and redox balances for XADH (NADH and $FADH_2$) and NADPH [%] of *C. glutamicum* ATCC 13032, *C. glutamicum Δpgi, C. glutamicum ΔmalE* and *C. glutamicum ΔmalE Δpgi* with corresponding oxygen consumptions [%].

	ATCC 13032			Δpgi			ΔmalE			ΔmalE Δpgi		
CO_2 production[a]												
gluconate 6PDH	44.9	±	1.3	97.8	±	0.1	43.0	±	3.6	97.7	±	0.1
pyruvate DH	78.8	±	0.4	73.8	±	0.7	95.6	±	0.3	80.1	±	1.3
ICDH	47.3	±	0.4	45.7	±	0.9	68.9	±	1.0	54.1	±	1.6
α-ketoglutarate DH	35.0	±	0.4	34.6	±	0.9	58.4	±	1.1	44.0	±	1.8
anabolism[b]	10.1	±	0.4	9.2	±	0.2	9.5	±	0.2	8.4	±	0.1
CO_2 consumption												
anaplerosis	29.0	±	0.0	25.9	±	0.2	24.6	±	0.2	23.9	±	0.4
Total$_{calc}$ [%][a]	187.2	±	1.5	235.2	±	1.4	250.9	±	3.6	260.3	±	2.8
Total$_{meas}$[%][c]	189.5	±	4.1	228.7	±	2.9	238.0	±	4.9	247.2	±	5.0
NADH production												
G3P DH	153.7	±	0.4	140.1	±	0.3	159.3	±	0.9	141.9	±	0.4
pyruvate DH	78.8	±	0.4	73.8	±	0.7	95.6	±	0.8	80.1	±	1.3
α-ketoglutarate DH[d]	105.0	±	1.2	103.8	±	2.7	175.2	±	3.3	132.0	±	5.4
anabolism	31.7	±	0.3	28.8	±	0.6	29.8	±	0.6	26.2	±	1.6
Total XADH [%]	369.2	±	1.4	346.5	±	2.9	459.9	±	3.6	380.2	±	5.8
O_2 consumption [%]	183.1	±	4.5	208.4	±	6.2	229.2	±	6.8	237.0	±	6.9
Redox balance [%]	-3.0	±	9.1	70.3	±	12.7	-1.5	±	14.1	93.8	±	15.0
NADPH production												
G6P DH	44.9	±	2.6	97.8	±	0.1	43.0	±	3.6	97.7	±	0.1
gluconate 6PDH	44.9	±	2.6	97.8	±	0.1	43.0	±	3.6	97.7	±	0.1
ICD	47.3	±	0.4	45.7	±	0.8	68.9	±	1.1	54.1	±	1.6
NADPH consumption												
anabolism	151.1	±	8.0	143.1	±	3.2	148.2	±	3.2	130.4	±	8.0
Total NADPH [%]	-14.0	±	8.2	98.1	±	0.9	6.7	±	7.4	119.2	±	8.1

[a] calculated from carbon flux distributions (Table V-4).

[b] anabolism with a stoichiometric CO_2 generation of 1.025 mmol g_{CDW}^{-1} was considered as producing reaction (Yang et al., 2005).

Upon *pgi* deletion (*C. glutamicum Δpgi* and *C. glutamicum ΔmalE Δpgi*) the oxygen uptake rates significantly surpassed the demand for XADH reoxidation (Table V-5). Further, a physiological phenomenon emerged in those strains comprising the *pgi* deletion, *i.e. C. glutamicum Δpgi* and *C. glutamicum ΔmalE Δpgi,* manifesting itself in a reoccurring complete growth stagnation of 24 h in synthetic, minimal medium which depicts the severe effects of this perturbation. The growth arrest was observed when switching from complex medium, used in the first precultures, to minimal medium used in the second precultures. After a short growth period (increase of the biomass concentration from $0.04 \, \text{g L}^{-1}$ to $0.08 \, \text{g L}^{-1}$), cellular growth completely stopped for approximately 24 h. The reasons for this aberrant growth behavior have not been revealed in detail. Due to the cultivation of the first precultures on complex medium, carry-over of complex components or intracellular metabolite storage might explain the initial (slight) increase of biomass concentration. Resumption of growth after approximately 24 h due to contamination was excluded by microscopic investigation and plating of the cultivation broth on agar plates. In addition, PCR analysis confirmed the presence of the corynespecific *pgi* deletion and the absence of the native wild type *pgi* sequence.

This reoccurring phenotype suggests a massive adaptation process which finally leads to a tolerance for this perturbation. The severity of this genetic manipulation has been addressed before for *pgi* deletion mutants of *E. coli* (Canonaco et al., 2001; Fischer and Sauer, 2003a; Fischer and Sauer, 2003b; Hua et al., 2003; Kabir and Shimizu, 2003; Nor 'Aini et al., 2006) as well as for *C. glutamicum* (Blombach et al., 2008; Marx et al., 2003), revealing a reduction in growth as a common phenotypical consequence due to the massive imbalance concerning NADPH metabolism which is consistent with the results obtained in this work.

It has to be mentioned that the increased oxygen uptake rates determined for *C. glutamicum Δpgi* and *C. glutamicum ΔmalE Δpgi* are, however, not implicitly linked with a direct oxidation of NADPH in the respiratory chain via molecular oxygen. The participation of MalE, assumed to account for the NADPH adjustments in terms of NADPH oxidation (Becker et al., 2007), is directly coupled to oxygen consumption, as this reaction operates as a transhydrogenase-like cycle, transferring electrons from NADPH (catalyzed by MalE) to NADH (catalyzed by malate dehydrogenase). The latter is further oxidized in the respiratory chain by molecular oxygen.

The potential oxygen utilization for NADPH reoxidation, accounted for 70.3% in *C. glutamicum Δpgi* and 93.8% in *C. glutamicum ΔmalE Δpgi* (Table V-6). In *C. glutamicum Δpgi* the increased oxygen consumption, exceeding the XADH demand, cannot be distinguished between malic enzyme and the respiratory chain reoxidizing NADPH, since both reactions are coupled to oxygen consumption. As oxidation via the respiratory chain is reported to be linked with ROS generation (Nantapong et al., 2005), reoxidation of NADPH by malic enzyme seems to be most likely in *C. glutamicum Δpgi* concerning the unfavorable ROS generation coupled to NADPH reoxidation via the respiratory chain.

Regarding the double deletion mutant (*C. glutamicum ΔmalE Δpgi)* however a participation of the malic enzyme can be excluded and the exceeding oxygen consumption might be attributed to a direct participation in reoxidation of NADPH via molecular oxygen as no other NADPH-NADH converting systems has been described for *C. glutamicum* to our knowledge. As a NADPH oxidizing capacity of the NADH-ubiquinone-1 oxidoreductase of *C. glutamicum* has been reported (Matsushita et al., 2001), direct NADPH oxidation via the respiratory chain seems possible. The reported K_m and V_{max} values for NADPH oxidation are approximately 30 times higher ($K_{m;NADPH}$) (Nantapong et al., 2005) and 10 times lower ($V_{max;NADPH}$) (Matsushita et al., 2001). The kinetic behavior of the respiratory chain, comprising several interconnected reactants, is however very complex (Nicholls and Ferguson, 2002) and direct consequences of

increased NADPH concentrations can only be assumed. Furthermore, determination of K_m and V_{max} values greatly depend on *in vitro* conditions of the enzymatic assays.

It can be noted however, that the intracellular NADPH concentrations were drastically increased in *C. glutamicum ΔmalE Δpgi*, while *C. glutamicum Δpgi* exhibited only a slight increase in the NADPH concentration (Table V-5). As this alteration of intracellular redox concentrations was caused by the *malE* deletion, it seems quite likely that MalE – at least partly – contributes to the reoxidation of NADPH in *C. glutamicum Δpgi*. This reoxidation system is deleted in *C. glutamicum ΔmalE Δpgi* and the direct participation of the respiratory chain in NADPH oxidation was thus questioned in this study. In this context the drastically increased NADPH concentrations and the reduced $NADP^+$ concentrations in *C. glutamicum ΔmalE Δpgi* might indicate at an increased acceptance of NADPH by the NADH-ubiquinone-1 oxidoreductase. The exact elucidation of these interactions was however beyond the scope of the present thesis.

The activation of the glyoxylate shunt, as a consequence of *pgi* deletion in *E. coli* (Hua et al., 2003) bypassing the NADPH generating reaction of ICD reflects another possibility to prevent excessive NADPH production. However no activity of the initializing enzyme isocitrate lyase was determined and an active participation of this pathway branch was therefore excluded.

Conclusions

In summary, the investigation of the NADPH metabolism in *C. glutamicum* by ^{13}C metabolic flux analysis provided valuable information concerning the flexibility of the metabolic network of this organism. One key point, supporting this flexibility, is the alternating nature of the metabolic network allowing to compensate various genetic manipulations by redirections of carbon fluxes (Becker et al., 2008). However, if this flexibility is restricted by a linearization of the network caused by deletion of essential genes, *e.g. pgi* and therefore withdrawing the ability for compensatory adjustment as previously suggested (Marx et al., 1999; Wittmann and Heinzle, 2002), the whole system has to be reconstructed. In the present work, it seems likely that one of these readjustments is the NADPH reoxidation via the respiratory chain. This is however linked to a distinct growth perturbation, as expressed by a phase of growth stagnation for 24 h observed for all *pgi* deletion strains which might be provoked only by tremendous stress-induction, as was reported previously for an *E. coli* mutant by Auriol et al. (2011). This genetically modified strain forced to produce an exceeding amount of NADPH without the ability to convert NADH to NADPH via transhydrogenases, actively modified the enzymatic properties of the NADH-ubiquinone-1 oxidoreductase in order to allow NADPH reoxidation via the respiratory chain, even linked to direct energy generation. This example additionally demonstrates the enormous flexibility and capacity to adapt to (stress-) induced perturbations and opens up a way for future in-depth analyses concerning the redox metabolism of *C. glutamicum*.

PART II

Phenotype characterization on complex medium

Analyses performed in previous chapters of **Part I** revealed the tight regulation of the purine intermediate distributions by NADH and ATP supply. In addition, deletion of the *pgi* gene resulted in adverse effects of the overall growth performance due to tremendous NADPH overabundances. The NADPH imbalances, representing a common metabolic characteristic of *pgi* deletion strains, were linked to the sole metabolization of glucose via the pentose phosphate pathway.

The results obtained from cultivations on complex medium are presented in the following chapters of **Part II**. Thereby, detrimental impacts on growth performance *e.g.* growth stagnation for 24 h were investigated. In addition, the metabolic shift, determined for *C. glutamicum ΔpurA ΔguaB2 purF^{K348Q} Δpgi* on glucose, was analyzed and related to the utilization of complex medium components. These topics are described in:

- Metabolic flux analysis using metabolite balancing with off-gas analysis provides detailed information about metabolic dynamics of *C. glutamicum* grown on complex substrates (**Chapter VI**).
- Comparative fluxome and dynamic metabolite analysis in a genetically engineered *C. glutamicum* strain cultivated on complex medium (**Chapter VII**).

Chapter VI

Uncovering dynamic structures

Metabolic flux analysis using metabolite balancing
with off-gas analysis provides detailed information
about metabolic dynamics of *C. glutamicum*
grown on complex substrates

Abstract*

Large-scale biotechnological processes often rely on complex substrates complicating *in vivo* metabolic flux quantification due to inherent multi-phase growth and varying metabolic activities. We present a metabolite balancing approach relying on metabolite balancing with additional constraints such as CO_2 production and O_2 consumption combined with balancing of redox equivalents. Using this scale-independent approach, precise determination of the split between glycolysis and pentose phosphate pathway during different growth phases on complex substrates was determined which increased from 22.8% to 44.6%. In addition, the amino acid content in the media was determined concerning free pools and peptide-bound amino acids resulting in completely closed carbon balances for each growth phase. Verification of these findings was carried out using ^{13}C based metabolic flux analysis (on glucose) resulting in comparable flux distributions and thereby confirmed the applicability and reproducibility of the extended metabolite balancing approach.

Introduction

Systems biology has evolved towards a field of increasing importance in biological sciences (Heinemann and Sauer, 2010; Kohlstedt et al., 2010; Niklas and Heinzle, 2011; Otero and Nielsen, 2009) aiming for a comprehensive understanding of the function of biological systems. One focus of this research area deals with the study of metabolic networks (Klapa et al., 2003; Mahadevan et al., 2002; Papin et al., 2003) and thereby with the analysis of *in vivo* carbon flux distributions. These metabolic distributions represent the quantitative and integrative endpoint of the cell physiology (Noh and Wiechert, 2011; Sauer, 2006), comprising regulations on the levels of DNA, RNA, proteins and metabolites. However, whereas other omic platforms, *i.e. genomics, proteomics* and *metabolomics*, target the concentration-based determination (Zamboni and Sauer, 2009), quantification of carbon fluxes, *fluxomics,* aims for the disclosure of the time-dependent conversion of intracellular metabolites, resulting in a snapshot of the actual physiological *in vivo* state of a biological system, the phenotype.

The quantification of the *in vivo* carbon fluxes, the so-called *metabolic flux analysis* (MFA), was applied in different fields of research, focusing on the metabolic engineering of pathway fluxes for biotechnology (Blombach et al., 2008; Kohlstedt et al., 2010; Wittmann, 2010; Wittmann and Becker, 2007), the discovery of novel pathways (Beste et al., 2011; Kromer et al., 2006; Nanchen et al., 2006; Tang et al., 2008), latent pathway activations (Fong et al., 2006) and many others (Benyamini et al., 2010; Bonarius et al., 1996; Bonarius et al., 2001; Niklas et al., 2010; Tang et al., 2008; van Gulik and Heijnen, 1995; Zamboni and Sauer, 2009).

A direct consequence of the time-dependent flux behavior is the inability to directly measure the *in vivo* carbon flux distributions or their determination from intracellular concentrations (Noh and Wiechert, 2011). Thus, in order to derive these fluxes, two major approaches have emerged: metabolite balancing and tracer-based flux determination employing ^{13}C labeled, stable isotopes (Stephanopoulos, 1998; Stephanopoulos et al., 1998; Wittmann and de Graaf, 2005).

The incorporation of ^{13}C labeled substrates in ^{13}C based MFA, leads to a distinct distribution of the labeled carbon atom(s) throughout the entire metabolic network. This results in a specific ^{13}C-enrichment found in intracellular free metabolites or macromolecules of the cell (*isotopic steady state condition*) (Marx et al., 1996; Wittmann, 2007). The specific ^{13}C enrichment is a direct consequence of the cellular metabolism, reflecting the activity of metabolic pathways and can thus be used to determine the alternative pathway partitioning of carbon fluxes throughout the carbon metabolism. Due to considerable improvements and substantial progress in experimental, but especially analytical and computational techniques (Bonarius et al., 2001; Klapa et al., 2003; Wiechert and de Graaf, 1997; Wiechert et al., 1997; Wittmann, 2007; Wittmann et al., 2002), nowadays, ^{13}C tracer-based metabolic flux analysis is commonly applied in academia as well as in industry.

One of the main disadvantages of isotope-based MFA are the associated high costs for the applied ^{13}C labeled compounds (Goudar et al., 2010) calling for small-scale experiments to keep the costs in reasonable ranges. However, these conditions may not reflect the actual conditions in large-scale industrial processes, since several process parameters, such as mixing, are not linearly scaled. In addition, industrial fermentation broths typically comprise an enormous fraction of complex components, further restricting the application of tracer-based metabolic flux analysis. Of additional relevance is the requirement of a metabolic and isotopic steady or pseudo-steady state (Marx et al., 1996; Provost and Bastin, 2004; Wiechert, 2001) for stationary MFA with constant intracellular concentrations and pathway activities, *i.e.* balanced growth conditions. However, application of complex substrates and the associated adaptation to varying nutritional conditions often bears multi-phase growth and thus a dynamic behavior of metabolite concentrations and pathway activities, demanding a switch from stationary to in-stationary MFA (Noack et al., 2011; Noh and Wiechert, 2011; Wiechert and Noh, 2005).

The second approach, metabolite balancing (Varma and Palsson, 1994), has been employed even longer than tracer-based MFA, due to its increased experimental, analytical and computational simplicity (Aiba and Matsuoka, 1978; Goudar et al., 2010). The mathematical approach is based on balancing intracellular metabolites resulting in a set of linearly dependent equations. Determined extracellular and anabolic fluxes, together with

the reaction stoichiometry of the metabolic network are used to calculate intracellular fluxes. This approach, since it is neither scale-dependent nor relies on labeling data that come along with high costs in case of large-scale experiments, is well suited to be applied at larger, industrially relevant scales. This method, however, exhibits limitations, since flux partitioning in cyclic pathways and reversible reactions cannot be determined without further simplification of the network, either by a priori assumption of pathway activities, complementation by linear objective functions (Feist and Palsson, 2010; Wiechert, 2001) or additional constraints. The latter was mostly achieved by including mass balances of cofactors such as ATP or NAD(P)H (Bonarius et al., 1998; Schmidt et al., 1998; van Gulik and Heijnen, 1995). Since for some of these cofactors only an approximate balance can be estimated, implementation is thus based on certain assumptions, *i.e.* concerning ATP requirements for maintenance processes and the P/O ratio in the respiratory chain.

The metabolite balancing approach in this study only implies the reoxidation of NADH and $FADH_2$ by molecular oxygen in order to maintain cellular functionality, as well as carbon dioxide production as additional constraints. The associated ATP supply and its efficiency are not required and therefore can be resigned. Metabolite dynamics of *C. glutamicum* grown on complex substrates, as used in large-scale industrial processes, were investigated applying this metabolite balancing approach in order to gain increased knowledge on physiological behavior under these industrially relevant conditions.

Materials and methods

Microorganism

The wild type strain *C. glutamicum* ATCC 13032 was obtained from the American Type Culture Collection (Manassas, VA, USA).

Growth media

The first preculture was grown on complex medium (pH 6.8) containing per liter: 10.0 g glucose, 2.5 g NaCl, 2.0 g urea, 5.0 g yeast extract, 5.0 g beef extract, 5.0 g polypeptone and 20.0 g casamino acids. For agar plates, the complex medium was supplemented with 20.0 g L^{-1} agar. Minimal medium for second precultures and main cultures (pH 7.2) contained per liter: 15.0 g glucose, 4.0 g KH$_2$PO$_4$, 16.0 g Na$_2$HPO$_4$, 500 mg MgCl$_2 \cdot$ 6 H$_2$O, 300 mg 3,4-dihydroxybenzoic acid, 100 mg CaCl$_2 \cdot$ 2 H$_2$O, 100 µg cyanocobalamin, 750 µg thiamine, 4 µg pyridoxal phosphate, 100 µg biotin, 400 µg calcium pantothenate, 2 µg folic acid, 400 µg nicotinic acid, 200 µg 4-aminobenzoic acid, 400 µg pyridoxine $\cdot$ HCl, 2 mg inositol, 10 mg FeCl$_2 \cdot$ 4 H$_2$O, 1 mg ZnCl$_2$, 100 µg CuCl$_2$, 20 µg NiCl$_2 \cdot$ 6 H$_2$O, 20 µg Na$_2$MoO$_4 \cdot$ 2 H$_2$O, 500 µg boric acid, 100 µg KI, 100 µg CoCl$_2 \cdot$ 6 H$_2$O, 10 mg MnCl$_2 \cdot$ 4 H$_2$O. For tracer studies, naturally labeled glucose was replaced by 99% ^{13}C enriched [1-^{13}C] glucose.

Second precultures and main cultures on complex media (pH 7.2) contained per liter: 4.0 g KH$_2$PO$_4$, 16.0 g K$_2$HPO$_4$, 4.0 g peptone, 20.0 g glucose, 10.0 g MgSO$_4$, 6.0 g urea, 100 mg CaCl$_2 \cdot$ 2 H$_2$O, 1 mg ZnSO$_4 \cdot$ 7 H$_2$O, 20 mg FeSO$_4$, 17 mg MnSO$_4$, 20 mg cysteine, 30 mg biotin, 10 mg calcium pantothenate and 5 mg thiamine.

Cultivations

Shake flask cultivations

Cultivations were carried out on an orbital shaker (Multitron 2, Infors AG, Bottmingen, Switzerland) at 230 rpm and 30°C. Precultures on complex medium (25 mL medium in 250 mL baffled shake flasks) were inoculated with a single colony from an agar plate and incubated for 16 h. Cells were harvested by centrifugation (3 min, 6,500 *g*, 4°C, Laborfuge 400R, Heraeus, Hanau, Germany), washed twice with sterile 0.9% NaCl and used for the inoculation of the second preculture. Second precultures (25 mL medium in 250 mL baffled shake flasks) on minimal medium were cultivated for 12 h and on complex medium for 8 h. Main cultures on minimal medium were performed in duplicates using 500 mL baffled shake flasks with 50 mL medium. Tracer experiments for ^{13}C MFA were carried out in 50 mL baffled flasks with 5 mL minimal medium containing 15.0 g L^{-1} [1-^{13}C] glucose.

Bioreactor cultivations

Cultivations were performed in a 500 mL stirred tank bioreactor (Meredos, Bovenden, Germany) in a liquid volume of 75 mL at 30°C and 1,000 rpm. Dissolved oxygen concentrations during fermentation were always above 60% air saturation thus avoiding oxygen limitation. The airflow was controlled at 1 vvm (vessel volume per minute) by a mass flow controller (WMR Compact 4, Brooks Instruments, Veenedaal, Netherlands). Composition of air and exhaust gas was quantified using a quadrupole mass spectrometer (Omnistar, Inficon, Vaduz, Liechtenstein). All relevant process parameters were collected and stored by a process control system (Lucullus PIMS 2.1, Biospectra, Schlieren, Switzerland).

Chemicals

Yeast extract, beef extract, polypeptone and casamino acids were purchased from Difco Laboratories (Detroit, USA). [1-^{13}C] glucose (99% enriched) was obtained from Cambridge Isotope Laboratories (Andover, Mass., USA). All other chemicals were

purchased from Sigma-Aldrich (Steinheim, Germany), Merck (Darmstadt, Germany), Fluka (Buchs, Switzerland) or Roth (Karlsruhe, Germany) and were of analytical grade unless stated otherwise.

Substrate and product analysis

Cell concentrations were determined by measurement of optical density at 660 nm (OD_{660nm}) using a photometer (Marsha Pharmacia Biotech, Freiburg, Germany) and gravimetrically correlated with the cell dry weight. The correlation factors were determined as $0.414\ g_{CDW}\ OD_{660nm}^{-1}$ for cultivations on minimal medium and $0.419\ g_{CDW}\ OD_{660nm}^{-1}$ for cultivations on complex medium.

The concentrations of extracellular substrates and products in cultivation supernatants were determined after 3 min centrifugation at 16,000 g. Glucose, α-ketoglutarate and trehalose were quantified in diluted supernatants by HPLC (Kontron Instruments, Neufahrn, Germany). Separation was performed using an Aminex HPX-87H Bio-Rad column (300 x 7.8 mm; Hercules, USA) at 55°C with a constant flow rate of $0.8\ mL\ min^{-1}$ (7 mM H_2SO_4 as mobile phase). Quantification of sugars was carried out using refraction index (RI) detection; organic acids were quantified applying UV detection (218 nm). Amino acids were quantified as described previously (Kromer et al., 2005). Total amino acid concentrations in complex media were determined after acidic hydrolysis of the peptides contained in the corresponding supernatants. For this purpose, cultivation supernatants were separated from cells by centrifugation (5 min, 16,000 g) and 90 µL were mixed with 10 µL α-amino-butyrate to a final concentration of 1 mM as internal standard. Subsequently 100 µL 12 M HCl were added and incubated for 24 h at 105°C. Neutralization was performed by adding adequate amounts of 6 M NaOH and insoluble matter was separated by centrifugation (5 min, 7,000 g; Ultrafee-MS filter units, 0.22 µm-pore-size Durapore membrane; Millipore, Darmstadt, Germany). The remaining clear solution was used for quantification of amino acids as described above. To ensure complete hydrolysis of peptide-bound amino acids and to determine the degradation degree, incubation times were varied between 12 and 24 h. In addition, the amount of HCl (12 M) added, was increased from 50% volume fraction up to 200% volume fraction. The

effect on the corresponding total amino acid content was determined as described previously (Kromer et al., 2005).

Cell disruption and enzymatic determination of the glyoxylate pathway activity

For quantification of the glyoxylate pathway activity of *C. glutamicum* wild type grown on glucose, cells were cultivated in 50 mL minimal medium in 500 mL baffled shake flasks (for descriptions see *"Shake flask cultivation – Materials and Methods"*). Disruption of cells was performed as described previously (Becker et al., 2005). Potential activity of the glyoxylate shunt was assessed measuring the enzymatic activity of the first enzyme of this pathway, isocitrate lyase. The enzymatic assay was performed as described previously by de Jong-Gubbels et al. (1995).

Mass spectrometric ^{13}C-labeling analysis

The labeling patterns of amino acids from cellular protein were analyzed by gas chromatography-mass spectrometry (GC-MS) and corresponding single mass isotopomer fractions were determined (Kiefer et al., 2004; Wittmann et al., 2004a). Therefore, 1 mg cell dry mass was harvested from an exponentially growing culture by centrifugation (5 min, 16,000 g) and washed twice with purified water. Cells were then incubated with 50 µL 6 M HCl at 105°C for 24 h. Subsequently neutralization was performed with adequate volumes of 6 M NaOH and insoluble matter was separated by filtration (5 min, 7,000 g; Ultrafee-MS filter units, 0.22 µm-pore-size Durapore membrane; Millipore, Darmstadt, Germany). The remaining clear solution was then lyophilized. Amino acid mass isotopomers were analyzed after derivatization using MBDSTFA (N-methyl-N-*t*-butyldimethylsilyl-trifluoroacetamide; Macherey-Nagel, Düren Germany) and conversion into the corresponding *t*-butyldimethylsilyl (TBDMS)-derivatives (Wittmann et al., 2002). The labeling pattern of secreted trehalose was determined from supernatants. Derivatization of trehalose was carried out using BSTFA (N,O-bis-

(trimethylsilyl)trifluoroacetamide; Macherey-Nagel Düren Germany), resulting in its trimethylsilyl-derivate. All samples were first analyzed in scan mode, thereby excluding isobaric interferences between analytes and sample components. Mass isotopomer fractions of amino acids were determined using selective ion monitoring (SIM) mode in duplicates. ^{13}C enrichment was determined on the basis of the [M-57] fragments except for leucine ([M-157]). The mass isotopomer distribution of trehalose was analyzed for the *m/z* 361 fragment consisting of one glucose moiety.

Biochemical network and biomass requirements

The metabolic network of *C. glutamicum* (Figure VI-1) includes all main metabolic pathways utilized during growth on glucose, *i.e.* glycolysis, pentose phosphate pathway (PPP), tricarboxylic acid (TCA) cycle and anaplerosis.
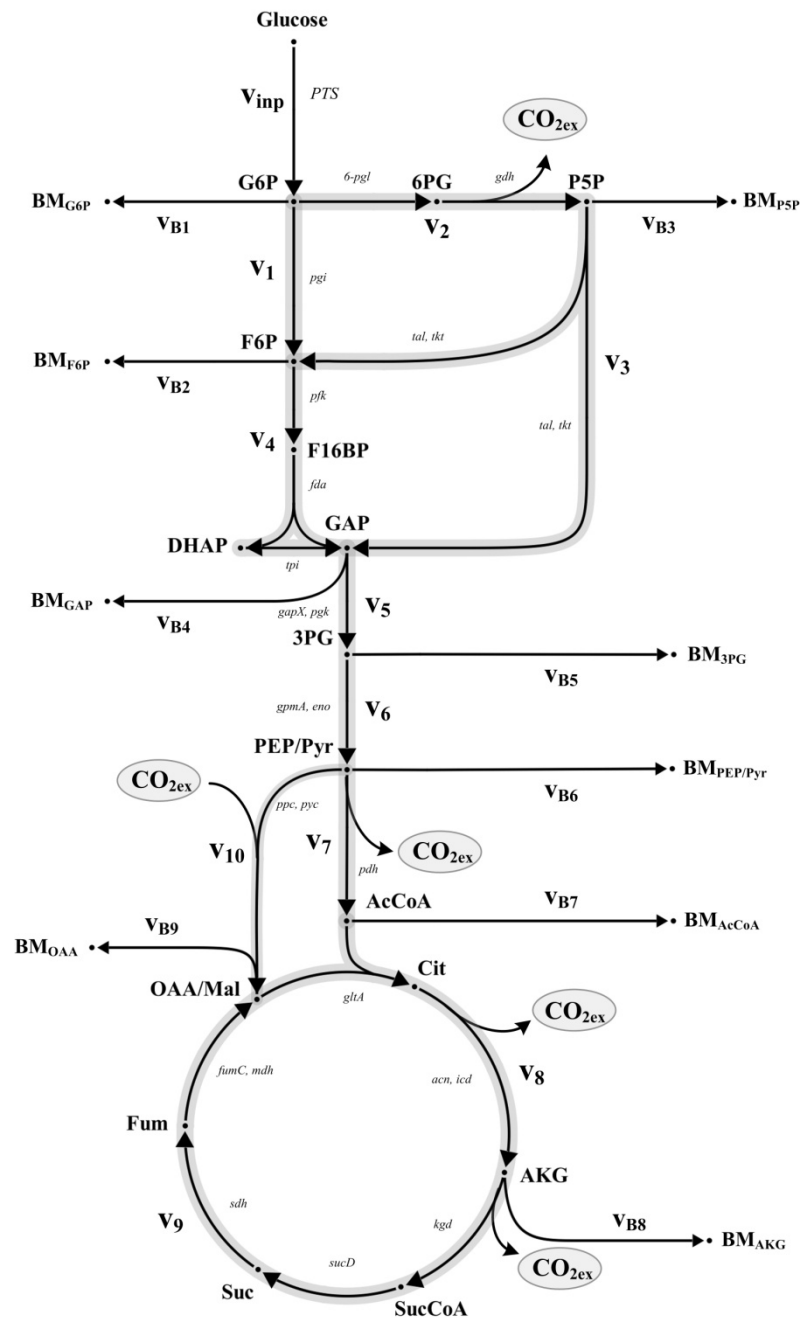
Figure VI-1. Metabolic network model for isotopomer-based flux estimation and metabolite balancing. v_i, intracellular fluxes; v_{Bi}, anabolic fluxes; abbreviations: **G6P**, glucose 6-phosphate; **6PG**, 6-phosphogluconate; **P5P**, pentose 5-phosphate; **F6P**, fructose 6-phosphate; **F16BP**, fructose 1,6-bisphosphate; **DHAP**, dihydroxyacetone phosphate; **GAP**, glyceraldehyde 3-phosphate; **3PG**, 3-phosphoglycerate; **PEP**, phosphoenolpyruvate; **Pyr**, pyruvate; **AcCoA**, acetyl-CoA; **Cit**, citrate; **AKG**, α-ketoglutarate; **SucCoA**, succinyl-CoA; **Suc**, succinate; **Fum**, fumarate; **OAA**, oxaloacetate; **Mal**, malate; **BM$_i$** biomass.

Since usage of [1-^{13}C] labeled glucose is insufficient to distinguish between phosphoenolpyruvate and pyruvate as well as oxaloacetate and malate pools, these pools were lumped and only the net fluxes were calculated. No activity of the glyoxylate shunt associated enzyme isocitrate lyase was experimentally detected and was therefore neglected. Anabolic pathways towards biomass production and production pathways for α-ketoglutarate, trehalose and glycine were incorporated in the metabolic network topology.

For metabolite balancing analysis, decarboxylating and carboxylating reactions located in anabolic and catabolic pathways were additionally balanced, as well as NADH and FADH$_2$ generating and consuming reactions (Table VI-1).

Table VI-1. Molar balance equations for the metabolite balancing model of glucose metabolism used for MFA of *C. glutamicum* wild type strain.

1.	v_{G6P}:	$0 =$	$v_{inp} - v_1 - v_2 - v_{B1}$
2.	v_{F6P}:	$0 =$	$v_1 - v_4 + 0.667v_3 - v_{B2}$
3.	v_{P5P}:	$0 =$	$v_2 - v_3 - v_{B3}$
4.	v_{GAP}:	$0 =$	$v_4 + 0.333v_3 - v_5 - v_{B4}$
5.	v_{3PG}:	$0 =$	$v_5 - v_{B5} - v_6$
6.	$v_{PEP/Pyr}$:	$0 =$	$v_6 - v_{B6} - v_7 - v_{10}$
7.	v_{AcCoA}:	$0 =$	$v_7 - v_{B7} - v_8$
8.	v_{AKG}:	$0 =$	$v_8 - v_{B8} - v_9$
9.	v_{OAA}:	$0 =$	$v_9 + v_{10} - v_8$
10.	v_{CO2}:	$0 =$	$v_2 + v_7 + v_8 + v_9 - v_{10} - 0.636v_{B3}{}^{a} - 0.154v_{B8}{}^{a} + 0.186v_{B9}{}^{a}$ $+ 0.502v_{B6}{}^{a} - v_{CO2exp}{}^{b}$
11.	$v_{XADH}{}^{c}$:	$0 =$	$v_5 + v_7 + 3v_9 + 0.313v_{inp}{}^{d} - 2qO_2$

v_i intracellular fluxes, v_{Bi} anabolic fluxes.

[a] stoichiometric coefficients denote the amount of CO$_2$ consumed or released by anabolism accounting for the usage of the precursor molecules in different anabolic reactions.

[b] v_{CO2exp} depicts the experimentally determined net CO$_2$ production.

[c] v_{XADH} corresponds to NADH and FADH$_2$ generating reactions.

[d] stoichiometric coefficient denotes the amount of NADH produced by anabolism.

Redox balancing

The amount of XADH (NADH and FADH$_2$) reoxidized by the respiratory chain is:

$$v_{XADH} = 2qO_2 \qquad\qquad [3]$$

where qO_2 denotes the specific oxygen uptake rate and v_{XADH} the combined specific net consumption of NADH and FADH$_2$ in the respiratory chain. Reoxidation of NADPH by the respiratory chain was not considered since NADPH – provided by glucose 6-phosphate dehydrogenase, 6-phosphogluconate dehydrogenase and isocitrate dehydrogenase – was reported to be completely used by anabolic reactions of *C. glutamicum* wild type (Kromer et al., 2008; Chapter V). Thus an active participation of malic enzyme in NADPH generation was supposed to be insignificant – under the prevailing conditions – and thus negligible. All rates were normalized to the glucose consumption rate. Production of XADH (catabolic and anabolic) in the metabolism is given by the reactions defined in Figure VI-1:

$$v_{XADH} = v_5 + v_7 + 3v_9 + 0.313v_{inp} \qquad\qquad [4]$$

The anabolic NADH production of 3.2 mmol NADH per gram biomass, as expressed in $0.313v_{inp}$, was adopted from literature for *C. glutamicum* (Yang et al., 2006).

Metabolic flux estimation and visualization

^{13}C metabolic flux analysis

In vivo metabolic fluxes of the *C. glutamicum* central carbon metabolism were calculated by fitting simulated mass isotopomer distributions to experimentally determined, GC-MS derived mass isotopomer fractions of measured amino acid fragments following the approach of Yang et al. (2009; 2008) implemented in Matlab (version 2008b, Mathworks Inc., Nattick, USA) applying metabolite and isotopomer balancing. Measured GC-MS data were corrected for naturally occurring isotopes in the amino acid fragments and derivatization reagent respectively (van Winden et al., 2002; Wittmann and Heinzle, 1999).

In addition extracellular rates and anabolic demands for biomass formation were used for flux estimation. Initial free randomized fluxes resulted in comparable metabolic flux distributions after optimization indicating the achievement of a global minimum. Statistical analysis was carried out using a Monte Carlo approach with 100 independent runs (Mollney et al., 1999; Wittmann and Heinzle, 2002; Yang et al., 2008). Fluxes are given with corresponding 90% confidence intervals.

Metabolite balancing

Metabolite balancing was based on extracellular measurable consumption and production rates and anabolic demands for biomass formation depicted in the metabolic network of Figure VI-1. In addition carbon dioxide production and oxygen consumption were used to balance carbon and XADH, allowing the determination of the split between glycolysis and pentose phosphate pathway. Flux estimation was carried out using a Monte Carlo approach varying extracellular rates within their corresponding standard deviation applying 1000 independent runs. Metabolic fluxes are given with 90% confidence intervals or with corresponding standard deviations.

Visualization was performed using Omix software (Droste et al., 2011).

Results and discussion

The information generated by metabolic flux analysis strongly depends on applicability and accuracy of the constraints applied (Schmidt et al., 1998). We therefore compared the reliability of two different approaches – isotopic tracer-based metabolic flux analysis and an extended metabolite balancing approach – in order to overcome limitations associated with both approaches. These two approaches were first compared and verified by investigating intracellular carbon fluxes during growth on glucose and then the extended metabolite balancing approach was applied for growth on complex compounds.

Metabolism of C. glutamicum wild type grown on glucose

C. glutamicum wild type (ATCC 13032) was grown in duplicate on minimal medium applying glucose as sole carbon source. Exponential growth was reached after one generation, indicated by constant biomass and by-product yields as well as constant glucose consumption and specific growth rate (Table VI-2). 64.3% of the carbon contained in glucose was used for biomass production, whereas only 1.5% was directed towards by-product formation.

Based on kinetic parameters and the stoichiometry of the underlying metabolic network (Figure VI-1), isotope tracer experiments allowed for the determination of intracellular *in vivo* carbon fluxes. The determined growth parameters and production rates obtained from tracer experiments and from main cultivations of *C. glutamicum* wild type performed on naturally labeled glucose were highly reproducible (Table VI-2) and data from both cultivations were used for flux estimation.

Table VI-2. Kinetic parameters for *C. glutamicum* ATCC 13032 grown on minimal medium with glucose as sole carbon source obtained from parallel main (naturally labeled glucose) and tracer ([1-^{13}C] glucose) cultivations[a].

parameter	main cultivations			tracer cultivations		
	mean value		standard deviation	mean value		standard deviation
μ	0.443	$\pm$	0.004	0.451	$\pm$	0.006
$Y_{X/S}$	0.095	$\pm$	0.005	0.099	$\pm$	0.003
$Y_{Gly/S}$	8.662	$\pm$	0.183	9.192	$\pm$	0.201
$Y_{Tre/S}$	4.767	$\pm$	0.004	5.220	$\pm$	0.012
$Y_{AKG/S}$	1.995	$\pm$	0.069	1.781	$\pm$	0.089
q_s	4.665	$\pm$	0.090	4.510	$\pm$	0.051

[a] specific growth rate μ [h^{-1}], biomass yield $Y_{X/S}$ [g mmol^{-1}], yields for glycine $Y_{Gly/S}$, trehalose $Y_{Tre/S}$ and α-ketoglutarate $Y_{AKG/S}$ [mmol mol^{-1}] and specific glucose consumption rate q_s [mmol g^{-1} h^{-1}].

Metabolic flux distributions applying ^{13}C MFA

The isotope labeling approach is based on experimentally determined production and consumption rates, the stoichiometry of the underlying network, the anabolic demand for biomass production and additionally comprises isotopomer balances and corresponding labeling patterns derived from biomass components and secreted products.

In this study, tracer experiments were carried out using [1-^{13}C] glucose. During mid-exponential growth phase, the labeling patterns of proteinogenic amino acids derived from protein hydrolyzates and of trehalose secreted during the entire cultivation were determined at two different time points during cultivation verifying isotopic steady state. Stationary ^{13}C metabolic flux analysis was performed using an iterative optimization process by minimizing the differences between simulated ($M_{i,\,sim}$) and calculated ($M_{i,\,calc}$) labeling patterns (Yang et al., 2009). The obtained fluxes determined for key reactions of the metabolism and the corresponding fit of simulated and calculated mass isotopomers are summarized in Tables VI-3 and IV-4, respectively. Deviations for each flux, as shown in

Table VI-3, correspond to 90% confidence intervals resulting from 100 independent Monte Carlo runs.

Table VI-3. *In vivo* carbon flux distribution and statistical evaluation of central metabolism key reactions of the *C. glutamicum* wild type strain during growth on [1-^{13}C] glucose, obtained by tracer-based flux analysis and by the metabolite balancing approach.

net flux	[13]C MFA		metabolite balancing approach	
	mean value	90% confidence intervals	mean value	90% confidence intervals
v_1	0.522	[0.520 ; 0.524]	0.503	[0.501 ; 0.504]
v_2	0.449	[0.446 ; 0.451]	0.467	[0.465 ; 0.468]
v_3	0.361	[0.360 ; 0.363]	0.353	[0.352 ; 0.355]
v_4	0.723	[0.723 ; 0.724]	0.709	[0.708 ; 0.709]
v_5	1.537	[1.536 ; 1.537]	1.521	[1.521 ; 1.522]
v_6	1.400	[1.399 ; 1.401]	1.384	[1.384 ; 1.385]
v_7	0.788	[0.787 ; 0.789]	0.785	[0.785 ; 0.786]
v_8	0.473	[0.473 ; 0.474]	0.471	[0.471 ; 0.472]
v_9	0.350	[0.350 ; 0.351]	0.348	[0.348 ; 0.348]
v_{10}	0.290	[0.290 ; 0.290]	0.286	[0.286 ; 0.287]
v_{CO2}	1.872[a]	[1.869; 1.874]	1.895[b]	[1.894; 1.896]
v_{XADH}	3.679	[3.678 ; 3.681]	3.662	[3.660; 3.664]

[a] calculation of CO_2 production was based on the corresponding flux distribution.

[b] CO_2 production was experimentally determined.

Table VI-4. Relative mass isotopomer fractions of proteinogenic amino acids derived from cellular protein and of trehalose secreted during cultivation of *C. glutamicum* ATCC 13032 on 99% [1-^{13}C] glucose[a].

metabolite	mass isotopomer fraction									
	M_0	M_1	M_2	M_3	M_4	M_5	M_6	M_7	M_8	M_9
ala (*m/z* 260; c_1-c_3)										
calc	0.648	0.337	0.015	0.000						
exp	0.650	0.335	0.014	0.001						
gly (*m/z* 246; c_1-c_2)										
calc	0.961	0.039	0.000							
exp	0.961	0.038	0.001							
val (*m/z* 288; c_1-c_5)										
calc	0.529	0.392	0.075	0.004	0.000	0.000				
exp	0.437	0.432	0.124	0.007	0.000	0.000				
leu (*m/z* 200; c_1-c_5)										
calc	0.314	0.439	0.210	0.037	0.001	0.000				
exp	0.315	0.425	0.214	0.043	0.002	0.001				
ser (*m/z* 390; c_1-c_3)										
calc	0.656	0.333	0.011	0.000						
exp	0.655	0.337	0.008	0.000						
thr (*m/z* 404; c_1-c_4)										
calc	0.507	0.400	0.087	0.006	0.000					
exp	0.505	0.399	0.091	0.004	0.000					
phe (*m/z* 336; c_1-c_9)										
calc	0.345	0.429	0.187	0.035	0.003	0.000	0.000	0.000	0.000	0.000
exp	0.341	0.421	0.187	0.034	0.003	0.004	0.002	0.004	0.002	0.002
asp (*m/z* 418; c_1-c_4)										
calc	0.507	0.400	0.087	0.006	0.000					
exp	0.504	0.402	0.090	0.004	0.000					
glu (*m/z* 432; c_1-c_5)										
calc	0.377	0.435	0.164	0.023	0.001	0.000				
exp	0.379	0.427	0.167	0.025	0.001	0.000				
arg (*m/z* 442; c_1-c_6)										
calc	0.298	0.422	0.221	0.053	0.006	0.000	0.000			
exp	0.314	0.403	0.205	0.050	0.015	0.009	0.004			
tyr (*m/z* 466; c_1-c_9)										
calc	0.345	0.429	0.187	0.035	0.003	0.000	0.000	0.000	0.000	0.000
exp	0.339	0.415	0.181	0.034	0.014	0.004	0.003	0.003	0.003	0.004
tre (*m/z* 361; c_1-c_6)										
calc	0.053	0.886	0.059	0.002	0.000	0.000	0.000			
exp	0.032	0.886	0.068	0.009	0.004	0.001	0.000			

[a] GC-MS data experimentally determined (exp) and corresponding calculated values (calc) obtained by an interative optimization applying 100 Monte Carlo runs with statistically varying initial values. M_0 denotes the non-labeled mass isotopomer fraction and M_i the corresponding higher-labeled fractions.

An excellent fit between calculated and simulated mass isotopomer ratios was reached, indicating the consistency of the underlying metabolic network. Using this approach, *C. glutamicum* wild type revealed a split at the glucose 6-phosphate node of 52.2% and 44.9% towards glycolysis and PPP, respectively. As indicated by the small confidence intervals, this flux partitioning could be determined with excellent precision.

This approach combining stoichiometric mass balances with isotopomer patterns of central metabolites allowed the accurate determination of key fluxes in the central metabolism, including the split at the glucose 6-phosphate node as shown in various studies for different organisms (Becker et al., 2005; Fuhrer et al., 2005; Goel et al., 1993; Kromer et al., 2008; Sauer et al., 2004).

However, these additional measurements are both analytically and computationally challenging and there is no guaranty that the final objective reaches the global minima during the iterative optimization process. Furthermore, the tracer experiments are routinely carried out in smaller scales that may not be transferrable to large-scale processes due to scale-dependent parameters such as mixing and aeration. Thus, in order to reflect industrial large-scale processes, scale-independent approaches, like the metabolite balancing approach, have to be applied.

Metabolic flux distributions using metabolite balancing

The metabolite balancing approach based on the metabolic network depicted in Figure VI-1 contains stoichiometric balances for 13 metabolites, 18 measured fluxes including biomass formation and 10 intracellular fluxes to be determined comprising one alternative route (glycolysis and PPP). The activities of the alternative fluxes at the glycolysis-PPP branch could not be determined without further constraints since the stoichiometry is based on linear dependencies and cannot be solved. The statistical evaluation therefore did not result in a defined solution but in a solution space for the linear dependent fluxes in glycolysis and reactions through the whole metabolic network. The only determinable flux not depending on varying input fluxes obtained from Monte Carlo simulations was the anabolic flux v_{10}, connecting the pools of PEP/Pyr and OAA/Mal. This non-dependency is based on the function to replenish the TCA cycle compensating for the draining reactions

v_{B8} and v_{B9} leaving the TCA cycle towards biomass formation. Thus, the activity of the anaplerotic flux v_{10} is solely determined by the anabolic demand of the cells. Flux determination resulted in tremendous deviations of the estimated fluxes. In addition obtained fluxes partly exhibited physiologically non-feasible values in terms of thermodynamics, as indicated by negative fluxes for the oxidative branch of the PPP (v_2) (data not shown).

In order to overcome this problem, the metabolic network has either to be further simplified, *i.e.* the flux through the oxidative branch of the PPP has to be assumed to be accountable solely for precursor supply and the non-oxidative branch has to be neglected, specific fluxes have to be assumed a priori or additional constraints or objective functions have to be implemented (Niklas and Heinzle, 2011). Since simplification or a priori assumption of flux activities are seldom physiologically justified (Schmidt et al., 1998), several reports aimed towards the establishment and validation of additional constraints, like the balance of metabolites involved in energy and redox metabolism (ATP, NADPH and NADH). Incorporation of balances for such metabolites, however, emerged being difficult, as for ATP neither requirements for maintenance or futile cycles nor the efficiency of the respiratory chain generating ATP from NADH, expressed as the P/O ratio, can be determined directly. As for the case of NADPH, all reactions involved in generation and consumptions and especially their feasible direction, evoked by the physiological state, have to be accounted for.

In *C. glutamicum* four strictly NADP$^+$-dependent enzymes are supplying NADPH for anabolism *i.e.* glucose 6-phosphate dehydrogenase and 6-phosphogluconate dehydrogenase (PPP), isocitrate dehydrogenase (TCA cycle) and malic enzyme (MalE, anaplerotic node) (Eikmanns et al., 1995; Gourdon et al., 2000; Marx et al., 1996; Sugimoto and Shiio, 1987a; Sugimoto and Shiio, 1987b; Wittmann and de Graaf, 2005). The participation of MalE however, was reported to be insignificant for the wild type strain of *C. glutamicum* during growth on glucose (Kromer et al., 2008; Chapter V). Furthermore, no transhydrogenase activity interconverting NADH and NADPH is reported for *C. glutamicum* (Dominguez et al., 1998), allowing a separate consideration of NADH and NADPH pools and corresponding reducing and oxidizing reactions.

To elude these uncertainties, we extended the stoichiometric approach by the directly measurable parameters, carbon dioxide production rate (qCO_2) and oxygen consumption rate (qO_2), both determined by exhaust gas analysis. The latter was further coupled to the oxidation of XADH in the respiratory chain, expressed by equation 3 **[3]**, implying that consumed oxygen is used for the oxidation of reduced equivalents NADH and $FADH_2$. The advantage relying solely on XADH for balancing is to circumvent uncertainties associated with ATP balancing (such as futile cycles, hydrolysis and unknown efficiencies of the ATP synthases namely the P/O ratios in the respiratory chain). Consideration of the net CO_2 efflux allowed the combined determination of the fluxes v_2, v_7, v_8 and v_{10}. In combination with the qO_2-XADH constraint, the glucose 6-phosphate partitioning could be estimated, resulting in a precise determination of all linear dependent fluxes (Figure VI-2). Furthermore, calculated flux activities solely exhibit physiologically feasible values (Figure VI-2).
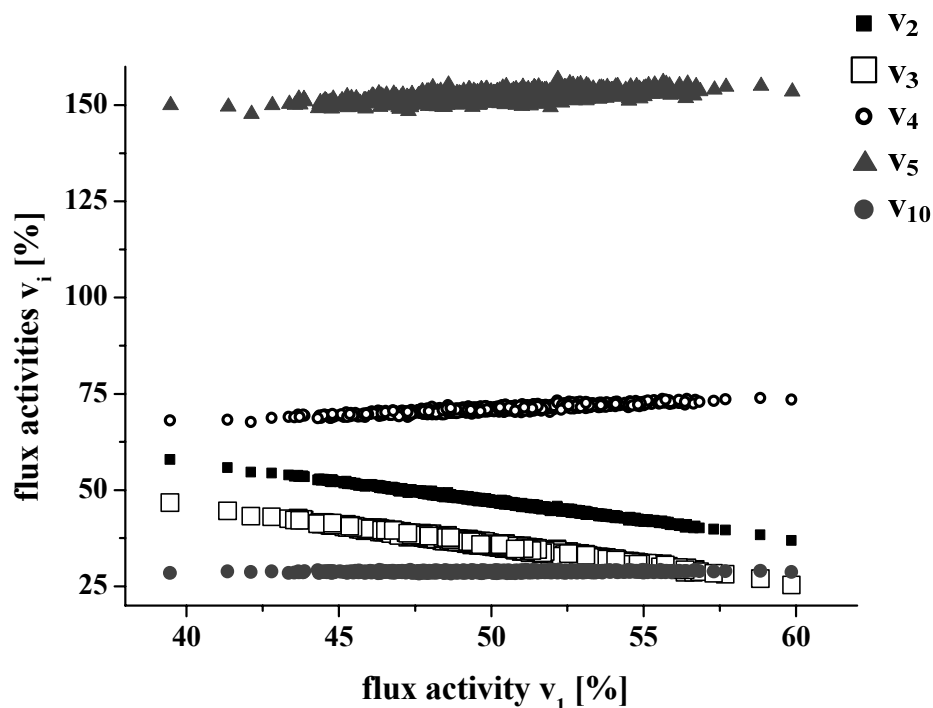
Figure VI-2. Correlation of flux activities and precision of flux estimations, showing obtained values for 1000 Monte Carlo simulations with varying initial values. Fluxes (v_i) of glycolysis (i=4, 5) and PPP (i=2, 3) and anaplerosis (i=10) are related to the initiating step of glycolysis (v_1). Values are displayed as relative values (in %) normalized to the glucose uptake rate, which was set to 100%. Determination of flux distributions was performed with balancing of XADH (Table VI-1). Flux calculations were carried out without thermodynamic restrictions, allowing physiologically non-feasible values to be calculated.

The implementation of the CO_2 and XADH balances introduces two additional constraints that were further analyzed and physiologically validated in direct comparison with the tracer-based flux determination in minimal medium. As depicted in Table VI-3, pathway activities estimated by the two different approaches resulted in almost identical flux distribution patterns, revealing the reliability and applicability of the extended metabolite balancing approach. Importantly, this approach can only be applied, when separation of NADPH and NADH is provided, as is not the case for organisms capable of NADPH-NADH interconversion by transhydrogenases as described for *Paracoccus versutus,*

Bacillus subtilis and *Escherichia coli* (Fuhrer and Sauer, 2009). In this context, participation of MalE, transferring electrons from NADH to NADPH, has to be ensured to be not active or insignificant, as was reported to be the case for *C. glutamicum* wild type strain (Kromer et al., 2008; Chapter V).

Metabolic flux analysis for industrial large-scale processes

Cultivation profile of C. glutamicum on complex medium

Industrial manufacturing of biotechnological products is mainly performed as scale-up process applying complex fermentation broths as substrates for the production process. Due to the complex nature of the substrate and changing environmental conditions, microbiological growth seldom features a single-phased growth behavior, resulting in substantial increased experimental and analytical demands for in-depth analysis.

In this study, fluxome analysis of *C. glutamicum* in a complex medium mimicking industrial fermentation conditions was performed applying the aforementioned extended metabolite balancing approach. The cultivation profile of *C. glutamicum* ATCC 13032 on complex medium is depicted in Figure VI-3. Consumption and production of amino acids (free and peptide-bound) were quantified and monitored over the complete cultivation period and are illustrated in Figure VI-4.
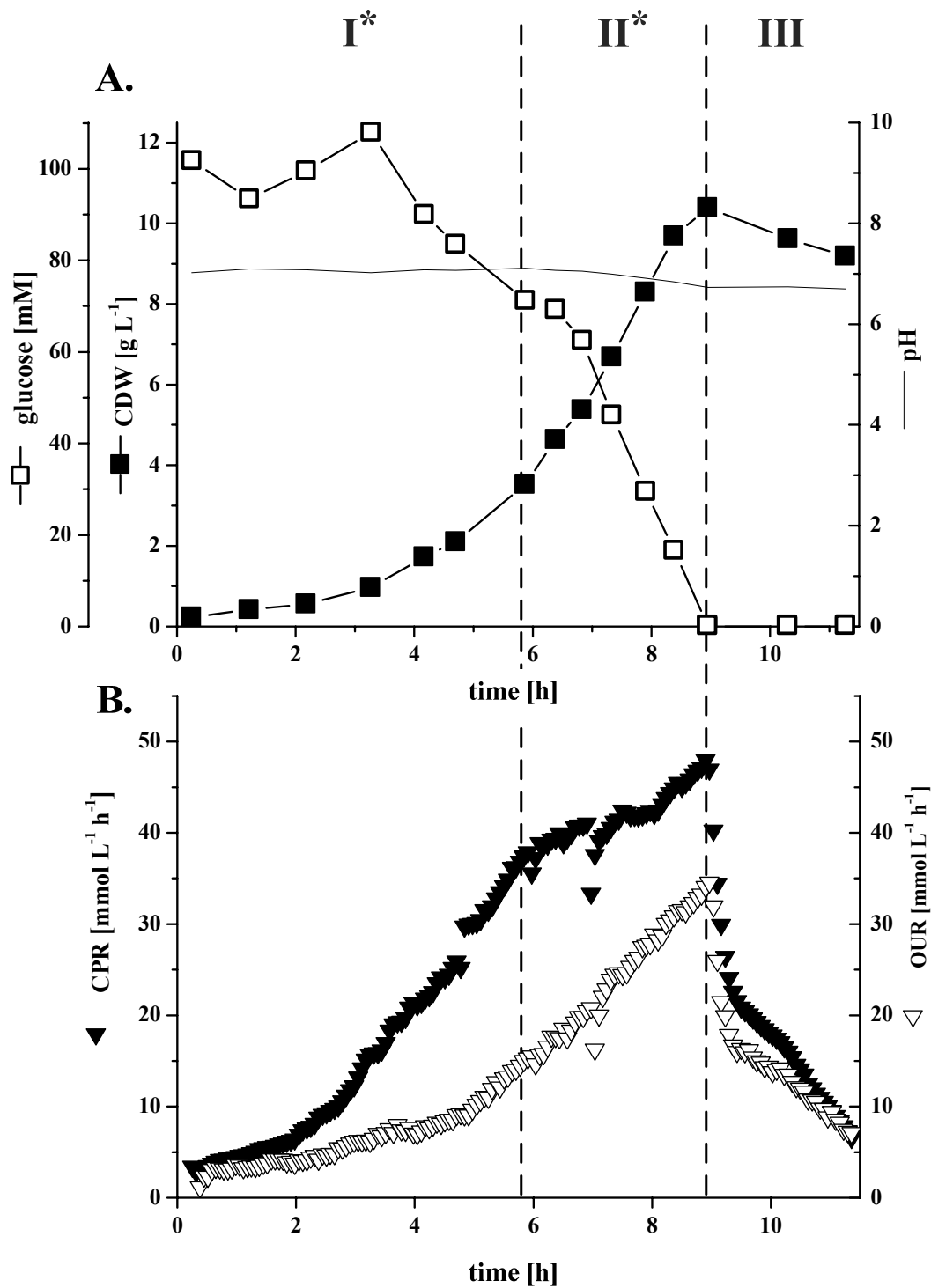
Figure VI-3. Profile of the batch fermentation of *C. glutamicum* ATCC 13032 on complex media, resulting in multi-phase growth behavior. Asterisks mark the growth phases, which were further analyzed by MFA. (**A.**) Growth profile, showing biomass production [g_{CDW} L^{-1}] and glucose consumption [mM]. (**B.**) CO_2 production rate [CPR; mmol L^{-1} h^{-1}] and O_2 uptake rate [OUR; mmol L^{-1} h^{-1}]. All data are shown with respect to the observed growth phases.
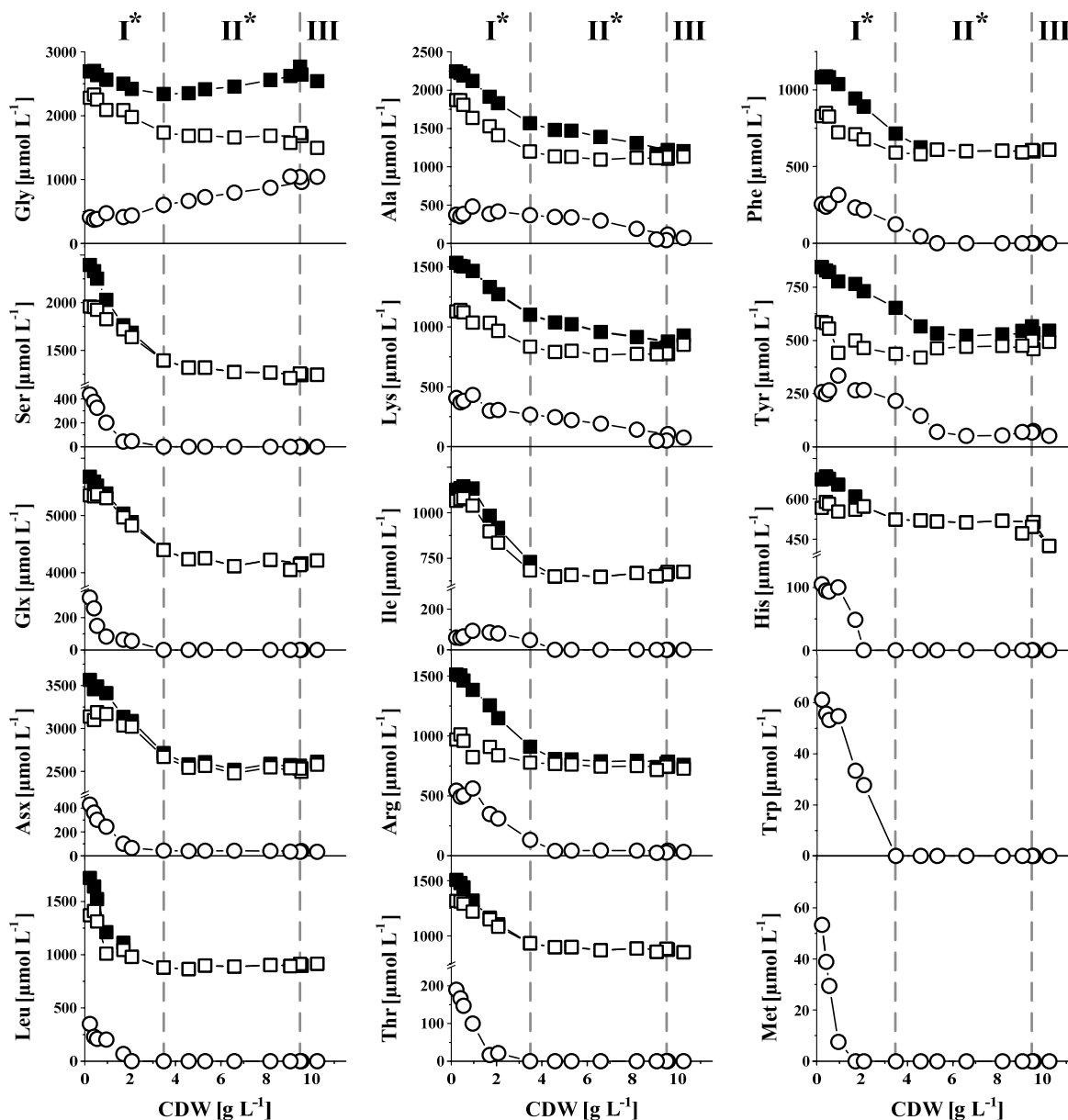
Figure VI-4. Time course of amino acid concentrations [µmol L^{-1}] of *C. glutamicum* ATCC 13032 during growth on complex medium in relation to biomass concentration [g L^{-1}]: free amino acids (open circles), peptide-bound amino acids (open squares) and hydrolyzates (both combined; full squares) of cultivation supernatants. Dashed lines mark different growth phases.

The resulting amino acid consumptions and glycine production with respect to biomass formation were determined for each growth phase and are summarized in Table VI-5.

To ensure total hydrolysis of peptide-bound amino acids and to determine the degree of degradation caused by acidic hydrolysis, incubations times and added volumes of HCl

were varied (see *"Substrate and product analysis – Materials and Methods"*). Neither increasing degradation times nor increasing volumes of 12 M HCl showed any effect on the concentration of released free amino acids.

Table VI-5. Amino acid consumption and production values [μmol g_{CDW}^{-1}], obtained for *C. glutamicum* ATCC 13032 grown in 75 ml complex medium for growth phases I and II[a,b].

amino acid	phase I	phase II
alanine (Ala)	216.7	60.0
arginine (Arg)	193.2	--
aspartate/asparagine (Asx)	259.9	--
glutamate/glutamine (Glx)	369.2	--
glycine (Gly)	147.6	52.1[c]
histidine (His)	51.7	--
isoleucine (Ile)	156.6	--
leucine (Leu)	213.8	--
lysine (Lys)	137.4	33.0
methionine (Met)[d]	62.1	--
phenylalanine (Phe)	57.4	--
serine (Ser)	438.9	--
threonine (Thr)	238.1	--
tryptophan (Trp)[d]	18.6	--
tyrosine (Tyr)	62.8	--

[a] values are obtained from hydrolyzates of the cultivation supernatants and represent the net consumptions of peptides and free amino acids.

[b] for phase III no substrate consumption was detected.

[c] glycine secretion in terms of free amino acids for growth phase II.

[d] for methionine and tryptophan, values were obtained exclusively from free amino acids due to instabilities during acid hydrolysis (for reference see Figure VI-4).

Quantification of methionine and tryptophan was carried out only for free amino acids due to instabilities of these two compounds during acidic hydrolysis. Furthermore, quantitative

determination of asparagine and aspartate as well as of glutamine and glutamate was performed for the combined pools of these compounds.

During 11 h of cultivation, $10\,g\,L^{-1}$ biomass were produced and 100 mM glucose were consumed. Considering growth parameters like specific growth rate, biomass yield and substrate consumption rates, the cultivation profile was divided into three major growth phases. For the first 8-9 h exponential growth was observed, characterizing the first two phases. In contrast, the third phase exhibited a decrease in OD_{660nm}, entire depletion of the main carbon source glucose and further lacked any amino acid consumption, indicating the death phase. The shift between these phases is indicated by dashed lines.

During phase I, the specific growth rate was found to be at maximum with $0.508\,h^{-1}$, corresponding to a doubling time of less than 90 min. Biomass production was covered mainly by glucose uptake, though a substantial part of the needed carbon was provided by peptide-bound as well as free amino acids available in the complex medium (Figure VI-4 and Table VI-5). 28% of the produced biomass during this period were covered by assimilated amino acids leaving a biomass-glucose yield of $0.079\,g_{CDW}\,mmol_{glucose}^{-1}$ derived solely from glucose. The carbon contained in glucose was thus converted to biomass and carbon dioxide with 54.0% and 48.9%, respectively (Table VI-6). During this phase all amino acid consumptions except for serine were lower than the amount required for biomass formation (Wittmann and Heinzle, 2008).

Serine uptake was determined with a constant yield of $438.9\,\mu mol\,g_{CDW}^{-1}$, exceeding the required demand of $225\,\mu mol\,g_{CDW}^{-1}$ by almost 100%. As consequence, amino acid uptake for all amino acids except for serine was assumed to be directly incorporated into cellular protein, whereas the consumed surplus of serine is most likely converted to pyruvate via serine dehydratase as described by Netzer et al. (2004b).

Table VI-6. Carbon balances for the first two growth phases of *C. glutamicum* ATCC 13032 grown in 75 mL complex medium[a].

	consumed carbon sources		produced carbon sources		
phase I	glucose	13.7 C-mmol	biomass[c] (CDW)	7.4 C-mmol	(= 0.54 C-mol$_{CDW}$ C-mol$_{glu}$)
	serine[b]	0.2 C-mmol	CO_2	6.7 C-mmol	(= 0.49 C-mol$_{CO2}$ C-mol$_{glu}$)
	balance	13.9 C-mmol		14.1 C-mmol	
phase II	glucose	31.5 C-mmol	biomass[c] (CDW)	19.8 C-mmol	(= 0.63 C-mol$_{CDW}$ C-mol$_{glu}$)
			CO_2	11.7 C-mmol	(= 0.37 C-mol$_{CO2}$ C-mol$_{glu}$)
			glycine	0.1 C-mmol	
	balance	31.5 C-mmol		31.6 C-mmol	

[a] for the third phase, no carbon balance was established, since neither carbon consumption nor production were detected, thus indicating the death phase.

[b] for serine balance, only the metabolized fraction (213.9 µmol g$_{CDW}^{-1}$) and not the total fraction (438.9 µmol g$_{CDW}^{-1}$) was considered.

[c] for biomass balance, only fractions derived from glucose were considered: for phase I 72% of the corresponding CDW were derived from glucose (28% from peptides and amino acids); for phase II only 1% of the CDW was derived from peptides and amino acids.

The second growth phase was initialized by the depletion of the free amino acid pools, except for alanine and lysine which were further consumed during the second growth phase. During this period, the specific growth rate decreased to 0.431 h^{-1}, which is consistent with growth on minimal medium containing glucose as sole carbon source (Table VI-2). Amino acid consumption (alanine and lysine during the second growth phase; Figure VI-4), drastically dropped and accounted for only 1% of the synthesized biomass during this phase. In addition, a constant glycine secretion of 58.2 µmol g$_{CDW}^{-1}$ was observed. In this phase the nitrogen demand was covered by supplemented urea. The

carbon contained in glucose (70 mM) was converted to biomass (62.9%), CO_2 (37.1%) and glycine (0.2%) (Table VI-6). The increased biomass yield of 0.093 g_{CDW} per mmol glucose thereby depicted the altered carbon usage from an amino acid/glucose-co-consumption in phase I (0.079 g_{CDW} $mmol_{glucose}^{-1}$) to glucose metabolization during phase II (0.093 g_{CDW} $mmol_{glucose}^{-1}$): in phase II glucose was used for biomass formation by converting 62.9% of the contained carbon into cellular components, whereas during phase I solely 54.0% of the glucose derived carbon were converted into biomass and almost 50% were lost as CO_2 (Table VI-6). Except for glycine no further by-product secretion was observed.

The results of the fermentation were further analyzed by metabolic flux analysis applying the metabolite balancing approach, thereby enabling a separate determination of the *in vivo* carbon fluxes for the two observed growth phases. The underlying metabolite model from Figure VI-1 was extended by uptake reactions for all amino acids determined and serine metabolization. The anabolic demand for NADH as described in the literature for sole glucose consumption (Yang et al., 2006) was adjusted accordingly. Carbon balances were set up for each growth phase and are listed in Table VI-6. Inclusion of CO_2 production yielded closed carbon balances indicating that all relevant substrates and products concerning all growth phases had been taken into account.

Fluxome profile of C. glutamicum, observed for different growth phases

Carbon flux distributions and corresponding standard deviations were estimated and are summarized in Figures VI-5 and VI-6. All fluxes could be determined with excellent precision including flux partitioning at the glucose 6-phosphate node.
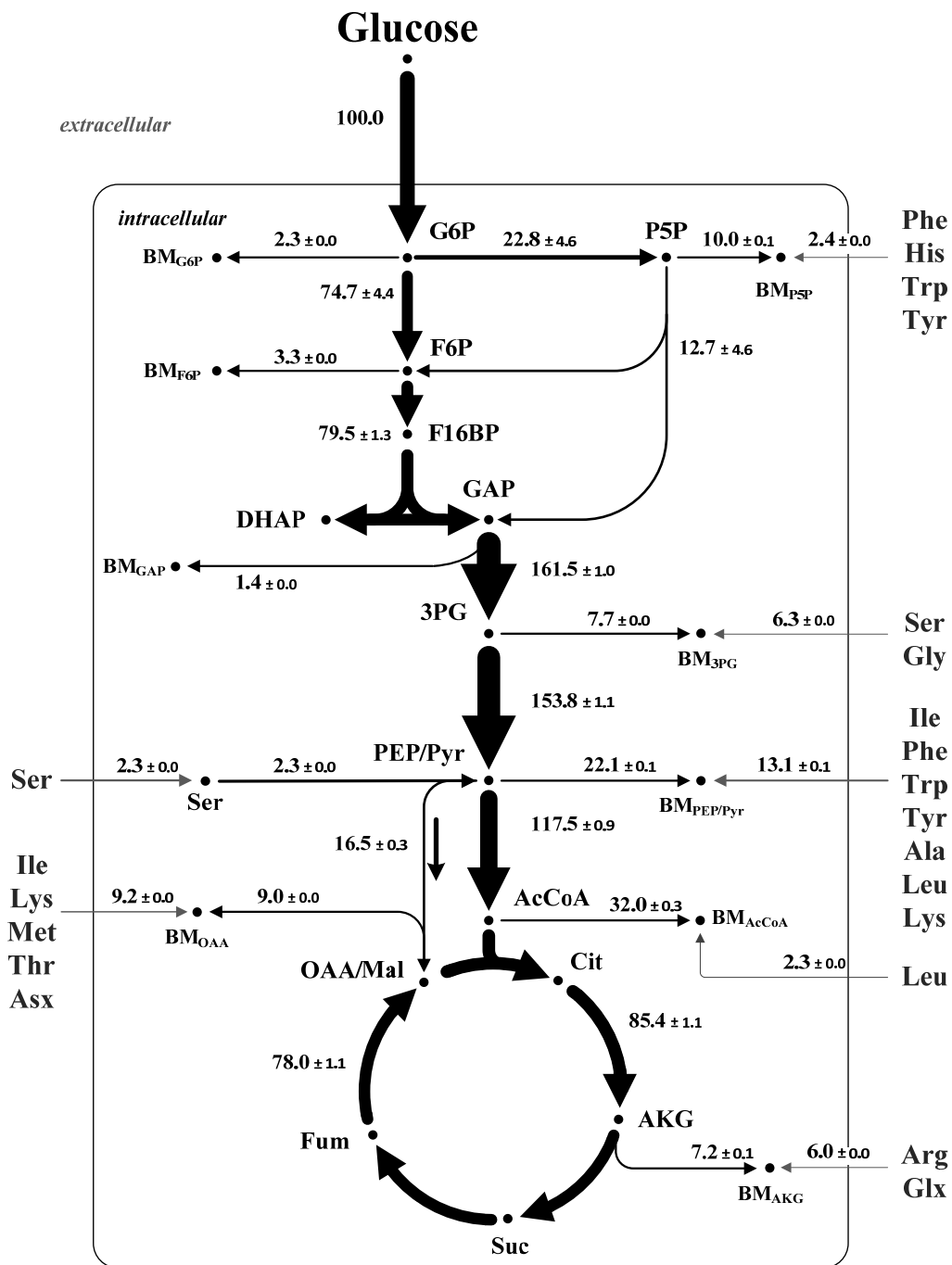
Figure VI-5. *In vivo* carbon flux distribution of the central metabolism of *C. glutamicum* ATCC 13032 during growth on complex media, resulting in multi-phase growth behavior: Phase I. Fluxes are standardized to the specific glucose uptake rate (phase I q_S = 4.70 mmol g^{-1} h^{-1}) which was set to 100%. PEP and Pyr, as well as Mal and OAA are lumped together. Net fluxes are displayed with corresponding standard deviations.
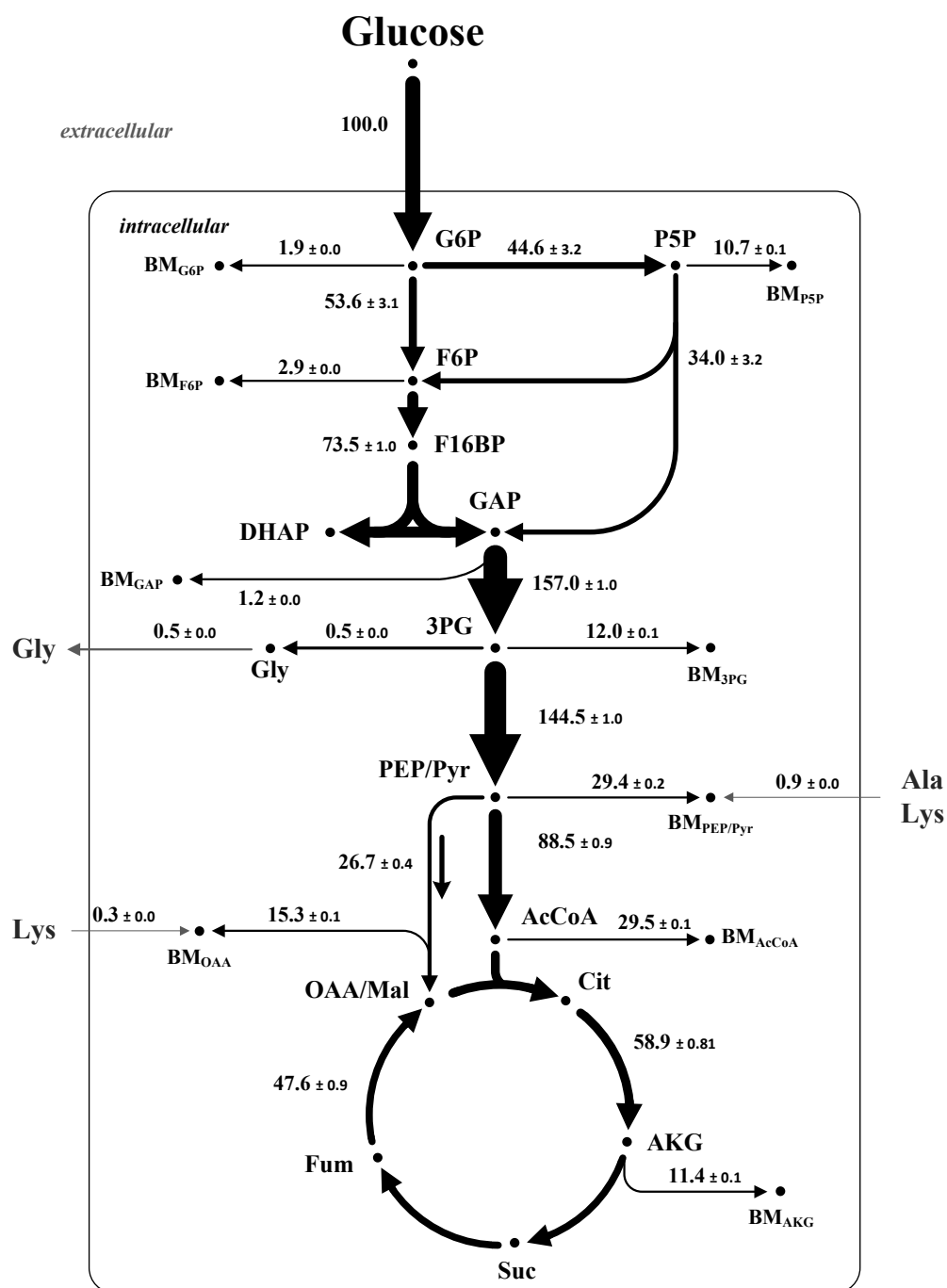
Figure VI-6. *In vivo* carbon flux distribution of the central metabolism of *C. glutamicum* ATCC 13032 during growth on complex media, resulting in multi-phase growth behavior: Phase II. Fluxes are standardized to the specific glucose uptake rate (phase II q_S = 5.46 mmol g^{-1} h^{-1}), which was set to 100%. PEP and Pyr, as well as Mal and OAA are lumped together. Net fluxes are displayed with corresponding standard deviations.

The flux partitioning at the branch point between glycolysis and PPP is of special interest as it allows assessing the amount of NADPH delivered by the oxidative branch of the PPP as well as the accompanying carbon loss and the precursor supply via this pathway. PPP activity during the first phase was drastically reduced compared to the second phase, indicating the reduced demand of NADPH for anabolic reactions due to the considerable amino acid consumption. Thus less carbon had to be dedicated for biomass production and NADPH supply and could therefore be channeled through the pathways generating energy in terms of NADH and eventually ATP. This reduced requirement of consumed glucose for precursor supply was also reflected in a high TCA activity of over 80%. During the second growth phase the PPP activity was increased according to the increased anabolic demand of glucose as precursor supplier and the enhanced requirements for NADPH for biomass production, deduced from the main usage of glucose as sole carbon source. TCA activity dropped to only 59%, which could be caused by the increased requirement of the biomass precursors acetyl-CoA, pyruvate and phosphoenolpyruvate.

Metabolic flux partitioning at the glucose 6-phosphate node during the second growth phase on complex substrate was identical to that obtained from ^{13}C MFA on glucose as sole carbon source. Since glucose was also the sole carbon source during the second growth phase on complex medium one would expect a similar flux distribution as it was the case in the ^{13}C MFA experiment. A further validation of the applicability of this approach was performed, analyzing the NADPH consuming and producing reactions, based on the estimated fluxes depicted in Figures VI-5 and VI-6. The anabolic NADHP demand of 15.9 mmol NADPH per gram biomass during sole glucose consumption (Yang et al., 2006) was corrected for both growth phases considering the consumption of amino acids and their direct incorporation into biomass. For the first growth phase, a NADPH generation of 131.0% (related to the glucose uptake rate) and a NADPH demand of 127.0% were determined, indicating a closed NADPH balance for this phase. Due to the reduced amino acid uptake in the second growth, the anabolic demand of NADPH was increased and calculated with 146.0%. The NADPH supply was determined to account for 148.1% likewise matching the requirements.

In summary, both growth phases exhibited closed carbon as well as NADPH balances, ensuring a correct determination of the intracellular *in vivo* carbon flux distributions under dynamic metabolite conditions using balance equations listed in Table VI-1. Thus, the supposed non-participation of the malic enzyme during glucose sustained growth (Kromer et al., 2008; Chapter V) was validated.

Conclusions

The metabolite balancing approach was seen to be best suited for fluxome estimation on complex medium for multiple reasons. First, growth-phase dependent changes in the fluxome are challenging for stationary ^{13}C-MFA, since it is based on an isotopic steady state in the main biomass components like the cellular protein. However, during dynamic changes isotopic steady state may not be reached in cellular protein. Thus, the only labeling-based alternative would be a dynamic labeling approach, employing free intracellular metabolites for determination of the corresponding labeling patterns. This approach also requires the determination of intracellular metabolite concentrations that are often difficult to accomplish (Bolten et al., 2007; Wittmann et al., 2004c). Furthermore potential protein degradation (turnover), resulting in the release of labeled amino acids representative for a previous phase, could corrupt the results. Even if all experimental problems are solved, such a dynamic labeling approach is experimentally, analytically and also computationally demanding.

Another reason for applying metabolite balancing is the scale-independency of this approach. A tracer-based analysis is always scale-dependent as information obtained from small-scale tracer cultivations that are required due to their inherent cost for labeled substrates have to be transferred to large-scale fermentations. Only gas chromatography combustion isotope ratio mass spectrometry (GC-C-IRMS) can solve the cost issue of ^{13}C labeled substrates to a certain extent (Heinzle et al., 2008; Yuan et al., 2010).

Chapter VII

Bringing the facts together

Comparative fluxome and dynamic metabolite analysis in a genetically engineered *C. glutamicum* strain cultivated on complex medium

Abstract*

In the following research, important insights into the metabolizing pathways and especially into the cellular adaptation capability of *C. glutamicum ΔpurA ΔguaB2 purF^{K348Q} Δpgi* were revealed. In small-scale fermentation with peptone-supplemented medium, the utilization of complex medium components were analyzed. The supplementation with peptone was applied to prevent glucose metabolism specific limitations of this *C. glutamicum* mutant determined for cultivations on minimal medium strain due to the *pgi* deletion (Chapters IV and V). The utilization of complex medium components was found to delay the *pgi* specific phenomenon *i.e.* the reductive burden due to excess NADPH delivery and the associated growth stagnation. Furthermore, peptone-supported growth resulted in an increased NADH and ATP supply. This promoted enhanced intracellular IMP concentrations of 40.66 μmol g_{CDW}^{-1} (12.88 μmol g_{CDW}^{-1} on minimal medium with glucose as sole carbon source; Chapter IV). The change of the carbon and precursor sources – from considerable peptide/amino acid supported growth (45.8% peptone derived biomass formation and metabolization of aspartate/asparagine, glutamate/glutamine and serine) to mainly glucose supported growth – however led to a progression of the NADPH surplus and the initiation of a growth stagnation period.

Introduction

In the field of the biotechnological industry, *Corynebacterium glutamicum* and related species provide an excellent production platform for food and feed additives, pharmaceuticals, fine chemicals, polymers and bio-based fuels (Becker and Wittmann, 2012). Rational strain optimization employing *metabolic engineering* strongly contributed to further broaden the product portfolio of this organism (Becker and Wittmann, 2012). In this study the potential of this organism for biotechnological production of the flavor-enhancing compound IMP was investigated. Various parameters and key points – supplying, regulating or constraining the purine biosynthesis capability – have been investigated in previous studies (Chapters IV and V) and were included in an approach focusing on intracellular IMP accumulation. In the course of these works, some of the parameters proofed to be detrimental for cellular growth, as was determined for the *pgi* deletion (Chapter V). In addition, redirection of the metabolic carbon fluxes caused by an entry block into glycolysis and aiming at an increased precursor supply of ribose 5-phosphate led to a metabolic shift of the intracellular distribution of the purine intermediates, favoring the accumulation of the corresponding degradation products – especially hypoxanthine – at the expense of IMP (Chapter IV). This metabolic shift was reported to be influenced mainly by a decreasing ATP supply via oxidative phosphorylation (Noguchi et al., 2003) which was consistent with the results obtained and discussed in Chapter IV. The decreased ATP delivery was caused by a diminished generation of NADH due to the forced metabolization of the sole carbon source glucose through the pentose phosphate pathway and the associated decarboxylating reaction of the 6-phosphogluconate dehydrogenase. In addition to the carbon loss due to the release of one molecule CO_2 per mol glucose 6-phosphate entering the oxidative branch of the PPP as initiating step of the metabolization, the redirection through the PPP was accompanied by a rigorous overabundance of NADPH (unbalanced supply and demand), resulting in a growth arrest for 24 h (Chapter V). This particular growth behavior developed after switching from complex medium to minimal medium employing glucose as sole carbon source and proofed to be detrimental with regard to the specific growth rate.

However, these two burdens are clearly linked to the utilization of glucose as carbon source and its sole metabolization via the oxidative branch of the PPP upon *pgi* deletion. As industrial biotechnological fermentation processes are seldom based on minimal medium containing expensive or purified compounds, the utilization of complex and low priced substances, *e.g.* peptone, and associated consequences on the intracellular purine accumulation should be investigated in this study. Thereby the main focus was put on the NADH generation using the provided complex substances in comparison to the usage of glucose as sole carbon source. In addition, the disturbance of the growth performance by excessive NADPH supply, determined on glucose sustained growth, was analyzed likewise and the impact on the purine concentrations was investigated.

Materials and methods

Bacterial strains

In the present study, the wild type strain of *Corynebacterium glutamicum* (ATCC 13032) and the site-directed mutant *C. glutamicum ΔpurA ΔguaB2 purF^{K348Q} Δpgi* were investigated. The wild type strain (*C. glutamicum* ATCC 13032) was purchased from the American Type Culture Collection (Manassas, VA, USA) and the site-directed mutant was constructed as described previously (Chapter IV).

Media and growth conditions

Precultures were carried out on an orbital shaker (Multitron 2, Infors AG, Bottmingen, Switzerland) at 230 rpm and 30°C. First precultures were performed on complex medium (pH 6.8) in baffled shake flasks (25 mL medium in 250 mL baffled shake flasks) containing per liter: 10.0 g glucose, 2.5 g NaCl, 2.0 g urea, 5.0 g yeast extract, 5.0 g beef extract, 5.0 g polypeptone and 20.0 g casamino acids. For agar plates, the complex medium was supplemented with 20.0 g L^{-1} agar. Second precultures (50 mL medium in 500 mL baffled shake flasks) and main cultures on complex media (pH 7.2) contained per liter: 4.0 g KH$_2$PO$_4$, 16.0 g K$_2$HPO$_4$, 4.0 g peptone, 20.0 g glucose, 10.0 g MgSO$_4$, 6.0 g urea, 100 mg CaCl$_2 \cdot 2$ H$_2$O, 1 mg ZnSO$_4 \cdot 7$ H$_2$O, 20 mg FeSO$_4$, 17 mg MnSO$_4$, 20 mg cysteine, 30 mg biotin, 10 mg calcium pantothenate and 5 mg thiamine. For cultivation of the site-derived mutant *C. glutamicum ΔpurA ΔguaB2 purF^{K348Q} Δpgi* exhibiting deletions of adenylosuccinate synthetase (*purA*) and IMP dehydrogenase (*guaB2*), the medium was additionally supplemented with 200 mg L^{-1} adenine sulfate and 80 mg L^{-1} guanine hydrochloride, due to auxotrophy-derived requirements (Chapter IV).

Main cultivations were performed in a stirred tank bioreactor (500 mL, Meredos, Bovenden, Germany) in a volume of 75 mL at 30°C and 1,000 rpm. Dissolved oxygen concentrations during fermentation were always above 60% air saturation thus avoiding

oxygen limitation. The airflow was controlled at 1 vvm (vessel volume per minute) by a mass flow controller (WMR Compact 4, Brooks Instruments, Veenedaal, Netherlands) and composition of air and exhaust gas was quantified using a quadrupole mass spectrometer (Omnistar, Inficon, Vaduz, Liechtenstein). Process parameters were collected and stored by a process control system (Lucullus PIMS 2.1, Biospectra, Schlieren, Switzerland).

Chemicals

Yeast extract, polypeptone, casamino acids and beef extract were obtained from Difco Laboratories (Detroit, USA). All other chemicals and reagents were purchased from Sigma-Aldrich (Steinheim, Germany), Merck (Darmstadt, Germany), Fluka (Buchs, Switzerland), Roth (Karlsruhe, Germany) and Roche Diagnostics (Mannheim, Germany) and were of analytical grade unless stated otherwise.

Extracellular substrate and product analysis

Biomass concentrations were determined by measuring the optical density of the culture at 660 nm (OD_{660nm}) using a photometer (Marsha Pharmacia Biotech, Freiburg, Germany) which was gravimetrically correlated with the cell dry weight. Extracellular substrates and secreted products were analyzed after 3 min centrifugation at 16,000 *g*. Quantification of glucose was performed in diluted supernatants by HPLC (Kontron Instruments, Neufahrn, Germany) by RI detection as described previously (Chapter VI). Total amino acid concentrations in complex media were determined after acidic hydrolysis of the peptides contained in the corresponding supernatants as described previously (Kromer et al., 2005; Chapter VI). Extracellular concentrations of adenine and guanine were quantified by HPLC (Agilent 1290 Infinity, Agilent Technologies, Waldbronn, Germany) as described previously (Chapter IV).

Intracellular metabolite analysis

Extraction and quantification of intracellular purine intermediates by LC-ESI-MS/MS was performed as described previously (Peifer et al., 2012; Chapter III).

Determination of the in vitro malic enzyme activity

Determination of *in vitro* malic enzyme activity was performed in crude cell extracts. Cultivations and cell disruption were performed as described previously (Chapter V). The specific activity was determined using the molar extinction coefficient of NADPH ($\varepsilon_{340nm} =$ 6.22 mM^{-1}) and the corresponding protein content contained in the crude cell extracts. The final protein concentration was between 0.2-0.4 g L^{-1}. The reaction mixture contained 100 mM Tris/HCl (pH 7.8), 200 mM KCl, 2 mM MgCl$_2$, 1 mM NADP$^+$, 40 mM malate and 50 µL of the crude cell extract. Determination of the *in vitro* malic enzyme activity was based on the change of absorption at 340 nm due to NADPH formation. The protein content was determined by the method of Bradford (1976) and the reagent solution from Sigma-Aldrich with bovine serum albumin as external standard.

Measurements were started by addition of the substrates, performed at 30°C and monitored for 15-30 min. Negative controls were performed without substrate or crude cell extract, respectively. All measurements were done in a total volume of 1 mL and carried out in triplicate.

Fluxome analysis

Carbon flux distribution of *C. glutamicum ΔpurA ΔguaB2 purF^{K348Q} Δpgi* was determined by a metabolite balancing approach. Briefly, extracellular measurable rates (glucose consumption, biomass formation, amino acid and peptide consumption and amino acid secretion) and anabolic demand for biomass formation were used to determine the metabolic fluxes of a simplified model containing reactions of glycolysis/gluconeogenesis, TCA cycle, PPP and anaplerotic carboxylation (as combined fluxes of the anaplerosis).

Statistical evaluation was carried out using a Monte Carlo approach applying 1000 independent runs (for detailed description see Chapter VI).

Visualization was performed using Omix software (Droste et al., 2011).

Results and discussion

In the present study, the availability of compounds – peptides and free amino acids – derived from peptone as complex medium supplement, their utilization and corresponding influences on the intracellular distribution and accumulation of the purine biosynthetic pathway intermediates in *C. glutamicum ΔpurA ΔguaB2 purF^{K348Q} Δpgi* were analyzed. Utilization of those complex components, which can directly serve as precursors for protein formation, led to a direct reduction of the ATP demand for protein synthesis. The overall ATP availability – as a key parameter for the purine distribution to be optimized in this study – was thus improved. In addition, the amount of carbon drained from the main pathways and spend for protein synthesis was diminished, resulting in comparatively increased fluxes (normalized to the glucose consumption rate) of the different pathway branches. The connection between the postulated increased flux activities and the cofactor delivery, *i.e.* NADH and ATP, was investigated and discussed below.

Dynamics of intracellular purine pathway metabolites during multi-phase growth

As described in Chapter VI, the wild type strain of *C. glutamicum* grown on complex medium exhibited exponential growth during the whole cultivation period, although two distinct growth phases were detected switching from amino acid and peptide supported growth (phase I) to primary glucose consumption (phase II) (for a detailed description see Chapter VI). The concentrations of the main purine intermediates were determined for the second growth phase and compared to those obtained during growth on minimal medium (Chapter IV). As illustrated in Table VII-1, the distribution of the purine intermediates on complex medium was similar to those obtained during growth on minimal medium. The concentration of AMP was found to be decreased and the concentration of GMP to be increased, however no significant intracellular accumulation of IMP or hypoxanthine were detected for both cases. The determination was likewise performed for the site-directed

mutant *C. glutamicum ΔpurA ΔguaB2 purF^{K348Q} Δpgi* for the first and additionally the third growth phase.

Table VII-1. Concentrations of purine intermediates [μmol g_{CDW}^{-1}] in *C. glutamicum* wild type (ATCC 13032) and *C. glutamicum ΔpurA ΔguaB2 purF^{K348Q} Δpgi*, determined during growth on minimal medium (MM) and complex medium (CM).

	concentrations [μmol g_{CDW}^{-1}]										
compound	ATCC 13032						*ΔpurA ΔguaB2 purF^{K348Q} Δpgi*				
	MM[a]			CM			MM			CM[b]		
AMP	8.13	±	0.50	6.57	±	0.94	3.57	±	0.20	5.83 (4.18)	±	0.04 (0.37)
GMP	2.63	±	0.16	5.04	±	0.33	0.51	±	0.03	1.30 [c]	±	0.02
IMP	0.49	±	0.06	0.38	±	0.04	12.88	±	0.74	40.66 (11.86)	±	0.53 (1.49)
hypoxanthine	0.28	±	0.03	0.10	±	0.03	101.53	±	1.09	7.57 (7.31)	±	0.95 (0.55)

[a] data on minimal medium were taken from Chapter IV.

[b] concentrations for *C. glutamicum ΔpurA ΔguaB2 purF^{K348Q} Δpgi* on complex medium were determined for the first (top) and third growth phase (in brackets, bottom) as depicted with asterisks in Figure VII-1.

[c] below detection limit.

The genetically engineered strain *C. glutamicum ΔpurA ΔguaB2 purF^{K348Q} Δpgi* exhibited a significantly different growth behavior compared to the wild type, which was reflected in four distinct growth phases (Figure VII-1). For neither strain grown on complex medium, any nucleosides were detected, which even on minimal medium solely exhibited small concentrations (Table VII-1). During the whole cultivation no secretion of purine compounds into the extracellular environment was observed and solely the intracellular concentrations were determined.
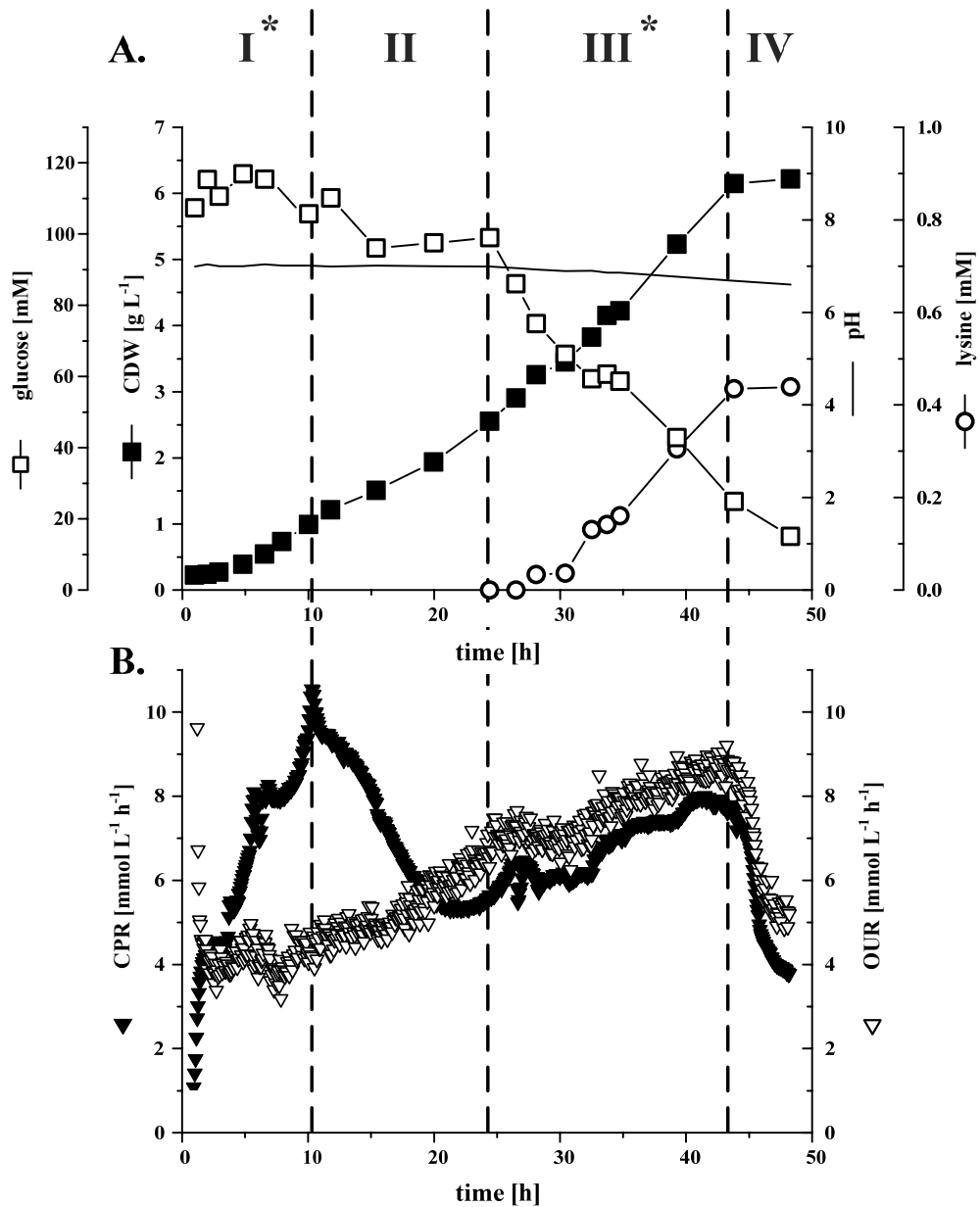
Figure VII-1. Batch fermentation profile of *C. glutamicum ΔpurA ΔguaB2 purF^{K348Q} Δpgi* on complex medium, resulting in multi-phase growth. Asterisks mark the corresponding growth phases further investigated. (**A.**) Growth profile with biomass production [g_{CDW} L^{-1}], glucose consumption [mM], lysine production [mM] and pH. (**B.**) CO_2 production rate [CPR; mmol L^{-1} h^{-1}] and O_2 uptake rate [OUR; mmol L^{-1} h^{-1}]. All data are shown with respect to observed growth phases.

In direct comparison to the wild type strain, the distribution of the detected purine compounds differed significantly. The IMP concentration of *C. glutamicum ΔpurA ΔguaB2 purF^{K348Q} Δpgi* significantly exceeded the wild type level in phase I (amino acid- and peptide-supported growth) (Table VII-1). The IMP concentration (40.66 µmol g_{CDW}^{-1}) even surpassed the concentration determined during growth on minimal medium significantly (12.88 µmol g_{CDW}^{-1}). In addition, AMP and GMP concentrations were drastically reduced compared to the wild type, which is consistent with results obtained in Chapter IV from growth experiments on minimal medium. The shift towards glucose-supported growth, however, led to a decrease of the intracellular IMP pool by 70% to a final concentration of 11.86 µmol g_{CDW}^{-1} which is in excellent agreement with the concentration determined for growth on glucose as sole carbon source in minimal medium (Chapter IV – Table IV-1).

One of the major objectives of this study was the investigation of *C. glutamicum ΔpurA ΔguaB2 purF^{K348Q} Δpgi* cultivated on peptone-supplemented medium. Thereby, the quantitation of purine intermediates and their intracellular distribution was put into focus.

Up to this point it can be concluded that the supplementation with peptides and free amino acids positively influenced the distribution of the purine metabolites. Especially the accumulation of the monophosphorylated nucleotide IMP was increased. Former results (Chapter IV) indicated a decrease of the IMP concentration due to a diminished ATP supply upon *pgi* deletion in combination with the deletion of IMP depleting reactions (*purA* and *guaB2*). The increased IMP concentration (40.66 µmol g_{CDW}^{-1}) determined in this study, might indicate that the adverse effect of the *pgi* deletion on the purine distribution was compensated to a certain extend. Due to the fact that the former decline was supposed to be caused by a decreased activity of NADH generating reactions, the phase-dependent metabolic growth behavior and the distribution of the underlying carbon fluxes on complex medium were determined.

Metabolization of alternating carbon sources

Most strikingly, the so far observed unique adaptation process concerning a complete growth stagnation caused by the disruption of the *pgi* gene (Chapter V), was completely absent during cultivation on complex medium for the period investigated and illustrated in Figure VII-1 and was thus determined to be directly linked to sole glucose consumption. In this context, the degree of amino acid/peptide utilization was determined and its impact on the flux distribution was investigated.

In accordance with the results obtained for the amino acid consumption of *C. glutamicum* wild type (Chapter VI) the site-directed mutant *C. glutamicum ΔpurA ΔguaB2 purF^{K348Q} Δpgi* exhibited constant amino acid uptake rates for growth phases I, II and III. In contrast to the wild type growth behavior, the majority of the amino acid uptakes of *C. glutamicum ΔpurA ΔguaB2 purF^{K348Q} Δpgi* however exceeded the anabolic demand, *i.e.* determined for alanine, arginine, aspartate/asparagine, glutamate/glutamine, lysine, serine and threonine (Table VII-2). For *C. glutamicum* ATCC 13032 (wild type) solely serine consumption exceeded the anabolic demand (Chapter VI – Table VI-5). During the second and third growth phases of *C. glutamicum ΔpurA ΔguaB2 purF^{K348Q} Δpgi*, the amino acid consumption declined significantly (Table VII-2), exceeding the anabolic demand solely in the case of alanine during the second growth phase (consumption: 665 µmol g$_{CDW}^{-1}$; anabolic demand: 606 µmol g$_{CDW}^{-1}$).

Table VII-2. Amino acid consumption and production values [µmol g_{CDW}^{-1}], obtained for *C. glutamicum ΔpurA ΔguaB2 purF^{K348Q} Δpgi* grown in 75 ml complex medium for growth phases I, II and III[a].

amino acid	anabolic demand[b]	phase I	phase II	phase III
alanine (Ala)	606	665	665	--[c]
arginine (Arg)	189	315	155	155
aspartate/asparagine (Asx)	399	1045	--	--
glutamate/glutamine (Glx)	806	1426	--	--
glycine (Gly)	361	281	--	--
histidine (His)	71	66	66	66
isoleucine (Ile)	202	163	163	115
leucine (Leu)	440	402	402	226
lysine (Lys)	202	313	--	132[d]
methionine (Met)[e]	146	41	41	--
phenylalanine (Phe)	133	133	133	133
serine (Ser)	225	989	--	--
threonine (Thr)	275	530	--	--
tryptophan (Trp)[e]	54	29	--	--
tyrosine (Tyr)	81	75	75	--

[a] values are obtained from hydrolyzates of the cultivation supernatants and represent the net consumptions of peptides and free amino acids.

[b] data for anabolic demand were taken from Wittmann and Heinzle (2008).

[c] – indicates uptake <1 µmol g_{CDW}^{-1}.

[d] lysine secretion in terms of free amino acids for growth phase III.

[e] for methionine and tryoptophan, values were obtained exclusively from free amino acids due to instabilities during acid hydrolysis.

data for *C. glutamicum* wild type strain on complex medium are depicted in Chapter VI – Table VI-5.

The amino acids taken up exceeding the anabolic demand, *i.e.* alanine, arginine, aspartate/asparagine, glutamate/glutamine, lysine, serine and threonine, are either stored – leading towards increasing intracellular pool sizes – or used as additional carbon sources and hence are metabolized. In order to determine their corresponding pool sizes, the *fast filtration method* for the quantitative determination of free intracellular amino acids in *C. glutamicum*, described by Wittmann et al. (2004c) was applied. The presence of the complex supplement peptone in the medium however precluded an accurate quantification as complex medium components seemed to attach to the cells thus disturbing the precise quantification of intracellular amino acid pools. Therefore, a carbon balance was set up and a possible metabolization of those amino acids was evaluated (Table VII-3).

Table VII-3. Carbon balance for the first growth phase of *C. glutamicum ΔpurA ΔguaB2 purF^{K348Q} Δpgi* grown in 75 mL complex medium.

consumed carbon sources		**produced carbon sources**	
glucose	2.31 C-mmol	biomass (CDW)	2.97 C-mmol
amino acids[a]	2.12 C-mmol (1.95 C-mmol)	CO_2	1.31 C-mmol
Total[b]	4.43 C-mmol (**4.26** C-mmol)		**4.28** C-mmol

[a.] consumption of amino acids was determined comprising all amino acids detected (including those exceeding the anabolic demand): numbers on top; and in addition comprising amino acid below or with balanced anabolic demand (Gly, His, Ile, Leu, Met, Phe, Trp and Tyr) and those reported to be metabolizable (excluding surpluses of Arg, Lys and Thr): numbers in brackets.

[b] carbon balance considering different amino acid utilization.

This evaluation was based on the assumption that an increase in amino acid pools sizes inevitably leads to a reduced carbon supply as these compounds are not metabolized and not used as carbon sources. Table VII-3 illustrates the results obtained in case of exhaustive metabolization (upper numbers) and for the case of a possible storage by

increasing pool sizes (lower numbers). As is clearly indicated in Table VII-3, a thorough metabolization comprising all amino acids detected would lead to an imbalance of consumed and produced carbon sources with a consumption surplus. This is further supported by the fact that the genome of *C. glutamicum* does not comprise gene sequences for the metabolization of arginine, lysine and threonine/isoleucine (Kalinowski et al., 2003) and is thus not able to utilize these compounds as carbon sources. Therefore the surplus of those amino acids that cannot be metabolized and that are exceeding the anabolic demand was assumed to be stored thus increasing the corresponding intracellular pools. The estimation of metabolic fluxes during phase I solely accounted for the metabolized carbon sources, *i.e.* glucose, alanine, aspartate/arginine, glutamate/glutamine and serine.

The second growth phase of *C. glutamicum ΔpurA ΔguaB2 purF^{K348Q} Δpgi* exhibited constantly decreasing specific CO_2 production rates while an increasing biomass formation was observed (Figure VII-1), clearly indicating a metabolic adaptation process involving inconstant consumption and production rates. As depicted in Table VII-2, the amino acid consumption profile significantly changed from phase I to phase III, switching from an amino acid-supported growth during phase I (45.8% peptone-derived biomass formation), to mainly glucose-supported growth. During phase III, CO_2 production increased proportional to biomass concentration (Figure VII-1). Most interestingly biomass formation as well as glucose consumption during phase III showed a linear production/consumption behavior (Figure VII-2) characterized by constant rates (q_{CDW} = 0.203 g L^{-1} h^{-1}, q_{Glu} = 0.308 mmol L^{-1} h^{-1}; Figure VII-2A.) and thus a constant biomass yield ($Y_{X/S}$ = 0.064 g$_{CDW}$ mmol$_{glu}$; Figure VII-2B.).
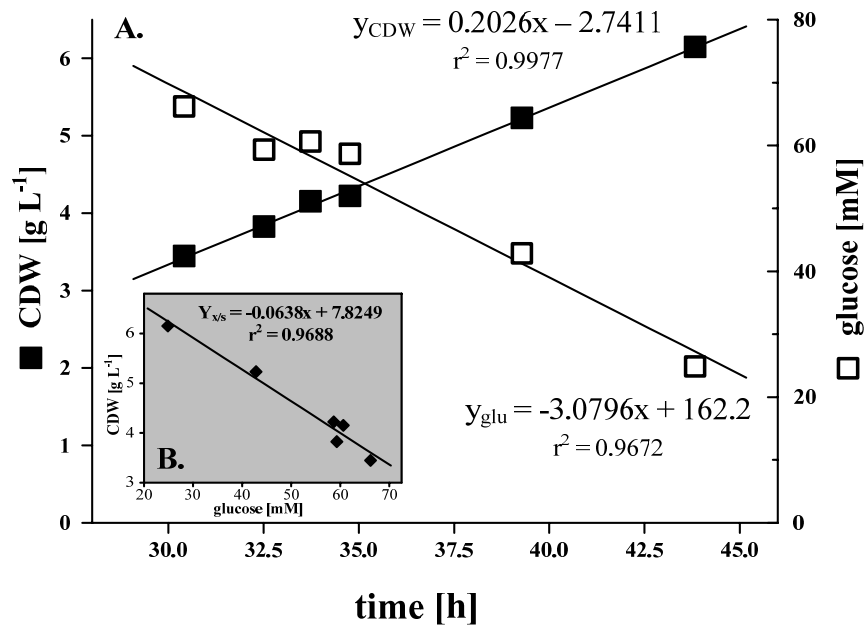
Figure VII-2. Linear biomass formation [g_{CDW} L^{-1}] and glucose consumption [mM] (**A.**) and biomass yield [g_{CDW} mmol$_{glu}$$^{-1}$] (**B.**) during the third growth phase of *C. glutamicum ΔpurA ΔguaB2 purF^{K348Q} Δpgi* on complex medium over time.

It has to be noted however, that the linear growth is directly linked to a constantly decreasing specific growth rate, as the average period for duplication is constantly increasing. The decreasing specific growth rate might be caused by several parameters: one possibility is the insufficient availability of an essential compound *e.g.* limited carbon sources, medium supplements or insufficient oxygen supply. These possible limitations however can be excluded as neither carbon sources nor supplements were limiting and the dissolved oxygen concentration was above 60% throughout the entire cultivation. Another growth-inhibiting parameter is the accumulation of harmful secretion products normally observed as initiation of cell lysis and the death phase. This was observed for the cultivation of the wild type strain of *C. glutamicum* as a reduction of the final biomass concentration (Chapter VI – Figure VI-4). However, for *C. glutamicum ΔpurA ΔguaB2 purF^{K348Q} Δpgi* no reduction in biomass concentration was detected (Figure VII-1). The cultivation time was thus prolonged up to 80 h and the growth behavior was monitored (Figure VII-3).
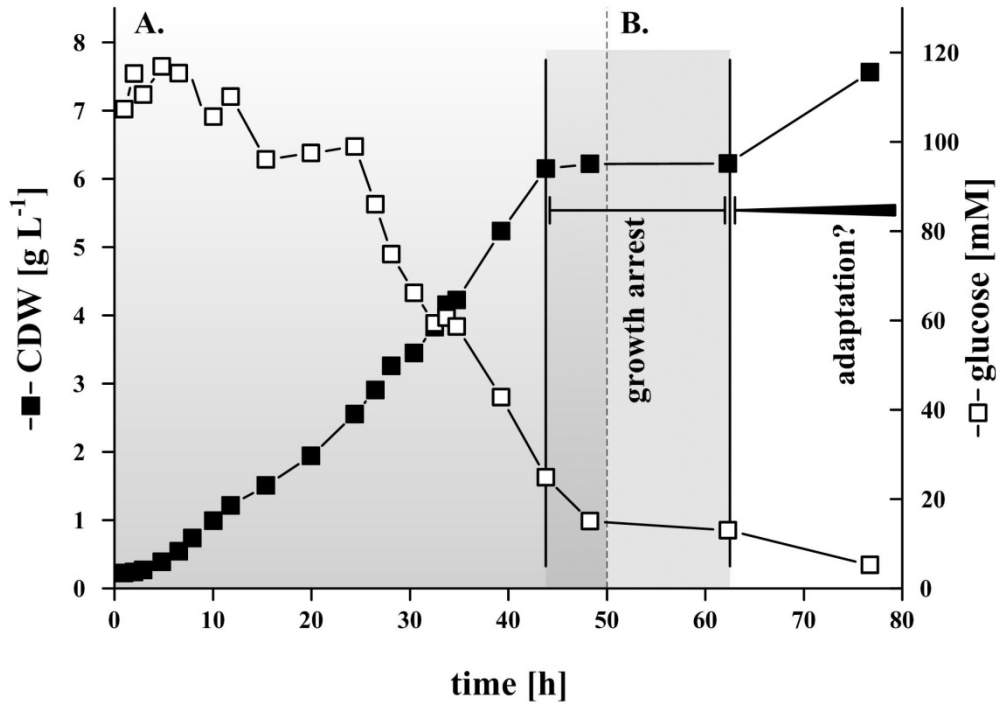
Figure VII-3. Batch fermentation profile of *C. glutamicum ΔpurA ΔguaB2 purF^{K348Q} Δpgi* on complex medium, resulting in multi-phase growth. (**A.**) Growth profile with biomass production [g_{CDW} L^{-1}] and glucose consumption [mM] taken from Figure VII-1; (**B.**). Period of growth arrest without biomass formation and potential adaptation phase resulting in growth recovery.

The growth stagnation, starting after 45 h was found to persist for another 20 h. The glucose consumption, however, further decreased (slightly) which became even more pronounced after 65 h with a simultaneous increase of the biomass concentration (Figure VII-3B.). Due to the almost exhaustive utilization of glucose, the growth behavior was solely monitored until that point of the cultivation. Resumption of growth after 65 h due to contamination was excluded by microscopic investigation and plating on agar plates.

In summary, it seems quite likely that the growth stagnation observed during this cultivation did not depict the death phase but a temporary growth arrest, found to be a mutual characteristic for *pgi* deletion strains of *C. glutamicum* grown on glucose as sole carbon source as shown in previous studies (Chapter V). This is further supported by the fact that no substrate or supplement limitations were detected, that glucose was

continuously depleted and that the growth stagnation was first initialized by a substrate change, *i.e.* from amino acid to glucose consumption.

Considering these facts, it seems quite likely that the growth stagnation, determined for all *pgi* deletion strains, was not circumvented by the addition of complex medium components, *i.e.* peptone, but solely delayed. In order to verify these findings, cultivation conditions should be modified, *e.g.* increasing the glucose concentrations or decreasing the peptone concentrations and thus provoking an earlier shift towards the growth stagnation period, which could be further analyzed in more detail. Besides, it would be beneficial to determine whether an additional glucose supplementation during the growth stagnation, *e.g.* as glucose pulse, would prolong and sustain cellular growth after the stagnation period.

The consequences of the substrate switch – from amino acid-supported growth during phase I to mainly glucose consumption during phase III – on the redox metabolism (NADH/NADPH) were analyzed in detail and possible connections to the initiation of the growth stagnation were suggested. The reduced NADPH demand for protein due to the usage of amino acids from the medium and the consequences for the NADH generation were considered in the following.

Metabolic flux distribution in C. glutamicum ΔpurA ΔguaB2 purF^{K348Q} Δpgi during phase I

The distribution of intracellular carbon fluxes of *C. glutamicum ΔpurA ΔguaB2 purF^{K348Q} Δpgi* was determined for the first growth phase. Due to the metabolic adjustments during phase II and the linear growth behavior in phase III, these two phases were not considered for flux estimation. The consequences of the drastically reduced amino acid consumption in phase III were however related to the overall growth behavior and the consequences are discussed in the overall context (see *"Metabolic activity and NADPH metabolism during phase III – Results and Discussion"*).
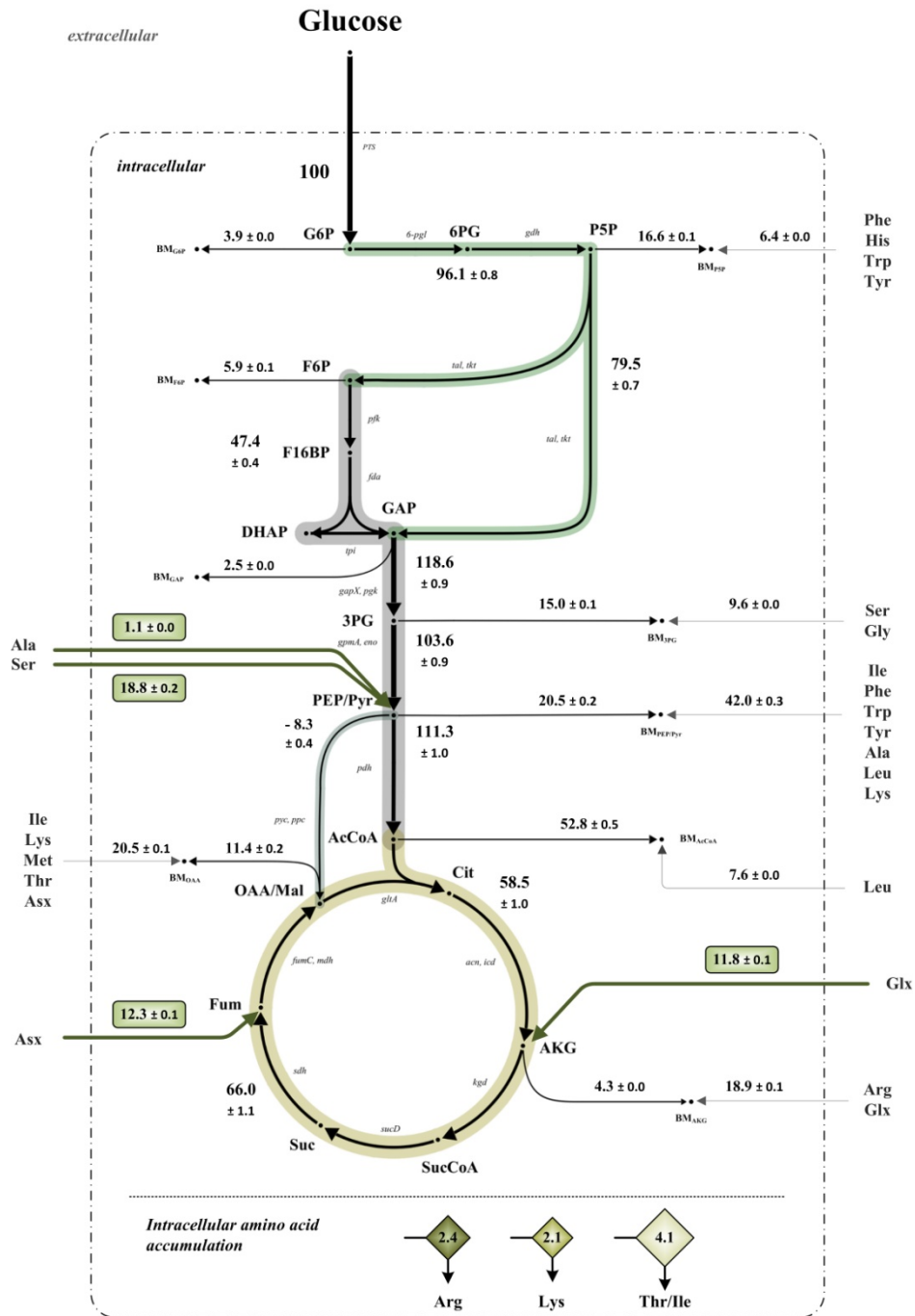
Figure VII-4. *In vivo* carbon flux distribution of the central metabolism of *C. glutamicum ΔpurA ΔguaB2 purF^K348Q Δpgi* during growth on complex media (phase I). Fluxes are standardized to the specific glucose uptake rate (q_S = 0.97 mmol g^-1 h^-1) which was set to 100%. PEP and Pyr, as well as Mal and OAA are lumped together. Net fluxes are depicted with corresponding standard deviations derived from 1000 Monte Carlo simulations. Intracellular accumulation of arginine, lysine and threonine/isoleucine is illustrated with estimated flux activities normalized to the glucose uptake rate (for explanations see Table VII-3 and text).

The *pgi* deletion led to a redirection of the carbon flux and an exclusive metabolization of glucose via the oxidative branch of the PPP (Figure VII-4). This was directly linked to a tremendous increase of NADPH formation and carbon release in terms of CO_2 due to the decarboxylating reaction in the PPP.

The increased CO_2 formation as well as the enhanced NADPH generation, exhibited both adverse effects: first affecting the NADH supply as the ratio of PPP and TCA cycle dictates the potential for an efficient NADH supply mainly provided in the TCA cycle (Marx et al., 1999; Noguchi et al., 2003); and secondly affecting the growth performance due to an NADPH overabundance and the associated reductive burden. Both points will be discussed in detail, especially focusing on the consequences for the overall growth performance and the intracellular distribution of purine pathway intermediates.

The increase of the PPP activity led to a substantial CO_2 production and an initial carbon loss of 17% of the consumed glucose in the first metabolizing pathway (PPP). In addition, the comparatively high biomass yield of 0.19 g mmol^{-1} on complex medium ($0.076 \text{ g mmol}^{-1}$ on minimal medium; Chapter IV) required large amounts of precursors. This anabolic demand, however, was covered to a significant extent by the amino acid consumption (Table VII-2) and 45.8% of the composed biomass were synthesized from these compounds. Furthermore, the enormous uptake of serine, glutamate/glutamine, aspartate/asparagine and – to a lesser extent – alanine led to a carbon replenishment in the lower glycolysis and the TCA cycle (Figure VII-4). Due to the increased uptake especially of glutamate, an increase of the TCA cycle activity to 66%, leading from α-ketoglutarate to succinyl-CoA, and an even further increase due to the aspartate metabolization to 72.3%, leading from fumarate to malate were determined. Considering these findings, the peptone-supplemented metabolic activity provided an overall XADH supply of 472.8% compared to 387.1% generated during growth on glucose as sole carbon source (Figure VII-5 and Chapter IV). As the generated XADH can be directly used to generate ATP via the respiratory chain, the total ATP supply can be assumed to be significantly improved during growth on peptone-supplemented media (at least for the first growth phase).
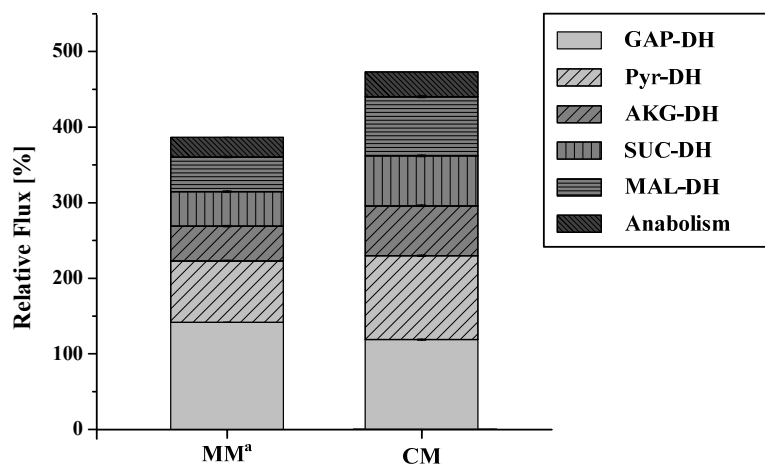
Figure VII-5. XADH supply for *C. glutamicum ΔpurA ΔguaB2 purF[K348Q] Δpgi*. Glyceraldehyde 3-phosphate dehydrogenase (GAP-DH), pyruvate dehydrogenase (Pyr-DH), α-ketoglutarate dehydrogenase (AKG-DH) and malate dehydrogenase (MAL-DH) were considered as NADH supplying reactions and succinate dehydrogenase (SUC-DH) as $FADH_2$ supplying reaction. In addition, metabolization of excessive Asx (Table VII-2 and Figure VII-4) to fumarate, resulting in an increased flux towards malate, was considered. Anabolic derived NADH was corrected for reduced amino acid synthesis due to amino acid consumption (Table VII-2) and considered with 1.7 mmol g_{CDW}^{-1} for growth on peptone supplemented medium and 3.2 mmol g_{CDW}^{-1} for growth on minimal medium (Yang et al., 2006).

[a] data for cultivation on minimal medium were taken from Chapter IV.

The second consequence of the *pgi* deletion was the excessive NADPH generation, mainly caused by the tremendous PPP activity of 96.1%. For the first growth phase the produced NADPH was determined to account for 263.6%, delivered by the activities of glucose 6-phosphate dehydrogenase, 6-phosphogluconate dehydrogenase and isocitrate dehydrogenase (Figure VII-4). Due to the pronounced amino acid uptake, the anabolic demand of NADPH was reduced from 15.9 mmol per gram biomass (Yang et al., 2006) to 8.0 mmol per gram biomass, accounting for a total NADPH demand of 152.0%. Thus, generated and consumed NADPH could not be balanced and caused an apparent NADPH surplus of 111.6%. A potential participation of the malic enzyme (MalE) operating in carboxylating direction and thereby reoxidizing excessive NADPH was then considered.

The possible role of MalE in *pgi* deletion strains of *C. glutamicum* has already been discussed in Chapter V and was determined to be linked with increased oxygen uptake rates, exceeding the requirements for NADH oxidation. The active participation of this enzyme would lead to an additional flux towards malate, and thus inevitably from malate to oxaloacetate transferring the electrons from NADPH (reoxidized by MalE) to NADH (generated by malate dehydrogenase). The increased NADH generation would however require an elevated O_2 consumption to oxidize NADH (Chapter V). In order to assess a potential MalE participation, the oxygen consumption rate – normalized to the glucose uptake rate – was determined and the maximal capacity for NADH reoxidation was calculated. The oxygen consumption rate during phase I accounted for 292.7%, comprising an oxidation potential – in terms of NADH reoxidation – of 585.5%, exceeding the aforementioned NADH generation of 472.8% (Figure VII-5) by 112.7%. As the NADPH overabundance was determined to constitute 111.6%, the increased oxygen consumption could compensate the overproduction of NADPH. It should be mentioned that due to the metabolite balancing approach solely the net-reaction of the anaplerotic decarboxylation and carboxylation could be determined and the participation of MalE and its operating direction can only be speculated about. The verification was thus extended and the *in vitro* enzyme activity of MalE was investigated. With a specific activity of 122 U $mg_{protein}^{-1}$, the *in vitro* activity of this enzyme allowed a maximal conversion of 3.7 mmol g_{CDW} h^{-1} (381.4% normalized to the specific glucose uptake rate of 0.97 mmol g_{CDW} h^{-1}) and thus significantly surpassed the potentially required 111.6%. A participation of MalE in NADPH reoxidation therefore seems quite likely.

Metabolic activity and NADPH metabolism during phase III

The third growth phase is characterized by linear growth (Figure VII-2), with a constant biomass formation rate (0.203 g L^{-1} h^{-1}) and glucose consumption rate (3.08 mmol L^{-1} h^{-1}) and a biomass yield of 0.064 g $mmol^{-1}$. The overall metabolic performance and the consequences of the altered biomass formation and amino acid consumption were qualitatively assessed and compared to the first growth phase.

The biomass yield ($Y_{X/S;PIII} = 0.06$ g mmol^{-1}) was significantly reduced compared to phase I ($Y_{X/S;PI} = 0.19$ g mmol^{-1}) as was the amino acid uptake (Table VII-2). These two alterations should lead to a further increase of the NADPH generation: first, due to the relatively decreased biomass yield, the NADPH consumption for biomass formation will decrease likewise as the NADPH demand is directly linked to the biomass formation; in addition, the lowered biomass yield will cause a reduction in the anabolic precursor demand, inevitably increasing the relative glucose metabolization expressed in relatively increased flux activities. As the generation of NADPH is provided by those reactions, the NADPH supply is supposed to increase proportionally. Thus, the metabolic adjustment – from peptone-supported growth to mainly glucose-supported growth – and the observed decline of the biomass yield seem to further increase the NADPH supply while reducing the NADPH demand which leads to an even more pronounced NADPH surplus and a reductive burden. In this context, the phase III-specific initiation of the lysine secretion (Figure VII-1) might additionally indicate an overloading in the NADPH supply, as the synthesis of this amino acid provides another NADPH oxidizing reaction with a capacity of 0.5 mmol NADPH g_{CDW}^{-1}. In the context of the supposedly tremendous NADPH overabundance, the comparatively minor NADPH oxidizing capacity of lysine secretion ($<1\%$ mM$_{Lys}$ mM$_{Glu}^{-1}$) does not really balance NADPH, but may be regarded as an additional indication for a reductive – and in this case even growth-deleterious – burden.

As phase III was now assessed to not represent a balanced or constant metabolic state, the quantified purine intermediate concentrations for that phase (Table VII-1) cannot be regarded as representative values for the whole phase period, but only as time- and especially (metabolic) state-dependent. Even so, a clear trend, leading from increased (40.66 µmol g_{CDW}^{-1}) to decreased (11.83 µmol g_{CDW}^{-1}) intracellular IMP concentrations was determined and in addition linked to the metabolic consequences provoked by the *pgi* deletion.

Chapter VIII

Outlook

Reflections and future directions

Reflections

The overall objective of the research presented in this study addressed the in-depth analysis of the purine biosynthetic pathway of the Gram-positive soil bacterium *Corynebacterium glutamicum*. Several experimental platforms have been employed, targeting a comprehensive investigation of the underlying system. In order to increase the existing knowledge about the essential pathway of the purine biosynthesis, it is of utmost importance to establish the foundations of systems-level understanding and to identify system structures, *e.g.* interacting parameters, and to comprehend and reconstruct dynamic structures. Furthermore, system redesign, *e.g.* modification and construction, allows the identification of basic principles and regulatory concepts, and helps uncovering cellular responses in terms of *when* and *how* readjustments of metabolic activity are initiated.

In **Chapter I**, a general introduction into the field of systems biotechnology is presented and in addition the possibilities of targeted strain manipulation *e.g.* of *C. glutamicum* as model organism within this field, are addressed. Fundamental principles about this organism, its metabolic physiology as well as the analytical techniques – targeted metabolite profiling employing LC-ESI-MS/MS and metabolic flux analysis – and strain construction principles are summarized in **Chapter II**.

In **Chapter III**, an analytical method for intracellular purine intermediate quantitation in *Corynebacteria* was implemented and validated. Thereby, a suitable extraction procedure for Gram-positive bacteria was especially investigated, that could be directly coupled to a precise and accurate quantitation by LC-ESI-MS/MS.

Following a targeted metabolic engineering approach, site-directed mutant strains of *C. glutamicum* were created: the initial wild type properties were altered, leading to a degradation-deactivated, supposedly feedback-released and precursor-improved purine pathway. To this end several key factors have been identified which positively influence the deregulation towards increased intracellular IMP levels (**Chapter IV**) *e.g.* the deletion of the degrading reactions towards AMP and GMP. Simultaneously, detrimental factors have been exposed, *i.e.* excessively increased PPP activity – targeting an improved

precursor availability – on glucose as sole carbon source (**Chapters IV** and **V**). The deletion of the key enzyme glucose 6-phosphate isomerase caused a tremendous reduction of the intracellular IMP concentrations in combination with a metabolic shift, favorising the intracellular accumulation of the degradation product hypoxanthine (**Chapter IV**). Furthermore, growth-deleterious impacts were determined, which – due to NADPH imbalances – led to a complete growth stagnation of the *pgi* deletion strains for 24 h (**Chapter V**).

This phenomenon was further addressed in **Part II** applying small-scale fermentations with a broadened substrate spectrum. In **Chapter VI**, a suitable method for the determination of intracellular carbon fluxes on complex substrates was implemented. Combining a metabolite balancing approach with off-gas analysis allowed for the quantitation of intracellular fluxes during multi-phase growth. This approach was further validated in direct comparison with ^{13}C MFA on minimal medium with glucose as sole carbon source. Applying this method, multi-phase growth of the wild type strain of *C. glutamicum* (**Chapter VI**) and the site-directed mutant strain *C. glutamicum ΔpurA ΔguaB2 purF^{K348Q} Δpgi* were analyzed in great detail, also determining intracellular pool sized of purine intermediates (**Chapter VII**). In the last chapter of **Part II (Chapter VII)**, the individual aspects, presented and discussed in previous chapters are recapitulated and the tight interconnection of these aspects is highlighted. As a direct consequence, the reductive burden in terms of excessive NADPH – leading to the inability to further sustain cellular growth – and the purine intermediate distribution were significantly improved, but not prevented completely.

The different steps and factors were presented and discussed thoroughly in the previous chapters, conclusions were drawn and future objectives and recommendations have been proposed. The last chapter of this thesis is dedicated to additional aspects and observations made but not presented in the previous chapters as well as challenges not approached directly in the scope of this thesis.

Future directions

Investigation of the redox metabolism in C. glutamicum:
an extended approach

Background

One parameter that has been intensely studied in this thesis was the situation of excessive NADPH production, resulting in an imbalance between supply and demand. The direct cause of this phenomenon and the corresponding consequences have been examined and discussed in detail in Chapter V. Even though a unique adaptation process was discovered and related to the site-directed genetic perturbation of the initiating step of the glycolysis, *i.e.* the disruption of the *pgi* gene, a significant amount of NADPH still needing to be reoxidized, remained unassigned. The issue about additional oxidizing capacities was not entirely resolved and will now be addressed in this context.

Network remodeling using in silico predictions

Metabolization of carbon sources such as glucose leads to the distribution of substrate-derived carbon throughout the entire metabolic network, delivering precursor molecules and redox equivalents. Metabolization thereby generates products either more reduced or oxidized compared to the substrate(s) taken up by the cells. Either way, the sum of all feasible pathways must be redox neutral, meaning that NADH as well as NADPH balances have to be closed (Nielsen et al., 2003). This was the case for all strains analyzed in this thesis except for the *pgi* deletion strains, exhibiting an unassigned NADPH surplus. However, to assure unimpaired cellular growth, additional, so far unconsidered, reduced products must be accumulated or secreted or the reductive state of present products must be higher than supposed, *e.g.* the biomass. As carbon balances were closed and the flux estimations yielded accurate results, the possibility of additional reduced products can be

excluded, pointing at an underestimation of the NADPH demand in terms of a changed reductive state of presently synthesized compounds. Thus the determined products must exhibit a higher degree of reduction as was assumed for setting up the redox balances.

Since the by-products are characterized by a distinct degree of reduction precisely calculable, the only product potentially comprising a higher degree of reduction is the biomass. In turn, the reductive state of the cell dry weight is purported by relative content of the different contributing macromolecules, *i.e.* lipids, carbohydrates, proteins, DNA, RNA and inorganic compounds. In conclusion, changes of the intracellular macromolecular composition of the cell inevitably lead to readjustments of NADPH and NADH delivery and demand, possibly balancing the redox metabolism in *pgi* deletion strains. As especially lipid and protein contents dictate the anabolic demand of NADPH, these two fractions were varied in percentage and the consequences for the NADPH demand were analyzed. In order to establish redox balances for these hypothetically modified conditions, the individual precursor demands were adapted and *in silico* flux distributions, contributing to the NADH and NADPH supply, were calculated.

Under simplified assumption two scenarios were investigated, the first (Scenario A) reflecting increasing lipid content, and the second (Scenario B), reflecting increasing protein content. In order to highlight trends in metabolic adjustments and redox equivalent deliveries, broad ranges were simulated comprising increased as well as decreased fractions of lipids and proteins compared to the wild type biomass composition (Figure VIII-1).

The composition of the cell dry weight was adopted from Kjeldsen and Nielsen (2009) and the precursor demands were modified accordingly as illustrated in Figure VIII-2.
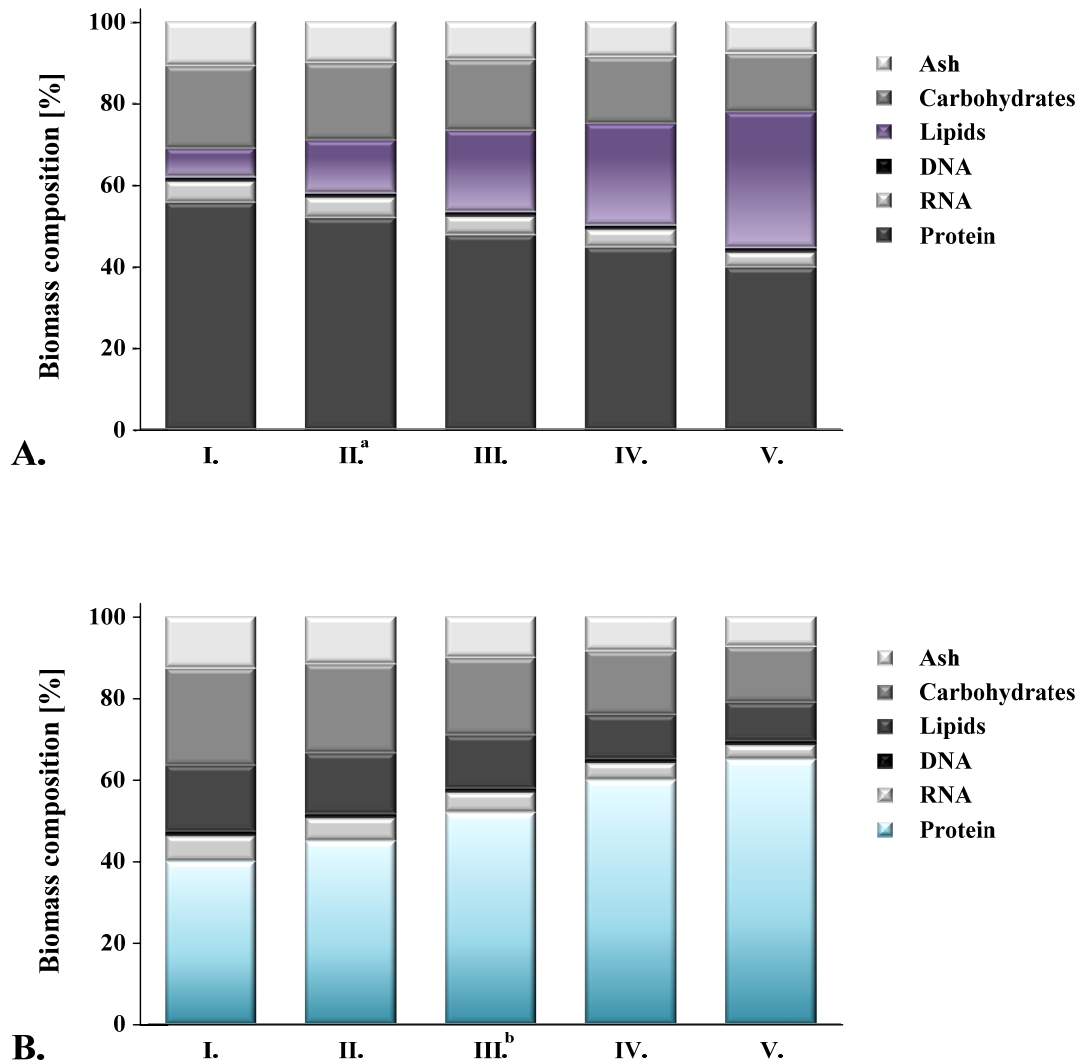
Figure VIII-1. *In silico* varied biomass compositions of *C. glutamicum*, comprising increasing lipid (**A.**) and protein contents (**B.**). Relative fractions were adjusted accordingly, except for DNA content which was assumed to be constant with one DNA molecule per cell exhibiting 1% by weight (for references see *"Supplementary material – Outlook"*).

[a,b] initial biomass compositions adopted from Kjeldsen and Nielsen (2009) for scenario A (modified lipid content) and scenario B (modified protein content), respectively.
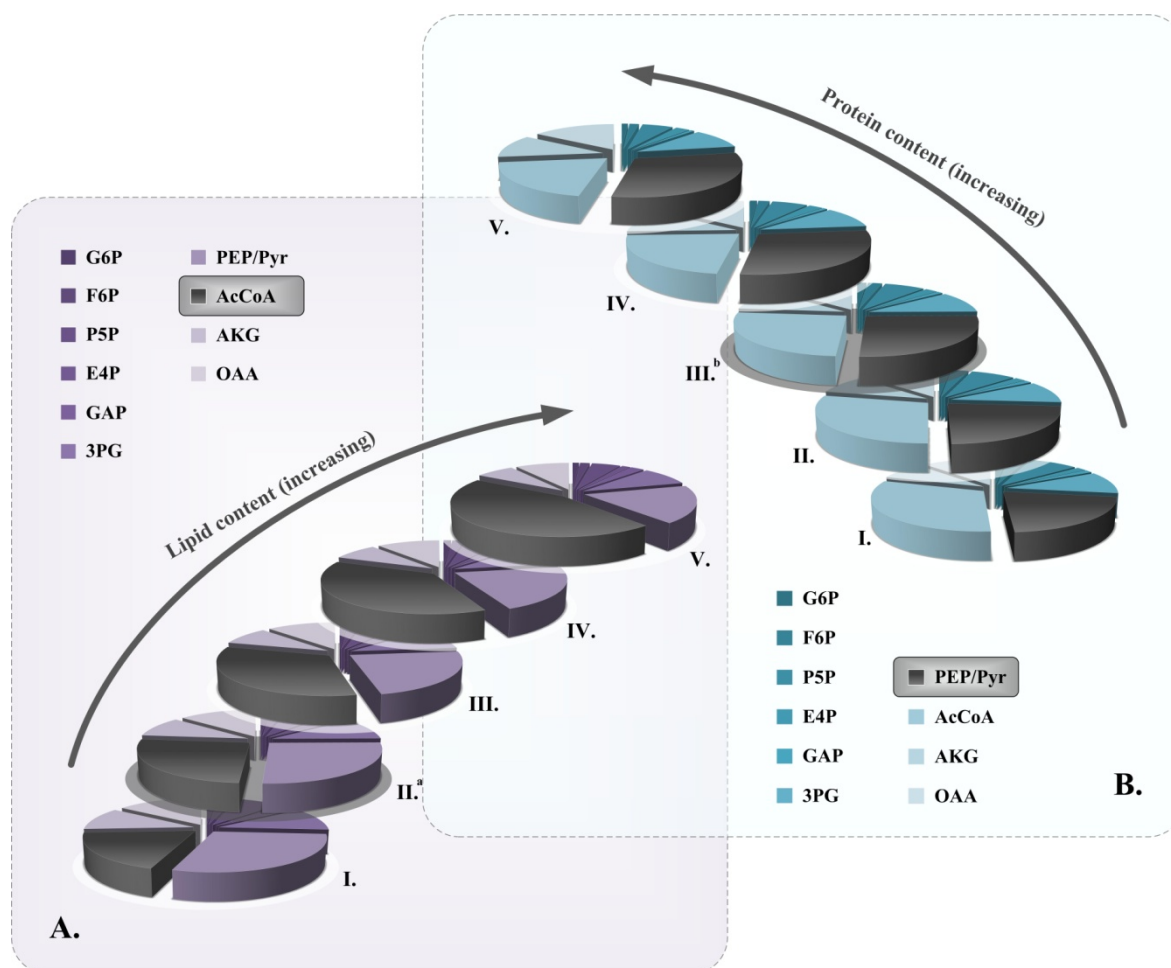
Figure VIII-2. Variation-caused alterations of precursor distribution in *C. glutamicum*, for increasing lipid (**A.**) and protein contents (**B.**). Calculation of precursor fractions were based on the *in silico* cell dry weight remodeling illustrated in Figure VIII-1. Most influenced precursor species are highlighted in dark grey.

[a,b] initial precursor distributions for scenario A (modified lipid content) and scenario B (modified protein content), respectively (adopted from Wittmann and Heinzle (2008)).

Modifications of biomass composition (Figure VIII-1) were reflected in increasing demands of the main precursor for lipid biosynthesis acetyl-CoA (Scenario A; Figure VIII-2A) and in increasing demands of especially phosphoenolpyruvate and pyruvate (PEP/Pyr) as major building blocks for protein biosynthesis (Scenario B; Figure VIII-2B). In consequence, anabolic effluxes of precursors located upstream and downstream of acetyl-CoA and PEP/Pyr were significantly reduced. Impacts on intracellular carbon fluxes were

analyzed by ^{13}C MFA employing strain specific parameters (biomass yield, by-product formations and labeling data derived from Chapters IV and V) and modified precursor demands (Figure VIII-2).
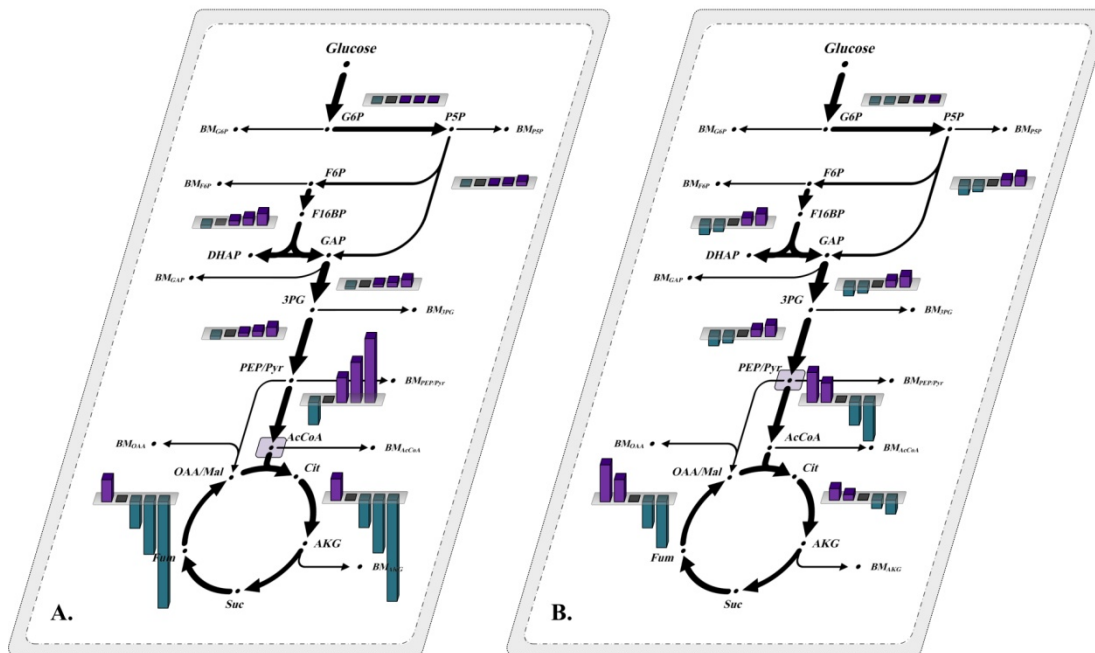
Figure VIII-3. *In silico* predictions of metabolic flux activities based on strain specific parameters ($Y_{X/S}$, $Y_{P/S}$, MDVs) and modified biomass compositions for increasing lipid content (**A.**) and increasing protein content (**B.**). Relative flux changes are shown in turquoise (attenuation) and purple (amplification) comprising altered biomass compositions depicted in Figure VIII-2 (five different compositions for each scenario, from left – lowest lipid/protein content –, to right – highest lipid/protein content). The unmodified (native) biomass composition-related flux distribution (relative changes equal to zero) is shown for each scenario in dark grey (**A.**: second from left; **B.**: third from left; for references see Figures VIII-1 and VIII-2 and *"Supplementary material – Outlook"*).

The resulting predictions of metabolic flux activities are illustrated in Figure VIII-3 for scenario A (increasing lipid content) and scenario B (increasing protein content). It has to

be mentioned however, that these estimations represent simplified *in silico* predictions and have to be validated, requiring an explicit determination of the actual biomass composition.

Variations of the macromolecule content featured significant, content-specific alterations possessing the major modification sites at the acetyl-CoA- and PEP/Pyr-nodes for increasing lipid and protein contents, respectively.

Scenario A

With acetyl-CoA representing the main precursor for lipid synthesis, pronounced carbon withdrawal was observed at this metabolic node assuming an increased lipid fraction in the biomass compositions. Consequently, while increasing lipid content, glycolysis – from glycose 6-phosphate to acetyl-CoA – was increased likewise as the relative anabolic precursor demands, except for acetyl-CoA, were reduced (Figure VIII-2). Oxidative and reversible PPP branches were not affected significantly. Most distinct shifts of the metabolic activities were observed for those reactions directly leading towards or from acetyl-CoA, namely pyruvate dehydrogenase and citrate synthase (Figure VIII-3), marking acetyl-CoA as the major precursor for lipid biosynthesis.

Scenario B

Variations of the protein content revealed a similar trend exhibiting amplified activities upstream of the PEP/Pyr-node and attenuated ones downstream. However, relative flux changes were as pronounced as in scenario A. This is on one side caused by the fact that protein synthesis drains carbon at multiple points within the metabolic network; PEP and pyruvate thereby solely depicting the major contributors while other metabolic pathway branches provide additional precursor, *e.g.* α-ketoglutarate (AKG) and oxaloacetate (OAA) from the TCA cycle. The second point is the difference between absolute contents: while lipids account for 13% of the cell dry weight, proteins account for 52% (Figure VIII-1).

Similar absolute variations, *e.g.* 12% increase in scenario A and 13% in scenario B, lead to tremendous effects in relative percentages leading to an increase of approximately 100% in lipids but only 25% in proteins. In summary, variations of the protein content caused a rather global network adjustment while variation of the lipid content resulted in a more pronounced and primarily punctual modulation.

In addition to remodeling metabolic fluxes, the alteration of the biomass composition drastically altered the reduction degree of the biomass, meaning that the anabolic demands of NADPH and the anabolic synthesis of NADH are depending on these compositions. Stoichiometric demands for both redox equivalents were calculated for each case and are depicted in Table VIII-1.

As illustrated in Table VIII-1, modifications of the lipid content caused a significant increase in the anabolic NADPH demand, whereas an identical increase in the protein fraction – 26% (scenario A) and 25% (scenario B) absolute increase – resulted in a significantly lower NADPH demand. In addition, anabolic supply of NADH decreased to 2.7 mmol g_{CDW}^{-1} in scenario A, but was almost unaffected by changing relative protein contents in scenario B.

Table VIII-1. Stoichiometric demands for NADPH and generation of NADH [mmol g_{CDW}^{-1}] determined from modified biomass compositions, *i.e.* lipid and protein contents[a].

	biomass contents [%]	NADPH [mmol g_{CDW}^{-1}]	NADH [mmol g_{CDW}^{-1}]
Scenario A: increasing lipid content	7	15.0	3.3
	13[b]	15.9	3.2
	20	17.1	3.0
	25	17.9	2.9
	33	19.2	2.7
max. difference[c]	**26**	**4.2**	**0.6**
Scenario B: increasing protein content	40	14.8	3.1
	45	15.3	3.1
	52[b]	15.9	3.2
	60	16.7	3.2
	65	17.1	3.2
max. difference[c]	**25**	**2.3**	**0.1**

[a] calculations based on the theoretical scenarios illustrated in Figures VIII-1 and VIII-2.

[b] initial values for lipid and protein contents, respectively.

[c] in absolute terms.

The complete redox balances were then established (Tables VIII-2 and VIII-3) including the experimentally determined specific oxygen consumption rate and biomass yield as strain-specific, unchanged variables (Chapter V).

Table VIII-2. Predictions for XADH and NADPH redox balances [%] for (*in silico*) increasing lipid content (scenario A) with experimentally determined oxygen consumption [%] (*in vivo*).

lipid content [%][a]	7	13[b]	20	25	33
NADPH production					
G6P DH	97.6	97.8	97.9	97.9	98.0
6PG DH	97.6	97.8	97.9	97.9	98.0
isocitrate DH	48.8	45.7	42.1	39.0	33.7
	244.0	241.3	237.9	234.8	229.7
NADPH consumption					
anabolism	135.0	143.1	153.9	161.1	172.8
Total [%]	109.0	98.2	84.0	73.7	56.9
XADH production					
G3P DH	139.2	140.1	141.4	142.0	143.3
pyruvate DH	69.0	73.8	79.6	83.4	89.6
α-ketoglutarate DH[c]	111.0	103.8	96.0	88.5	75.3
anabolism	29.7	28.8	27.0	26.1	24.3
Total [%]	348.9	346.5	344.0	340.0	332.5
O$_2$ consumption [%]			208.4		
Redox balance [%]	-41.1	-27.9	-11.2	3.1	27.4

[a] expressed as percent of the cell dry weight.

[b] initial values for lipid content (wild type).

[c] comprises combined NADH and FADH$_2$ production by α-ketoglutarate dehydrogenase, succinate dehydrogenase and malate dehydrogenase.

Exclusive variation of lipid content allowed an evenly closed redox balance solely after increasing the corresponding fraction up to 25% of the biomass (Table VIII-2). Due to the tremendous withdrawal of acetyl-CoA, the activity of the TCA cycle dropped significantly, causing an overall reduction in the supply of NADPH. The increased degree of reduction

of the cell dry weight (Table VIII-1), however, led to an increased anabolic demand for NADPH (30% increase). Despite increasing activities of the glycolysis (Figure VIII-3), the net XADH supply decreased, mainly caused by the diminished activity of the TCA cycle. It is however doubtful, whether an increase of the lipid content to 25% reflects a physiologically feasible condition.

Table VIII-3. Predictions for XADH and NADPH redox balances [%] for (*in silico*) increasing protein content (scenario B) with experimentally determined oxygen consumption [%] (*in vivo*).

protein content [%][a]	40	45	52[b]	60	65
NADPH production					
G6P DH	97.3	97.4	97.8	98.1	98.2
6PG DH	97.3	97.4	97.8	98.1	98.2
isocitrate DH	47.4	46.4	45.7	44.7	44.0
	242.0	241.2	241.3	240.9	240.4
NADPH consumption					
anabolism	133.2	137.7	143.1	150.3	153.9
Total [%]	108.8	103.5	98.2	90.6	86.5
XADH production					
G3P DH	136.5	137.9	140.1	142.6	144.2
pyruvate DH	80.8	77.7	73.8	69.3	66.4
α-ketoglutarate DH[c]	116.1	110.1	103.8	96.6	91.5
anabolism	27.9	27.9	28.8	28.8	28.8
Total [%]	361.3	353.6	346.5	337.3	330.9
O₂ consumption [%]			208.4		
Redox balance [%]	-53.3	-40.3	-27.9	-11.1	-0.6

[a] expressed as percent of the cell dry weight.

[b] initial values for protein content (wild type).

[c] comprises combined NADH and $FADH_2$ production by α-ketoglutarate dehydrogenase, succinate dehydrogenase and malate dehydrogenase.

Increase of the protein content also led to an even-balanced redox metabolism which was achieved with an assumed protein content of 65%. Separate investigations of the XADH and NADPH metabolism, however, revealed significant differences between scenario A and scenario B: in scenario A, redox balancing was mainly achieved by decreasing NADPH surpluses (relative reduction of 50%), in scenario B by a decreasing XADH allocation, highlighting different adjustment processes for both scenarios. It is, however, questionable too, whether a protein augmentation to 65% of the total cell dry weight, represents an *in vivo* feasible situation.

In summary, both scenarios – theoretically - allowed even-balanced redox supply and demand. The changes permitting these adjustments might however reflect extreme non-physiological solutions due to the distinct requirements compared to the reported biomass composition (Figure VIII-4).
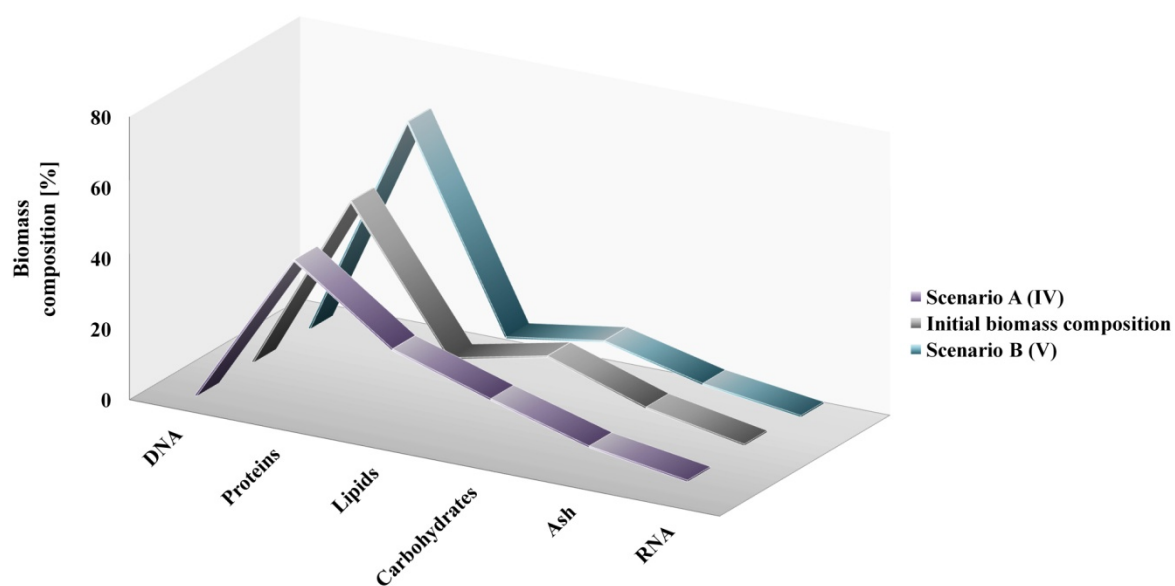
Figure VIII-4. *In silico* alterations of the biomass composition with even-balanced redox metabolism (scenario A: 25% lipid fraction (IV); scenario B: 65% protein fraction (V); derived from Tables VIII-2 and VIII-3) in comparison with the reported, initial biomass composition derived from Wittmann and Heinzle (2008).

Concluding, a combination of scenario A and B with a slightly increased lipid fraction (15%) and an increased protein fraction (58%) were investigated (Scenario C; Figure VIII-5), combining the differential balancing mechanisms determined for scenario A and B.
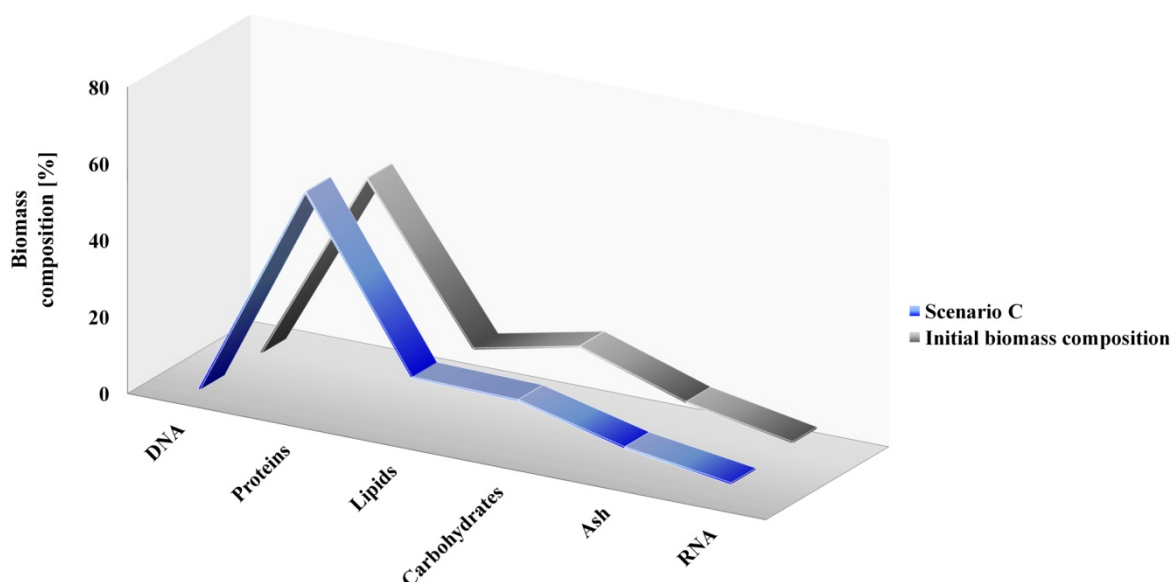
Figure VIII-5. *In silico* alterations of biomass compositions, comprising a lipid fraction of 15% and a protein fraction of 58% (scenario C) in comparison with the initial biomass composition derived from Wittmann and Heinzle (2008).

As depicted in Figure VIII-5, the overall composition changes were less pronounced as those highlighted in Figure VIII-4, more likely representing physiologically feasible conditions. The protein content was solely increased by 6% (absolute) and the lipid content by 2% (absolute). Most importantly, the composition presumed for scenario C generated an even-balanced redox metabolism: the stoichiometric NADPH demand was increased to 17.4 mmol g_{CDW}^{-1} and the stoichiometric NADH supply was slightly decreased to 3.1 mmol g_{CDW}^{-1}. Thus, the NADPH supply accounted for 238.9%, the anabolic consumption for 156.6%, while the XADH production dropped to 335.5%. In total, the reduced redox equivalents accounted for 417.8% needing to be oxidized. Considering the unchanged

specific oxygen consumption with 208.4% (Chapter V), which comprised an oxidation potential for 416.8% of reduced redox equivalents, the redox balance was closed with -1%.

It has to be mentioned, that this scenario just represents one of many possibilities and actual *in vivo* variations of the biomass composition might turn out to be far more complex than considered in this chapter. The predictions demonstrated and discussed here were meant to allow first estimations about composition-dependent balancing mechanisms and to evaluate their range of influence and general feasibility.

In summary, variations of biomass compositions might partly be involved in balancing supply and demand of redox equivalents, resulting in evened redox balances inevitable for balanced cellular growth. Furthermore, the magnitude of the reductive state – the degree of reduction – cannot be deduced solely from *in silico* calculation but has to be determined experimentally, providing the basis for detailed analyses such as the establishment of redox balances.

An additional target towards increasing productivity: secretory processes

Background

Besides increasing knowledge and understanding of the essential pathway of the purine biosynthesis, part of this thesis focused on the intracellular accumulation of flavor-enhancing compounds. The last section of this chapter intends to further broaden the knowledge about targeted intracellular accumulation of the phosphorylated purine nucleotide, IMP.

In the general introduction key targets – identified and analyzed in this study – are summarized, focusing on precursor availability, deleting depleting reactions and neutralizing feedback inhibition. These parameters represented crucial hurdles to be overcome in order to increase intracellular metabolite concentration.

The bacterial cell, however, is a complex system comprising evolutionary developed definite and optimized regulation mechanisms that are (sometimes) not known or understood in great detail. One mechanism – addressed in Chapter IV – is the distinct inhibition by feedback regulation of the amidophosphoribosyltranferase (PurF) preventing unnecessary metabolite synthesis, *i.e.* any kind of intracellular concentration increase that cannot be used to improve cellular growth behavior (Marx et al., 1999). With increasing intracellular metabolite concentrations, the corresponding feedback inhibitions become even more pronounced, eventually blocking the afferent pathway branch (Figure VIII-6A). In consequence, either all inhibitory processes have to be tackled, the causative compounds have to be removed from the system or their corresponding pool sizes have to be kept at a non-inhibitory level (Figure VIII-6B).
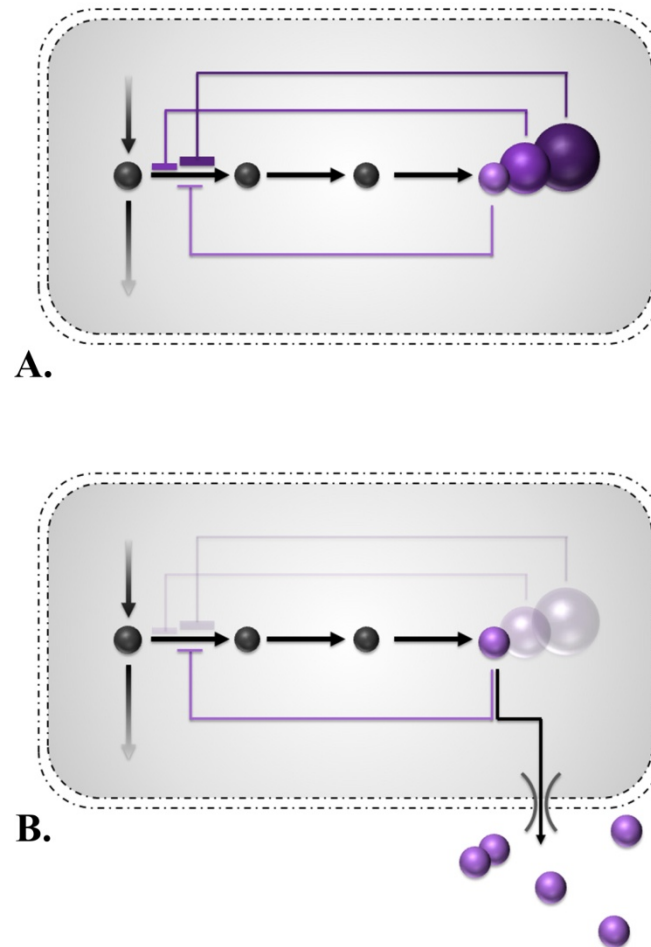
Figure VIII-6. Increasing feedback inhibition of an intracellular metabolite (purple), caused by rising intracellular pool sizes (**A.**). Unchanged feedback inhibition, maintained by a constant – low – intracellular metabolite pool size (purple; **B.**) due to improved secretory processes.

Principle of secretion

The principle of metabolite export as maximizing productivity process has been investigated and proven to be successful for the excretion of amino acids (Bellmann et al., 2001; Dassler et al., 2000; Diesveld et al., 2009; Doroshenko et al., 2007; Kennerknecht et al., 2002; Livshits et al., 2003; Vrljic et al., 1999; Zakataeva et al., 1999), indicating that export facilitation might also beneficially affect the productivity for nucleotides (Livshits et al., 2003). While many systems have been identified for various substances in bacteria (Eggeling and Sahm, 2003; Jack et al., 2001; Zakataeva et al., 2007), efflux systems for

purine nucleotides and derivatives have only been rarely studied (Kakehi et al., 2007; Zakataeva et al., 2007) up to date. The hydrophilic nature of phosphorylated nucleotides thereby precludes any diffusion through the cell membrane working as a permeability barrier – except for small molecules like gases and water or apolar substances like glycerol (Dassler et al., 2000; Gronskiy et al., 2005). Translocation of polar substances, *e.g.* nucleotides, therefore depends on active transport mechanisms (Kramer, 1994).

Mechanisms for IMP secretion in Corynebacteria

The study of the purine biosynthetic pathway and associated efflux systems is not only of fundamental but also of industrial interest as those compounds exhibit several properties making them promising candidates for biotechnological production. Over the last decades, especially one *Corynebacterium* species – *Corynebacterium ammoniagenes* – was successfully employed for the biotechnological production of purine nucleotides and their derivatives, exhibiting substantial potential for their secretion.

These production strains, derived and optimized by classical breeding, *i.e.* random mutagenesis and selection processes, featured a mutual characteristic: their increased capability for the translocation of phosphorylated (polar) nucleotides from the cell interior into extracellular environment. Although the genetic backgrounds allowing these transport mechanisms were not known – and still aren't – the existing potential for nucleotide secretion led to a wide application range of this bacterial species for the biotechnological production. In contrast, the well studied close relative, *Corynebacterium glutamicum*, exhibiting an immense industrial importance (Burkovski, 2008) but missing comparable secretory capabilities for purine nucleotides, did not find successful application for the industrial production of purine compounds.

A direct comparison regarding the ability for intracellular accumulation of the flavor-enhancing substance IMP in *Corynebacterium glutamicum* – performed in this thesis – and a high-scale production strain of *Corynebacterium ammoniagenes* – adopted from Teshiba and Furuya (1983) – clearly demonstrates comparable capacities (Figure VIII-7). While the investigation of the purine biosynthesis in *C. glutamicum,* carried out in this work, did not include any working points for improving secretory mechanisms, the industrial

applications of *C. ammoniagenes* for purine accumulation, seem to be based – at least partly – on these secretory properties: the intracellular IMP concentrations, determined for both species, exhibited similar maximum concentrations, possibly indicating an upper limit for intracellular pool sizes and the need for pool size reduction, either by secretion – observed in *C. ammoniagenes* – or by degradation – as shown in *C. glutamicum* (for reference see Chapter IV).
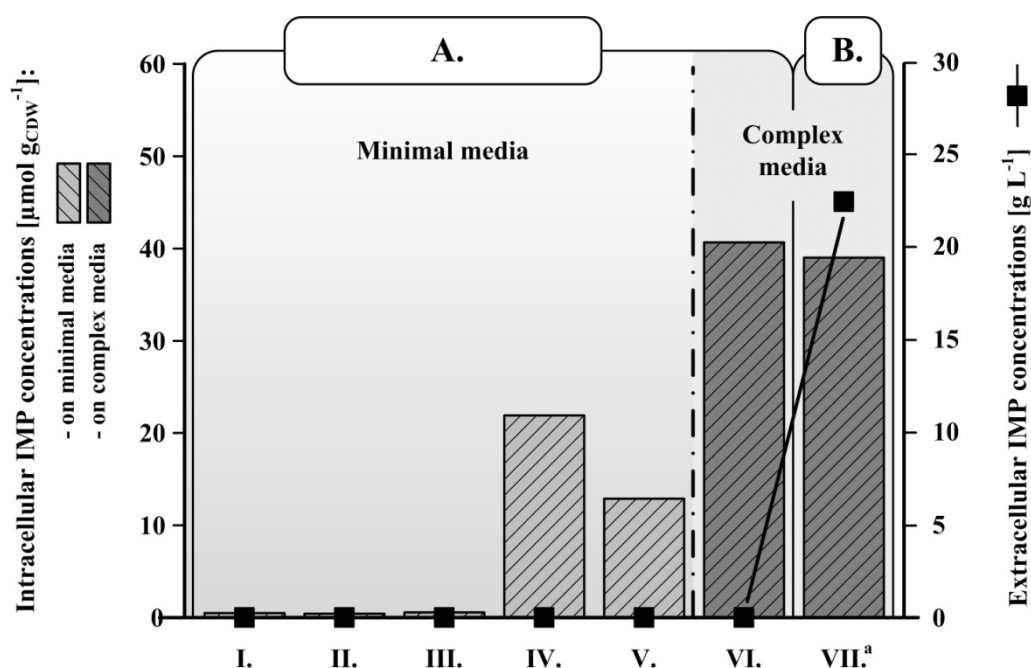
Figure VIII-7. Correlation between intracellular IMP accumulation [μmol g_{CDW}^{-1}] and extracellular IMP secretion [g L^{-1}] on minimal medium and complex media.

Abbreviations: I. – V.: results obtained during growth on minimal medium (for reference see Chapter IV): **I.**, *C. glutamicum* wild type (ATCC 13032); **II.**, *C. glutamicum Δpgi*; **III.**, *C. glutamicum purF*^{K348Q}; **IV.**, *C. glutamicum ΔpurA ΔguaB2*; **V.**, *C. glutamicum ΔpurA ΔguaB2 purF*^{K348Q} *Δpgi*. **VI. – VII.**: results obtained during growth on complex media (for reference see Chapter VII and Teshiba and Furuya (1983), respectively): **VI.**, *C. glutamicum ΔpurA ΔguaB2 purF*^{K348Q} *Δpgi*, **VII.**: *C. ammoniagenes* KY13369. **A.**, processes not optimized for IMP secretion. **B.**, process optimized for IMP secretion.

[a] data for *C. ammoniagenes* KY13369 were taken from Teshiba and Furuya (1983) and represent maximum values for intracellular as well as extracellular IMP concentration.

In conclusion, the increase of the intracellular IMP concentration in *C. glutamicum*, targeted and investigated as a part of this work (Chapter IV) completely excluded any extracellular secretion. Targeting different working points within the metabolic network (Chapter IV) and implementing different strategies concerning varying cultivation conditions (Chapters VI and VII), allowed an iterative optimization process also disclosing basic regulatory fundamentals (Chapter IV) and crucial points for genetic modifications (Chapter V).

Based on the information gained in this study, it seems quite likely that a further significant increase of IMP productivity can only be achieved by including – so far not considered – secretory processes.

References

Abbouni B, Elhariry HM and Auling G (2003). Arrest of cell cycle by inhibition of ribonucleotide reductase induces accumulation of NAD^+ by Mn^{2+}-supplemented growth of *Corynebacterium ammoniagenes*. *Biotechnol Lett* **25,** 143-147.

Abbouni B, Elhariry HM and Auling G (2004). Overproduction of NAD^+ and 5'-inosine monophosphate in the presence of 10 µM Mn^{2+} by a mutant of *Corynebacterium ammoniagenes* with thermosensitive nucleotide reduction (nrd^{ts}) after temperature shift. *Arch Microbiol* **182,** 119-125.

Aiba S and Matsuoka M (1978). Citrate production from n-alkane by *Candida lipolytica* in reference to carbon fluxes *in vivo*. *Eur. J. Appl. Microbiol. Biotechnol.* **5,** 247-261.

Auriol C, Bestel-Corre G, Claude JB, Soucaille P and Meynial-Salles I (2011). Stress-induced evolution of *Escherichia coli* points to original concepts in respiratory cofactor selectivity. *Proc Natl Acad Sci U S A* **108,** 1278-1283.

Auriola S, Frith J, Rogers MJ, Koivuniemi A and Monkkonen J (1997). Identification of adenine nucleotide-containing metabolites of bisphosphonate drugs using ion-pair liquid chromatography-electrospray mass spectrometry. *J. Chromatogr., B* **704,** 187-195.

Bebenek K, Roberts JD and Kunkel TA (1992). The effects of dNTP pool imbalances on frameshift fidelity during DNA replication. *J Biol Chem* **267,** 3589-3596.

Becker J, Klopprogge C, Herold A, Zelder O, Bolten CJ and Wittmann C (2007). Metabolic flux engineering of L-lysine production in *Corynebacterium glutamicum*--over expression and modification of G6P dehydrogenase. *J Biotechnol* **132,** 99-109.

Becker J, Klopprogge C and Wittmann C (2008). Metabolic responses to pyruvate kinase deletion in lysine producing *Corynebacterium glutamicum*. *Microb Cell Fact* **7,** 8.

Becker J, Klopprogge C, Zelder O, Heinzle E and Wittmann C (2005). Amplified expression of fructose 1,6-bisphosphatase in *Corynebacterium glutamicum* increases *in vivo* flux through the pentose phosphate pathway and lysine production on different carbon sources. *Appl Environ Microbiol* **71,** 8587-8596.

Becker J and Wittmann C (2012). Bio-based production of chemicals, materials and fuels - *Corynebacterium glutamicum* as versatile cell factory. *Curr Opin Biotechnol* **23,** 631-640.

Becker J, Zelder O, Hafner S, Schroder H and Wittmann C (2011). From zero to hero--design-based systems metabolic engineering of *Corynebacterium glutamicum* for L-lysine production. *Metab Eng* **13,** 159-168.

Bellmann A, Vrljic M, Patek M, Sahm H, Kramer R and Eggeling L (2001). Expression control and specificity of the basic amino acid exporter LysE of *Corynebacterium glutamicum*. *Microbiology* **147,** 1765-1774.

Benyamini T, Folger O, Ruppin E and Shlomi T (2010). Flux balance analysis accounting for metabolite dilution. *Genome Biol* **11,** R43.

Bernofsky C and Swan M (1973). An improved cycling assay for nicotinamide adenine dinucleotide. *Anal Biochem* **53,** 452-458.

Beste DJ, Bonde B, Hawkins N, Ward JL, Beale MH, Noack S, Noh K, Kruger NJ, Ratcliffe RG and McFadden J (2011). ^{13}C metabolic flux analysis identifies an unusual route for pyruvate dissimilation in mycobacteria which requires isocitrate lyase and carbon dioxide fixation. *PLoS Pathog* **7,** e1002091.

Bidlingmeyer BA, Deming SN, Price Jr WP, Sachok B and Petrusek M (1979). Retention mechanism for reversed-phase ion-pair liqiod chromatography. *J Chromatogr* **186,** 419-434.

Blombach B, Schreiner ME, Bartek T, Oldiges M and Eikmanns BJ (2008). *Corynebacterium glutamicum* tailored for high-yield L-valine production. *Appl Microbiol Biotechnol* **79,** 471-479.

Boehlke JK, de Laeter JR, De Bièvre P, Hidaka H, Peiser HS, Rosman KJR and Taylor PDP (2005). Isotopic compositions of the elements, 2001. *J. Phys. Chem. Ref. Data* **34,** 57-67.

Bolten CJ, Kiefer P, Letisse F, Portais JC and Wittmann C (2007). Sampling for metabolome analysis of microorganisms. *Anal Chem* **79,** 3843-3849.

Bonamy C, Labarre J, Cazaubon L, Jacob C, Le Bohec F, Reyes O and Leblon G (2003). The mobile element IS1207 of *Brevibacterium lactofermentum* ATCC 21086: isolation and use in the construction of Tn5531, a versatile transposon for insertional mutagenesis of *Corynebacterium glutamicum*. *J Biotechnol* **104,** 301-309.

Bonarius HP, Hatzimanikatis V, Meesters KP, de Gooijer CD, Schmid G and Tramper J (1996). Metabolic flux analysis of hybridoma cells in different culture media using mass balances. *Biotechnol Bioeng* **50,** 299-318.

Bonarius HP, Ozemre A, Timmerarends B, Skrabal P, Tramper J, Schmid G and Heinzle E (2001). Metabolic-flux analysis of continuously cultured hybridoma cells using $^{13}CO_2$ mass spectrometry in combination with ^{13}C-lactate nuclear magnetic resonance spectroscopy and metabolite balancing. *Biotechnol Bioeng* **74,** 528-538.

Bonarius HP, Timmerarends B, de Gooijer CD and Tramper J (1998). Metabolite-balancing techniques vs. ^{13}C tracer experiments to determine metabolic fluxes in hybridoma cells. *Biotechnol Bioeng* **58,** 258-262.

Bonnassie S, Burini JF, Oreglia J, Trautwetter A, Patte JC and Sicard AM (1990). Transfer of plasmid DNA to *Brevibacterium lactofermentum* by electrotransformation. *J Gen Microbiol* **136,** 2107-2112.

Bradford MM (1976). A rapid and sensitive method for the quantitation of microgram quantities of protein utilizing the principle of protein-dye binding. *Anal Biochem* **72,** 248-254.

Buchholz A, Hurlebaus J, Wandrey C and Takors R (2002). Metabolomics: quantification of intracellular metabolite dynamics. *Biomol Eng* **19,** 5-15.

Burkovski A (2008). *Corynebacteria - Genomics and Molecular Biology*. Caister Academic Press.

References

Buziol S, Bashir I, Baumeister A, Claassen W, Noisommit-Rizzi N, Mailinger W and Reuss M (2002). New bioreactor-coupled rapid stopped-flow sampling technique for measurements of metabolite dynamics on a subsecond time scale. *Biotechnol Bioeng* **80,** 632-636.

Cai Z, Song F and Yang MS (2002). Capillary liquid chromatographic-high-resolution mass spectrometric analysis of ribonucleotides. *J Chromatogr A* **976,** 135-143.

Cameron DC and Tong IT (1993). Cellular and metabolic engineering. An overview. *Appl Biochem Biotechnol* **38,** 105-140.

Canonaco F, Hess TA, Heri S, Wang T, Szyperski T and Sauer U (2001). Metabolic flux response to phosphoglucose isomerase knock-out in *Escherichia coli* and impact of overexpression of the soluble transhydrogenase UdhA. *FEMS Microbiol Lett* **204,** 247-252.

Carlucci F, Tabucchi A, Consolmagno E, Tagliaferri P, Porcelli B, Marinello E, Leoncini R and Pagani R (1992). Levels and variability of purine nucleotides in normal human lymphocytes. *Biomed Pharmacother* **46,** 109-114.

Christensen B and Nielsen J (1999). Isotopomer analysis using GC-MS. *Metab Eng* **1,** 282-290.

Cohen S, Jordheim LP, Megherbi M, Dumontet C and Guitton J (2010). Liquid chromatographic methods for the determination of endogenous nucleotides and nucleotide analogs used in cancer therapy: a review. *J. Chromatogr., B* **878,** 1912-1928.

Cohn WE (1950). The anion-exchange separation of ribonucleotides. *J Am Chem Soc* **72,** 1471-1478.

Cordell RL, Hill SJ, Ortori CA and Barrett DA (2008). Quantitative profiling of nucleotides and related phosphate-containing metabolites in cultured mammalian cells by liquid chromatography tandem electrospray mass spectrometry. *J Chromatogr B Analyt Technol Biomed Life Sci* **871,** 115-124.

Crauste C, Lefebvre I, Hovaneissian M, Puy JY, Roy B, Peyrottes S, Cohen S, Guitton J, Dumontet C and Perigaud C (2009). Development of a sensitive and selective LC/MS/MS method for the simultaneous determination of intracellular 1-beta-D-arabinofuranosylcytosine triphosphate (araCTP), cytidine triphosphate (CTP) and deoxycytidine triphosphate (dCTP) in a human follicular lymphoma cell line. *J Chromatogr B Analyt Technol Biomed Life Sci* **877,** 1417-1425.

Czarnecka J, Cieslak M and Michal K (2005). Application of solid phase extraction and high-performance liquid chromatography to qualitative and quantitative analysis of nucleotides and nucleosides in human cerebrospinal fluid. *J Chromatogr B Analyt Technol Biomed Life Sci* **822,** 85-90.

Dassler T, Maier T, Winterhalter C and Bock A (2000). Identification of a major facilitator protein from *Escherichia coli* involved in efflux of metabolites of the cysteine pathway. *Mol Microbiol* **36,** 1101-1112.

de Abreu RA, Van Baal JM, de Bruyn CH, Bakkeren JA and Schretlen ED (1982). High-performance liquid chromatographic determination of purine and pyrimidine bases, ribonucleosides, deoxyribonucleosides and cyclic ribonucleotides in biological fluids. *J. Chromatogr.* **229,** 67-75.

de Graaf AA, Eggeling L and Sahm H (2001). Metabolic engineering for L-lysine production by *Corynebacterium glutamicum*. *Adv Biochem Eng Biotechnol* **73,** 9-29.

de Jong-Gubbels P, Vanrolleghem P, Heijnen S, van Dijken JP and Pronk JT (1995). Regulation of carbon metabolism in chemostat cultures of *Saccharomyces cerevisiae* grown on mixtures of glucose and ethanol. *Yeast* **11,** 407-418.

de Koning W and van Dam K (1992). A method for the determination of changes of glycolytic metabolites in yeast on a subsecond time scale using extraction at neutral pH. *Anal Biochem* **204,** 118-123.

Demain AL, Jackson M, Viatali RA, Hendlin D and Jacob TA (1965). Production of xanthosine-5'-monophosphate and inosine-5'-monophosphate by auxotrophic mutants of a coryneform bacterium. *Appl Microbiol* **13,** 757-761.

Demain AL, Jackson M, Vitali RA, Hendlin D and Jacob TA (1966). Production of guanosine-5'-monophosphate and inosine-5'-monophosphate by fermentation. *Appl Microbiol* **14,** 821-825.

Deng Q, Kauri LM, Qian WJ, Dahlgren GM and Kennedy RT (2003). Microscale determination of purines in tissue samples by capillary liquid chromatography with electrochemical detection. *Analyst* **128,** 1013-1018.

Diesveld R, Tietze N, Furst O, Reth A, Bathe B, Sahm H and Eggeling L (2009). Activity of exporters of *Escherichia coli* in *Corynebacterium glutamicum*, and their use to increase L-threonine production. *J Mol Microbiol Biotechnol* **16,** 198-207.

Dominguez H, Rollin C, Guyonvarch A, Guerquin-Kern JL, Cocaign-Bousquet M and Lindley ND (1998). Carbon-flux distribution in the central metabolic pathways of *Corynebacterium glutamicum* during growth on fructose. *Eur J Biochem* **254,** 96-102.

Doroshenko V, Airich L, Vitushkina M, Kolokolova A, Livshits V and Mashko S (2007). YddG from *Escherichia coli* promotes export of aromatic amino acids. *FEMS Microbiol Lett* **275,** 312-318.

Droste P, Miebach S, Niedenfuhr S, Wiechert W and Noh K (2011). Visualizing multi-omics data in metabolic networks with the software Omix: a case study. *Biosystems* **105,** 154-161.

Dunn WB (2008). Current trends and future requirements for the mass spectrometric investigation of microbial, mammalian and plant metabolomes. *Phys Biol* **5,** 011001.

Eggeling L and Bott M (2005). *Handbook of Corynebacterium glutamicum*. CRC Press.

Eggeling L, Morbach S and Sahm H (1997). The fruits of molecular physiology: engineering the L-isoleucine biosynthesis pathway in *Corynebacterium glutamicum*. *J Biotechnol* **56,** 167-182.

Eggeling L and Sahm H (2003). New ubiquitous translocators: amino acid export by *Corynebacterium glutamicum* and *Escherichia coli*. *Arch Microbiol* **180,** 155-160.

Eikmanns BJ, Follettie MT, Griot MU and Sinskey AJ (1989). The phosphoenolpyruvate carboxylase gene of *Corynebacterium glutamicum*: molecular cloning, nucleotide sequence, and expression. *Mol Gen Genet* **218,** 330-339.

Eikmanns BJ, Rittmann D and Sahm H (1995). Cloning, sequence analysis, expression, and inactivation of the *Corynebacterium glutamicum icd* gene encoding isocitrate dehydrogenase and biochemical characterization of the enzyme. *J Bacteriol* **177,** 774-782.

Faletto MB, Miller WH, Garvey EP, St Clair MH, Daluge SM and Good SS (1997). Unique intracellular activation of the potent anti-human immunodeficiency virus agent 1592U89. *Antimicrob Agents Chemother* **41,** 1099-1107.

Feist AM and Palsson BO (2010). The biomass objective function. *Curr Opin Microbiol* **13,** 344-349.

Fernandez CA, Des Rosiers C, Previs SF, David F and Brunengraber H (1996). Correction of ^{13}C mass isotopomer distributions for natural stable isotope abundance. *J Mass Spectrom* **31,** 255-262.

Fiehn O (2001). Combining genomics, metabolome analysis, and biochemical modelling to understand metabolic networks. *Comp Funct Genomics* **2,** 155-168.

Fiehn O (2002). Metabolomics--the link between genotypes and phenotypes. *Plant Mol Biol* **48,** 155-171.

Fischer E and Sauer U (2003a). Metabolic flux profiling of *Escherichia coli* mutants in central carbon metabolism using GC-MS. *Eur J Biochem* **270,** 880-891.

Fischer E and Sauer U (2003b). A novel metabolic cycle catalyzes glucose oxidation and anaplerosis in hungry *Escherichia coli*. *J Biol Chem* **278,** 46446-46451.

Fong SS, Nanchen A, Palsson BO and Sauer U (2006). Latent pathway activation and increased pathway capacity enable *Escherichia coli* adaptation to loss of key metabolic enzymes. *J Biol Chem* **281,** 8024-8033.

Franco CMM, Smith JE and Berry DR (1984). Effect of nitrogen and phosphate on the levels of intermediates in baker's yeast grown in continuous culture. *J Gen Microbiol* **130,** 2465-2472.

Fuhrer T, Fischer E and Sauer U (2005). Experimental identification and quantification of glucose metabolism in seven bacterial species. *J Bacteriol* **187,** 1581-1590.

Fuhrer T and Sauer U (2009). Different biochemical mechanisms ensure network-wide balancing of reducing equivalents in microbial metabolism. *J Bacteriol* **191,** 2112-2121.

Furuya A, Abe S and Kinoshita S (1968). Production of nucleic acid-related substances by fermentative processes. XIX. Accumulation of 5'-inosinic acid by a mutant of *Brevibacterium ammoniagenes*. *Appl Microbiol* **16,** 981-987.

Furuya A, Abe S and Kinoshita S (1969). Production of nucleic acid-related substances by fermentative processes. XXVIII. Accumulation of 5' inosinic acid by a manganese-insensitive mutant of *Brevibacterium ammoniagenes*. *Appl Microbiol* **18,** 977-984.

Furuya A, Abe S and Kinoshita S (1970). Production of nucleic acid-related substances by fermentation processes. XXXIII. Accumulation of inosine by a mutant of *Brevibacterium ammoniagenes*. *Appl Microbiol* **20,** 263-270.

Gayden RH, Watts BA, 3rd, Beach RE and Benedict CR (1991). Quantitation of adenosine, inosine and hypoxanthine in biological samples by microbore-column isocratic high-performance liquid chromatography. *J Chromatogr* **536,** 265-272.

Georgi T, Rittmann D and Wendisch VF (2005). Lysine and glutamate production by *Corynebacterium glutamicum* on glucose, fructose and sucrose: roles of malic enzyme and fructose-1,6-bisphosphatase. *Metab Eng* **7,** 291-301.

Giannattasio S, Gagliardi S, Samaja M and Marra E (2003). Simultaneous determination of purine nucleotides, their metabolites and beta-nicotinamide adenine dinucleotide in cerebellar granule cells by ion-pair high performance liquid chromatography. *Brain Res Protoc* **10,** 168-174.

Gill BD and Indyk HE (2007). Determination of nucleotides and nucleosides in milks and pediatric formulas: a review. *J AOAC Int* **90,** 1354-1364.

Goel A, Ferrance J, Jeong J and Ataai MM (1993). Analysis of metabolic fluxes in batch and continuous cultures of *Bacillus subtilis. Biotechnol Bioeng* **42,** 686-696.

Goudar C, Biener R, Boisart C, Heidemann R, Piret J, de Graaf A and Konstantinov K (2010). Metabolic flux analysis of CHO cells in perfusion culture by metabolite balancing and 2D [^{13}C, ^{1}H] COSY NMR spectroscopy. *Metab Eng* **12,** 138-149.

Gourdon P, Baucher MF, Lindley ND and Guyonvarch A (2000). Cloning of the malic enzyme gene from *Corynebacterium glutamicum* and role of the enzyme in lactate metabolism. *Appl Environ Microbiol* **66,** 2981-2987.

Gronskiy SV, Zakataeva NP, Vitushkina MV, Ptitsyn LR, Altman IB, Novikova AE and Livshits VA (2005). The *yicM (nepI)* gene of *Escherichia coli* encodes a major facilitator superfamily protein involved in efflux of purine ribonucleosides. *FEMS Microbiol Lett* **250,** 39-47.

Guimaraes PM and Londesborough J (2008). The adenylate energy charge and specific fermentation rate of brewer's yeasts fermenting high- and very high-gravity worts. *Yeast* **25,** 47-58.

Gutmann M, Hoischen C and Kramer R (1992). Carrier-mediated glutamate secretion by *Corynebacterium glutamicum* under biotin limitation. *Biochim Biophys Acta* **1112,** 115-123.

Halpern BP (2002). What's in a name? Are MSG and umami the same? *Chem Senses* **27,** 845-846.

Hanahan D (1983). Studies on transformation of *Escherichia coli* with plasmids. *J Mol Biol* **166,** 557-580.

Heinemann M and Sauer U (2010). Systems biology of microbial metabolism. *Curr Opin Microbiol* **13,** 337-343.

Heinzle E, Oeggerli A and Dettwiler B (1990). On-line fermentation gas analysis: error analysis and application of mass spectrometry. *Anal Chim Acta* **238,** 101-115.

Heinzle E, Yuan Y, Kumar S, Wittmann C, Gehre M, Richnow HH, Wehrung P, Adam P and Albrecht P (2008). Analysis of ^{13}C labeling enrichment in microbial culture applying metabolic tracer experiments using gas chromatography-combustion-isotope ratio mass spectrometry. *Anal Biochem* **380,** 202-210.

Hirasawa T, Wachi M and Nagai K (2000). A mutation in the *Corynebacterium glutamicum ltsA* gene causes susceptibility to lysozyme, temperature-sensitive growth, and L-glutamate production. *J Bacteriol* **182,** 2696-2701.

References

Ho SN, Hunt HD, Horton RM, Pullen JK and Pease LR (1989). Site-directed mutagenesis by overlap extension using the polymerase chain reaction. *Gene* **77,** 51-59.

Hoffman NE and Liao JC (1977). Reversed phase high performance liquid chromatographic separations of nucleotides in the presence of solvophobic ions. *Anal Chem* **49,** 2231-2234.

Hofmann U, Heinkele G, Angelberger S, Schaeffeler E, Lichtenberger C, Jaeger S, Reinisch W and Schwab M (2012). Simultaneous quantification of eleven thiopurine nucleotides by liquid chromatography-tandem mass spectrometry. *Anal. Chem.* **84,** 1294-1301.

Hua Q, Yang C, Baba T, Mori H and Shimizu K (2003). Responses of the central metabolism in *Escherichia coli* to phosphoglucose isomerase and glucose 6-phosphate dehydrogenase knockouts. *J Bacteriol* **185,** 7053-7067.

Ikeda M (2003). Amino acid production processes. *Adv Biochem Eng Biotechnol* **79,** 1-35.

Ikeda M and Nakagawa S (2003). The *Corynebacterium glutamicum* genome: features and impacts on biotechnological processes. *Appl Microbiol Biotechnol* **62,** 99-109.

Inoue H, Nojima H and Okayama H (1990). High efficiency transformation of *Escherichia coli* with plasmids. *Gene* **96,** 23-28.

Jack DL, Yang NM and Saier MH, Jr. (2001). The drug/metabolite transporter superfamily. *Eur J Biochem* **268,** 3620-3639.

Jager W, Schafer A, Puhler A, Labes G and Wohlleben W (1992). Expression of the *Bacillus subtilis sacB* gene leads to sucrose sensitivity in the gram-positive bacterium *Corynebacterium glutamicum* but not in *Streptomyces lividans*. *J Bacteriol* **174,** 5462-5465.

Jetten M and Sinskey AJ (1993). Characterization of phosphoenolpyruvate carboxykinase from *Corynebacterium glutamicum*. *FEMS Microbiol Lett* **111,** 183-188.

Jetten MS and Sinskey AJ (1995). Purification and properties of oxaloacetate decarboxylase from *Corynebacterium glutamicum*. *Antonie Van Leeuwenhoek* **67,** 221-227.

Kabir MM and Shimizu K (2003). Gene expression patterns for metabolic pathway in *pgi* knockout *Escherichia coli* with and without *phb* genes based on RT-PCR. *J Biotechnol* **105,** 11-31.

Kakehi M, Usuda Y, Tabira Y and Sugimoto S (2007). Complete deficiency of 5'-nucleotidase activity in *Escherichia coli* leads to loss of growth on purine nucleotides but not of their excretion. *J Mol Microbiol Biotechnol* **13,** 96-104.

Kalinowski J, Bathe B, Bartels D, Bischoff N, Bott M, Burkovski A, Dusch N, Eggeling L, Eikmanns BJ, Gaigalat L, Goesmann A, Hartmann M, Huthmacher K, Kramer R, Linke B, McHardy AC, Meyer F, Mockel B, Pfefferle W, Puhler A, Rey DA, Ruckert C, Rupp O, Sahm H, Wendisch VF, Wiegrabe I and Tauch A (2003). The complete *Corynebacterium glutamicum* ATCC 13032 genome sequence and its impact on the production of L-aspartate-derived amino acids and vitamins. *J Biotechnol* **104,** 5-25.

Kamada N, Yasuhara A, Takano Y, Nakano T and Ikeda M (2001). Effect of transketolase modifications on carbon flow to the purine-nucleotide pathway in *Corynebacterium ammoniagenes*. *Appl Microbiol Biotechnol* **56,** 710-717.

Kennerknecht N, Sahm H, Yen MR, Patek M, Saier Jr MH, Jr. and Eggeling L (2002). Export of L-isoleucine from *Corynebacterium glutamicum*: a two-gene-encoded member of a new translocator family. *J Bacteriol* **184,** 3947-3956.

Kiefer P, Heinzle E, Zelder O and Wittmann C (2004). Comparative metabolic flux analysis of lysine-producing *Corynebacterium glutamicum* cultured on glucose or fructose. *Appl Environ Microbiol* **70,** 229-239.

Kim HM, Heinzle E and Wittmann C (2006). Deregulation of aspartokinase by single nucleotide exchange leads to global flux rearrangement in the central metabolism of *Corynebacterium glutamicum*. *J Microbiol Biotechnol* **16,** 1174-1179.

Kind S, Jeong WK, Schroder H and Wittmann C (2010). Systems-wide metabolic pathway engineering in *Corynebacterium glutamicum* for bio-based production of diaminopentane. *Metab Eng* **12,** 341-351.

Kinoshita S, Shigezo U and Shimono M (1957). Studies on the amino acid fermentation: Part I: Production of L-glutamic acid by various microorganisms. *J. Gen. Appl. Microbiol.* **3,** 193-205.

Kirchner O and Tauch A (2003). Tools for genetic engineering in the amino acid-producing bacterium *Corynebacterium glutamicum*. *J Biotechnol* **104,** 287-299.

Kissinger PT (1977). Comments on reverse-phase ion-pair partition chromatography. *Anal Chem* **49,** 883.

Kjeldsen KR and Nielsen J (2009). In silico genome-scale reconstruction and validation of the *Corynebacterium glutamicum* metabolic network. *Biotechnol Bioeng* **102,** 583-597.

Klapa MI, Aon JC and Stephanopoulos G (2003). Systematic quantification of complex metabolic flux networks using stable isotopes and mass spectrometry. *Eur J Biochem* **270,** 3525-3542.

Klawitter J, Schmitz V, Klawitter J, Leibfritz D and Christians U (2007). Development and validation of an assay for the quantification of 11 nucleotides using LC/LC-electrospray ionization-MS. *Anal Biochem* **365,** 230-239.

Klein S and Heinzle E (2012). Isotope labeling experiments in metabolomics and fluxomics. *Wiley Interdiscip Rev Syst Biol Med* **4,** 261-272.

Kohlstedt M, Becker J and Wittmann C (2010). Metabolic fluxes and beyond-systems biology understanding and engineering of microbial metabolism. *Appl Microbiol Biotechnol* **88,** 1065-1075.

Kramer R (1994). Systems and mechanisms of amino acid uptake and excretion in prokaryotes. *Arch Microbiol* **162,** 1-13.

Kromer JO, Bolten CJ, Heinzle E, Schroder H and Wittmann C (2008). Physiological response of *Corynebacterium glutamicum* to oxidative stress induced by deletion of the transcriptional repressor McbR. *Microbiology* **154,** 3917-3930.

Kromer JO, Fritz M, Heinzle E and Wittmann C (2005). In vivo quantification of intracellular amino acids and intermediates of the methionine pathway in *Corynebacterium glutamicum*. *Anal Biochem* **340,** 171-173.

References

Kromer JO, Heinzle E, Schroder H and Wittmann C (2006). Accumulation of homolanthionine and activation of a novel pathway for isoleucine biosynthesis in *Corynebacterium glutamicum* McbR deletion strains. *J Bacteriol* **188,** 609-618.

Kromer JO, Sorgenfrei O, Klopprogge K, Heinzle E and Wittmann C (2004). In-depth profiling of lysine-producing *Corynebacterium glutamicum* by combined analysis of the transcriptome, metabolome, and fluxome. *J Bacteriol* **186,** 1769-1784.

Lee HC, Kim JS, Jang W and Kim SY (2010). High NADPH/NADP$^+$ ratio improves thymidine production by a metabolically engineered *Escherichia coli* strain. *J Biotechnol* **149,** 24-32.

Li H, Zhang G, Deng A, Chen N and Wen T (2011). De novo engineering and metabolic flux analysis of inosine biosynthesis in *Bacillus subtilis*. *Biotechnol Lett* **33,** 1575-1580.

Liebl W (2005). *Corynebacterium* Taxonomy in Eggeling L and Bott M (Eds), *Handbook of Corynebacterium glutamicum*, CRC Press, pp. 9-34.

Livshits VA, Zakataeva NP, Aleshin VV and Vitushkina MV (2003). Identification and characterization of the new gene *rhtA* involved in threonine and homoserine efflux in *Escherichia coli*. *Res Microbiol* **154,** 123-135.

Luo B, Groenke K, Takors R, Wandrey C and Oldiges M (2007). Simultaneous determination of multiple intracellular metabolites in glycolysis, pentose phosphate pathway and tricarboxylic acid cycle by liquid chromatography-mass spectrometry. *J Chromatogr A* **1147,** 153-164.

Mahadevan R, Edwards JS and Doyle FJ, 3rd (2002). Dynamic flux balance analysis of diauxic growth in *Escherichia coli*. *Biophys J* **83,** 1331-1340.

Malloy CR, Sherry AD and Jeffrey FM (1988). Evaluation of carbon flux and substrate selection through alternate pathways involving the citric acid cycle of the heart by ^{13}C NMR spectroscopy. *J Biol Chem* **263,** 6964-6971.

Marx A, de Graaf A, Wiechert W, Eggeling L and Sahm H (1996). Determination of the fluxes in the central metabolism of *Corynebacterium glutamicum* by Nuclear Magnetic Resonance Spectroscopy combined with metabolite balancing. *Biotechnol Bioeng* **49 (2),** 111-129.

Marx A, Eikmanns BJ, Sahm H, de Graaf AA and Eggeling L (1999). Response of the central metabolism in *Corynebacterium glutamicum* to the use of an NADH-dependent glutamate dehydrogenase. *Metab Eng* **1,** 35-48.

Marx A, Hans S, Mockel B, Bathe B, de Graaf AA, McCormack AC, Stapleton C, Burke K, O'Donohue M and Dunican LK (2003). Metabolic phenotype of phosphoglucose isomerase mutants of *Corynebacterium glutamicum*. *J Biotechnol* **104,** 185-197.

Mascarenhas D, Ashworth DJ and Chen CS (1991). Deletion of *pgi* alters tryptophan biosynthesis in a genetically engineered strain of *Escherichia coli*. *Appl Environ Microbiol* **57,** 2995-2999.

Mathews CK (2006). DNA precursor metabolism and genomic stability. *Faseb J* **20,** 1300-1314.

Matsui H, Kawasaki H, Shimaoka M and Kurahashi O (2001a). Investigation of various genotype characteristics for inosine accumulation in *Escherichia coli* W3110. *Biosci Biotechnol Biochem* **65,** 570-578.

Matsui H, Shimaoka M, Takenaka Y, Kawasaki H and Kurahashi O (2001b). *gsk* disruption leads to guanosine accumulation in *Escherichia coli. Biosci Biotechnol Biochem* **65,** 1230-1235.

Matsushita K, Otofuji A, Iwahashi M, Toyama H and Adachi O (2001). NADH dehydrogenase of *Corynebacterium glutamicum*. Purification of an NADH dehydrogenase II homolog able to oxidize NADPH. *FEMS Microbiol Lett* **204,** 271-276.

Messenger LJ and Zalkin H (1979). Glutamine phosphoribosylpyrophosphate amidotransferase from *Escherichia coli*. Purification and properties. *J Biol Chem* **254,** 3382-3392.

Meyer R and Wagner KG (1985). Determination of nucleotide pools in plant tissue by high-performance liquid chromatography. *Anal. Biochem.* **148,** 269-276.

Molenaar D, van der Rest ME, Drysch A and Yucel R (2000). Functions of the membrane-associated and cytoplasmic malate dehydrogenases in the citric acid cycle of *Corynebacterium glutamicum*. *J Bacteriol* **182,** 6884-6891.

Mollney M, Wiechert W, Kownatzki D and de Graaf AA (1999). Bidirectional reaction steps in metabolic networks: IV. Optimal design of isotopomer labeling experiments. *Biotechnol Bioeng* **66,** 86-103.

Moon MW, Kim HJ, Oh TK, Shin CS, Lee JS, Kim SJ and Lee JK (2005). Analyses of enzyme II gene mutants for sugar transport and heterologous expression of fructokinase gene in *Corynebacterium glutamicum* ATCC 13032. *FEMS Microbiol Lett* **244,** 259-266.

Moon MW, Park SY, Choi SK and Lee JK (2007). The phosphotransferase system of *Corynebacterium glutamicum*: features of sugar transport and carbon regulation. *J Mol Microbiol Biotechnol* **12,** 43-50.

Mori H, Iida A, Fujio T and Teshiba S (1997). A novel process of inosine 5'-monophosphate production using overexpressed guanosine/inosine kinase. *Appl Microbiol Biotechnol* **48,** 693-698.

Mori M and Shiio I (1987). Phosphoenolpyruvate: sugar phosphotransferase systems and sugar metabolism in *Brevibacterium flavum*. *Agric. Biol. Chem.* **51,** 2671-2678.

Moritz B, Striegel K, De Graaf AA and Sahm H (2000). Kinetic properties of the glucose 6-phosphate and 6-phosphogluconate dehydrogenases from *Corynebacterium glutamicum* and their application for predicting pentose phosphate pathway flux *in vivo*. *Eur J Biochem* **267,** 3442-3452.

Nakayama K, Araki K and Kase H (1978). Microbial production of essential amino acid with *Corynebacterium glutamicum* mutants. *Adv Exp Med Biol* **105,** 649-661.

Nanchen A, Schicker A and Sauer U (2006). Nonlinear dependency of intracellular fluxes on growth rate in miniaturized continuous cultures of *Escherichia coli*. *Appl Environ Microbiol* **72,** 1164-1172.

Nantapong N, Otofuji A, Migita CT, Adachi O, Toyama H and Matsushita K (2005). Electron transfer ability from NADH to menaquinone and from NADPH to oxygen of type II NADH dehydrogenase of *Corynebacterium glutamicum*. *Biosci Biotechnol Biochem* **69,** 149-159.

References

Naydenova Z, Rose JB and Coe IR (2008). Inosine and equilibrative nucleoside transporter 2 contribute to hypoxic preconditioning in the murine cardiomyocyte HL-1 cell line. *Am J Physiol Heart Circ Physiol* **294,** H2687-2692.

Nesvera J and Patek M (2011). Tools for genetic manipulations in *Corynebacterium glutamicum* and their applications. *Appl Microbiol Biotechnol* **90,** 1641-1654.

Netzer R, Krause M, Rittmann D, Peters-Wendisch PG, Eggeling L, Wendisch VF and Sahm H (2004a). Roles of pyruvate kinase and malic enzyme in *Corynebacterium glutamicum* for growth on carbon sources requiring gluconeogenesis. *Arch Microbiol* **182,** 354-363.

Netzer R, Peters-Wendisch PG, Eggeling L and Sahm H (2004b). Cometabolism of a nongrowth substrate: L-serine utilization by *Corynebacterium glutamicum*. *Appl Environ Microbiol* **70,** 7148-7155.

Neuner A and Heinzle E (2011). Mixed glucose and lactate uptake by *Corynebacterium glutamicum* through metabolic engineering. *Biotechnol J* **6,** 318-329.

Nicholls DG and Ferguson SJ (2002). *Bioenergetics 3*. Academic Press.

Nichthauser J and Stepnowski P (2009). Retention mechanism of selected ionic liquids on a pentafluorophenylpropyl polar phase: investigation using RP-HPLC. *J Chromatogr Sci* **47,** 247-253.

Nielsen J (2003). It is all about metabolic fluxes. *J Bacteriol* **185,** 7031-7035.

Nielsen J and Oliver S (2005). The next wave in metabolome analysis. *Trends Biotechnol* **23,** 544-546.

Nielsen J, Villadsen J and Lidén G (2003). *Bioreaction engineering principles*, Second edition edn. Kluwer Academic/Plenum Publishers.

Niklas J and Heinzle E (2011). Metabolic flux analysis in systems biology of mammalian cells. *Adv Biochem Eng Biotechnol* **127,** 109-132.

Niklas J, Schneider K and Heinzle E (2010). Metabolic flux analysis in eukaryotes. *Curr Opin Biotechnol* **21,** 63-69.

Nissen TL, Anderlund M, Nielsen J, Villadsen J and Kielland-Brandt MC (2001). Expression of a cytoplasmic transhydrogenase in *Saccharomyces cerevisiae* results in formation of 2-oxoglutarate due to depletion of the NADPH pool. *Yeast* **18,** 19-32.

Noack S, Noh K, Moch M, Oldiges M and Wiechert W (2011). Stationary versus non-stationary ^{13}C-MFA: a comparison using a consistent dataset. *J Biotechnol* **154,** 179-190.

Noguchi Y, Shimba N, Kawahara Y, Suzuki E and Sugimoto S (2003). ^{31}P NMR studies of energy metabolism in xanthosine-5'-monophosphate overproducing *Corynebacterium ammoniagenes*. *Eur J Biochem* **270,** 2622-2626.

Noh K and Wiechert W (2011). The benefits of being transient: isotope-based metabolic flux analysis at the short time scale. *Appl Microbiol Biotechnol* **91,** 1247-1265.

Nor 'Aini AR, Shirai Y, Hassan MA and Shimizu K (2006). Investigation on the metabolic regulation of *pgi* gene knockout *Escherichia coli* by enzyme activities and intracellular metabolite concentrations. *Malaysian Journal of Microbiology* **2(2),** 24-31.

Ohnishi J, Mitsuhashi S, Hayashi M, Ando S, Yokoi H, Ochini K and Ikeda M (2002). A novel methodology employing *Corynebacterium glutamicum* genome information to generate a new L-lysine-producing mutant. *Appl Microbiol Biotechnol* **58,** 217-223.

Otero JM and Nielsen J (2009). Industrial systems biology. *Biotechnol Bioeng* **105,** 439-460.

Pang B, McFaline JL, Burgis NE, Dong M, Taghizadeh K, Sullivan MR, Elmquist CE, Cunningham RP and Dedon PC (2011). Defects in purine nucleotide metabolism lead to substantial incorporation of xanthine and hypoxanthine into DNA and RNA. *Proc Natl Acad Sci U S A*.

Papin JA, Price ND, Wiback SJ, Fell DA and Palsson BO (2003). Metabolic pathways in the post-genome era. *Trends Biochem Sci* **28,** 250-258.

Parche S, Burkovski A, Sprenger GA, Weil B, Kramer R and Titgemeyer F (2001). *Corynebacterium glutamicum*: a dissection of the PTS. *J Mol Microbiol Biotechnol* **3,** 423-428.

Peifer S, Schneider K, Nürenberg G, Volmer DA and Heinzle E (2012). Quantitation of intracellular purine intermediates in different *Corynebacteria* using electrospray LC-MS/MS. *Anal Bioanal Chem* **DOI: 10.1007/s00216-012-6388-6**.

Petersen S, de Graaf AA, Eggeling L, Mollney M, Wiechert W and Sahm H (2000). *In vivo* quantification of parallel and bidirectional fluxes in the anaplerosis of *Corynebacterium glutamicum*. *J Biol Chem* **275,** 35932-35941.

Pfefferle W, Mockel B, Bathe B and Marx A (2003). Biotechnological manufacture of lysine. *Adv Biochem Eng Biotechnol* **79,** 59-112.

Provost A and Bastin G (2004). Dynamic metabolic modelling under the balanced growth condition. *Journal of Process Control* **14,** 717-728.

Qian J, Cai X, Chu J, Zhuang Y and Zhang S (2006). Nucleotide mutations in *purA* gene and *pur* operon promoter discovered in guanosine- and inosine-producing *Bacillus subtilis* strains. *Biotechnol Lett* **28,** 937-941.

Qian T, Cai Z and Yang MS (2004). Determination of adenosine nucleotides in cultured cells by ion-pairing liquid chromatography-electrospray ionization mass spectrometry. *Anal Biochem* **325,** 77-84.

Rowlands RT (1984). Industrial strain improvement: mutagenesis and random screening procedures. *Enzyme Microb. Technol.* **6,** 3-10.

Sahm H, Eggeling L and de Graaf AA (2000). Pathway analysis and metabolic engineering in *Corynebacterium glutamicum*. *Biol Chem* **381,** 899-910.

Sahm H, Eggeling L, Eikmanns BJ and Reinhard K (1995). Metabolic design in amino acid producing bacterium *Corynebacterium glutamicum*. *FEMS Microbiol Rev* **16,** 243-252.

Sauer U (2006). Metabolic networks in motion: ^{13}C-based flux analysis. *Mol Syst Biol* **2,** 62.

Sauer U, Canonaco F, Heri S, Perrenoud A and Fischer E (2004). The soluble and membrane-bound transhydrogenases UdhA and PntAB have divergent functions in NADPH metabolism of *Escherichia coli*. *J Biol Chem* **279,** 6613-6619.

References

Sauer U and Eikmanns BJ (2005). The PEP-pyruvate-oxaloacetate node as the switch point for carbon flux distribution in bacteria. *FEMS Microbiol Rev* **29,** 765-794.

Sauer U and Zamboni N (2008). From biomarkers to integrated network responses. *Nat Biotechnol* **26,** 1090-1092.

Saxild HH and Nygaard P (1991). Regulation of levels of purine biosynthetic enzymes in *Bacillus subtilis*: effects of changing purine nucleotide pools. *J Gen Microbiol* **137,** 2387-2394.

Schaechter M, Kolter R and Buckley M (2004). Microbiology in the 21st century: Where are we and where are we going? *American Society for Microbiology*.

Schmidt K, Carlsen M, Nielsen J and Villadsen J (1997). Modeling isotopomer distributions in biochemical networks using isotopomer mapping matrices. *Biotechnol Bioeng* **55,** 831-840.

Schmidt K, Marx A, de Graaf AA, Wiechert W, Sahm H, Nielsen J and Villadsen J (1998). ^{13}C tracer experiments and metabolite balancing for metabolic flux analysis: comparing two approaches. *Biotechnol Bioeng* **58,** 254-257.

Schneider J, Peters-Wendisch P, Stansen KC, Gotker S, Maximow S, Kramer R and Wendisch VF (2012). Characterization of the biotin uptake system encoded by the biotin-inducible *bioYMN* operon of *Corynebacterium glutamicum*. *BMC Microbiol* **12,** 6.

Seifar RM, Ras C, van Dam JC, van Gulik WM, Heijnen JJ and van Winden WA (2009). Simultaneous quantification of free nucleotides in complex biological samples using ion-pair reversed phase liquid chromatography isotope dilution tandem mass spectrometry. *Anal. Biochem.* **388,** 213-219.

Shimaoka M, Kawasaki H, Takenaka Y, Kurahashi O and Matsui H (2005). Effects of *edd* and *pgi* disruptions on inosine accumulation in *Escherichia coli*. *Biosci Biotechnol Biochem* **69,** 1248-1255.

Shimaoka M, Takenaka Y, Kurahashi O, Kawasaki H and Matsui H (2007). Effect of amplification of desensitized *purF* and *prs* on inosine accumulation in *Escherichia coli*. *J Biosci Bioeng* **103,** 255-261.

Shulaev V (2006). Metabolomics technology and bioinformatics. *Brief Bioinform* **7,** 128-139.

Stackebrandt E, Rainey FA and Ward-Rainey NL (1997). Proposal for a new hierarchic classification system, *Actinobacteria* classis nov. *Int. J. Syst. Evol. Microbiol.* **47,** 479-491.

Stephanopoulos G (1998). Metabolic engineering. *Biotechnol Bioeng* **58,** 119-120.

Stephanopoulos G, Aristidou A and Nielsen J (1998). *Metabolic Engineering - Principles and Methodologies*. Academic Press.

Stephanopoulos G and Vallino JJ (1991). Network rigidity and metabolic engineering in metabolite overproduction. *Science* **252,** 1675-1681.

Sugimoto S and Shiio I (1987a). Regulation of 6-phosphogluconate dehydrogenase in *Brevibacterium flavum*. *Agric. Biol. Chem.* **51,** 1257-1263.

Sugimoto S and Shiio I (1987b). Regulation of glucose 6-phosphate dehydrogenase in *Brevibacterium flavum*. *Agric. Biol. Chem.* **51,** 101-108.

Sumner LW, Mendes P and Dixon RA (2003). Plant metabolomics: large-scale phytochemistry in the functional genomics era. *Phytochemistry* **62,** 817-836.

Tang YJ, Martin HG, Dehal PS, Deutschbauer A, Llora X, Meadows A, Arkin A and Keasling JD (2008). Metabolic flux analysis of *Shewanella* spp. reveals evolutionary robustness in central carbon metabolism. *Biotechnol Bioeng* **102,** 1161-1169.

Tauch A, Kirchner O, Loffler B, Gotker S, Puhler A and Kalinowski J (2002). Efficient electrotransformation of C*orynebacterium diphtheriae* with a mini-replicon derived from the *Corynebacterium glutamicum* plasmid pGA1. *Curr Microbiol* **45,** 362-367.

Taylor PJ (2005). Matrix effects: the Achilles heel of quantitative high-performance liquid chromatography-electrospray-tandem mass spectrometry. *Clin Biochem* **38,** 328-334.

Teshiba S and Furuya A (1983). Mechanisms of 5'-inosinic acid accumulation by permeability mutants of *Brevibacterium ammoniagenes*. III. Intracellular 5'-IMP pool and excretion mechanisms of 5'-IMP. *Agric. Biol. Chem.* **47,** 2357-2363.

Teshiba S and Furuya A (1989). *Production of Nucleotides and Nucleosides by Fermentation*. Gordon and Breach Science Publishers.

Tozzi MG, Camici M, Mascia L, Sgarrella F and Ipata PL (2006). Pentose phosphates in nucleoside interconversion and catabolism. *Febs J* **273,** 1089-1101.

Traut TW (1994). Physiological concentrations of purines and pyrimidines. *Mol Cell Biochem* **140,** 1-22.

Tzvetkov M, Klopprogge C, Zelder O and Liebl W (2003). Genetic dissection of trehalose biosynthesis in *Corynebacterium glutamicum*: inactivation of trehalose production leads to impaired growth and an altered cell wall lipid composition. *Microbiology* **149,** 1659-1673.

Udaka S (1960). Screening method for microorganisms accumulating metabolites and its use in the isolation of *Micrococcus glutamicus*. *J Bacteriol* **79,** 754-755.

Vallino JJ and Stephanopoulos G (1993). Metabolic flux distributions in *Corynebacterium glutamicum* during growth and lysine overproduction. *Biotechnol Bioeng* **41,** 633-646.

Vallino JJ and Stephanopoulos G (1994). Carbon flux distributions at the glucose 6-phosphate branch point in *Corynebacterium glutamicum* during lysine overproduction. *Biotechnol Prog* **10,** 327-334.

van der Rest ME, Lange C and Molenaar D (1999). A heat shock following electroporation induces highly efficient transformation of *Corynebacterium glutamicum* with xenogeneic plasmid DNA. *Appl Microbiol Biotechnol* **52,** 541-545.

van Gennip AH, Bierau J and Nyhan WL (2006). Physician's guide to the treatment and folluw-up of metabolic diseases in Blau N, FHoffmann GF, Leonard J and Clarke JTR (Eds), *Inborn errors of purine and pyrimidine metabolism*, Springer, pp. 245-253.

van Gulik WM and Heijnen JJ (1995). A metabolic network stoichiometry analysis of microbial growth and product formation. *Biotechnol Bioeng* **48,** 681-698.

van Winden WA, Wittmann C, Heinzle E and Heijnen JJ (2002). Correcting mass isotopomer distributions for naturally occurring isotopes. *Biotechnol Bioeng* **80,** 477-479.

References

Varma A and Palsson BO (1994). Metabolic flux balancing: basic concepts, scientific and practical use. *Nat Biotechnol* **12,** 994-998.

Veit A, Rittmann D, Georgi T, Youn JW, Eikmanns BJ and Wendisch VF (2009). Pathway identification combining metabolic flux and functional genomics analyses: acetate and propionate activation by *Corynebacterium glutamicum*. *J Biotechnol* **140,** 75-83.

Verho R, Londesborough J, Penttila M and Richard P (2003). Engineering redox cofactor regeneration for improved pentose fermentation in *Saccharomyces cerevisiae*. *Appl Environ Microbiol* **69,** 5892-5897.

Villas-Boas SG, Hojer-Pedersen J, Akesson M, Smedsgaard J and Nielsen J (2005). Global metabolite analysis of yeast: evaluation of sample preparation methods. *Yeast* **22,** 1155-1169.

Vrljic M, Garg J, Bellmann A, Wachi S, Freudl R, Malecki MJ, Sahm H, Kozina VJ, Eggeling L, Saier MH, Jr., Eggeling L and Saier MH, Jr. (1999). The LysE superfamily: topology of the lysine exporter LysE of *Corynebacterium glutamicum*, a paradyme for a novel superfamily of transmembrane solute translocators. *J Mol Microbiol Biotechnol* **1,** 327-336.

Wendisch VF, Bott M and Eikmanns BJ (2006a). Metabolic engineering of *Escherichia coli* and *Corynebacterium glutamicum* for biotechnological production of organic acids and amino acids. *Curr Opin Microbiol* **9,** 268-274.

Wendisch VF, Bott M, Kalinowski J, Oldiges M and Wiechert W (2006b). Emerging *Corynebacterium glutamicum* systems biology. *J Biotechnol* **124,** 74-92.

Werner A, Siems W, Kowalewski J and Gerber G (1989). Interrelationships between purine nucleotide degradation and radical formation during intestinal ischaemia and reperfusion: an application of ion-pair high-performance liquid chromatography of nucleotides, nucleosides and nucleobases. *J. Chromatogr.* **491,** 77-88.

Wheeler LJ, Rajagopal I and Mathews CK (2005). Stimulation of mutagenesis by proportional deoxyribonucleoside triphosphate accumulation in *Escherichia coli*. *DNA Repair (Amst)* **4,** 1450-1456.

Wiechert W (2001). ^{13}C metabolic flux analysis. *Metab Eng* **3,** 195-206.

Wiechert W and de Graaf A (1997). Bidirectional reaction steps in metabolic networks: I. Modeling and simulation of carbon isotope labeling experiments. *Biotechnol Bioeng* **55 (1),** 102-117.

Wiechert W and Noh K (2005). From stationary to instationary metabolic flux analysis. *Adv Biochem Eng Biotechnol* **92,** 145-172.

Wiechert W, Siefke C, de Graaf A and Marx A (1997). Bidirectional reaction steps in metabolic networks: II. Flux estimation and statistical analysis. *Biotechnol Bioeng* **55 (1),** 118-135.

Witters E, Roef L, Newton RP, Van Dongen W, Esmans EL and Van Onckelen HA (1996). Quantitation of cyclic nucleotides in biological samples by negative electrospray tandem mass spectrometry coupled to ion suppression liquid chromatography. *Rapid Commun. Mass Spectrom.* **10,** 225-231.

Witters E, Van Dongen W, Esmans EL and Van Onckelen HA (1997). Ion-pair liquid chromatography-electrospray mass spectrometry for the analysis of cyclic nucleotides. *J. Chromatogr., B* **694,** 55-63.

Wittmann C (2002). Metabolic flux analysis using mass spectrometry. *Adv Biochem Eng Biotechnol* **74,** 39-64.

Wittmann C (2007). Fluxome analysis using GC-MS. *Microb Cell Fact* **6,** 6.

Wittmann C (2010). Analysis and engineering of metabolic pathway fluxes in *Corynebacterium glutamicum*. *Adv Biochem Eng Biotechnol* **120,** 21-49.

Wittmann C and Becker J (2007). The L-lysine story: From metabolic pathways to industrial production, *Microbiology Monographs*, Springer Berlin/ Heidelberg

Wittmann C and de Graaf A (2005). Metabolic flux analysis in *Corynebacterium glutamicum* in Eggeling L and Bott M (Eds), *Handbook of Corynebacterium glutamicum*, CRC Press, pp. 277-304.

Wittmann C, Hans M and Heinzle E (2002). *In vivo* analysis of intracellular amino acid labelings by GC/MS. *Anal Biochem* **307,** 379-382.

Wittmann C and Heinzle E (1999). Mass spectrometry for metabolic flux analysis. *Biotechnol Bioeng* **62,** 739-750.

Wittmann C and Heinzle E (2002). Genealogy profiling through strain improvement by using metabolic network analysis: metabolic flux genealogy of several generations of lysine-producing corynebacteria. *Appl Environ Microbiol* **68,** 5843-5859.

Wittmann C and Heinzle E (2008). Metabolic network analysis and design in *Corynebacterium glutamicum* in Burkovski A (Ed), *Corynebacteria - Genomics and Molecular Biology*, Caister Academic Press, pp. 79-112.

Wittmann C, Kiefer P and Zelder O (2004a). Metabolic fluxes in *Corynebacterium glutamicum* during lysine production with sucrose as carbon source. *Appl Environ Microbiol* **70,** 7277-7287.

Wittmann C, Kim HM and Heinzle E (2004b). Metabolic network analysis of lysine producing *Corynebacterium glutamicum* at a miniaturized scale. *Biotechnol Bioeng* **87,** 1-6.

Wittmann C, Kromer JO, Kiefer P, Binz T and Heinzle E (2004c). Impact of the cold shock phenomenon on quantification of intracellular metabolites in bacteria. *Anal Biochem* **327,** 135-139.

Wu L, Mashego MR, van Dam JC, Proell AM, Vinke JL, Ras C, van Winden WA, van Gulik WM and Heijnen JJ (2005). Quantitative analysis of the microbial metabolome by isotope dilution mass spectrometry using uniformly ^{13}C-labeled cell extracts as internal standards. *Anal Biochem* **336,** 164-171.

Yamaoka N, Kudo Y, Inazawa K, Inagawa S, Yasuda M, Mawatari K, Nakagomi K and Kaneko K (2010). Simultaneous determination of nucleosides and nucleotides in dietary foods and beverages using ion-pairing liquid chromatography-electrospray ionization-mass spectrometry. *J. Chromatogr., B* **878,** 2054-2060.

Yang TH, Bolten CJ, Coppi MV, Sun J and Heinzle E (2009). Numerical bias estimation for mass spectrometric mass isotopomer analysis. *Anal Biochem* **388,** 192-203.

Yang TH, Frick O and Heinzle E (2008). Hybrid optimization for ^{13}C metabolic flux analysis using systems parametrized by compactification. *BMC Syst Biol* **2,** 29.

Yang TH, Heinzle E and Wittmann C (2005). Theoretical aspects of ^{13}C metabolic flux analysis with sole quantification of carbon dioxide labeling. *Comput Biol Chem* **29,** 121-133.

Yang TH, Wittmann C and Heinzle E (2006). Respirometric ^{13}C flux analysis. Part II. *In vivo* flux estimation of lysine-producing *Corynebacterium glutamicum*. *Metab Eng* **8,** 432-446.

Yokota A and Lindley ND (2005). Central metabolism: sugar uptake and conversion in Eggeling L and Bott M (Eds), *Handbook of Corynebacterium glutamicum*, CRC Press, pp. 215-240.

Yuan Y, Yang TH and Heinzle E (2010). ^{13}C metabolic flux analysis for larger scale cultivation using gas chromatography-combustion-isotope ratio mass spectrometry. *Metab Eng* **12,** 392-400.

Zakataeva NP, Aleshin VV, Tokmakova IL, Troshin PV and Livshits VA (1999). The novel transmembrane *Escherichia coli* proteins involved in the amino acid efflux. *FEBS Lett* **452,** 228-232.

Zakataeva NP, Gronskiy SV, Sheremet AS, Kutukova EA, Novikova AE and Livshits VA (2007). A new function for the *Bacillus* PbuE purine base efflux pump: efflux of purine nucleosides. *Res Microbiol* **158,** 659-665.

Zamboni N and Sauer U (2009). Novel biological insights through metabolomics and ^{13}C-flux analysis. *Curr Opin Microbiol* **12,** 553-558.

Zhou G, Charbonneau H, Colman RF and Zalkin H (1993). Identification of sites for feedback regulation of glutamine 5-phosphoribosylpyrophosphate amidotransferase by nucleotides and relationship to residues important for catalysis. *J Biol Chem* **268,** 10471-10481.

Zhou G, Smith JL and Zalkin H (1994). Binding of purine nucleotides to two regulatory sites results in synergistic feedback inhibition of glutamine 5-phosphoribosylpyrophosphate amidotransferase. *J Biol Chem* **269,** 6784-6789.

Zupke C and Stephanopoulos G (1994). Modeling of isotope distributions and intracellular fluxes in metabolic networks using atom mapping matrices. *Biotechnol Prog* **10,** 489-498.

Supplementary material

Chapters IV and V

Stoichiometric networks for ^{13}C metabolic flux analysis (MFA)
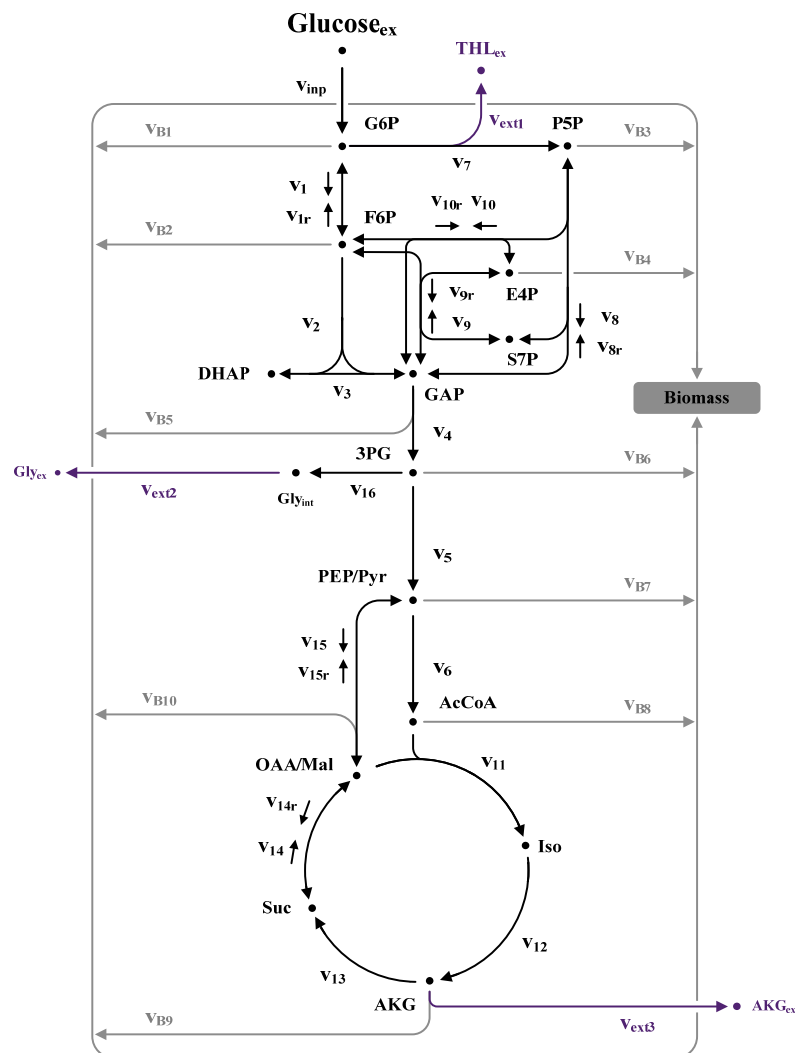
Figure S-1. Metabolic network of the central carbon metabolism of *Corynebacterium glutamicum* used for ^{13}C-MFA of *C. glutamicum* ATCC 13032, *C. glutamicum ΔpurA ΔguaB2* and *C. glutamicum ΔmalE*. The network contains mass balances for 15 metabolites linked by 15 intracellular fluxes (v_i; v_{ir}), 4 extracellular fluxes (vinp; $v_{ext\ i}$) and 10 anabolic fluxes (v_{Bi}).

Molar balance equations for metabolites illustrated in Figure S-1 are defined as follows:

$$v_{G6P}: \quad 0 = (v_{inp} + v_{1r}) - (v_1 + v_7 + v_{B1} + \tfrac{1}{2}v_{ext1})$$

$$v_{F6P}: \quad 0 = (v_1 + v_9 + v_{10}) - (v_{1r} + v_2 + v_{9r} + v_{10r} + v_{B2})$$

$$v_{DHAP}: \quad 0 = (v_2) - (v_3)$$

$$v_{GAP}: \quad 0 = (v_2 + v_3 + v_8 + v_{9r} + v_{10}) - (v_4 + v_{8r} + v_9 + v_{10r} + v_{B5})$$

$$v_{3PG}: \quad 0 = (v_4) - (v_5 + v_{16} + v_{B6})$$

$$v_{PEP/Pyr}: \quad 0 = (v_5 + v_{15r}) - (v_6 + v_{B7})$$

$$v_{P5P}: \quad 0 = (v_7 + 2v_{8r} + v_{10r}) - (2v_8 + v_{10} + v_{B3})$$

$$v_{E4P}: \quad 0 = (v_9 + v_{10r}) - (v_{9r} + v_{10} + v_{B4})$$

$$v_{S7P}: \quad 0 = (v_8 + v_{9r}) - (v_{8r} + v_9)$$

$$v_{AcCoA}: \quad 0 = (v_6) - (v_{11} + v_{B8})$$

$$v_{Iso}: \quad 0 = (v_{11}) - (v_{12})$$

$$v_{AKG}: \quad 0 = (v_{12}) - (v_{13} + v_{B9} + v_{ext3})$$

$$v_{Suc}: \quad 0 = (v_{13} + v_{14r}) - (v_{14})$$

$$v_{OAA/Mal}: \quad 0 = (v_{14} + v_{15}) - (v_{11} + v_{14r} + v_{15r} + v_{B10})$$

$$v_{Gly,int}: \quad 0 = (v_{16}) - (v_{ext2})$$
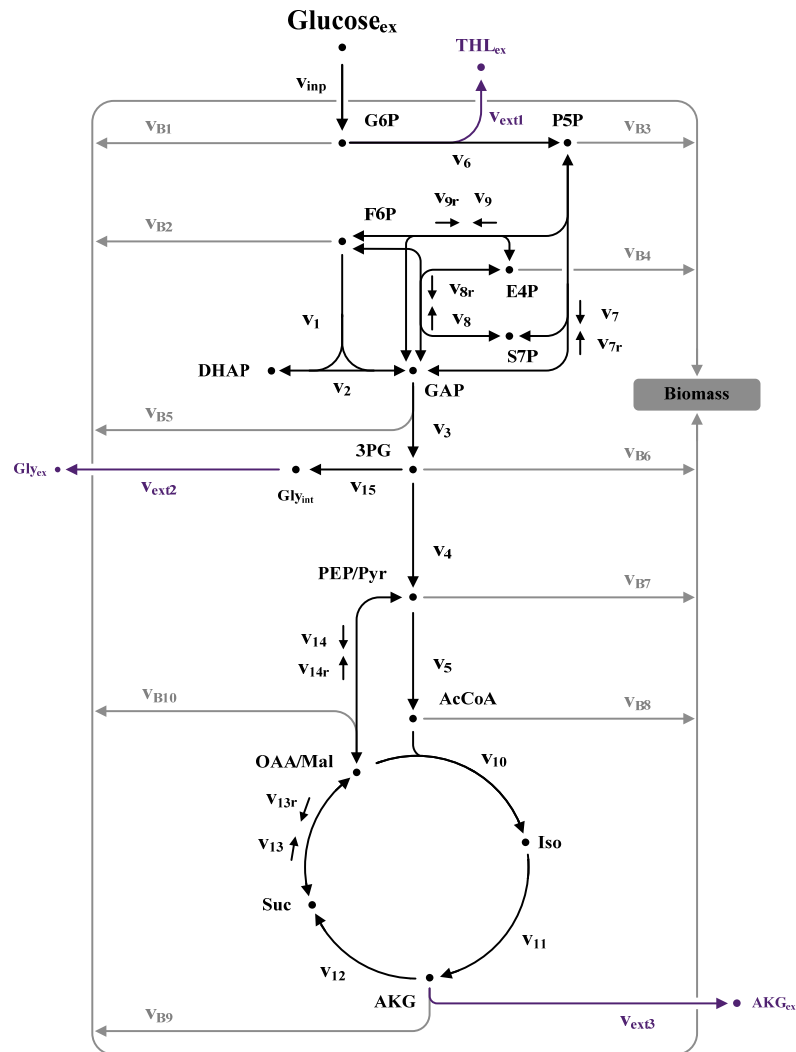
Figure S-2. Metabolic network of the central carbon metabolism of *Corynebacterium glutamicum* used for ^{13}C-MFA of *C. glutamicum Δpgi, C. glutamicum ΔpurA ΔguaB2 purF^{K348Q} Δpgi* and *C. glutamicum ΔmalE Δpgi*. The network contains mass balances for 15 metabolites linked by 14 intracellular fluxes (v_i; v_{ir}), 4 extracellular fluxes (v_{inp}; $v_{ext\ i}$) and 10 anabolic fluxes (v_{Bi}).

Molar balance equations for metabolites illustrated in Figure S-2 are defined as follows:

$$v_{G6P}: \quad 0 = (v_{inp}) - (v_6 + v_{B1} + \tfrac{1}{2}v_{ext1})$$

$$v_{F6P}: \quad 0 = (v_8 + v_9) - (v_1 + v_{8r} + v_{9r} + v_{B2})$$

$$v_{DHAP}: \quad 0 = (v_1) - (v_2)$$

$$v_{GAP}: \quad 0 = (v_2 + v_3 + v_7 + v_{8r} + v_9) - (v_3 + v_{7r} + v_8 + v_{9r} + v_{B5})$$

$$v_{3PG}: \quad 0 = (v_3) - (v_4 + v_{15} + v_{B6})$$

$$v_{PEP/Pyr}: \quad 0 = (v_4 + v_{14r}) - (v_5 + v_{B7})$$

$$v_{P5P}: \quad 0 = (v_6 + 2v_{7r} + v_{9r}) - (2v_7 + v_9 + v_{B3})$$

$$v_{E4P}: \quad 0 = (v_8 + v_{9r}) - (v_{8r} + v_9 + v_{B4})$$

$$v_{S7P}: \quad 0 = (v_7 + v_{8r}) - (v_{7r} + v_8)$$

$$v_{AcCoA}: \quad 0 = (v_5) - (v_{10} + v_{B8})$$

$$v_{Iso}: \quad 0 = (v_{10}) - (v_{11})$$

$$v_{AKG}: \quad 0 = (v_{11}) - (v_{12} + v_{B9} + v_{ext3})$$

$$v_{Suc}: \quad 0 = (v_{12} + v_{13r}) - (v_{13})$$

$$v_{OAA/Mal}: \quad 0 = (v_{13} + v_{14}) - (v_{10} + v_{13r} + v_{14r} + v_{B10})$$

$$v_{Gly,int}: \quad 0 = (v_{15}) - (v_{ext2})$$

Mass isotopomer distributions

The corresponding flux activities and standard deviations determined for *C. glutamicum* ATCC 13032, *C. glutamicum Δpgi*, *C. glutamicum ΔpurA ΔguaB2* and *C. glutamicum ΔpurA ΔguaB2 purF^{K348Q} Δpgi* are listed in Chapter IV, and for *C. glutamicum ΔmalE* and *C. glutamicum ΔmalE Δpgi* in Chapter V.

Comparison of experimentally determined and calculated mass isotopomer distributions of *C. glutamicum* ATCC 13032 is depicted in Chapter VI.

Computational modeling and mathematical optimization were performed by a Monte Carlo approach as described by Yang et al., (2008).

Table S-1. Relative mass isotopomer fractions of proteinogenic amino acids derived from cellular protein and of trehalose secreted during cultivation of *C. glutamicum ΔpurA ΔguaB2* on 99% [1-^{13}C] glucose[a].

metabolite	mass isotopomer fraction									
	M_0	M_1	M_2	M_3	M_4	M_5	M_6	M_7	M_8	M_9
ala (*m/z* 260; c_1-c_3)										
calc	0.604	0.365	0.030	0.001						
exp	0.622	0.364	0.013	0.000						
gly (*m/z* 246; c_1-c_2)										
calc	0.948	0.051	0.001							
exp	0.948	0.047	0.005							
val (*m/z* 288; c_1-c_5)										
calc	0.479	0.411	0.101	0.009	0.000	0.000				
exp	0.397	0.449	0.144	0.008	0.001	0.001				
leu (*m/z* 200; c_1-c_5)										
calc	0.273	0.435	0.240	0.050	0.003	0.000				
exp	0.273	0.429	0.243	0.052	0.002	0.001				
ser (*m/z* 390; c_1-c_3)										
calc	0.624	0.356	0.019	0.000						
exp	0.629	0.363	0.008	0.000						
thr (*m/z* 404; c_1-c_4)										
calc	0.462	0.415	0.112	0.011	0.000					
exp	0.465	0.423	0.106	0.006	0.000					
phe (*m/z* 336; c_1-c_9)										
calc	0.300	0.422	0.216	0.053	0.008	0.001	0.000	0.000	0.000	0.000
exp	0.308	0.430	0.209	0.041	0.004	0.003	0.001	0.003	0.001	0.001
asp (*m/z* 418; c_1-c_4)										
calc	0.462	0.415	0.112	0.011	0.000					
exp	0.465	0.423	0.106	0.006	0.000					
glu (*m/z* 432; c_1-c_5)										
calc	0.332	0.438	0.194	0.033	0.002	0.000				
exp	0.329	0.441	0.198	0.031	0.001	0.000				
tyr (*m/z* 466; c_1-c_9)										
calc	0.300	0.422	0.216	0.053	0.008	0.001	0.000	0.000	0.000	0.000
exp	0.306	0.428	0.209	0.041	0.006	0.002	0.002	0.002	0.002	0.002
tre (*m/z* 361; c_1-c_6)										
calc	0.017	0.928	0.053	0.002	0.000	0.000	0.000			
exp	0.026	0.928	0.030	0.001	0.007	0.005	0.003			

[a] GC-MS data experimentally determined (exp) and corresponding calculated values (calc) obtained by an interative optimization applying 100 Monte Carlo runs with statistically varying initial values. M_0 denotes the non-labeled mass isotopomer fraction and M_i the corresponding higher-labeled fractions.

Table S-2. Relative mass isotopomer fractions of proteinogenic amino acids derived from cellular protein and of trehalose secreted during cultivation of *C. glutamicum ΔmalE* on 99% [1-^{13}C] glucose[a].

metabolite	M$_0$	M$_1$	M$_2$	M$_3$	M$_4$	M$_5$	M$_6$	M$_7$	M$_8$	M$_9$
ala (*m/z* 260; c$_1$-c$_3$)										
calc	0.653	0.332	0.014	0.000						
exp	0.657	0.332	0.011	0.000						
gly (*m/z* 246; c$_1$-c$_2$)										
calc	0.962	0.037	0.000							
exp	0.963	0.037	0.000							
val (*m/z* 288; c$_1$-c$_5$)										
calc	0.535	0.388	0.073	0.004	0.000	0.000				
exp	0.445	0.431	0.116	0.005	0.001	0.001				
leu (*m/z* 200; c$_1$-c$_5$)										
calc	0.317	0.438	0.207	0.036	0.001	0.000				
exp	0.319	0.433	0.208	0.037	0.002	0.001				
ser (*m/z* 390; c$_1$-c$_3$)										
calc	0.662	0.328	0.010	0.000						
exp	0.662	0.332	0.006	0.000						
thr (*m/z* 404; c$_1$-c$_4$)										
calc	0.495	0.399	0.097	0.009	0.000					
exp	0.498	0.409	0.089	0.003	0.000					
phe (*m/z* 336; c$_1$-c$_9$)										
calc	0.353	0.428	0.182	0.034	0.003	0.000	0.000	0.000	0.000	0.000
exp	0.348	0.420	0.179	0.033	0.004	0.005	0.002	0.005	0.002	0.002
asp (*m/z* 418; c$_1$-c$_4$)										
calc	0.495	0.399	0.097	0.009	0.000					
exp	0.497	0.409	0.090	0.003	0.000					
glu (*m/z* 432; c$_1$-c$_5$)										
calc	0.372	0.431	0.169	0.026	0.002	0.000				
exp	0.370	0.432	0.173	0.023	0.000	0.000				
tyr (*m/z* 466; c$_1$-c$_9$)										
calc	0.353	0.428	0.182	0.034	0.003	0.000	0.000	0.000	0.000	0.000
exp	0.349	0.420	0.179	0.032	0.008	0.003	0.002	0.002	0.002	0.003
tre (*m/z* 361; c$_1$-c$_6$)										
calc	0.021	0.926	0.052	0.001	0.000	0.000	0.000			
exp	0.026	0.926	0.032	0.002	0.006	0.005	0.003			

[a] GC-MS data experimentally determined (exp) and corresponding calculated values (calc) obtained by an interative optimization applying 100 Monte Carlo runs with statistically varying initial values. M$_0$ denotes the non-labeled mass isotopomer fraction and M$_i$ the corresponding higher-labeled fractions.

Table S-3. Relative mass isotopomer fractions of proteinogenic amino acids derived from cellular protein and of trehalose secreted during cultivation of *C. glutamicum Δpgi* on 99% [1,2-^{13}C$_2$] glucose[a].

metabolite	M$_0$	M$_1$	M$_2$	M$_3$	M$_4$	M$_5$	M$_6$	M$_7$	M$_8$	M$_9$
ala (*m/z* 260; c$_1$-c$_3$)										
calc	0.597	0.217	0.182	0.004						
exp	0.601	0.213	0.183	0.003						
gly (*m/z* 246; c$_1$-c$_2$)										
calc	0.788	0.206	0.006							
exp	0.785	0.209	0.005							
val (*m/z* 288; c$_1$-c$_5$)										
calc	0.419	0.325	0.196	0.058	0.003	0.000				
exp	0.372	0.356	0.198	0.072	0.002	0.000				
leu (*m/z* 200; c$_1$-c$_5$)										
calc	0.244	0.431	0.262	0.060	0.003	0.000				
exp	0.241	0.422	0.267	0.064	0.004	0.001				
ser (*m/z* 390; c$_1$-c$_3$)										
calc	0.609	0.199	0.188	0.004						
exp	0.589	0.238	0.170	0.003						
thr (*m/z* 404; c$_1$-c$_4$)										
calc	0.341	0.417	0.184	0.056	0.001					
exp	0.347	0.412	0.182	0.057	0.001					
phe (*m/z* 336; c$_1$-c$_9$)										
calc	0.164	0.278	0.262	0.179	0.083	0.028	0.006	0.000	0.000	0.000
exp	0.160	0.274	0.264	0.181	0.083	0.028	0.006	0.001	0.001	0.001
asp (*m/z* 418; c$_1$-c$_4$)										
calc	0.341	0.417	0.184	0.056	0.001					
exp	0.344	0.412	0.186	0.059	0.000					
glu (*m/z* 432; c$_1$-c$_5$)										
calc	0.243	0.426	0.264	0.063	0.004	0.000				
exp	0.247	0.423	0.265	0.062	0.002	0.000				
tyr (*m/z* 466; c$_1$-c$_9$)										
calc	0.164	0.278	0.262	0.179	0.083	0.028	0.006	0.000	0.000	0.000
exp	0.161	0.276	0.264	0.180	0.082	0.028	0.006	0.001	0.001	0.001
tre (*m/z* 361; c$_1$-c$_6$)										
calc	0.000	0.0019	0.940	0.041	0.001	0.000	0.000			
exp	0.006	0.006	0.943	0.041	0.002	0.001	0.001			

[a] GC-MS data experimentally determined (exp) and corresponding calculated values (calc) obtained by an interative optimization applying 100 Monte Carlo runs with statistically varying initial values. M$_0$ denotes the non-labeled mass isotopomer fraction and M$_i$ the corresponding higher-labeled fractions.

Table S-4. Relative mass isotopomer fractions of proteinogenic amino acids derived from cellular protein and of trehalose secreted during cultivation of *C. glutamicum ΔmalE Δpgi* on 99% [1,2-$^{13}C_2$] glucose[a].

metabolite	M_0	M_1	M_2	M_3	M_4	M_5	M_6	M_7	M_8	M_9
ala (*m/z* 260; c_1-c_3)										
calc	0.604	0.208	0.185	0.004						
exp	0.608	0.209	0.180	0.002						
gly (*m/z* 246; c_1-c_2)										
calc	0.790	0.204	0.006							
exp	0.788	0.207	0.005							
val (*m/z* 288; c_1-c_5)										
calc	0.425	0.320	0.195	0.058	0.003	0.000				
exp	0.379	0.355	0.194	0.070	0.002	0.000				
leu (*m/z* 200; c_1-c_5)										
calc	0.240	0.432	0.265	0.060	0.003	0.000				
exp	0.244	0.429	0.264	0.060	0.003	0.000				
ser (*m/z* 390; c_1-c_3)										
calc	0.608	0.202	0.186	0.004						
exp	0.592	0.235	0.171	0.003						
thr (*m/z* 404; c_1-c_4)										
calc	0.355	0.416	0.186	0.041	0.001					
exp	0.355	0.409	0.179	0.057	0.001					
phe (*m/z* 336; c_1-c_9)										
calc	0.151	0.274	0.264	0.186	0.088	0.030	0.007	0.000	0.000	0.000
exp	0.159	0.272	0.263	0.181	0.083	0.029	0.007	0.002	0.001	0.001
asp (*m/z* 418; c_1-c_4)										
calc	0.355	0.416	0.186	0.041	0.001					
exp	0.351	0.410	0.183	0.055	0.000					
glu (*m/z* 432; c_1-c_5)										
calc	0.255	0.429	0.254	0.059	0.004	0.000				
exp	0.255	0.429	0.256	0.057	0.001	0.000				
tyr (*m/z* 466; c_1-c_9)										
calc	0.151	0.274	0.264	0.186	0.088	0.030	0.007	0.000	0.000	0.000
exp	0.156	0.269	0.259	0.185	0.087	0.030	0.007	0.003	0.002	0.002
tre (*m/z* 361; c_1-c_6)										
calc	0.000	0.019	0.940	0.041	0.001	0.000	0.000			
exp	0.041	0.023	0.885	0.034	0.007	0.004	0.006			

[a] GC-MS data experimentally determined (exp) and corresponding calculated values (calc) obtained by an interative optimization applying 100 Monte Carlo runs with statistically varying initial values. M_0 denotes the non-labeled mass isotopomer fraction and M_i the corresponding higher-labeled fractions.

Table S-5. Relative mass isotopomer fractions of proteinogenic amino acids derived from cellular protein and of trehalose secreted during cultivation of *C. glutamicum ΔpurA ΔguaB2 purF*[K348Q] *Δpgi* on 99% $[1,2\text{-}^{13}C_2]$ glucose[a].

metabolite	M_0	M_1	M_2	M_3	M_4	M_5	M_6	M_7	M_8	M_9
ala (*m/z* 260; c_1-c_3)										
calc	0.583	0.218	0.194	0.005						
exp	0.584	0.216	0.197	0.000						
gly (*m/z* 246; c_1-c_2)										
calc	0.757	0.237	0.006							
exp	0.726	0.255	0.019							
val (*m/z* 288; c_1-c_5)										
calc	0.402	0.326	0.205	0.064	0.003	0.000				
exp	0.353	0.350	0.210	0.081	0.006	0.000				
leu (*m/z* 200; c_1-c_5)										
calc	0.257	0.431	0.252	0.057	0.003	0.000				
exp	0.237	0.415	0.271	0.069	0.007	0.001				
ser (*m/z* 390; c_1-c_3)										
calc	0.608	0.182	0.206	0.004						
exp	0.593	0.226	0.179	0.002						
thr (*m/z* 404; c_1-c_4)										
calc	0.360	0.398	0.188	0.053	0.001					
exp	0.366	0.395	0.187	0.050	0.001					
phe (*m/z* 336; c_1-c_9)										
calc	0.283	0.318	0.234	0.119	0.035	0.010	0.002	0.000	0.000	0.000
exp	0.250	0.293	0.241	0.139	0.052	0.017	0.004	0.002	0.001	0.001
asp (*m/z* 418; c_1-c_4)										
calc	0.360	0.398	0.188	0.053	0.001					
exp	0.363	0.398	0.187	0.050	0.001					
glu (*m/z* 432; c_1-c_5)										
calc	0.273	0.418	0.245	0.061	0.004	0.000				
exp	0.253	0.419	0.258	0.064	0.005	0.001				
tyr (*m/z* 466; c_1-c_9)										
calc	0.283	0.318	0.234	0.119	0.035	0.010	0.002	0.000	0.000	0.000
exp	0.246	0.294	0.242	0.140	0.052	0.018	0.004	0.002	0.001	0.001
tre (*m/z* 361; c_1-c_6)										
calc	0.000	0.019	0.940	0.041	0.001	0.000	0.000			
exp	0.041	0.039	0.870	0.034	0.007	0.004	0.006			

[a] GC-MS data experimentally determined (exp) and corresponding calculated values (calc) obtained by an interative optimization applying 100 Monte Carlo runs with statistically varying initial values. M_0 denotes the non-labeled mass isotopomer fraction and M_i the corresponding higher-labeled fractions.

Plasmid charts
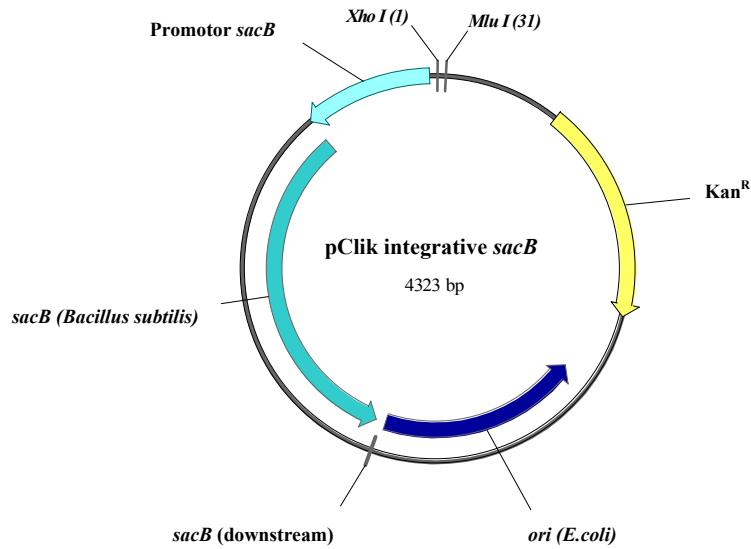
Figure S-3. Structure of the integrative plasmid pClik int *sacB* used for the introduction of stable modification into the genome of *Corynebacterium glutamicum* via homologous recombination.
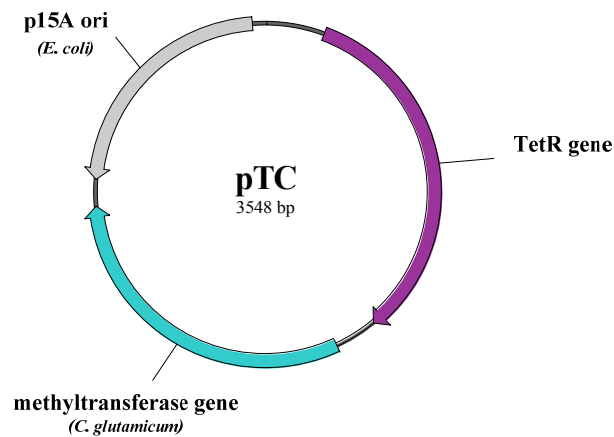
Figure S-4. Structure of the pTC plasmid, used for transfer of the corynespecific methylation pattern to the integrative pClik-derivates.

Outlook

Table S-6. *In silico* alterations of biomass composition of *C. glutamicum*[a].

	biomass fractions					
	ash	**carbohydrates**	**lipids**	**DNA**	**RNA**	**proteins**
Alteration of lipid fraction						
A.I.	10.7	20.3	7.0	1.0	5.3	55.7
A.II.[b]	10.0	19.0	13.0	1.0	5.0	52.0
A.III.	9.2	17.4	20.0	1.0	4.6	47.8
A.IV.	8.5	16.4	25.0	1.0	4.3	44.8
A.V.	7.6	14.5	33.3	1.0	3.8	39.8
Alteration of protein fraction						
B.I.	12.6	23.8	16.3	1.0	6.3	40.0
B.II.	11.5	21.9	14.9	1.0	5.7	45.0
B.III.[b]	10.0	19.0	13.0	1.0	5.0	52.0
B.IV.	8.3	15.7	10.8	1.0	4.2	60.0
B.V.	7.2	13.8	9.4	1.0	3.6	65.0
Scenario C						
	7.7	14.5	15.0	1.0	3.8	58.0

[a] relative fractions and abbreviations are highlighted in Figures VIII-1, VIII-4 and VIII-5.

[b] initial biomass composition adopted from Kjeldsen and Nielsen (2009).

Table S-7. Intracellular carbon flux distributions (*in silico*) with corresponding standard deviations determined for varying lipid content of *C. glutamicum Δpgi*[a].

lipid content [%] Flux parameter	7 (A.I.)	13[b] (A.II.)	20 (A.III.)	25 (A.IV.)	33 (A.V.)
G6P DH	97.6 ± 0.1	97.8 ± 0.1	97.9 ± 0.1	97.9 ± 0.3	98.0 ± 0.1
transketolase 1	30.7 ± 0.0	30.8 ± 0.0	30.9 ± 0.0	31.0 ± 0.1	31.2 ± 0.0
transketolase 2	28.1 ± 0.1	28.4 ± 0.0	28.8 ± 0.0	29.0 ± 0.1	29.4 ± 0.0
aldolase	55.8 ± 0.1	56.4 ± 0.1	57.2 ± 0.1	57.6 ± 0.2	58.5 ± 0.1
G3P DH	139.2 ± 0.3	140.1 ± 0.3	141.4 ± 0.3	142.0 ± 0.4	143.3 ± 0.2
enolase	127.6 ± 0.3	128.7 ± 0.3	130.1 ± 0.3	130.8 ± 0.5	132.3 ± 0.3
pyruvate DH	69.0 ± 0.6	73.8 ± 0.7	79.6 ± 0.5	83.4 ± 0.7	89.6 ± 0.6
citrate synthase	48.8 ± 0.6	45.7 ± 0.9	42.1 ± 0.7	39.0 ± 1.0	33.7 ± 0.9
α-ketoglutarate DH	37.0 ± 0.7	34.6 ± 0.9	32.0 ± 0.8	29.5 ± 1.1	25.1 ± 1.0
pyruvate carboxylase[c]	27.2 ± 0.1	25.9 ± 0.2	23.9 ± 0.1	22.5 ± 0.2	20.2 ± 0.1

data are given as relative fluxes [%] normalized to the specific glucose uptake rate q_S = 4.18 mmol g_{CDW}^{-1} h^{-1} (see Table V-3), which was set to 100%.

[a] mean values and standard deviations were calculated from 100 independent Monte Carlo runs.

[b] initial values for lipid content (wild type).

[c] given as net flux through anaplerotic reactions.

Table S-8. Intracellular carbon flux distributions (*in silico*) with corresponding standard deviations determined for varying protein content of *C. glutamicum Δpgi*[a].

protein content [%] Flux parameter	40 (B.I.)	45 (B.II.)	52[b] (B.III.)	60 (B.IV.)	65 (B.V.)
G6P DH	97.3 ± 0.0	97.4 ± 0.2	97.8 ± 0.1	98.1 ± 0.1	98.2 ± 0.1
transketolase 1	30.0 ± 0.0	30.3 ± 0.1	30.8 ± 0.0	31.3 ± 0.0	31.6 ± 0.0
transketolase 2	28.2 ± 0.0	28.3 ± 0.1	28.4 ± 0.0	28.5 ± 0.0	28.6 ± 0.0
aldolase	54.8 ± 0.0	55.5 ± 0.2	56.4 ± 0.1	57.5 ± 0.1	58.2 ± 0.1
G3P DH	136.5 ± 0.1	137.9 ± 0.5	140.1 ± 0.3	142.6 ± 0.2	144.2 ± 0.2
enolase	125.1 ± 0.1	126.5 ± 0.6	128.7 ± 0.3	131.1 ± 0.3	132.6 ± 0.3
pyruvate DH	80.8 ± 0.2	77.7 ± 1.0	73.8 ± 0.7	69.3 ± 0.6	66.4 ± 0.5
citrate synthase	47.4 ± 0.3	46.4 ± 1.3	45.7 ± 0.9	44.7 ± 0.7	44.0 ± 0.6
α-ketoglutarate DH	38.7 ± 0.3	36.7 ± 1.4	34.6 ± 0.9	32.2 ± 0.7	30.5 ± 0.7
pyruvate carboxylase[c]	21.4 ± 0.0	23.3 ± 0.2	25.9 ± 0.2	28.9 ± 0.1	30.8 ± 0.1

data are given as relative fluxes [%] normalized to the specific glucose uptake rate $q_S = 4.18$ mmol g_{CDW}^{-1} h^{-1} (see Table V-3), which was set to 100%.

[a] mean values and standard deviations were calculated from 100 independent Monte Carlo runs.

[b] initial values for protein content (wild type).

[c] given as net flux through anaplerotic reactions.

Table S-9. Intracellular carbon flux distribution (*in silico*) with corresponding standard deviations determined for initial biomass composition of *C. glutamicum Δpgi* and for Scenario C.

flux parameter	initial biomass composition	scenario C
G6P DH	97.8 ± 0.1	98.2 ± 0.1
transketolase 1	30.8 ± 0.0	31.4 ± 0.0
transketolase 2	28.4 ± 0.0	28.8 ± 0.0
aldolase	56.4 ± 0.1	58.1 ± 0.1
G3P DH	140.1 ± 0.3	143.7 ± 0.2
enolase	128.7 ± 0.3	132.3 ± 0.2
pyruvate DH	73.8 ± 0.7	72.7 ± 0.6
citrate synthase	45.7 ± 0.9	42.5 ± 0.7
α-ketoglutarate DH	34.6 ± 0.9	30.4 ± 0.8
pyruvate carboxylase[a]	25.9 ± 0.2	27.9 ± 0.2

data are given as relative fluxes [%] normalized to the specific glucose uptake rate q_S = 4.18 mmol g_{CDW}^{-1} h^{-1} (see Table V-3), which was set to 100%. Mean values and standard deviations were calculated from 100 independent Monte Carlo runs.

[a] given as net flux through anaplerotic reactions.

Table S-10. Relative flux changes of *in silico* predicted metabolic fluxes based on strain specific parameters ($Y_{X/S}$, $Y_{P/S}$, MDVs) and modified biomass compositions for increasing lipid content as depicted in Figure VIII-4.

lipid content [%][a] flux parameter	7 (A.I.)	13[b] (A.II.)	20 (A.III.)	25 (A.IV.)	33 (A.V.)
G6P DH	-0.20	-	0.10	0.10	0.20
transketolase 1	-0.33	-	0.32	0.65	1.29
transketolase 2	-1.06	-	1.40	2.09	3.46
aldolase	-1.07	-	1.41	2.11	3.66
G3P DH	-0.64	-	0.92	1.35	2.26
enolase	-0.86	-	1.08	1.62	2.76
pyruvate DH	-6.73	-	7.57	12.23	19.40
citrate synthase	6.56	-	-8.21	-15.85	-30.46
α-ketoglutarate DH	6.71	-	-7.81	-15.95	-32.10

data are given as relative changes (logarithmized and expressed in percent) in relation to fluxes determined for the initial biomass composition (A.II.)

[a] lipid contents are given as relative biomass fraction [%].

[b] initial biomass composition served as reference (- indicates: flux changes are equal to zero).

Table S-11. Relative flux changes of *in silico* predicted metabolic flux activities based on strain specific parameters ($Y_{X/S}$, $Y_{P/S}$, MDVs) and modified biomass compositions for increasing protein contents as depicted in Figure VIII-4.

protein content [%][a] flux parameter	40 (B.I.)	45 (B.II.)	52[b] (B.III.)	60 (B.IV.)	65 (B.V.)
G6P DH	-0.51	-0.41	-	0.31	0.41
transketolase 1	-2.63	-1.64	-	1.61	2.56
transketolase 2	-.071	-0.35	-	0.35	0.70
aldolase	-2.88	-1.61	-	1.93	3.14
G3P DH	-2.60	-1.58	-	1.77	2.88
enolase	-2.84	-1.72	-	1.85	2.99
pyruvate DH	9.06	5.15	-	-6.29	-10.57
citrate synthase	3.65	1.52	-	-2.21	-3.79
α-ketoglutarate DH	11.20	5.89	-	-7.19	-12.61

data are given as relative changes (logarithmized and expressed in percent) in relation to fluxes determined for the initial biomass composition (B.III.).

[a] protein contents are given as relative biomass fraction [%].

[b] initial biomass composition served as reference (-indicates: flux changes are equal to zero).

Curriculum vitae

Susanne Peifer

Diplom-Biologin, geboren am 28.12.1982 in Merzig

Aktuelle Tätigkeit

Wissenschaftl. Mitarbeiterin

seit 04/2012

Vorbereitende Arbeiten zur Einrichtung des neuen Lehrstuhls Systembiotechnologie; Erarbeitung und Umsetzung eines interdisziplinären Projektplans (Fakultäten der Chemie, Pharmazie und Bioinformatik); Kooperationsausbau mit der Université de la Grande Région (UniGR) (Université de Liège, Université de Lorraine, Université de Luxembourg, Universität des Saarlandes).

Akademische Ausbildung

Promotion

01/2008 – 09/2012

Institut für Technische Biochemie; Universität des Saarlandes.

Titel: **In-depth analysis of the purine biosynthetic pathway of *Corynebacterium glutamicum* – From local pathway analysis to global phenotype profiling.**

Diplomarbeit

01/2007 – 09/2007

Institut für Technische Biochemie; Universität des Saarlandes.

Titel: **Charakterisierung von Schwefelstoffwechsel und Methioninbiosynthese in *Corynebacterium glutamicum.***

Studium

10/2002 – 09/2007	Biologie mit Schwerpunkt Human- und Molekularbiologie.
	Zentrum für Human-und Molekularbiologie.
	Universität des Saarlandes und Universitätsklinikum Homburg Saar.

Schulische Ausbildung

08/1993 – 06/2002	Peter-Wust-Gymnasium, Merzig-Wadern.
	Abitur: Biologie, Mathematik, Geschichte.
08/1989 – 07/1993	Grundschule, Orscholz.

Publikationen

Peifer S, Schneider K, Nürenberg G, Volmer DA, Heinzle E (2012).
Quantitation of intracellular purine intermediates in different *Corynebacteria* using electrospray LC-MS/MS.
Anal Bioanal Chem. DOI: 10.1007/s00216-012-6388-6.

Neuner A, Wagner I, Sieker T, Ulber R, Schneider K, **Peifer S**, Heinzle E (2012).
Production of L-lysine on different silage juices using genetically engineered *Corynebacterium glutamicum*.
J Biotechnol http:// dx.doi.org/10.1016/j.jbiotec.2012.07.190.

Peifer S, Heinzle E (2012).
Nucleic acid metabolism in bacteria in Schomburg D and Michal G (Eds) Biochemical Pathways, 2nd Edition.

Peifer S, Lis AV, Heinzle E, Schneider K (2012).
Metabolic flux analysis using metabolite balancing with off-gas analysis provides detailed information about metabolic dynamics of *C. glutamicum* grown on complex substrates.
Submitted.

Peifer S, Barduhn T, Zimmet S, Volmer DA, Ho-Dac T, Heinzle E, Schneider K (2012).
Metabolic engineering of the purine biosynthetic pathway in *Corynebacterium glutamicum* results in increased intracellular pool sizes of IMP and hypoxanthine.
Submitted.

Castillo T, Heinzle E, **Peifer S**, Schneider K, Peña CF (2012).
Metabolic flux analysis of *Azotobacter vinelandii* under different aeration conditions and its relationship with alginate acetylation and poly-β-hydroxybutyrate production.
In preparation.

Peifer S, Höfner M, Heinzle E, Schneider K (2012).
Restriction of the metabolic flexibility due to *pgi* gene deletion triggers a unique adaptation process in *C. glutamicum* involving increased oxygen uptake.
In preparation.

Peifer S, Lis AV, Heinzle E, Schneider K (2012).
Comparative fluxome and dynamic metabolite analysis in a genetically engineered *C. glutamicum* strain cultivated on complex medium.
In preparation.

Konferenzbeiträge

Peifer S, Schneider K, Heinzle E.
IMP accumulation in coryneform bacteria: a comparison of rational strain design and classical mutagenesis. *Metabolic Engineering IX: Metabolic Engineering and synthetic biology* (03.-07.06.2012) Biarritz, France.

Peifer S, Schneider K, Barduhn T, Zimmet S, Volmer DA, Heinzle E.
Metabolic engineering of the purine biosynthesis pathway in *Corynebacterium glutamicum* results in increased IMP accumulation. *Meeting on UniGR research in systems biology* (19.-20.06.2012), Lultzhausen, Luxembourg.

Castillo T, **Peifer S**, Schneider K, Heinzle E, Peña CF.
Metabolic flux analysis of *Azotobacter vinelandii*: first approach under different oxygen concentrations. *8th European Congress of Chemical Engineering and 1st European Congress of Applied Biotechnology* (25.-29.09.2011), Berlin, Germany.

Peifer S, Yang TH, Heinzle E.

High overproduction of NADPH in the PPP reverses malic enzyme activity in *Corynebacterium glutamicum. Metabolic engineering VIII: Metabolic engineering for green growth* (13.-17.06.2010), Jeju Island, Korea.

Bolten CJ, **Peifer S**, Schröder H, Heinzle E, Wittmann C.

Utilization of sulfur sources by *Corynebacterium glutamicum* towards biotechnological methionine production. *BioPerspectives* (07.-09.10.2008), Hannover, Germany.

The outcome of any serious research can only be

to make two questions grow where only one grew before.

Thorstein Bunde Veblen

(1857-1929)